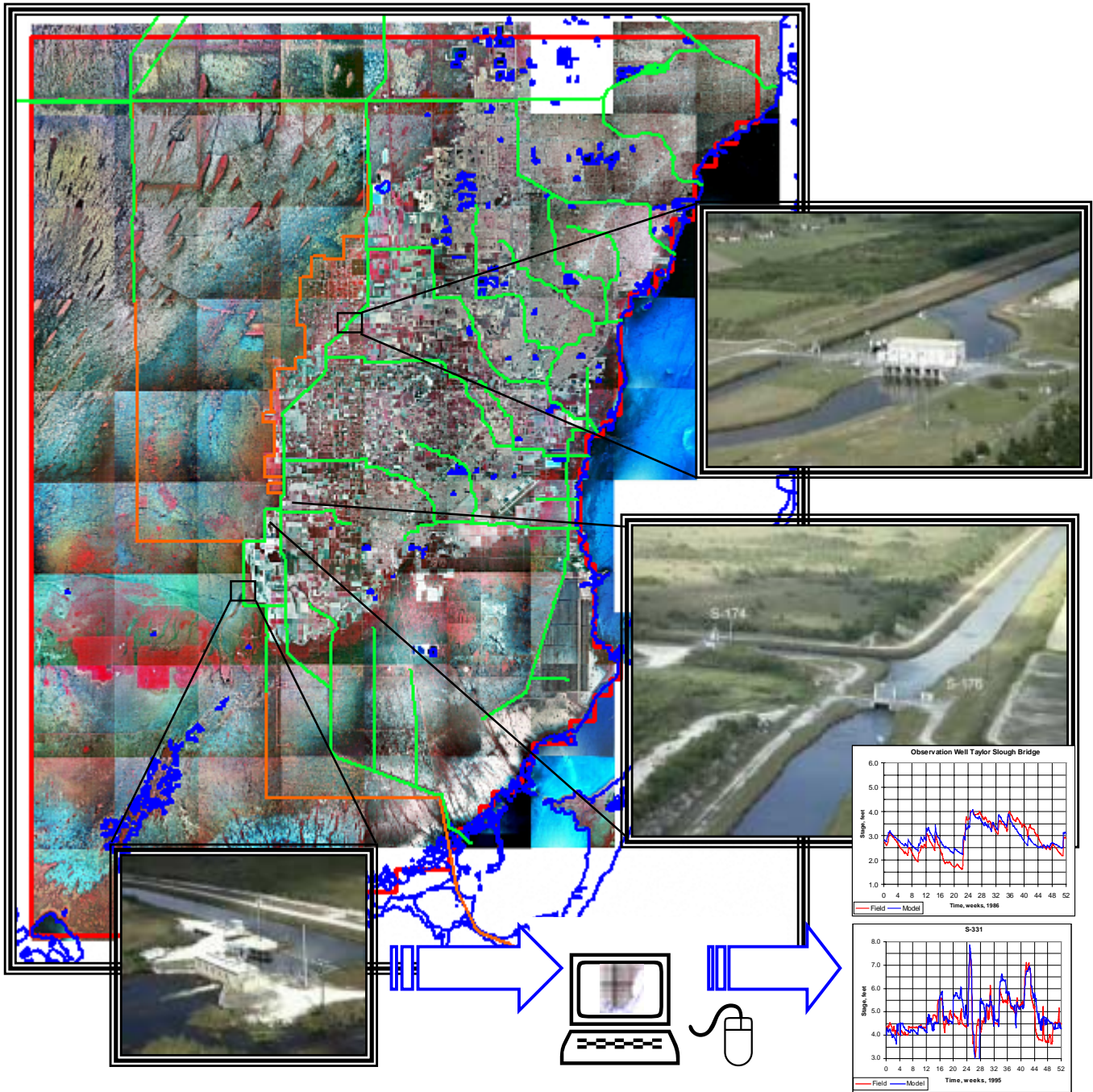


Calibration and Verification of the MODBRANCH Numerical Model of South Dade County, Florida



Robert A. Evans, Jr.

U. S. Army Corps of Engineers
Jacksonville District
February 2000



Table of Contents	
Section	Page
List of Figures	ii
Introduction	1
Model Domain and Description	1
Ground Water and Overland Flow	1
Canal Inputs	3
Model Boundary Conditions	7
Calibration and Verification	8
Ground Water Stages	9
Canal Flows and Stages	14
Sources of Error	23
Conclusions	25
References	26

List of Tables	
Table	Page
Table 1. MODBRANCH Leakage Coefficients	6
Table 2A. Ground Water Observation Wells, MODBRANCH vs Field Data	11-12
Table 2B. Summary of Statistical Performance Measures, Ground Water Observation Wells, MODBRANCH vs Field	13
Table 3A. 1986 Canal Stage Statistics	16
Table 3B. 1989 Canal Stage Statistics	17
Table 3C. 1995 Canal Stage Statistics	18
Table 4A. 1986 Canal Flow Statistics	19
Table 4B. 1989 Canal Flow Statistics	19
Table 4C. 1995 Canal Flow Statistics	20
Table 5. Summary of Canal Stage Statistics	21
Table 6. Summary of Canal Flow Statistics	21
Table 7. Structures Included in MODBRANCH Model of South Dade County	22

List of Figures

Figure	Description
1	Model Boundaries, major canals, ENP boundary, and land variations
2	Model Grid
3a	Contours of Layer 1 Bottom Elevations
3b	Contours of Layer 2 Bottom Elevations
3c	Contours of Layer 3 Bottom Elevations
4	Oblique View of Model Domain
5a	Contours of $\log_{10}(k)$, k = Hydraulic Conductivity, Layer 1
5b	Contours of $\log_{10}(T)$, T = Hydraulic Transmissivity, Layer 2
5c	Contours of $\log_{10}(T)$, T = Hydraulic Transmissivity, Layer 3
6a	Vertical Leakance, Layers 1 and 2
6b	Vertical Leakance, Layers 2 and 3
7	Locations of Production Wells
8a-e	Production Well Pumping Rates
9	Average Daily Rainfall and Cumulative Rainfall, 1986, 1989, and 1995
10	Average Daily ET and Cumulative ET, 1986, 1989, and 1995
11	Evaporation Surface and Extinction Depth
12a-b	Ground Water Observation Wells
13a	Contours of Correlation Coefficient (r), 1995 Ground Water Stages
13b	Contours of Average Absolute Error, 1995 Ground Water Stages
13c	Contours of Average Error, 1995 Ground Water Stages
14	Ground Water Stage, MODBRANCH vs Field Data, G-618
15	Ground Water Stage, MODBRANCH vs Field Data, NE-1
16	Ground Water Stage, MODBRANCH vs Field Data, NE-2
17	Ground Water Stage, MODBRANCH vs Field Data, L67 Extention, East
18	Ground Water Stage, MODBRANCH vs Field Data, L67 Extention, West
19	Ground Water Stage, MODBRANCH vs Field Data, NE-5
20	Ground Water Stage, MODBRANCH vs Field Data, NP-202
21	Ground Water Stage, MODBRANCH vs Field Data, G-3559
22	Ground Water Stage, MODBRANCH vs Field Data, Krome
23	Ground Water Stage, MODBRANCH vs Field Data, G-3558
24	Ground Water Stage, MODBRANCH vs Field Data, G-3556
25	Ground Water Stage, MODBRANCH vs Field Data, G-3552
26	Ground Water Stage, MODBRANCH vs Field Data, G-3555
27	Ground Water Stage, MODBRANCH vs Field Data, G-1487
28	Ground Water Stage, MODBRANCH vs Field Data, G-855
29	Ground Water Stage, MODBRANCH vs Field Data, G-596
30	Ground Water Stage, MODBRANCH vs Field Data, Angels Well
31	Ground Water Stage, MODBRANCH vs Field Data, G-3273
32	Ground Water Stage, MODBRANCH vs Field Data, G-1502
33	Ground Water Stage, MODBRANCH vs Field Data, G-3437
34	Ground Water Stage, MODBRANCH vs Field Data, Humble
35	Ground Water Stage, MODBRANCH vs Field Data, NP-206
36	Ground Water Stage, MODBRANCH vs Field Data, G-1363
37	Ground Water Stage, MODBRANCH vs Field Data, S-196A
38	Ground Water Stage, MODBRANCH vs Field Data, Rutzke
39	Ground Water Stage, MODBRANCH vs Field Data, G-789
40	Ground Water Stage, MODBRANCH vs Field Data, NTS10
41	Ground Water Stage, MODBRANCH vs Field Data, R-3110

List of Figures

Figure	Description
42	Ground Water Stage, MODBRANCH vs Field Data, NTS1
43	Ground Water Stage, MODBRANCH vs Field Data, L-31W
44	Ground Water Stage, MODBRANCH vs Field Data, Frog Pond
45	Ground Water Stage, MODBRANCH vs Field Data, Robblee
46	Ground Water Stage, MODBRANCH vs Field Data, NTS14
47	Ground Water Stage, MODBRANCH vs Field Data, E-112
48	Ground Water Stage, MODBRANCH vs Field Data, Taylor Slough Bridge
49	Ground Water Stage, MODBRANCH vs Field Data, R-158
50	Ground Water Stage, MODBRANCH vs Field Data, NP-72
51	Ground Water Stage, MODBRANCH vs Field Data, DO-1
52	Ground Water Stage, MODBRANCH vs Field Data, R-127
53	Ground Water Stage, MODBRANCH vs Field Data, Taylor Slough Hilton
54	Ground Water Stage, MODBRANCH vs Field Data, E-146
55	Ground Water Stage, MODBRANCH vs Field Data, G-1362
56	Ground Water Stage, MODBRANCH vs Field Data, S-182A
57	Ground Water Stage, MODBRANCH vs Field Data, G-614
58	Ground Water Stage, MODBRANCH vs Field Data, G-1486
59	Ground Water Stage, MODBRANCH vs Field Data, G-1183
60	Ground Water Stage, MODBRANCH vs Field Data, F-358
61	Ground Water Stage, MODBRANCH vs Field Data, G-3356
62	Ground Water Stage, MODBRANCH vs Field Data, G-3355
63	Ground Water Stage, MODBRANCH vs Field Data, G-613
64	Ground Water Stage, MODBRANCH vs Field Data, EVER1
65	Ground Water Stage, MODBRANCH vs Field Data, EVER8
66	Ground Water Stage, MODBRANCH vs Field Data, EVER3
67	Ground Water Stage, MODBRANCH vs Field Data, G-3354
68	Ground Water Stage, MODBRANCH vs Field Data, CV5N
69	Ground Water Stage, MODBRANCH vs Field Data, EVER4
70	Ground Water Stage, MODBRANCH vs Field Data, G-1251
71	Ground Water Stage, MODBRANCH vs Field Data, G-3353
72	Ground Water Stage, MODBRANCH vs Field Data, CV5S
73	Ground Water Stage, MODBRANCH vs Field Data, EP1R
74	Ground Water Stage, MODBRANCH vs Field Data, G-3439
75	Ground Water Stage, MODBRANCH vs Field Data, G-3473
76	Tail Water Stage, MODBRANCH vs Field Data, S-335
77	Flow, MODBRANCH vs Field Data, S-335
78	Head Water Stage, MODBRANCH vs Field Data, S-334
79	Head Water Stage, MODBRANCH vs Field Data, S-336
80	Tail Water Stage, MODBRANCH vs Field Data, S-336
81	Head Water Stage, MODBRANCH vs Field Data, S-25b
82	Flow, MODBRANCH vs Field Data, S-25b
83	Head Water Stage, MODBRANCH vs Field Data, S-121
84	Tail Water Stage, MODBRANCH vs Field Data, S-121
85	Flow, MODBRANCH vs Field Data, S-121
86	Head Water Stage, MODBRANCH vs Field Data, S-22
87	Head Water Stage, MODBRANCH vs Field Data, G-211
88	Tail Water Stage, MODBRANCH vs Field Data, G-211
89	Flow, MODBRANCH vs Field Data, G-211
90	Tail Water Stage, MODBRANCH vs Field Data, S-338

List of Figures

Figure	Description
91	Flow, MODBRANCH vs Field Data, S-338
92	Head Water Stage, MODBRANCH vs Field Data, S-118
93	Flow, MODBRANCH vs Field Data, S-173
94	Head Water Stage, MODBRANCH vs Field Data, S-331
95	Tail Water Stage, MODBRANCH vs Field Data, S-331
96	Flow, MODBRANCH vs Field Data, S-331
97	Head Water Stage, MODBRANCH vs Field Data, S-123
98	Head Water Stage, MODBRANCH vs Field Data, S-149
99	Head Water Stage, MODBRANCH vs Field Data, S-194
100	Tail Water Stage, MODBRANCH vs Field Data, S-194
101	Flow, MODBRANCH vs Field Data, S-194
102	Head Water Stage, MODBRANCH vs Field Data, S-148
103	Flow, MODBRANCH vs Field Data, S-148
104	Head Water Stage, MODBRANCH vs Field Data, S-195
105	Head Water Stage, MODBRANCH vs Field Data, S-165
106	Flow, MODBRANCH vs Field Data, S-165
107	Head Water Stage, MODBRANCH vs Field Data, S-21
108	Head Water Stage, MODBRANCH vs Field Data, S-196
109	Flow, MODBRANCH vs Field Data, S-196
110	Head Water Stage, MODBRANCH vs Field Data, S-21a
111	Head Water Stage, MODBRANCH vs Field Data, S-174/S-332D
112	Flow, MODBRANCH vs Field Data, S-174/S-332D
113	Head Water Stage, MODBRANCH vs Field Data, S-176
114	Tail Water Stage, MODBRANCH vs Field Data, S-176
115	Flow, MODBRANCH vs Field Data, S-176
116	Head Water Stage, MODBRANCH vs Field Data, S-20f
117	Head Water Stage, MODBRANCH vs Field Data, S-332
118	Flow, MODBRANCH vs Field Data, S-332
119	Head Water Stage, MODBRANCH vs Field Data, S-175
120	Head Water Stage, MODBRANCH vs Field Data, S-178
121	Tail Water Stage, MODBRANCH vs Field Data, S-178
122	Head Water Stage, MODBRANCH vs Field Data, S-18c
123	Tail Water Stage, MODBRANCH vs Field Data, S-18c
124	Head Water Stage, MODBRANCH vs Field Data, S-197

1.0 INTRODUCTION

A numerical model of the hydrology of South Dade County (Florida) was developed as a tool to determine impacts of canals, structures, and water use. The area in question has two significant hydrologic regimes that must be considered. The first is the movement of the water through the Biscayne (surficial) Aquifer and the second the movement of water through the various canals and structures of the region. For this reason the simulations were done using the MODBRANCH model, which is a hybrid model created from two USGS models. The first model is MODFLOW, which simulates the ground water hydrodynamics. The second model is BRANCH, which simulates the canal hydrodynamics. E. D. Swain and E. J. Wexler of the United States Geological Survey (USGS) coupled the models. More information on the creation of MODBRANCH may be found in "A Coupled Surface-Water and Ground-Water Flow Model for Simulation of Stream-Aquifer Interaction," (Swain and Wexler, USGS Open File Report 92-138). Further modifications were added to more accurately model the area of South Florida.

Three years were selected for the calibration and verification process. These years represented average, dry, and wet periods and were 1986, 1989, and 1995, respectively.

2.0 MODEL DOMAIN AND DESCRIPTION

Figure 1 shows the model domain on top of an aerial photograph of the area. This figure illustrates the complexity of the area. Land elevations vary from the high Atlantic Ridge to the low Everglades. Land use varies from urban to suburban to agricultural to wilderness.

2.1 GROUND WATER AND OVERLAND FLOW

Ground water and overland flow are simulated by the MODFLOW part of MODBRANCH. MODFLOW is a pseudo-three-dimensional, finite difference, ground water model (McDonald and Harbaugh, 1988). This model requires defining a model "grid" of specified numbers of rows, columns, and layers. The width of each row or column is determined by required resolution in specific areas. The model grid is shown in figure 2 with major canals superimposed. The domain runs north and south from approximately 3 miles north of the Tamiami Trail to Florida Bay. The western boundary is approximately 4.75 miles west of the L-67 Extension and runs eastward to Biscayne Bay. The model grid is made up of 103 rows, 90 columns, and 3 layers. The grid resolution varies in the horizontal from 431 to 10560 feet and in the vertical from 673 to 10560 feet. Levees are defined by using the *horizontal flow barrier* package of MODFLOW.

The hydrogeology of the study area has been studied extensively by many investigators. The study area is underlain by the porous Biscayne Aquifer which is a part of the Surficial Aquifer system. The location and extent of the Surficial Aquifer system has been defined by the Florida Geologic Survey based on

recommendations of the Southeastern Geological Society in 1986. It consists of undifferentiated sand and gravel or marine limestone. In this case, the marine limestone of primary importance is the Biscayne Aquifer. The Biscayne Aquifer, of Pleistocene age, is the main potable aquifer in South Florida. It covers an area of approximately 4,000 square miles including all of Dade County (Randazzo & Jones, 1997). The Biscayne Aquifer consists of beds of highly permeable limestone and sandy-limestone of marine origin. The bottom of the Biscayne Aquifer is characterized by an abrupt change in sediment type where clays and marls of the Tamiami Formation or Hawthorn Formation are present. The Biscayne Aquifer is mostly an unconfined aquifer, although segments may exhibit semi-confined conditions initially. In general, the Biscayne Aquifer is well connected to surface water features including the various drainage canals that are located in the study area.

South Florida's geology is extremely heterogeneous. Measurements and tests performed at one location can give distinctly different values when done 500 feet away. It is important to keep this in mind when considering the model results. The model considers the hydrogeologic parameters input to be homogenous within each grid cell. While hydraulic conductivity and transmissivity vary from cell to cell, each is isotropic within the cell. Additionally, the parameters do not vary significantly between adjacent cells, increasing the degree of homogeneity of the model. The real world is not homogenous. There are indications that there are preferential flow paths within the surficial aquifer including voids, fractures and cavities. These preferential flow paths are not represented by the model inputs. For this reason, the model results should be considered primarily on an areal basis, secondarily on a site-specific basis.

The top layer of the grid is used to simulate free surface, overland flow. As such, it is defined with a bottom elevation that is set at ground surface. Figure 3a shows the contours of the ground elevations. Elevation data were developed using various data sources by the Everglades National Park, the Corps of Engineers, and the United States Geological Survey. Included in these sources were East – West profile lines (approximately 2000 m apart) measured from April to June 1992 by Army Corps of Engineers Jacksonville District personnel.

The second layer is considered to be the upper part of the Biscayne Aquifer. It begins at the ground surface and extends downward to various elevations. These elevations are shown in figure 3b. The third layer extends from these elevations to the bottom of the Biscayne aquifer. The bottom elevations of the Biscayne aquifer are shown in figure 3c. An oblique view of the model domain is shown in figure 4.

The various hydraulic properties of the aquifers (layers 2 and 3) were derived primarily from "Hydrogeology of the Surficial Aquifer System, Dade County, Florida," (Fish and Stewart, USGS Water-Resources Investigations Report 90-4108). The hydraulic properties (horizontal conductivity and storage) of the top layer were assigned in order to mimic overland flow as closely as possible. Figure 5a shows layer 1 contours of $\log_{10}(K)$, where K is the hydraulic

conductivity in feet/day. The contours of layers 2 and 3 (figures 5b and 5c, respectively) show $\log_{10}(T)$, where T is the hydraulic transmissivity in ft^2/day . These data are presented in \log_{10} format due to the extreme range of values found in the area.

MODBRANCH simulates psuedo-three-dimensional ground water movement between adjacent aquifer layers through the use of a “vertical leakance” term. This term is calculated using a variation of a *harmonic mean* of the vertical conductivity. The formula for two successive layers is (Equation 49, p. 5-12, McDonald and Harbaugh, 1988):

$$V = 1 / (\Delta z_i / K_i + \Delta z_{i+1} / K_{i+1}), \text{ where}$$

Δz_i = half thickness of layer i,

K_i = vertical hydraulic conductivity of layer i.

The resulting vertical leakance values are shown in figure 6a (between layers 1 and 2) and figure 6b (between layers 2 and 3). Note that the values within 2 miles (10,560 feet) of the coast were set to low values in order to minimize movement of water along the coastal regions. This was done in conjunction with modification of the coastal *general head boundaries* (see below, section 2.3) in order to mimic the effects of salinity intrusion into the surficial aquifer.

Constant values that further define the hydrologic properties of the aquifers are the specific yield and storage coefficients. Since the surface layer represents overland flow, the specific yield was defined as 1. This indicates that the “material” in layer 1, which is essentially “air,” has 100% porosity and that a unit change in head will result in a unit change in volume of water input or output. The specific yield in layer 2 is defined as 0.2, which indicates a porosity of 20%. Layers 2 and 3 have a “confined storage coefficient” of 0.0001.

2.2 CANAL INPUTS

Canal stage and flow rates are simulated by the BRANCH part of MODBRANCH. Canals are represented by a series of one-dimensional “branches” each of which are defined by a number of “cross-sections” or “segments” of defined length, depth, and area. Structures can be defined as pumps, culverts, or spillways. The canal network is comprised of 178 branches (a total of 1024 cross-sections) and 41 structures of various types. The network represents over 260 miles of canals.

Each branch segment is assigned to a specific MODFLOW cell corresponding approximately to that segment’s geographic location. Canal location accuracy is therefore limited to the local grid resolution. Each canal segment is assigned to the 2nd layer, which corresponds to the top of the surficial aquifer. It is important to note that the model does not model flow between the canals and the 1st layer directly. Water which moves overland (i.e., within the 1st layer) must first move into the 2nd layer and then into the canals. Conversely, water moving out of the

canals into the 1st layer must first pass through the 2nd layer. There is no direct hydraulic link between any canal segment and overland flow.

Movement from the 2nd layer into the canal segment is controlled by a “leakage coefficient,” which is an input variable via the BRANCH portion of the code. The leakage coefficient (C_L) is defined as local reach transmissivity (T_R) divided by the wetted perimeter (p).

The leakage coefficient is an important parameter in producing accurate results using MODBRANCH. As such, the method of determining its values is as follows.

$$T_R = Q / (L \times \Delta h), \text{ where}$$

Q = flow into or out of the segment of length L ,
 L = length of the canal segment,
 Δh = head difference between the aquifer and canal.

Therefore, the leakage coefficient can be written as

$$C_L = T_R / p = Q / (L \times \Delta h \times p) = q / \Delta h, \text{ where}$$

q = the Darcy velocity expressed in the Darcy Equation as:

$$q = k \Delta h / \Delta z, \text{ where}$$

k = hydraulic conductivity of canal sediment,
 Δh = head change from canal to aquifer, and
 Δz = distance of head change = thickness of canal sediments.

Expressing the Darcy equation in terms of C_L gives:

$$q = k \Delta h / \Delta z = \Delta h \times C_L.$$

Therefore, $C_L = k / \Delta z$, or the leakage coefficient is equal to the canal sediment hydraulic conductivity divided by the canal sediment thickness. The value of C_L can change significantly based on the type of sediment (sand, clay, or silt) which settles in the canal, the age of the deposition (i.e., the older the deposit, the lower k is likely to be), and the thickness of the deposit. Data collected by Genereux and Guardiaro (“A Canal Drawdown Experiment for Determination of Aquifer Parameters,” David Genereux and Jose Guardiaro, Journal of Hydrologic Engineering, October 1998) gives a value of $k / \Delta z = 35.2/\text{day} = 0.0004/\text{second}$.

The MODBRANCH model stability is extremely sensitive to the value of the leakage coefficient. In general, large BRANCH time steps require small leakage coefficients in order to maintain numerical stability. Initial simulations of the area were done using a BRANCH time step of 3 hours. However, this allowed a

maximum leakage coefficient of 0.00016/s, which is approximately 40% of the value reported above. In order to use values closer to the field value of 0.0004/s while maintaining numerical stability, the BRANCH time step had to be reduced to 1 hour. The actual values used for the leakage coefficient varied based on whether or not the value used resulted in better agreement between the model and field results. The values ranged from 0.00048/s to 0.00016/s, as shown in Table 1.

The MODFLOW time step for the initial simulations was 6 hours (a stress period of 1 day divided into 4 steps). While it is possible to run MODBRANCH with different time steps for the MODFLOW and BRANCH parts, it is more stable if the time steps are equal. The final simulations of MODBRANCH used time steps of 1 hour for both the MODFLOW and BRANCH parts. Computationally, the number of branches and segments is the largest contributor to execution times; the MODFLOW routines run significantly faster than the BRANCH routines. Decreasing the MODFLOW time steps increases run times only marginally compared to decreasing the BRANCH time step. The small increase in run time is compensated by the increase in numerical stability that results in less numerical iteration.

TABLE 1. MODBRANCH LEAKAGE COEFFICIENTS		
Canal Name	Reach Limits	Leakage Coefficient (1/seconds)
C-1		0.00048
C-100, C-100A, C-100C		0.00048
C-102	L-31N to S-165	0.00016
C-102	S-165 to Biscayne Bay	0.00048
C-102N		0.00048
C-103	L-31N to C-103S	0.00016
C-103	C-103S to L-31E	0.00048
C-103N		0.00048
C-103S		0.00048
C-109		0.00016
C-110		0.00016
C-111	S-176 to C111E	0.00016
C-111	C-111E to south of S-18C	0.00048
C-111	South of S-18C to S-197	0.00016
C-111E		0.00048
C-113		0.00048
C-1N		0.00048
C-1W	L-31N to C-1	0.00048
C-2		0.00048
C-3		0.00048
C-4		0.00048
Card Sound Road Canal		0.00048
Florida City Canal		0.00048
Goulds Canal		0.00048
L-29		0.00048
L-30		0.00048
L-31E		0.00016
L-31N	S-335 to S-331	0.00048
L-31N	S-331 to S-176	0.00016
L-31W		0.00048
L-67		0.00048
Military Canal		0.00048
Model Lands Canal		0.00048
North Canal		0.00048

2.3 MODEL BOUNDARY CONDITIONS

The model requires a number of boundary conditions for proper simulation. These include head boundaries defined along the outer “edge” of the grid, rainfall and evapotranspiration defined along the upper surface, and stage or flow boundaries defined at “canal dead ends.” The MODFLOW portion of the model requires the first three boundary conditions. The BRANCH portion of the model requires the last.

The groundwater head boundaries were generated in three ways based on location. The first method was to retrieve the daily groundwater heads from the results of the SFWMM 2x2 model at all the locations that were along the northern edge of the grid. The SFWMM 2x2 stage values were comparable to field measurements taken at observation wells. However, the SFWMM 2x2 stage values extracted for the locations along the western edge of the grid did not agree well with measured field data. Therefore, head boundaries along the western edge were created by interpolating between ground water observation well stages (NP201, NP202, NP203, and NP44). The final method was to use harmonic tide data at six locations around the perimeter of the coast. The six National Ocean Survey (NOS) locations were Miami Marina, Cutler, Turkey Point, Pumpkin Key, Garden Cove, and Flamingo. All tidal elevations were adjusted to NGVD 29. Locations between NOS stations were interpolated. The MODBRANCH stress period is 1 day, therefore, the tidal values were averaged over 1 day. This is sufficient to include seasonal effects of the tides along the coasts.

MODBRANCH does not simulate density driven transport. Specification of the head at the ocean without a correction for the higher density salt water would decrease model accuracy. In order to maximize model accuracy, the tidal boundaries were changed to represent an *effective freshwater head* based on the density of ocean water. The derivation of this is found in Appendix A. As mentioned in section 2.1 above, the vertical leakance within 2 miles of the coast was decreased in order to mimic a salinity “wedge.”

Production (withdrawal) wells were included as boundary conditions. The locations of the well fields are shown in figure 7. The South Florida Water Management District (SFWMD) provided the monthly total pumping volumes. These values were converted into daily average values for input into MODBRANCH. The average daily pumping rates are shown, by month, in figures 8A through 8E.

The rainfall inputs were obtained directly from the SFWMM 2x2 inputs. The evapotranspiration (ET) rates were obtained from SFWMM 2x2 outputs. This was done in order to have rainfall and evapotranspiration that is not uniformly distributed and more accurately represents the patterns found in nature. Since the SFWMM 2x2 resolution is 2 miles and, in general, the MODBRANCH resolution is much smaller, the values of rainfall and evapotranspiration do not

have the finest resolution possible for the MODBRANCH grid. However, the SFWMM 2x2 was the only source of these data available for the years under study.

The three years that were simulated for this study (1986, 1989, and 1995) represent an average, dry, and wet year, respectively. Figure 9 shows the daily average rainfall/acre and cumulative rainfall for each year. Figure 10 shows the monthly average evapotranspiration/acre and cumulative evapotranspiration for each year.

Evapotranspiration losses are computed only for the MODFLOW portion of the model. This requires that the **ET surface** and the **extinction depth** be defined at every finite difference cell location. When the water table is at or above the ET surface, the ET rate is at the maximum value for that location and time. When the water table is at or below the (ET surface – extinction depth), no ET occurs. The ET varies linearly between these limits. The ET extracted from the SFWMM 2x2 was defined as the maximum ET. Figure 11 illustrates the variation of ET surface and extinction depth throughout the area.

Both the rainfall and the ET can dramatically affect the ground water head fluctuations on both a day to day and long term basis. The values and approach used in this study were the best available at the time. The actual areal variation over time of both ET and rainfall is not known and the amount of error induced by this lack of information is not known. However, this lack of information is assumed to be a significant source of error.

Evaporation from the canals is not included and is assumed to be negligible compared to the ET over the entire region.

3.0 CALIBRATION and VERIFICATION

“As far as the laws of mathematics refer to reality, they are not certain; and as far as they are certain, they do not refer to reality.” *Albert Einstein*

The MODBRANCH model was *calibrated* using the 1995 simulation. *Verification* was done using 1986 and 1989. As mentioned above, 1995 is considered a “wet” year, 1986 is an “average” year, and 1989 is a “dry” year.

The calibration procedure requires many simulations of a single time period (in this study the time period was the year 1995) and many adjustments of input parameters, boundary conditions and structure operation rules in order to get the best match possible between field (measured) and model (simulated) data. Hydrogeologic parameters such as conductivity, storage, and geometry definition are not varied once the model is calibrated. Verification of the model is not as rigorous and requires only minimum adjustments to structure operating rules and boundary conditions. Verification was performed using the years of 1986 and 1989.

3.1 Ground Water Stages

The locations of the ground water gages used in the calibration and verification process are shown in figures 12a and 12b. Ground water stages from both field measurements and model results are shown in figures 14 – 75. Note that 1995 (calibration year) had the most available data (62 stations), followed by 1989 (46 stations), and 1986 (38 stations). Table 2A gives a statistical description of the model performance for each available data set. The statistical description consists of correlation coefficient (r), average absolute error (ϵ), and average difference (Δ).

The correlation coefficient indicates if the model is accurately tracking the increases and decreases in ground water head. Correlation coefficient ranges between -1 and +1. A value of $r = +1$ indicates complete positive correlation; a plot of model results versus field data with complete positive correlation would lie on a straight line with a positive slope. A value of -1 indicates complete negative correlation. In this case, the plot of model results versus field data would fall on a straight line with a negative slope. Values of r near 0 indicate that the model results and field data are uncorrelated.

The correlation coefficient, r , is computed using the following equation:

$$r = \frac{\sum (X_i - \underline{X})(Y_i - \underline{Y})}{\{\text{sqrt}[\sum (X_i - \underline{X})^2] \text{sqrt}[\sum (Y_i - \underline{Y})^2]\}}, \text{ where}$$

X_i = model stage at time t ,
 \underline{X} = average model stage,
 Y_i = field stage at time t , and
 \underline{Y} = average field stage.

The correlation coefficient is excellent for determining if a model is mimicking variations due to changes in boundary conditions and other inputs in the same manner as the real world

A model may have complete positive correlation and still over or under predict the actual values. In order to further determine the “goodness of fit” between the model results and the field data, the average absolute error (ϵ) and the average difference (Δ) are used. The average absolute error is defined as

$$\epsilon = \frac{\sum | \text{model} - \text{field} |}{N}, \text{ where}$$

N = number of model and field pairs,
model = model stage at time t , and
field = field stage at time t .

Similarly, the average difference is defined as

$$\Delta = \frac{\sum (\text{model} - \text{field})}{N}.$$

A model which is a *perfect* simulator of field data will have $r = +1$, $\epsilon = 0$, and $\Delta = 0$. When $\epsilon > 0$ and $\Delta > 0$, then the model is over predicting stages. When $\epsilon > 0$ and $\Delta < 0$, then the model is under predicting stages. When $\epsilon > 0$ and $\Delta \sim 0$, then the model is “oscillating” about the field data. Since no model will perfectly fit any field data, the goal is to have as many locations with $r \sim +1$, $\epsilon \sim 0$, and $\Delta \sim 0$. The 1995 statistical measures are presented (figures 13a, b, and c) as contours in an effort to determine on an areal basis how well the model is performing. The correlation coefficient contours indicate that the model responds in a nearly identical manner to the field data (average $r = 0.89$, Table 2B).

The values of correlation coefficient (r) were contoured (figure 13a) in an attempt to determine on an areal basis the regions that have low values. There are basically two locations that have low correlation coefficients (i.e., $r < 0.8$). The first is along the upper part of L-31N (G-1487, G-3559, and Krome); the second is near the lower end of C-103 (G-1183). There are a number of possibilities for this discrepancy. Along the upper L-31N there are open pit mines which are not included in the model. Daily water level fluctuations in these mines may adversely affect the field data. The West 1 and West 2 well fields are also located nearby, which could be a source of error. It should be noted that other observation wells in the area have very good correlation coefficients.

The absolute average error (figure 13b) and the average error (figure 13c) indicate that the most significant differences are located along L-31N, near other production wells, and the lower end of C-111. The overall average value of average *absolute* error for 1995 is 0.40 feet and the overall average error for 1995 is -0.02 feet. The extremely high average value of r and the extremely small average value of Δ indicate that the model is calibrated. The differences reflected in ϵ between model and field measurements are primarily a product of inexact and unknown boundary conditions and geohydrologic variables.

The results of 1986 and 1989 simulations are also included in tables 2A and 2B. The average values for r (0.75, 0.82), ϵ (0.32, 0.44), and Δ (0.18, 0.28) are not as good as for the 1995 simulation. This is expected as these verification simulations did not require the same degree of effort that was applied to the calibration simulation.

**TABLE 2A. GROUND WATER OBSERVATION WELLS
MODBRANCH VERSUS FIELD DATA**

1986, 1989, 1995

STATION LOCATION	1986			1989			1995		
	r	AVERAGE ABSOLUTE ERROR	AVERAGE ERROR	r	AVERAGE ABSOLUTE ERROR	AVERAGE ERROR	r	AVERAGE ABSOLUTE ERROR	AVERAGE ERROR
Angels Well	0.85	0.25	0.06	0.79	0.68	0.62	0.86	0.34	-0.23
CV5N				0.60	0.41	0.34	0.88	0.53	-0.46
CV5S				0.50	0.27	-0.01	0.92	0.87	-0.84
DO1				0.99	0.84	0.28	0.95	0.45	0.44
E112							0.85	0.66	0.60
E146							0.97	0.14	0.09
EP1R				0.86	0.24	0.15	0.90	0.63	-0.63
EVER1	0.69	0.17	0.17	0.73	0.20	0.28	0.97	0.10	0.03
EVER3	0.28	0.25	0.10	0.79	0.32	0.29	0.91	0.17	0.00
EVER4	0.88	0.31	0.31	0.85	0.57	0.57	0.94	0.12	0.16
EVER8							0.97	0.37	-0.39
F358							0.91	0.62	0.60
Frog Pond	0.46	0.39	0.05	0.89	0.24	-0.10	0.94	0.37	0.36
G1183	0.82	0.23	0.12	0.82	0.43	-0.12	0.72	0.65	0.51
G1251				0.78	0.30	0.26	0.90	0.31	-0.29
G1362	0.72	0.36	0.32	0.61	0.51	0.40	0.91	0.32	-0.07
G1363	0.93	0.39	0.37	0.85	0.51	0.37	0.94	0.34	0.33
G1486	0.95	0.36	0.36	0.89	0.40	0.01	0.87	0.42	0.37
G1487	0.03	0.77	0.67	0.69	0.39	-0.36	0.51	0.72	-0.66
G1502	0.88	0.37	-0.32	0.84	0.73	0.63	0.85	0.17	-0.05
G3273	0.88	0.29	-0.22	0.82	0.78	0.70	0.86	0.21	0.09
G3353	0.56	0.24	-0.13	0.63	0.36	0.33	0.92	0.43	-0.42
G3354	0.69	0.25	-0.12	0.80	0.20	0.07	0.96	0.50	-0.49
G3355	0.83	0.18	-0.04	0.79	0.25	-0.10	0.87	0.51	-0.51
G3356	0.81	0.25	-0.20	0.80	0.31	-0.27	0.86	0.33	-0.33
G3437	0.71	0.31	0.12	0.86	0.57	0.55	0.90	0.24	-0.13
G3439				0.83	0.37	-0.03	0.91	0.39	-0.19
G3473							0.91	0.45	0.12
G3552							0.87	0.66	-0.58
G3555							0.87	0.45	-0.08
G3556							0.91	1.21	-1.19

**TABLE 2A. GROUND WATER OBSERVATION WELLS
MODBRANCH VERSUS FIELD DATA**

1986, 1989, 1995

STATION LOCATION	1986			1989			1995		
	r	AVERAGE ABSOLUTE ERROR	AVERAGE ERROR	r	AVERAGE ABSOLUTE ERROR	AVERAGE ERROR	r	AVERAGE ABSOLUTE ERROR	AVERAGE ERROR
G3558							0.86	0.40	-0.08
G3559							0.61	0.52	-0.31
G596	-0.03	0.69	0.67	0.74	0.38	0.21	0.84	0.39	-0.29
G613	0.81	0.41	0.41	0.80	0.45	0.44	0.88	0.28	0.29
G614	0.95	0.61	0.61	0.86	0.67	0.67	0.93	0.32	0.56
G618	0.97	0.14	0.14	0.99	0.22	0.22	0.96	0.19	0.17
G789	0.59	0.37	0.21	0.87	0.31	0.28	0.89	0.62	0.55
G855	0.57	0.47	0.44	0.62	0.40	0.11	0.88	0.41	-0.17
Humble	0.89	0.27	0.22	0.81	0.61	0.61	0.92	0.46	0.45
Krome	0.19	0.34	0.20	0.53	0.37	-0.18	0.77	0.74	-0.68
L31W				0.91	0.20	0.04	0.88	0.52	0.52
L67X-E	0.87	0.11	-0.03	0.86	0.32	0.30	0.85	0.25	0.00
L67X-W	0.92	0.21	0.18	0.93	0.38	0.50	0.99	0.23	0.27
NE1	0.81	0.14	0.00	0.84	0.40	0.39	0.83	0.28	0.15
NE2							0.82	0.27	-0.08
NE5							0.90	0.29	0.27
NP202	0.94	0.17	0.19	0.90	0.33	0.32	0.99	0.20	0.17
NP206	0.95	0.35	0.32	0.92	0.83	0.83	0.91	0.18	0.14
NP72	0.93	0.38	0.34	0.97	0.48	0.48	0.97	0.19	0.00
NTS1				0.92	0.22	0.01	0.92	0.21	-0.01
NTS10							0.94	0.21	0.04
NTS14							0.95	0.19	-0.52
R127	0.95	0.16	0.11	0.87	0.47	0.47	0.94	0.23	-0.19
R158	0.94	0.27	0.25	0.88	0.63	0.63	0.96	0.25	-0.03
R3110	0.89	0.30	0.07	0.97	0.41	0.42	0.89	0.34	0.09
Robblee							0.95	0.48	0.43
Rutzke	0.87	0.27	0.15	0.88	0.59	0.59	0.94	0.47	0.47
S182A	0.74	0.53	0.47	0.77	0.54	0.08	0.87	0.66	0.53
S196A	0.94	0.32	0.31	0.88	0.41	0.11	0.92	0.46	0.44
TS Bridge	0.87	0.30	0.09	0.94	0.54	0.42	0.92	0.57	-0.45
TS Hilton							0.93	0.18	-0.15

**TABLE 2B. SUMMARY OF STATISTICAL PERFORMANCE MEASURES
GROUND WATER OBSERVATION WELLS
MODBRANCH VERSUS FIELD DATA**

1986, 1989, 1995

	1986			1989			1995		
	R	AVERAGE ABSOLUTE ERROR	AVERAGE ERROR	R	AVERAGE ABSOLUTE ERROR	AVERAGE ERROR	R	AVERAGE ABSOLUTE ERROR	AVERAGE ERROR
Minimum	-0.03	0.00	-0.32	0.50	0.00	-0.36	0.51	0.00	-1.19
Maximum	0.97	0.67	0.67	0.99	0.83	0.83	0.99	0.60	0.60
Average	0.75	0.32	0.18	0.82	0.44	0.28	0.89	0.40	-0.02
Median	0.86	0.30	0.17	0.85	0.40	0.30	0.91	0.37	0.00
Standard Deviation	0.26	0.15	0.23	0.11	0.17	0.28	0.08	0.21	0.40
Absolute Deviation	0.19	0.10	0.18	0.09	0.14	0.23	0.05	0.16	0.32
Number of Stations Analyzed	38			46			62		

3.2 Canal Flows and Stages

The canal stages and flows predicted by MODBRANCH are shown with the corresponding field data in figures 76 – 125. Individual structure stage statistics are listed in Tables 3A, 3B, and 3C for the years 1986, 1989, and 1995, respectively. Individual structure flow statistics are listed in Tables 4A, 4B, and 4C for the same years. The values shown in tables 3A – 4C are the correlation coefficient (r), the average absolute error and its standard deviation, and the average error and its standard deviation. The stage statistics are summarized in Table 5. Flow statistics are summarized in Table 6.

The canal results are not as accurate as the ground water stages. There are four primary reasons for this. The first is that the actual operation of the structures is not known completely and the rules may be ambiguous. The second is that the performance of the structures in the real world is not the same as the performance in the “model” world. The third is that the field measurements of flow rates are not as accurate as ground water stage measurements. The fourth is that the model structure operations frequently result in rapid increases and decreases of stages that are not found in the real world.

An example of the first case is the way in which G-211 is operated. The USACE SAJ web page (<http://hw2.saj.usace.army.mil/strdsc/g211.html>) describes this structure as *“a manually operated structure with long response times and time-consuming operations. As a result, frequent gate operations at this structure are impracticable and stages outside this range may occur for several days.”*

The model does not make a distinction between manually or automatically operated structures. The model operates such that whenever the structure “trigger” criteria are met, the structure will either open or close (Note: For the purpose of clarity, “open” refers to both opening a gate and turning on a pump. Similarly, “close” refers to closing a gate and turning off a pump). There will be no delay which would occur in the real world due to shift changes, travel time, etc. Table 7 lists the structures that are included in the MODBRANCH model. Of the 38 structures, 20 are automatically operated (53%) and 15 are manually operated (39%). Two of the structures are remotely operated which indicates that the actual operation may fall between automatically and manually operated. The high number of manually operated structures is likely to be a significant source of discrepancy between model and field data.

Flows through the structures are computed using mathematical equations and turned on or off according to Boolean operations. This can induce errors if the structure parameters (culvert coefficient, weir coefficient, sill width, shape, etc.) are not accurately defined or known. The operation of the structures within the MODBRANCH model is both a numerical and incremental process. The “numerically” computed flow through a structure depends on the structure type, stage differentials, and structure “coefficients” as described above.

The process is “incremental” in that, once the specific criteria are met to open or close a structure, the structure opens in a certain number of time steps. The gradual opening or closing of structures maintains numerical stability. Many of the structures are opened or closed in incremental time steps (minimum duration of 1 hour), whereas, in the real world these structure operations occur in a fraction of the model time steps. Additionally, the opening (or closing) of a structure may change the trigger status such that in the next time step the structure will be closed (or opened). This frequently results in rapid oscillations of “flow/no-flow” through the structure. Rapidly opening and closing the structures does not occur in the real world, but it does in the model world. This is especially true of manually operated structures.

Flow rates measured through structures are frequently in error. Measured flow rates are normally a function of head differential (i.e., headwater versus tail water) and a structure rating curve. Therefore, the accuracy of the flow rates measured in the field depends primarily on the accuracy of the rating curves.

The simulation with the best canal stage results is for the dry year 1989. The average correlation coefficients of both the flow and stage values are higher (0.66, 0.81, respectively) than for either 1986 or 1995. The average of the average error is also lower for 1989 than for 1986 or 1995. The primary reason for this is that there were a number of structures that, according to field data, were closed for significant periods of time. These structures include S-173, S-174, S-176, S-196, S-331, S-332, S-335, S-334, S-336, and S-338. These structures significantly affect the water levels in the main canals. By limiting the flow through the principle structures, the simulations become primarily a ground water modeling exercise with canal stages determined by the amount of leakage into and out of the canal segments.

The 1995 simulation shows the second best results for canal stages and flows. This is primarily due to the fact that 1995 is the calibration year and more effort was expended in fine tuning the model inputs and canal structure operations. Each of the simulations shows the effects of the open/close cycling of structures, as evidenced by the large standard deviations of both flow and stage found for each of the performance measurements.

TABLE 3A. 1986 CANAL STAGE STATISTICS					
Location	r	Abs Error	σ of Abs Error	Ave Error	σ of Ave Error
S-331HW	0.28	1.09	0.52	1.08	0.55
S-331TW	0.62	0.51	0.34	-0.48	0.37
S-176HW	0.35	0.42	0.27	-0.33	0.37
S-176TW	0.09	0.42	0.34	-0.08	0.54
S-332HW	0.6	0.34	0.25	0.08	0.41
S-174HW	0.41	0.42	0.27	-0.35	0.36
S-194HW	0.43	0.33	0.22	-0.23	0.32
S-194TW	0.36	0.31	0.22	-0.21	0.32
S-196HW	0.65	0.26	0.16	0.05	0.31
S-196TW	0.78	0.24	0.18	0.13	0.27
S-338TW	0.13	1.19	0.64	1.17	0.67
S-165HW					
S-148HW	0.17	0.37	0.26	0.12	0.43
S-334HW	0.67	0.39	0.25	-0.36	0.28
S-335TW					
G211HW					
G211TW					
S-22HW					
S-25HW					
S-121HW	0.13	4.25	0.41	-4.25	0.41
S-121TW					
S-25bHW	-0.04	0.56	1.12	-0.29	1.22
S-336HW	0.17	0.92	0.5	0.85	0.61
S-336TW	0.3	0.35	0.28	-0.24	0.38
S-18cHW	-0.08	0.22	0.19	0.15	0.25
S-18cTW	-0.37	0.48	0.38	0.42	0.45
S-178HW	0.82	0.3	0.18	0.27	0.22
S-178TW	0.24	0.22	0.19	0.17	0.24
S-332TW					
S118HW	0.83	0.37	0.23	-0.36	0.25
S175HW	0.56	0.36	0.28	0.15	0.43
S197HW	-0.61	0.57	0.35	0.44	0.5
S21HW	-0.2	0.47	0.26	-0.43	0.32
S123HW	0.58	1.09	0.32	-1.09	0.32
S149HW	0.71	0.96	0.45	0.94	0.47
S195HW	0.72	0.75	0.32	0.75	0.32
S20fHW	0.26	0.3	0.32	-0.22	0.38
S21aHW	0.3	0.33	0.29	-0.27	0.35

TABLE 3B. 1989 CANAL STAGE STATISTICS					
Location	r	Abs Error	σ of Abs Error	Ave Error	σ of Ave Error
S-331HW	0.57	0.35	0.23	0.04	0.42
S-331TW	0.76	0.33	0.25	0.28	0.31
S-176HW	0.75	0.33	0.26	0.27	0.32
S-176TW	0.75	0.5	0.33	-0.44	0.4
S-332HW	0.91	0.2	0.17	-0.01	0.26
S-174HW	0.75	0.36	0.28	0.32	0.32
S-194HW	0.73	0.42	0.31	0.41	0.33
S-194TW	0.7	0.34	0.3	0.31	0.34
S-196HW	0.75	0.58	0.33	0.57	0.35
S-196TW	0.65	0.56	0.49	-0.35	0.65
S-338TW	0	0.64	0.41	0.26	0.71
S-165HW					
S-148HW	0.47	0.44	0.33	0.19	0.52
S-334HW	1	0.17	0.05	-0.17	0.07
S-335TW					
G211HW					
G211TW					
S-22HW					
S-25HW					
S-121HW	0.88	0.44	0.33	-0.38	0.41
S-121TW					
S-25bHW	0.61	0.54	0.37	-0.31	0.58
S-336HW	0.56	0.34	0.32	-0.13	0.45
S-336TW	0.35	0.8	0.57	-0.77	0.62
S-18cHW	0.67	0.4	0.26	0.37	0.3
S-18cTW	0.52	0.69	0.29	0.67	0.33
S-178HW	0.87	0.28	0.21	0.23	0.26
S-178TW	0.68	0.41	0.24	0.34	0.34
S-332TW					
S118HW	0.84	0.57	0.39	-0.26	0.64
S175HW	0.91	0.2	0.18	0.05	0.26
S197HW	0.43	0.67	0.29	0.64	0.34
S21HW	0.16	0.59	0.26	-0.58	0.29
S123HW	0.65	0.76	0.34	-0.76	0.34
S149HW	0.76	0.69	0.61	0.39	0.84
S195HW	0.79	0.78	0.28	0.78	0.28
S20fHW	0.68	0.3	0.12	-0.27	0.18
S21aHW	0.58	0.42	0.18	-0.41	0.21

TABLE 3C. 1995 CANAL STAGE STATISTICS					
Location	r	Abs Error	σ of Abs Error	Ave Error	σ of Ave Error
S-331HW	0.76	0.43	0.42	0.15	0.58
S-331TW	0.64	0.19	0.23	-0.09	0.29
S-176HW	0.46	0.22	0.19	0.11	0.26
S-176TW	0.84	0.3	0.24	0.21	0.32
S-332HW	0.85	0.37	0.32	0.3	0.38
S-174HW	0.48	0.23	0.19	0.13	0.26
S-194HW	0.63	0.36	0.26	0.21	0.39
S-194TW	0.37	0.82	0.51	-0.71	0.65
S-196HW	0.62	0.29	0.17	0.23	0.24
S-196TW					
S-338TW	0.56	0.82	0.46	-0.81	0.47
S-165HW	0.66	0.48	0.39	0.32	0.53
S-148HW	0.01	1.34	0.97	1.1	1.24
S-334HW	0.94	0.17	0.07	-0.17	0.07
S-335TW	0.75	0.6	0.43	-0.56	0.49
G211HW	0.74	0.55	0.43	-0.48	0.51
G211TW	0.73	0.43	0.44	0.09	0.61
S-22HW	-0.6	0.87	0.49	0.15	0.99
S-25HW					
S-121HW	0.48	0.59	0.44	-0.5	0.55
S-121TW	0.55	1.01	0.66	-0.97	0.72
S-25bHW	-0.51	0.96	0.65	0.72	0.91
S-336HW	0.79	0.53	0.41	-0.48	0.47
S-336TW	0.81	1.41	0.66	-1.39	0.7
S-18cHW	0.79	0.13	0.1	0.01	0.16
S-18cTW	0.86	0.41	0.25	-0.33	0.35
S-178HW	0.75	0.19	0.18	-0.07	0.26
S-178TW	0.83	0.13	0.1	-0.01	0.16
S-332TW					
S118HW	0.8	0.58	0.42	-0.49	0.53
S175HW	0.85	0.43	0.34	0.39	0.38
S197HW	0.81	0.44	0.28	-0.36	0.37
S21HW	0.04	0.33	0.23	-0.04	0.4
S123HW	-0.23	0.91	0.45	-0.69	0.74
S149HW	0.03	1.41	1.26	1.4	1.27
S195HW	0.74	0.81	0.35	0.81	0.35
S20fHW	0.37	0.22	0.19	-0.01	0.29
S21aHW	0.33	0.24	0.2	0.01	0.31

TABLE 4A. CANAL FLOW STATISTICS, 1986					
Location	r	Abs Error	σ of Abs Error	Ave Error	σ of Ave Error
S-25b_Q	0.57	129.56	124.88	-73.74	164.24
S-336_Q	0.07	71.6	72.27	71.34	72.53
S-332_Q	-0.01	3.2	29.59	0.48	29.76
S-338_Q	0.07	130.69	68.71	128.34	73
S-174_Q		72.38	105.63	-71.04	106.54
S-196_Q	0.12	90.78	57.86	46.04	97.4
S-334_Q	0.1	707.3	591.95	705.45	594.16
S-176_Q	0.23	444.82	270.53	321.36	409.93
S-335_Q	0.87	20.44	59.6	-5	62.82
S-331_Q		333.92	374.03	-333.92	374.03
S-173_Q	0.93	14.88	26.5	-1.21	30.38

TABLE 4B. CANAL FLOW STATISTICS, 1989					
Location	r	Abs Error	σ of Abs Error	Ave Error	σ of Ave Error
S-25b_Q	0.64	79.25	131.03	53.94	143.35
S-336_Q	0.98	6.06	12.28	-5.41	12.58
S-332_Q	0.97	11.89	10.2	-10.92	11.23
S-338_Q	0.91	6.22	21.43	-5.04	21.74
S-174_Q	0.56	29.95	37.37	-18.36	44.25
S-196_Q	0.63	38.17	27.11	28.46	37.2
S-176_Q	0.92	22.52	69.81	-12.74	72.24
S-335_Q	0.9	48.32	152.91	-41.94	154.79
S-331_Q	0.86	28.37	60.55	-21.78	63.22
S-173_Q	0.73	32.3	45.33	-31.16	46.13

TABLE 4C. CANAL FLOW STATISTICS, 1995					
Location	r	Abs Error	σ of Abs Error	Ave Error	σ of Ave Error
G211_Q	0.24	295.11	250.8	135.52	363.07
S-121_Q		21.24	101.77	21.06	101.81
S-25b_Q	0.16	219.84	162.55	-180.24	205.7
S-148_Q	0.62	103	154.96	-57.46	177.03
S-194_Q	0.51	82.55	61.55	75.07	70.49
S-332_Q	0.52	140.4	108.11	67.31	164.05
S-338_Q	0.5	72.15	53.89	-53.46	72.52
S-165_Q	0.62	84.07	71.57	56.76	94.76
S-174_Q	0.63	72.06	88.43	29.84	110.16
S-196_Q	-0.02	116.67	41.6	116.31	42.59
S-176_Q	0.51	146.21	205.78	-62.21	244.75
S-335_Q		25.39	95.62	-25.39	95.62
S-331_Q	0.77	102.45	105.79	1.56	147.35
S-173_Q	0.66	27.35	32.71	-7.83	41.93

TABLE 5. SUMMARY OF CANAL STAGE STATISTICS, 1986, 1989, AND 1995

	1986			1989			1995		
	r	Average Absolute Error, feet	Average Error, feet	r	Average Absolute Error, feet	Average Error, feet	r	Average Absolute Error, feet	Average Error, feet
Minimum	-0.61	0.22	-4.25	0.0	0.17	-0.77	-0.6	0.13	-1.39
Maximum	0.83	4.25	1.17	1.0	0.8	0.78	0.94	1.41	1.4
Average	0.33	0.63	-0.08	0.66	0.47	0.04	0.53	0.55	-0.05
Median	0.32	0.4	-0.02	0.69	0.43	0.12	0.66	0.43	-0.01
Standard Deviation	0.35	0.74	0.94	0.22	0.18	0.42	0.39	0.36	0.57
Absolute Deviation	0.28	0.39	0.53	0.16	0.15	0.36	0.29	0.29	0.42
Number of Stations	30			30			35		

TABLE 6. SUMMARY OF CANAL FLOW STATISTICS, 1986, 1989, AND 1995

	1986			1989			1995		
	r	Average Absolute Error cfs	Average Error cfs	r	Average Absolute Error cfs	Average Error cfs	r	Average Absolute Error cfs	Average Error cfs
Minimum	-0.01	3.2	-333.92	0.56	6.06	-41.94	-0.02	21.24	-180.24
Maximum	0.93	707.3	705.45	0.98	79.25	53.94	0.77	295.11	135.52
Average	0.33	183.6	71.65	0.81	30.3	-6.49	0.48	107.75	8.35
Median	0.12	90.78	0.48	0.88	29.16	-11.83	0.51	93.26	11.31
Standard Deviation	0.36	221.81	262.71	0.16	22	28.23	0.23	75.86	82.68
Absolute Deviation	0.31	170.05	170.95	0.14	15.36	19.59	0.18	54.21	63.35
Number of Stations	11			10			14		

TABLE 7. STRUCTURES INCLUDED IN MODBRANCH MODEL OF SOUTH DADE COUNTY		
Structure	Operation Mode	Type
G-093	manual	Gated Spillway
G-114	none	uncontrolled sheet pile weir
G-119	manual	Gated Pipe Culvert
G-211	manual	Gated Pipe Culvert
S-118	automatic	Gated Spillway
S-119	automatic	Gated Spillway
S-121	manual	Gated Box Culvert
S-123	automatic	Gated Spillway
S-148	automatic	Gated Spillway
S-149	automatic	Gated Pipe Culvert
S-165	automatic	Gated Spillway
S-166	automatic	Gated Spillway
S-167	automatic	Gated Spillway
S-173	manual	Gated Pipe Culvert
S-174	automatic/manual	Gated Spillway
S-175	manual	Gated Pipe Culvert
S-176	automatic	Gated Spillway
S-177	automatic	Gated Spillway
S-178	manual	Gated Box Culvert
S-179	automatic	Gated Spillway
S-18C	automatic	Gated Spillway
S-194	manual	Gated Pipe Culvert
S-195	manual	Gated Arch Culvert
S-196	manual	Gated Pipe Culvert
S-197	manual	Gated Pipe Culvert
S-20	automatic	Gated Spillway
S-20F	automatic	Gated Spillway
S-20G	automatic	Gated Spillway
S-21	automatic	Gated Spillway
S-21A	automatic	Gated Spillway
S-22	automatic	Gated Spillway
S-25B	automatic	Gated Spillway
S-331	manual	Pump
S-332	remote	Pump
S-334	manual	Gated Spillway
S-335	manual	Gated Spillway
S-338	remote	Gated Pipe Culvert
S-346	manual	Pipe Culvert

4.0 Sources of Error

There are seven primary sources of error resulting from inputs to the MODBRANCH model. These are (not necessarily in order of importance):

- 1- Rainfall boundary conditions,
- 2- Evapotranspiration boundary conditions and parameters,
- 3- General head boundary conditions,
- 4- Geologic parameters,
- 5- Canal leakance and hydraulic parameters,
- 6- Structure operations and implementation, and
- 7- Topography.

Although these have all been discussed to a limited degree above, it is worth going into more detail.

Rainfall boundary conditions

The rainfall is an important parameter, especially in the region of south Florida. The amount and timing of rainfall greatly affects the increase or decrease in stage (ground water and canal) and flows within the system. The rainfall boundary conditions used for this study were the same that is used as inputs for the SFWMM 2x2, as mentioned above. The spacial resolution is 2 miles x 2 miles and the temporal resolution is 1 day. The MODBRANCH model would give much better results if finer resolution rainfall information were available. This is especially important for simulating ground water stages. Unfortunately, these data are not presently available. Future studies could include rainfall derived from NEXRAD or other methods, which would give rainfall at fine resolutions in both temporal and spacial terms.

Evapotranspiration boundary conditions

The evapotranspiration boundary conditions used were produced by the SFWMM 2x2. However, the monthly total evapotranspiration output by SFWMM 2x2 was used, as opposed to the rainfall, which was daily. Again, there was no better source for these data. The only way to get better evapotranspiration is to establish more data collections sites throughout the area. The total yearly evapotranspiration can equal or exceed the total rainfall for average and dry years (see figures 9 and 10), which means that evapotranspiration is an equally important boundary condition.

General head boundary conditions

The general head boundaries, as mentioned above, were generated as a hybrid of SFWMM 2x2 output, ground water observation well data, and harmonic tide data. Future model accuracy could be improved by using more observation wells

and eliminating the inherent error found in using model output and harmonic tide data as boundary conditions.

Geologic parameters

South Florida's geology is extremely heterogeneous. Measurements and tests performed at one location can give distinctly different values when done 500 feet away. It is important to keep this in mind when considering the model results. The model considers the hydrogeologic parameters input to be homogenous within each grid cell. While hydraulic conductivity and transmissivity vary from cell to cell, each is isotropic within the cell. Additionally, the parameters do not vary significantly between adjacent cells, increasing the degree of homogeneity of the model. The real world is not homogenous. There are indications that there are preferential flow paths within the surficial aquifer. These preferential flow paths are not represented by the model inputs. For this reason, the model results should be considered primarily on an areal basis, secondarily on a site-specific basis.

Canal leakance and hydraulic parameters

The canal leakance has been discussed at length above. Other hydraulic parameters, which affect canal stage and flow, include Manning's n (roughness) and momentum coefficient. Nominal values of each were used throughout the study.

Structure operations and implementation

The affect of how the structures are operated and how they are numerically implemented is discussed above. Future refinement of structure operation routines, especially in opening and closing could result in better replication of field stages and flows.

Topography

The topography (as stated above) is a composite derived from Everglades National Park, Corps of Engineers, and USGS data sources. The accuracy of these data (on the order of 0.5 feet) can significantly affect both the results of the MODBRANCH model and the interpretation of the results. The model results can be affected by slight variations in elevations, since this would change the local land slope. A small change in topography could cause a significant change in flow direction due to the small water gradients found in the area. Comparison between model stages and observation well stages could have consistent errors based on the error in the observation well reference point. The average errors (see Table 2B) found between model and field data are less than the accuracy of the topography.

5.0 Conclusions

The MODBRANCH model of South Dade County has been tested using dry (1989), average (1986), and dry (1995) years. The results indicate that the model is adequate for testing scenarios in the region of the L-31N and C-111 canals and the eastern Everglades. The accuracy of the model, as is the case for any model, depends primarily on the accuracy of the inputs. Rainfall and evapotranspiration are especially important boundary conditions.

The results of the model, at the level of accuracy produced, can be used with confidence in determining the relative differences between different alterations and tests. However, the users of the model must not depend on the model to produce absolute values. Model results are an indication of what may happen under certain conditions.

“Do not quench your inspiration and your imagination; do not become the slave of your model.”
Vincent van Gogh

References

Swain, E.D., and Wexler, E.J., 1993, "A Coupled Surface-Water and Ground-Water Flow Model for Simulation of Stream-Aquifer Interaction," USGS Open File Report 92-138.

Swain, E.D., Howie, B., and Dixon, J., 1995, "Description and Field Analysis of a Coupled Ground-Water/Surface-Water Flow Model (MODFLOW/BRANCH) with Modifications for Structures and Wetlands in Southern Dade County, Florida," USGS Water-Resources Investigations Report 96-4118.

McDonald, M.G., and Harbaugh, A.W., 1988, "A Modular Three-Dimensional Finite-Difference Ground-Water Flow Model," U.S. Geological Survey Techniques of Water-Resources Investigations, book 6, chap. A1.

Klein, H., and Hull, J.E., 1978, "Biscayne Aquifer, Southeast Florida," USGS Water-Resources Investigations 78-107.

Fish, J.E., and Stewart, M., 1991, "Hydrogeology of the Surficial Aquifer System, Dade County, Florida," USGS Water-Resources Investigations Report 90-4108.

Causaras, C.R., 1986, "Geology of the Surficial Aquifer System, Dade County, Florida, Lithologic Logs," USGS Water-Resources Investigations Report 86-4126.

Randazzo, A.F., and Jones, D.S., 1997, "The Geology of Florida," University Press of Florida.

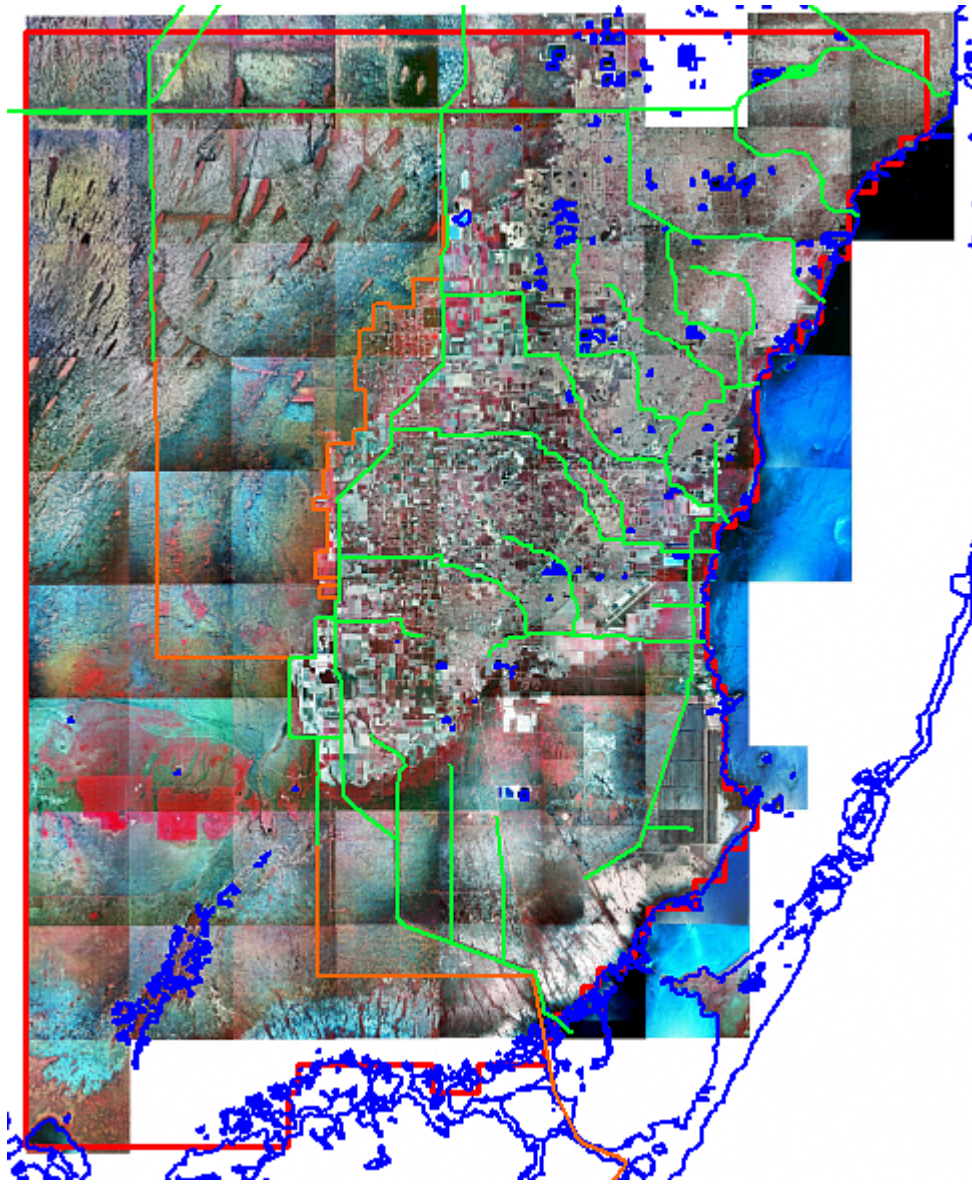


Figure1. Model boundaries (red), major canals (green), ENP boundary (orange), and land variations.

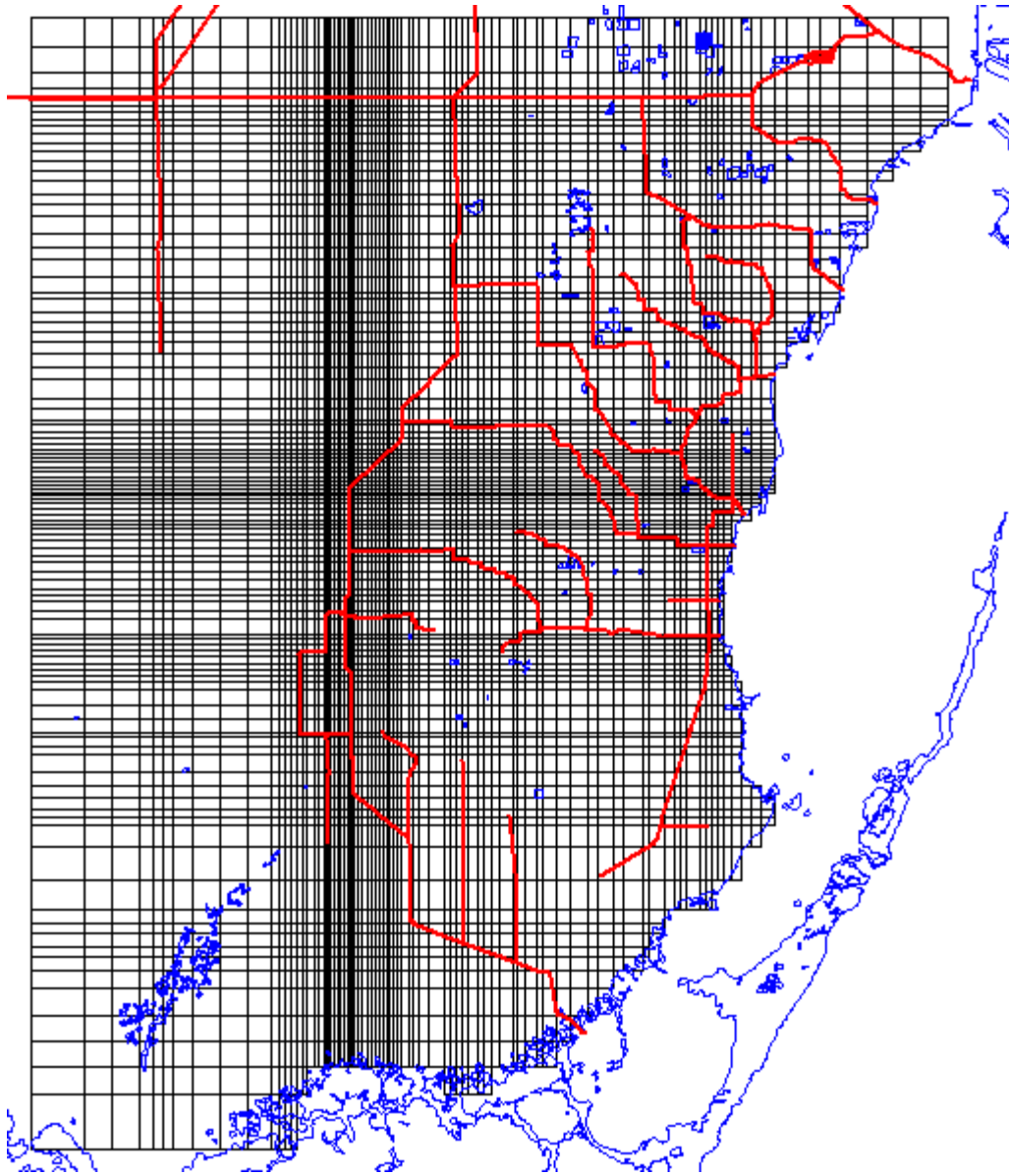


Figure 2. Model Grid: 103 rows and 90 columns

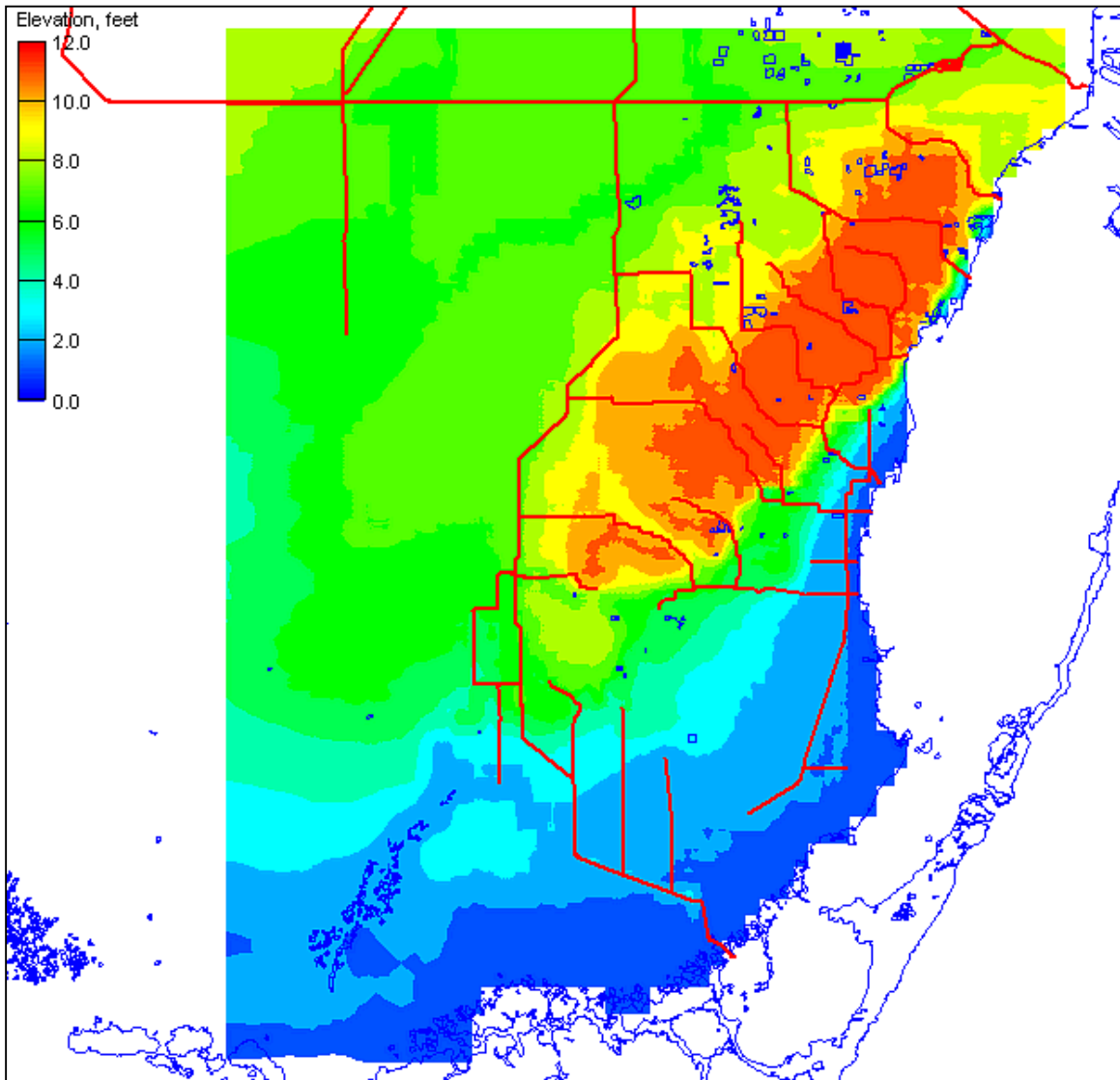


Figure 3a. Bottom elevation of layer 1 (ground elevation).

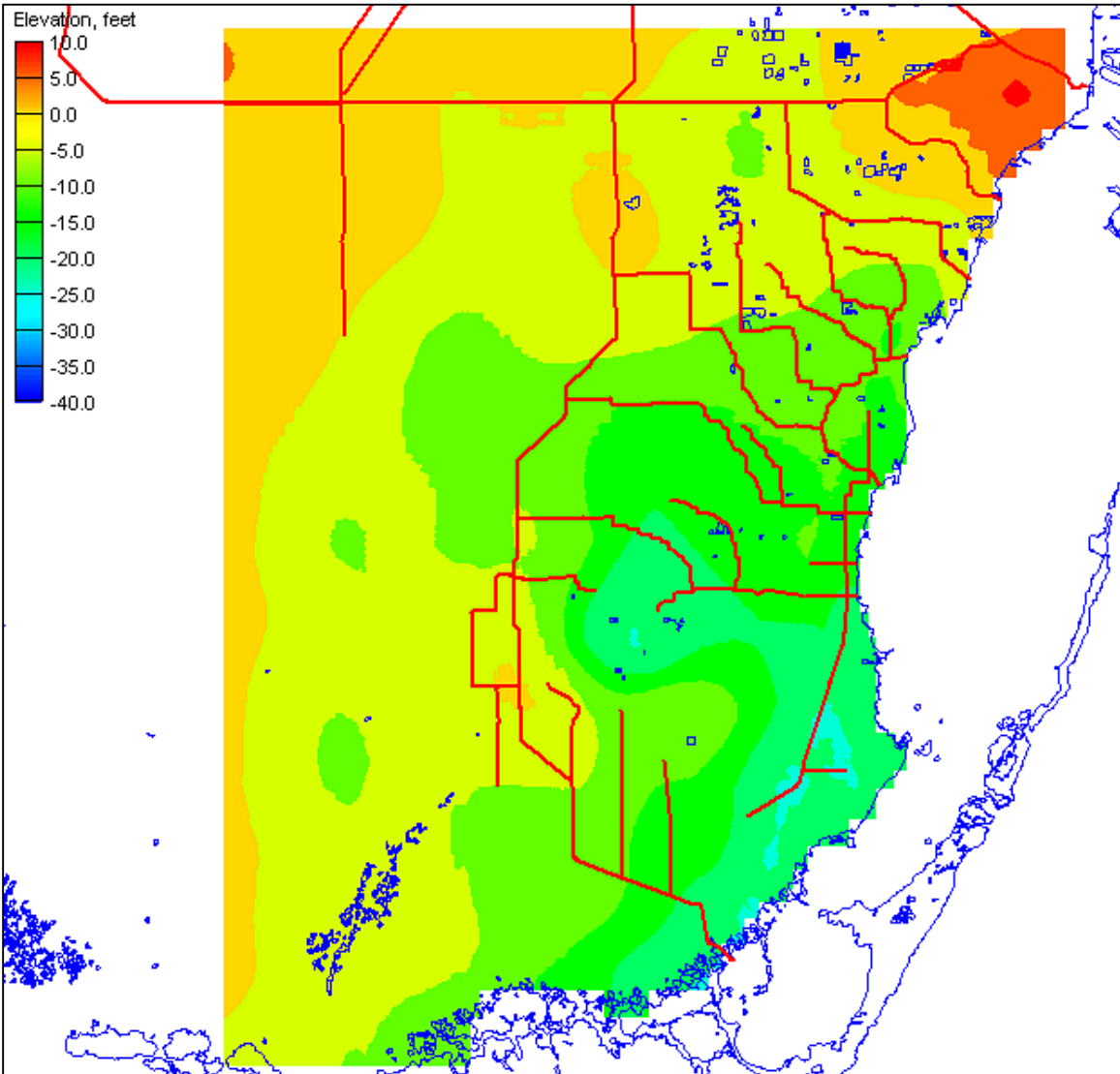


Figure 3b. Bottom elevation of layer 2.

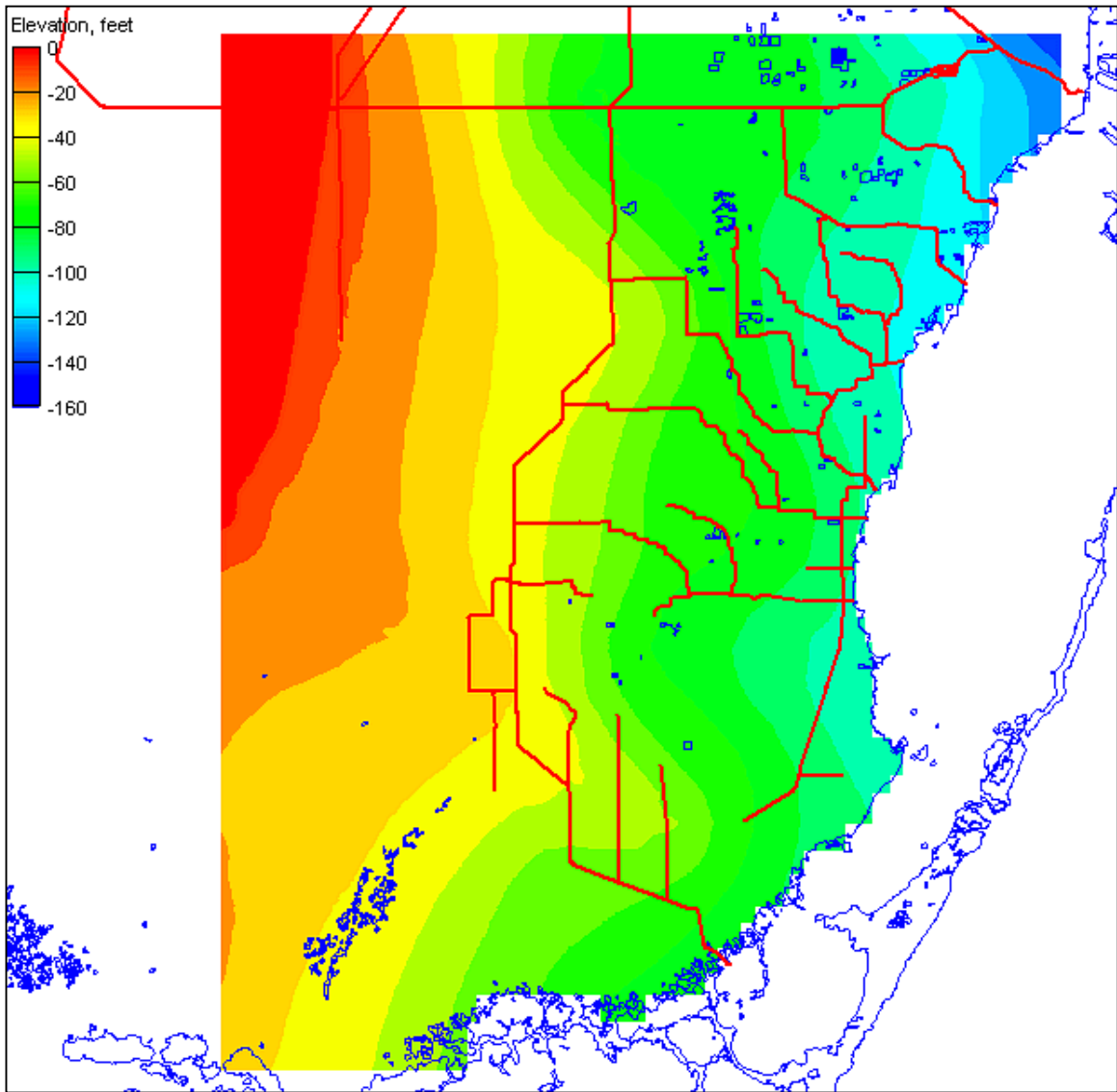


Figure 3c. Bottom elevation of layer 3.

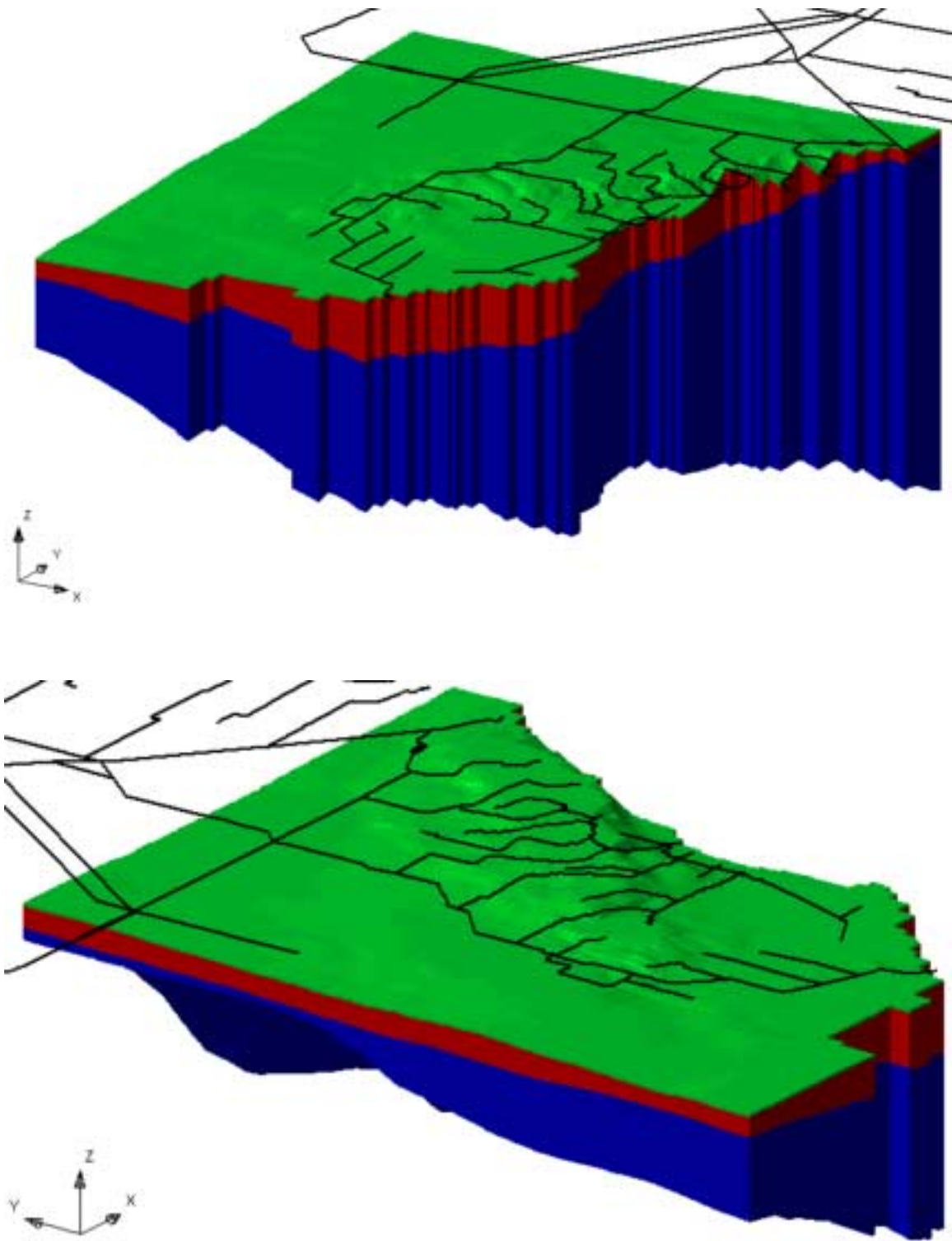


Figure 4. Oblique Views of the Model Domain.
Green represents surface layer.
Red represents upper Surficial Aquifer.
Blue represents lower Surficial Aquifer.

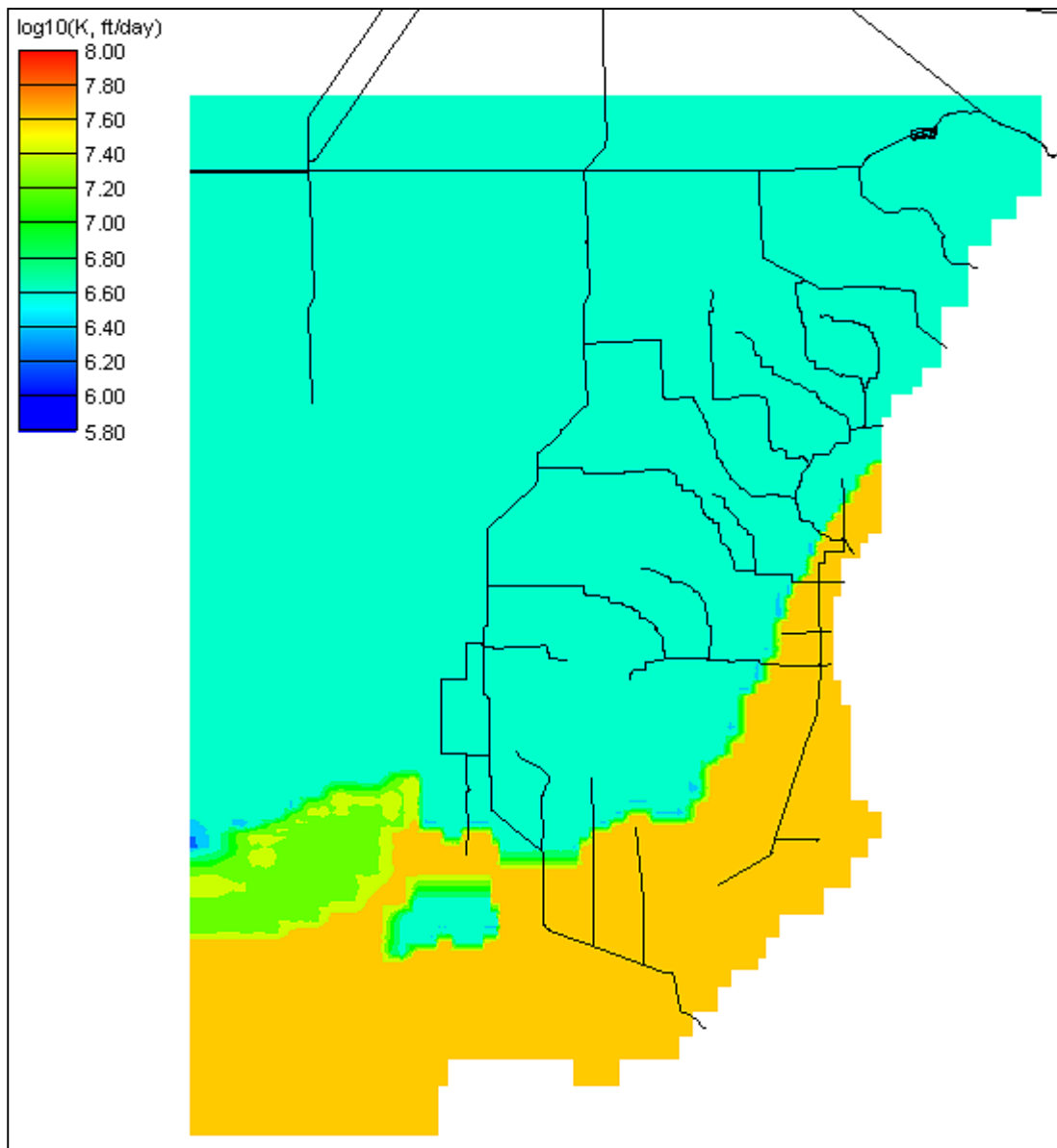


Figure 5a. Contours of $\log_{10}(K)$, K = hydraulic conductivity, ft/day.
Layer 1

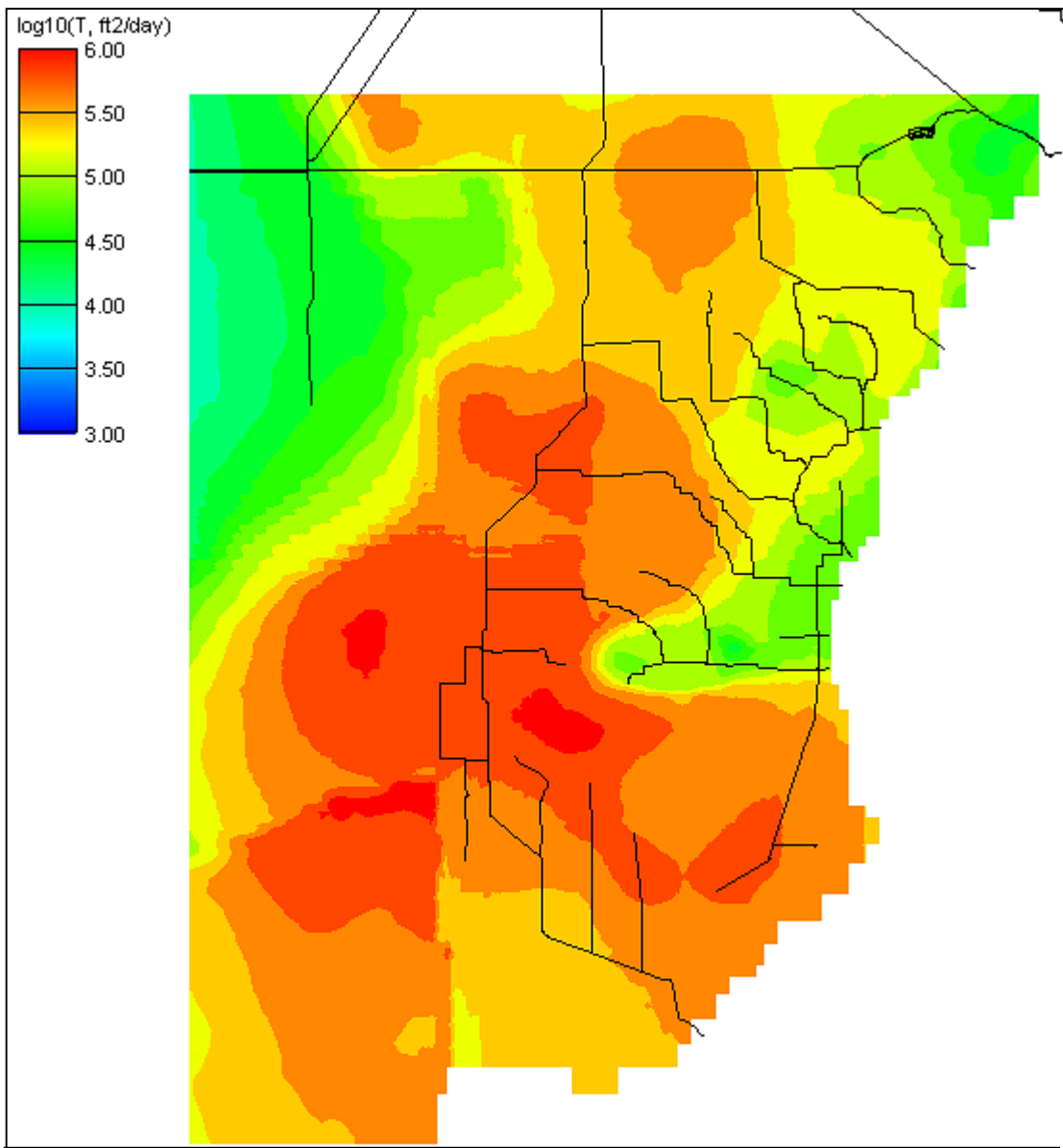


Figure 5b. Contours of $\log_{10}(T)$, T = hydraulic transmissivity, ft^2/day .
Layer 2

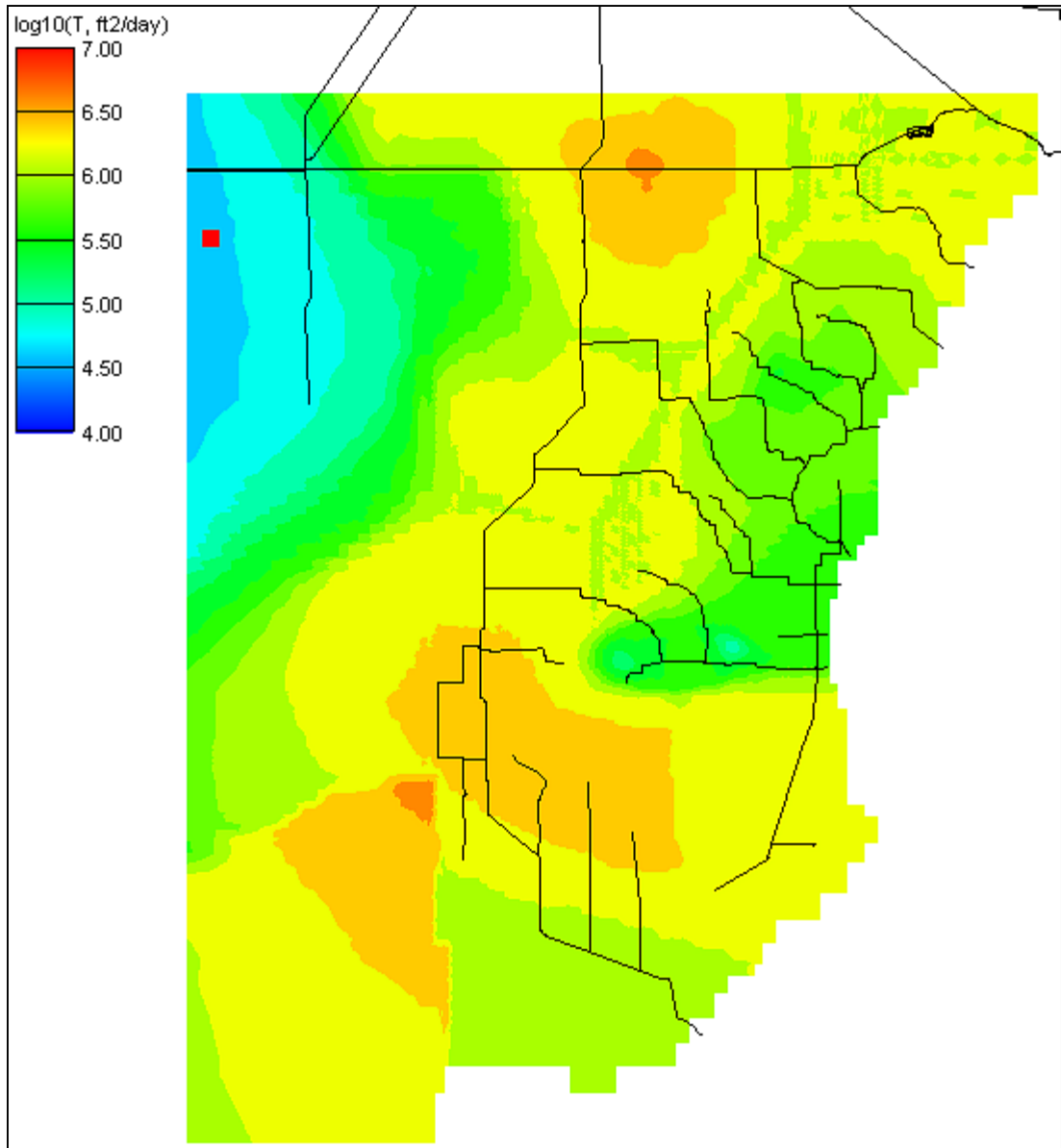


Figure 5c. Contours of $\log_{10}(T)$, T = hydraulic transmissivity, ft^2/day .
Layer 3

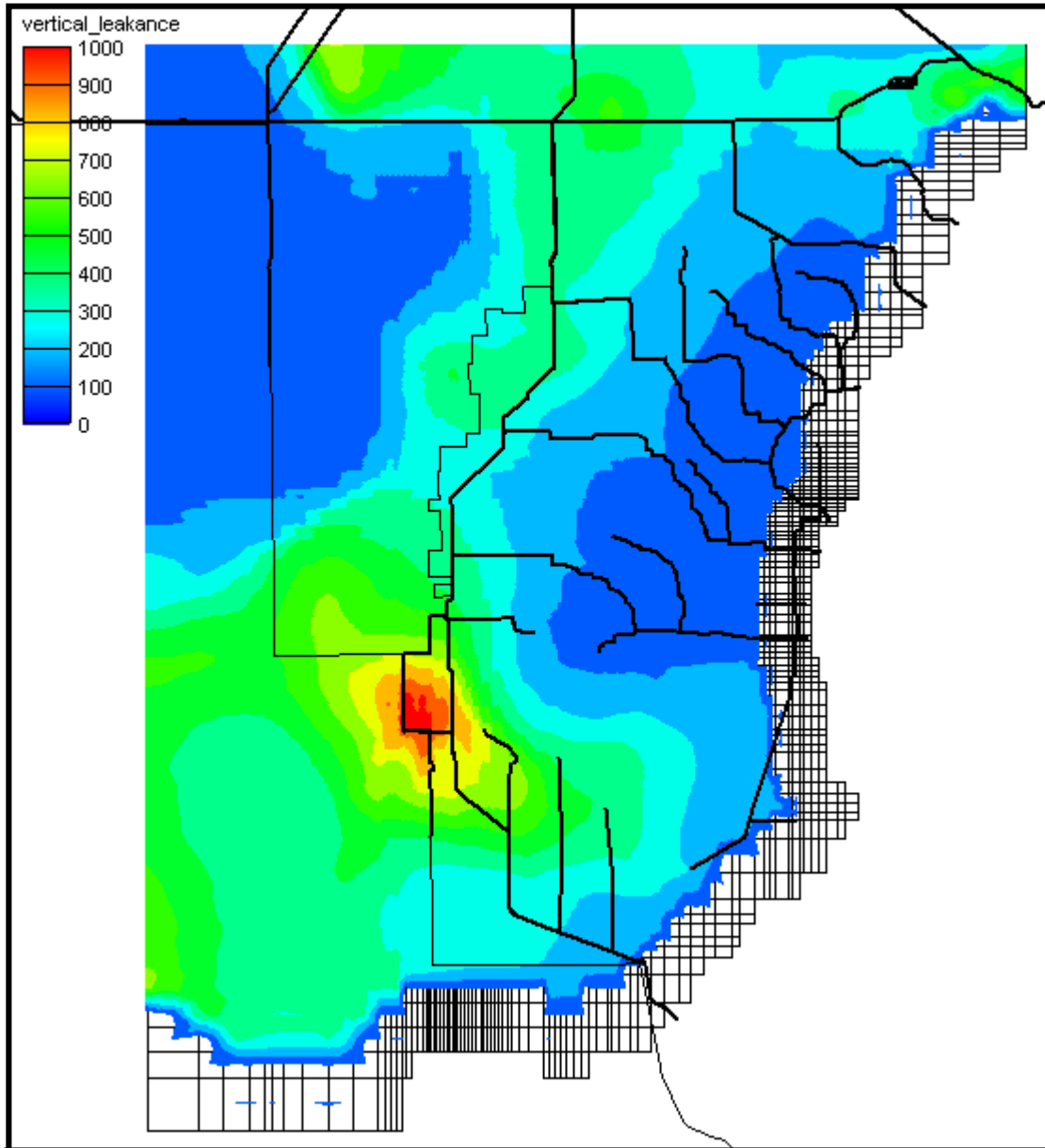


Figure 6a. Vertical Leakance Values between Layers 1 and 2.

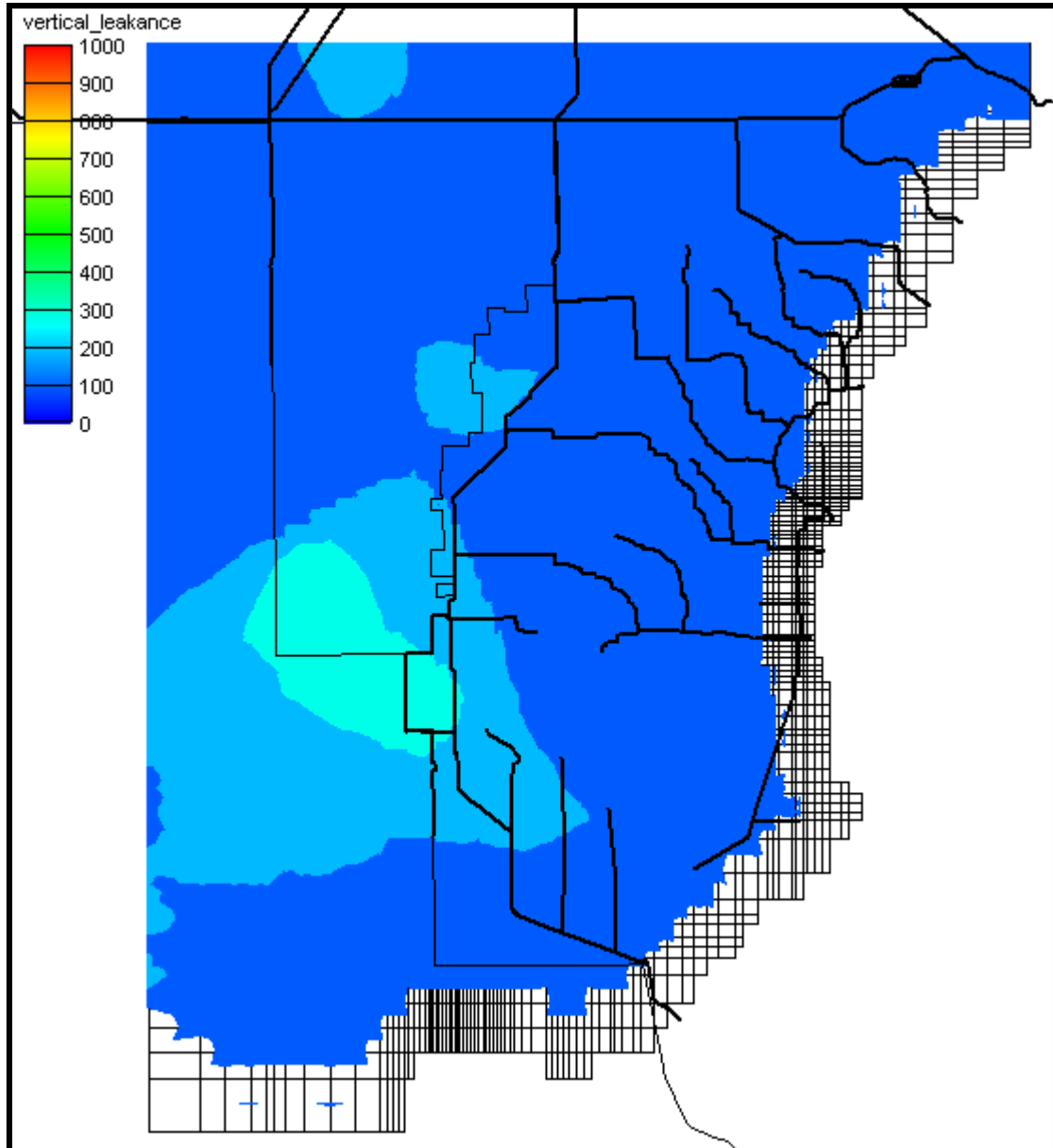


Figure 6b. Vertical Leakance Values between Layers 2 and 3.

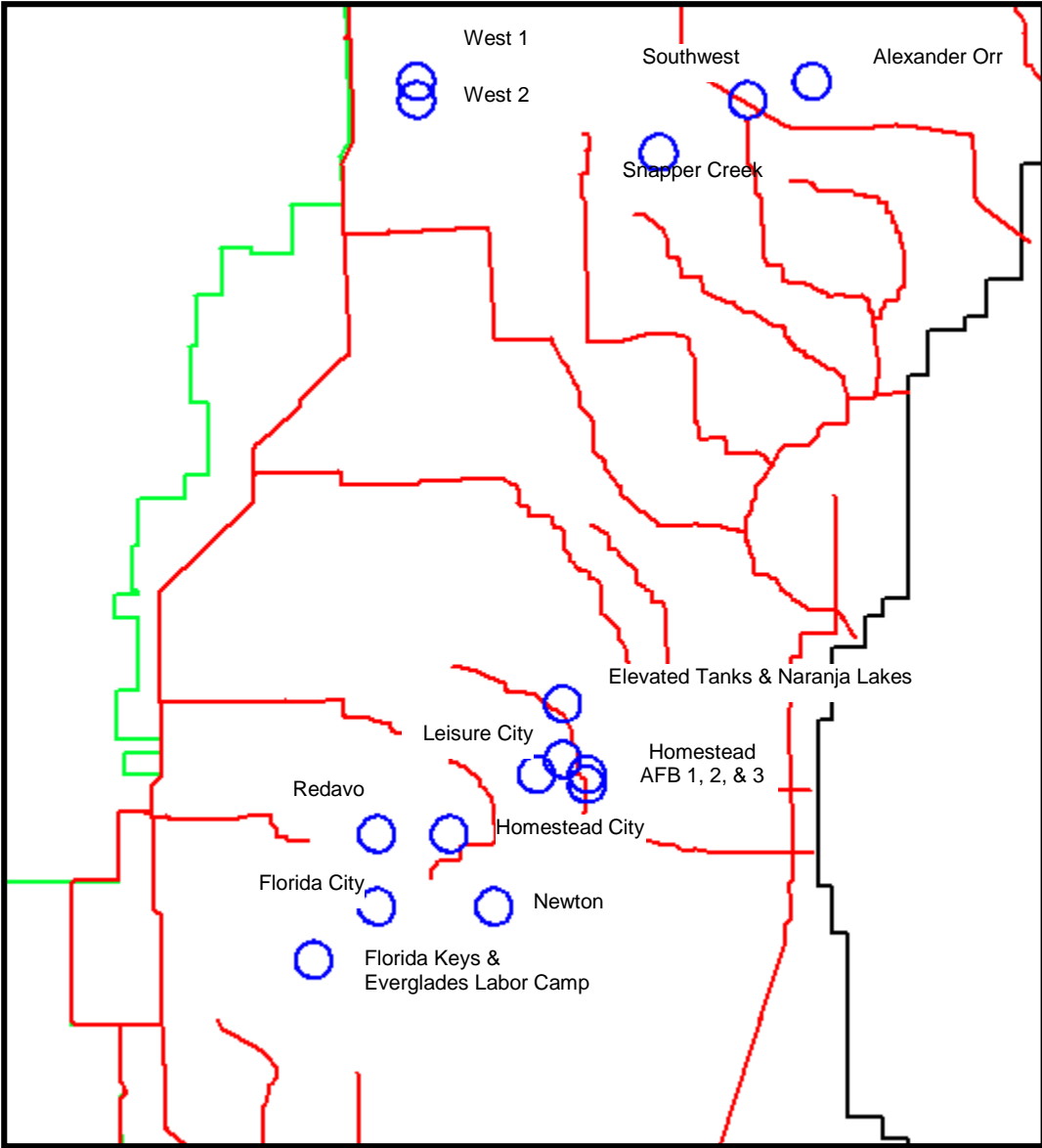


Figure 7. Location of Production Wells used in MODBRANCH Simulations.

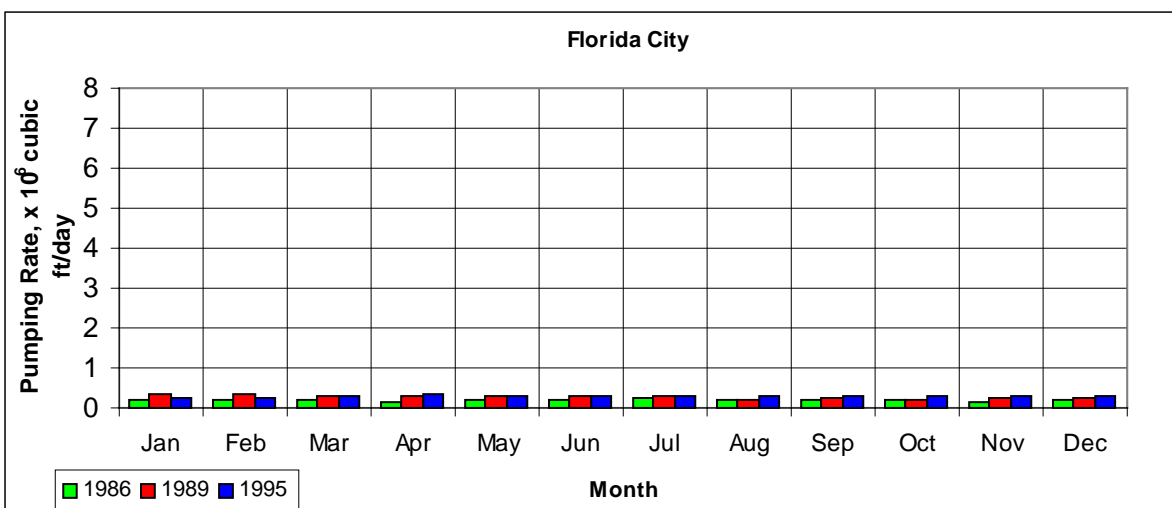
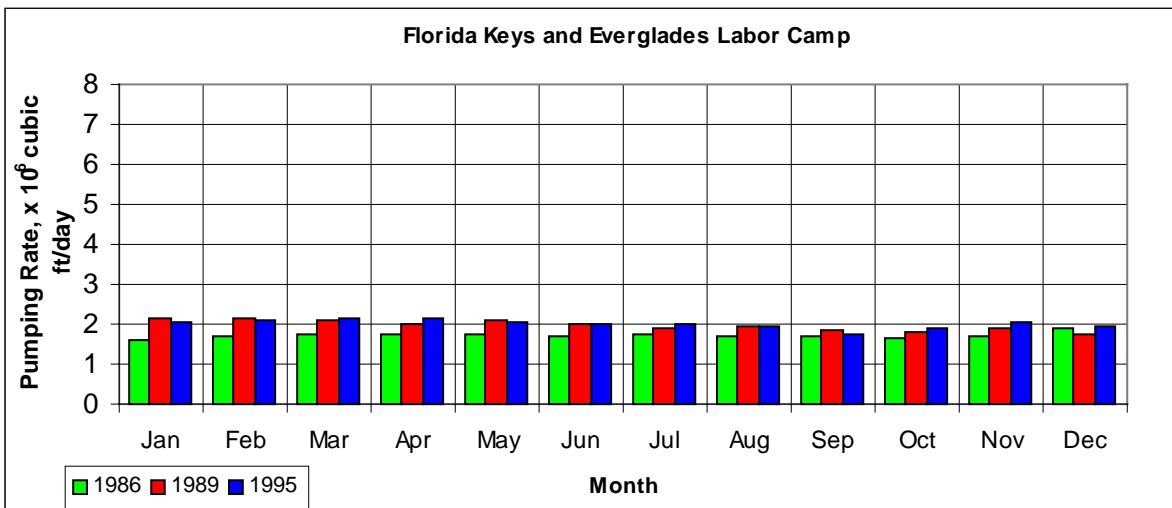
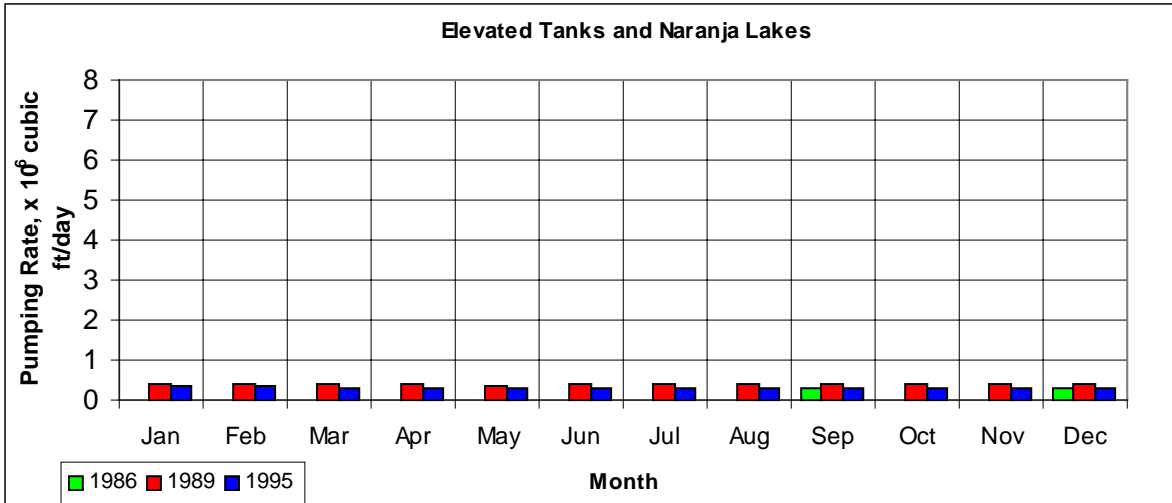


Figure 8a. 1986, 1989, and 1995 Production Well Pumping Rates for Elevated Tanks and Naranja Lakes, Florida Keys and Everglades Labor Camp, and Florida City.

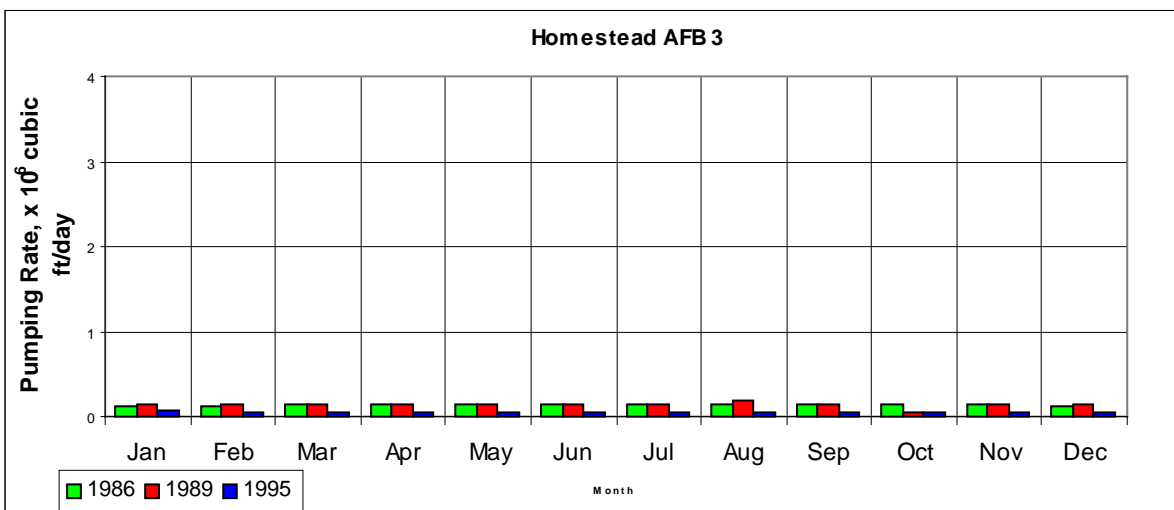
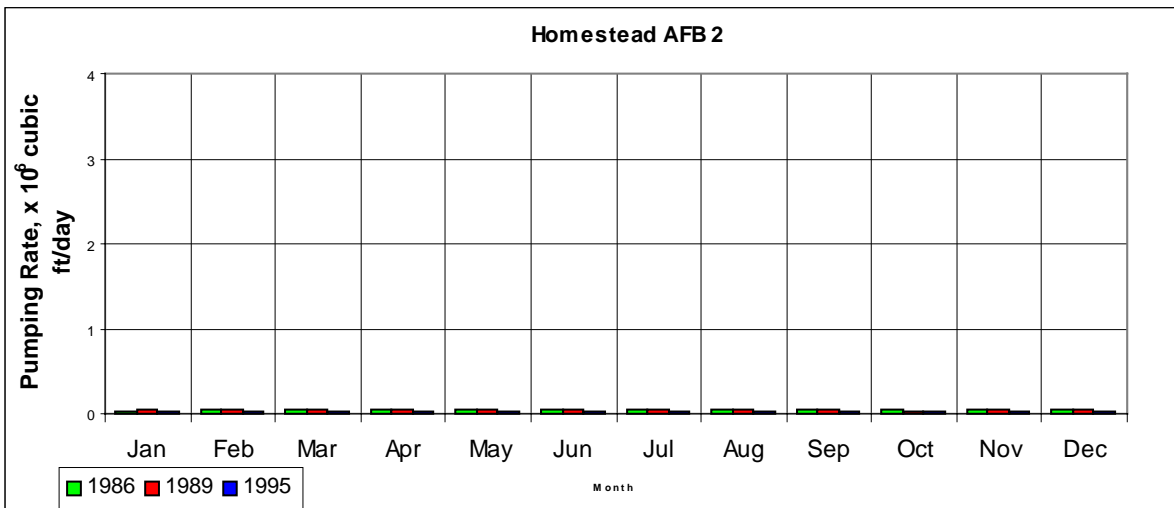
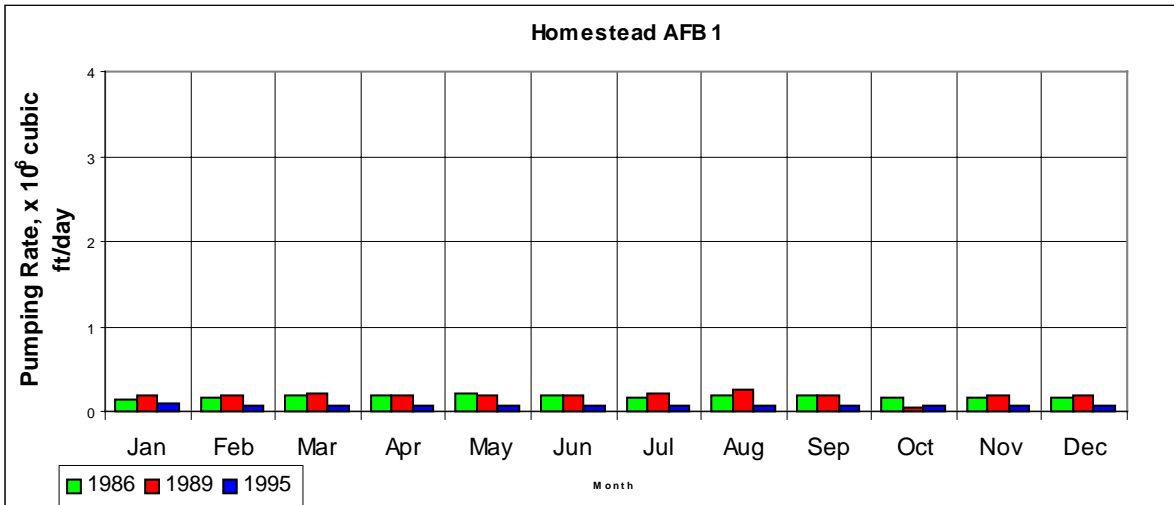


Figure 8b. 1986, 1989, and 1995 Production Well Pumping Rates for Homestead AFB 1, 2, and 3.

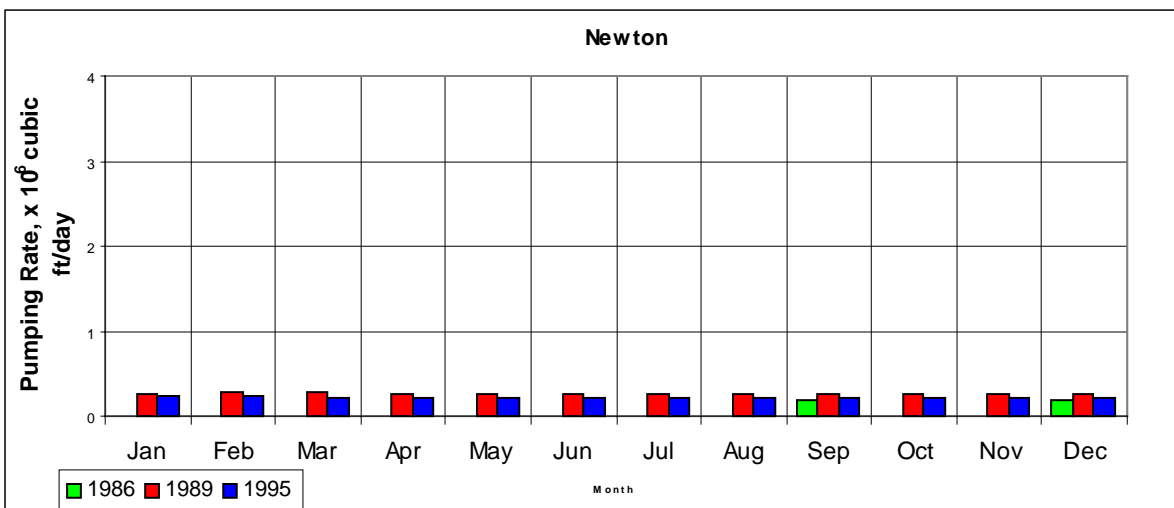
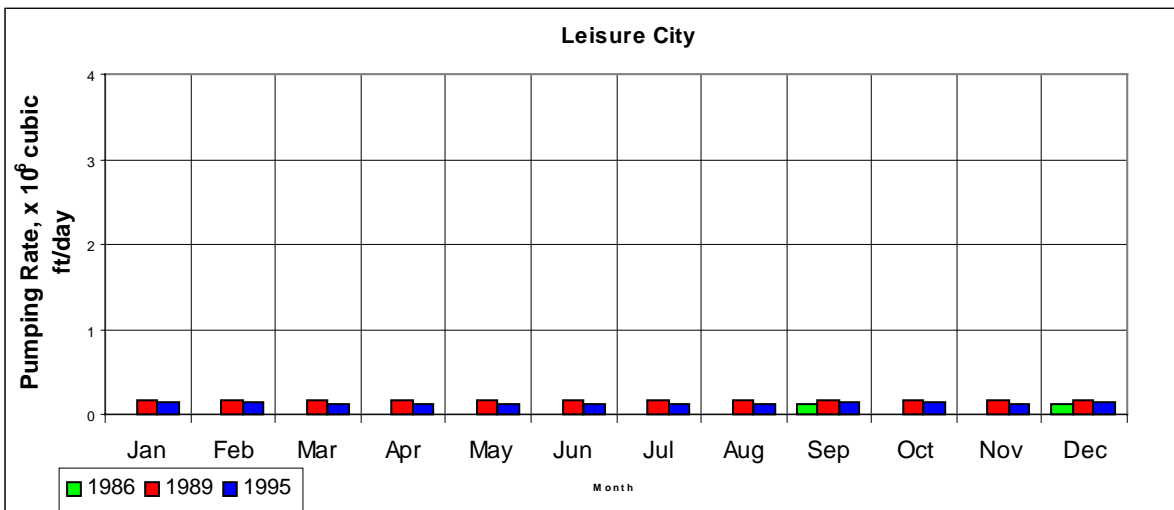
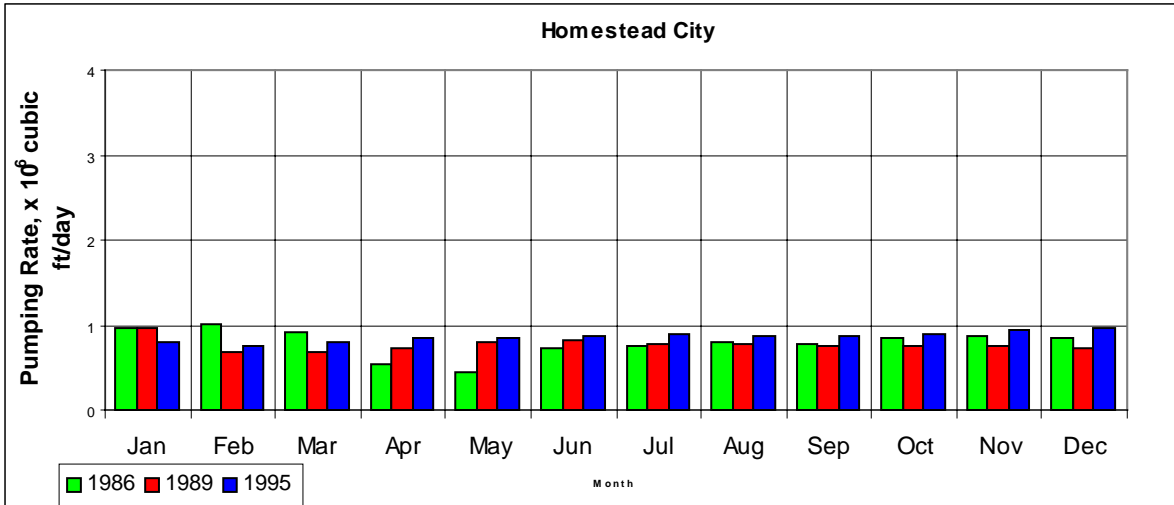


Figure 8c. 1986, 1989, and 1995 Production Well Pumping Rates for Homestead City, Leisure City, and Newton.

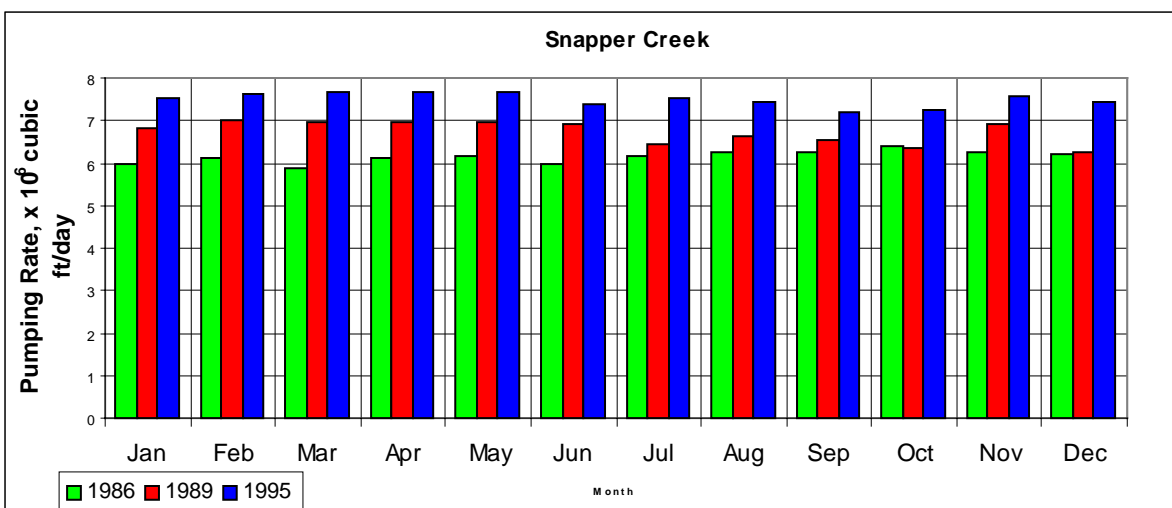
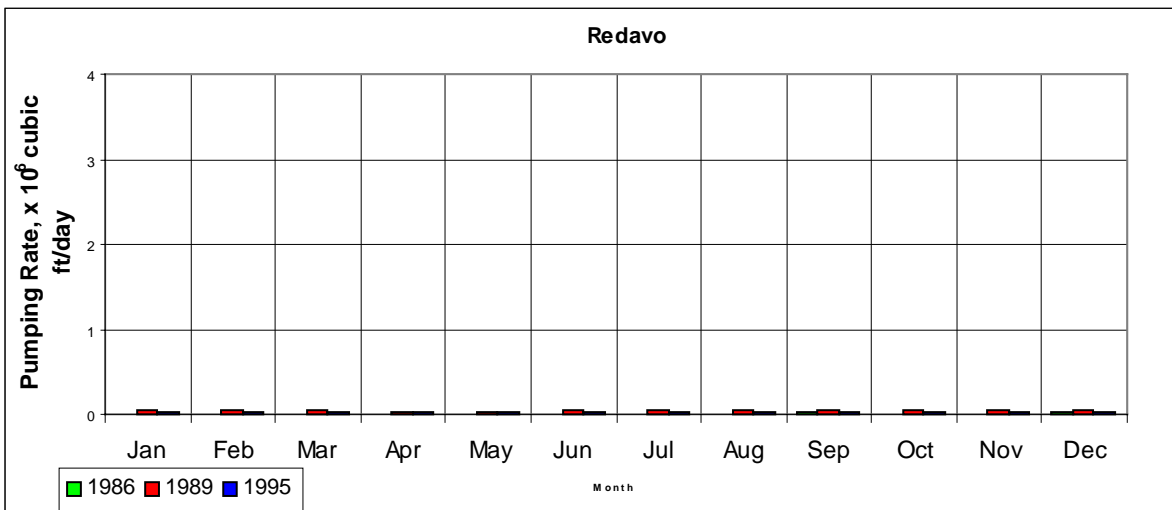
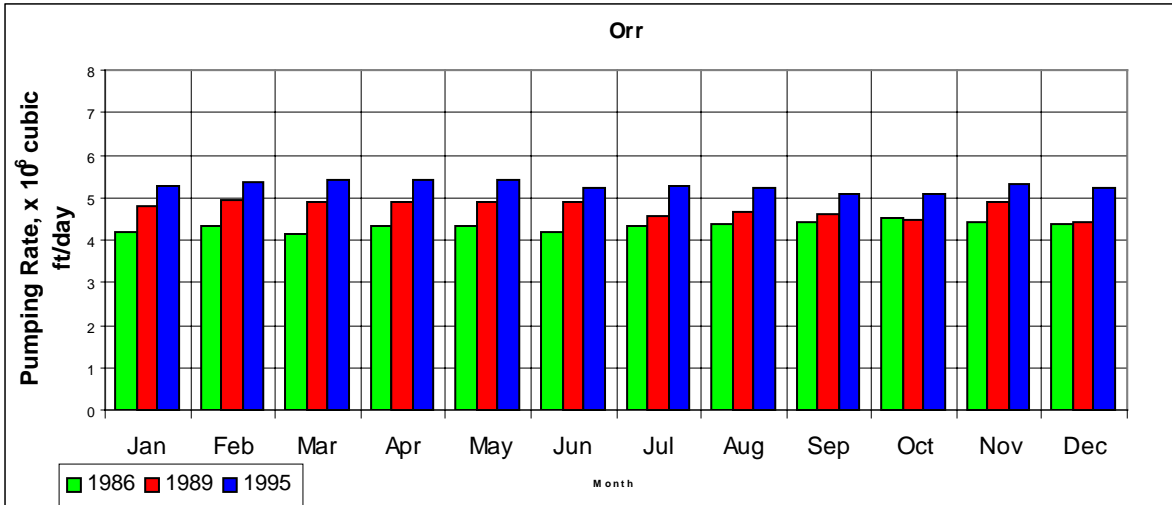


Figure 8d. 1986, 1989, and 1995 Production Well Pumping Rates for Orr, Redavo, and Snapper Creek.

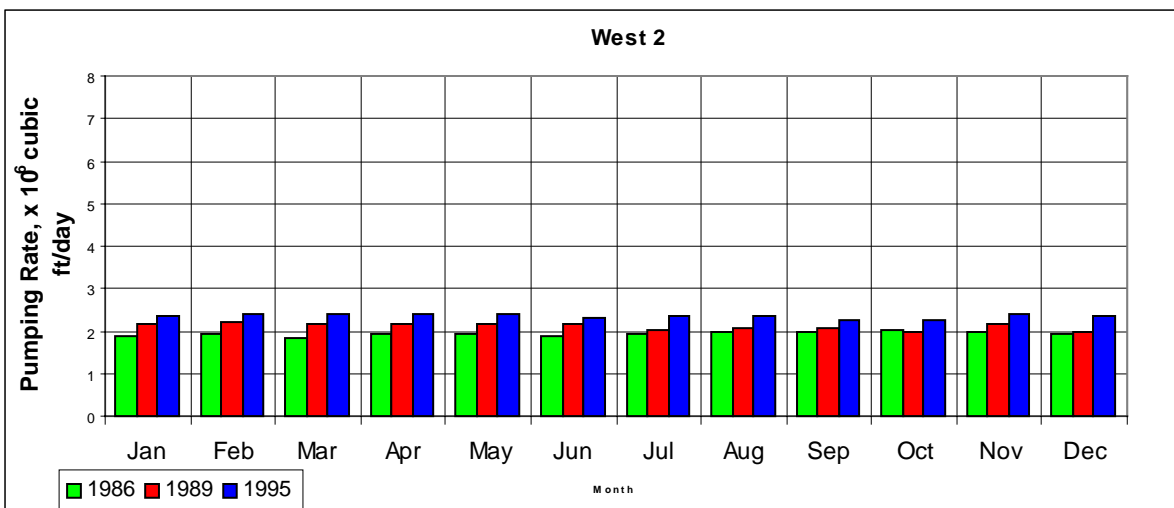
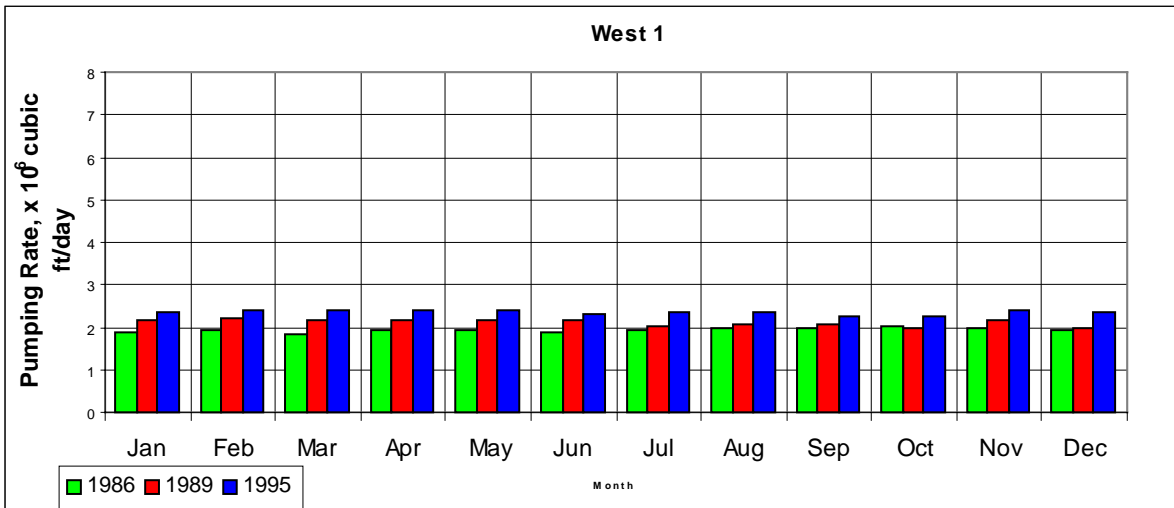
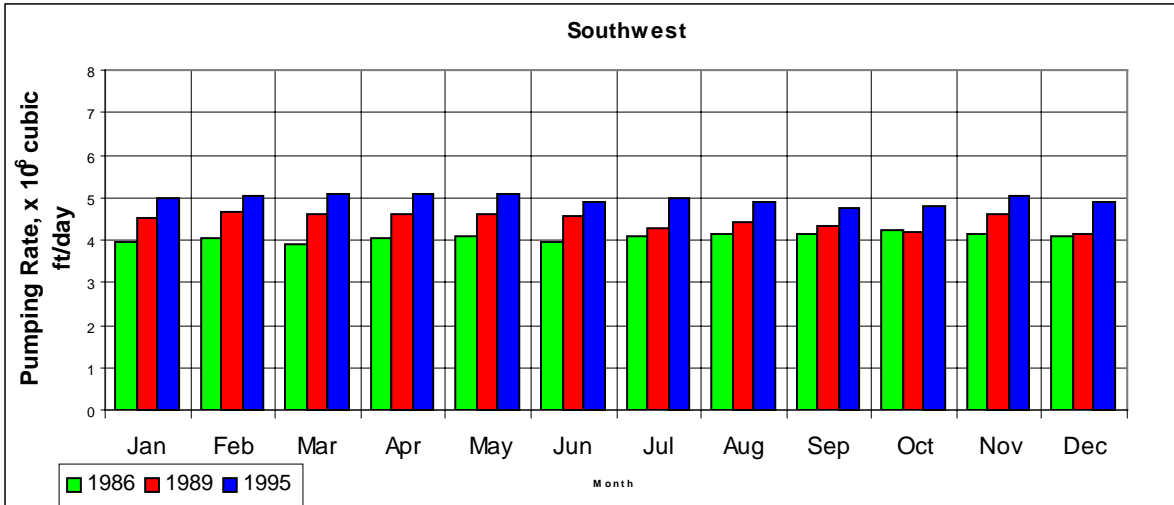


Figure 8e. 1986, 1989, and 1995 Production Well Pumping Rates for Southwest, West 1 and West 2.

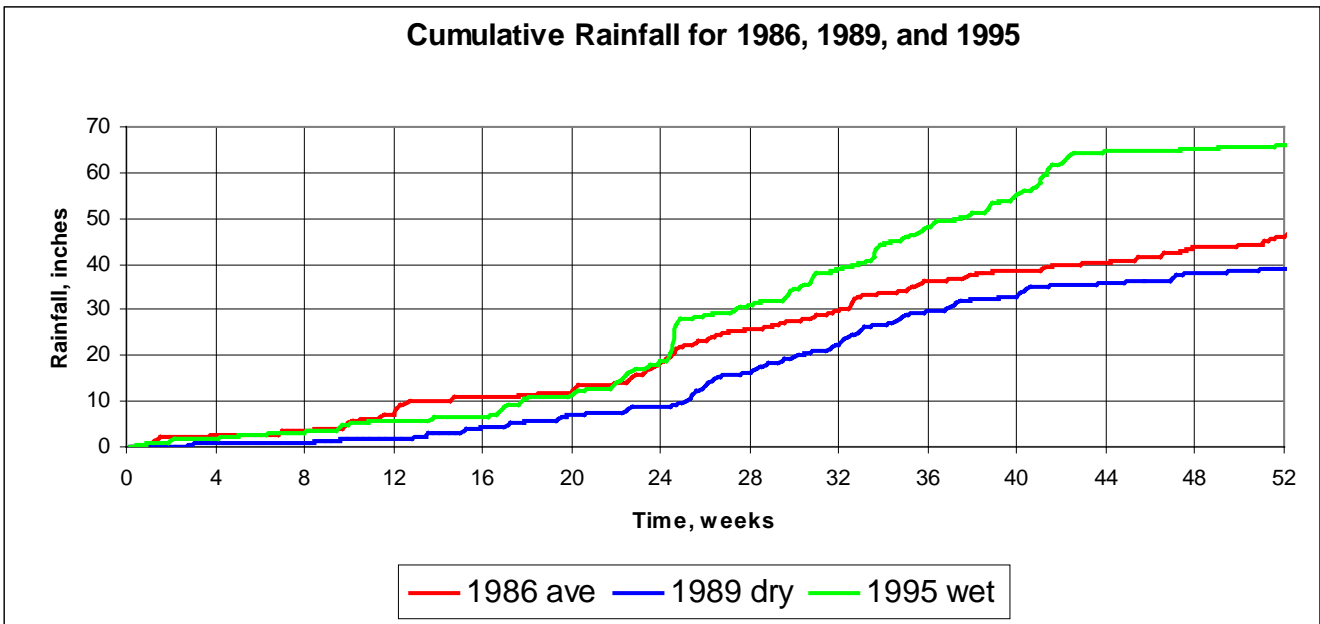
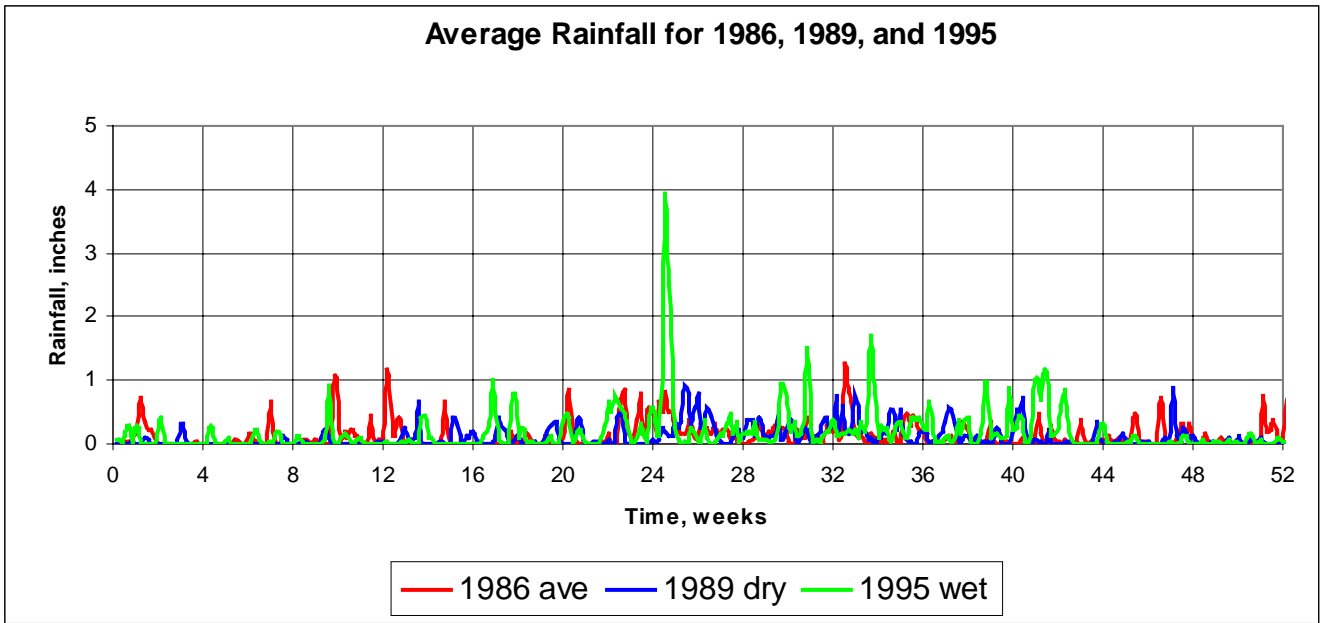


Figure 9. Rainfall for 1986, 1989, and 1995. (source: SFWMM 2x2 rainfall input)

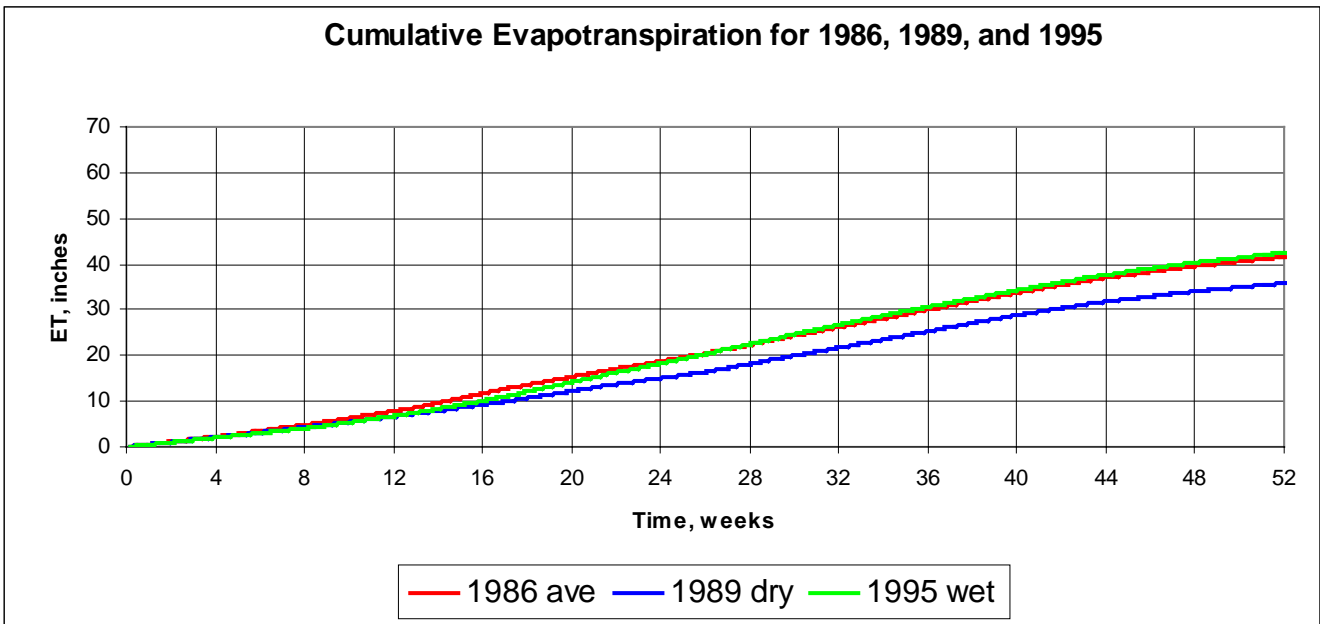
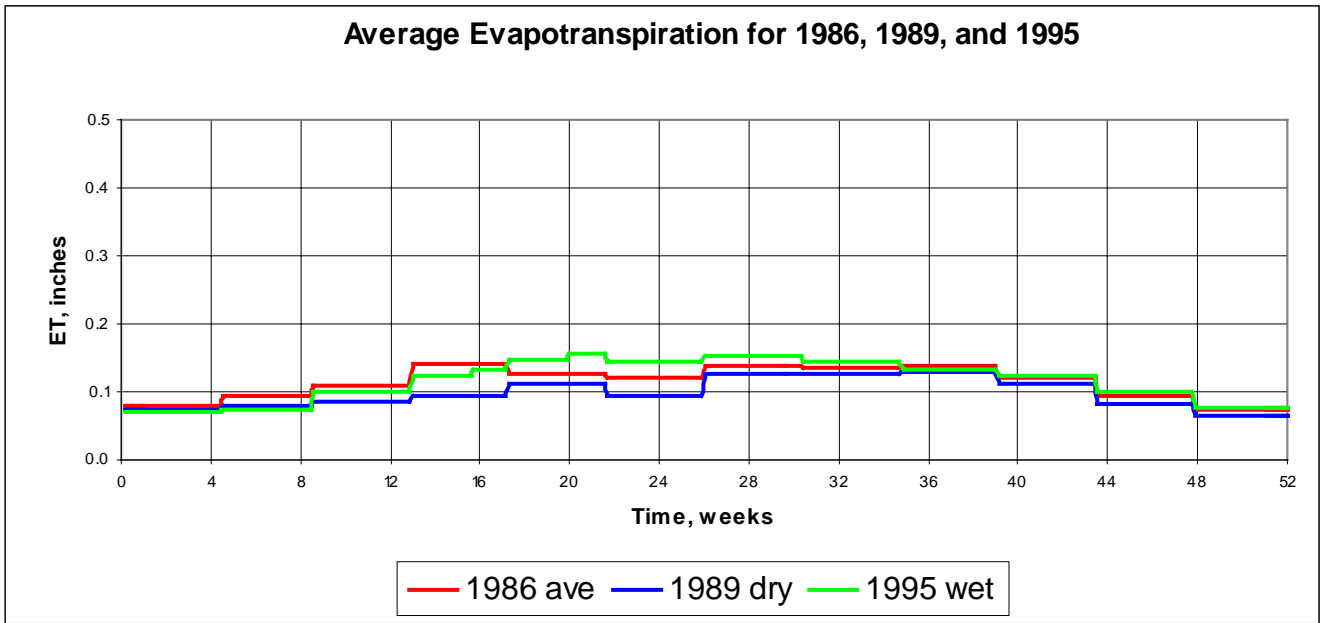


Figure 10. Evapotranspiration for 1986, 1989, and 1995. (source: SFWMM 2x2 ET output)

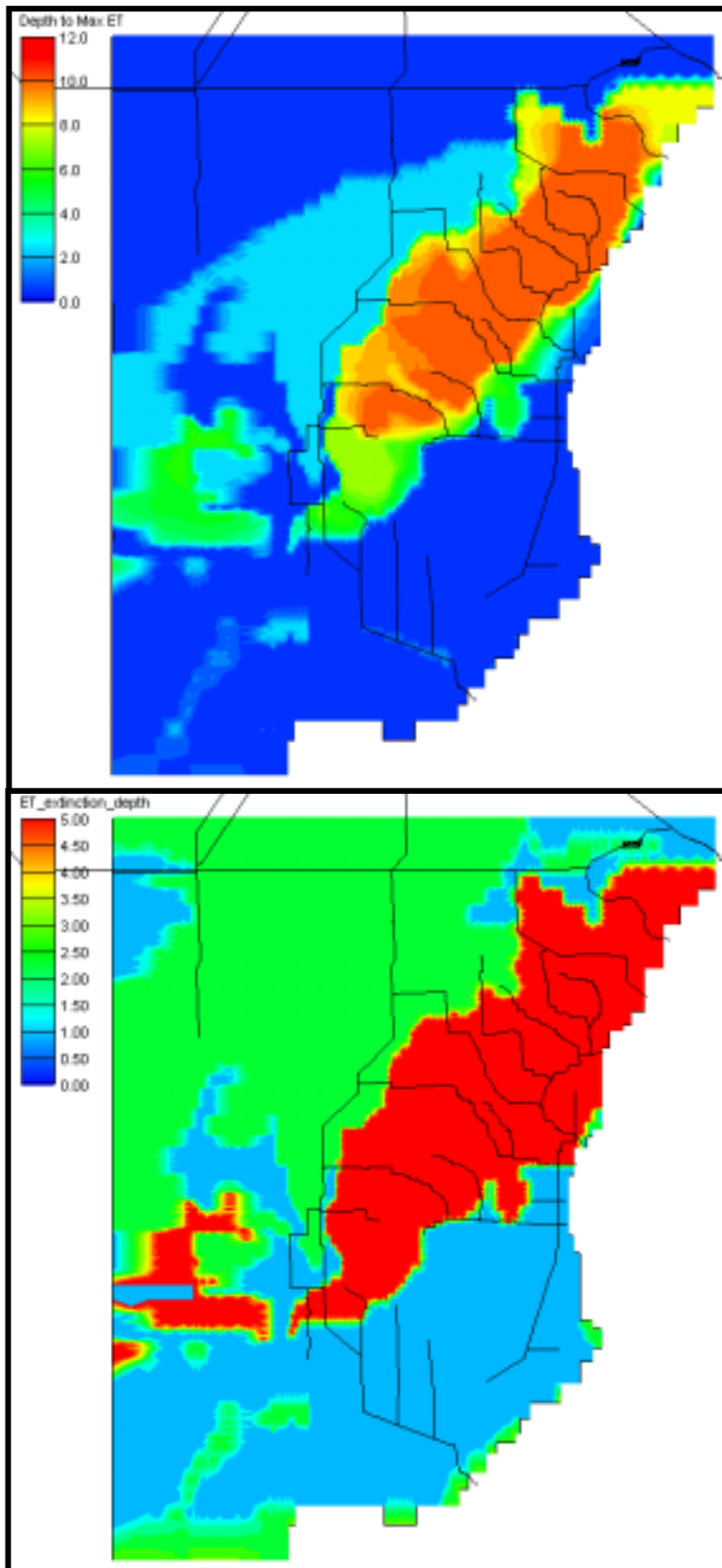


Figure 11. Maximum Evaporation Surface (top) and ET Extinction Depth (bottom) (units of feet).

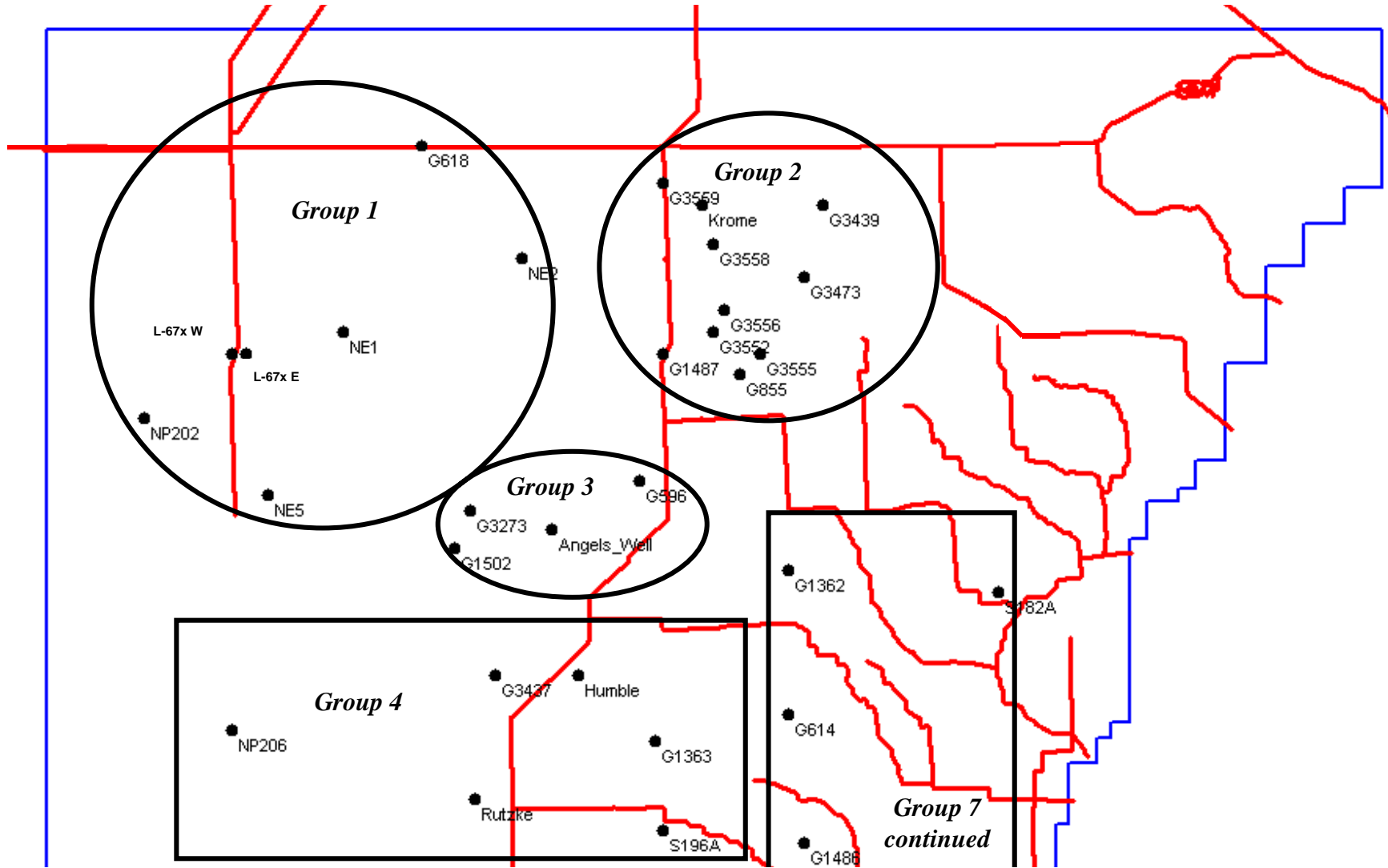


Figure 12a. Ground Water Observation Wells, North Model Domain.

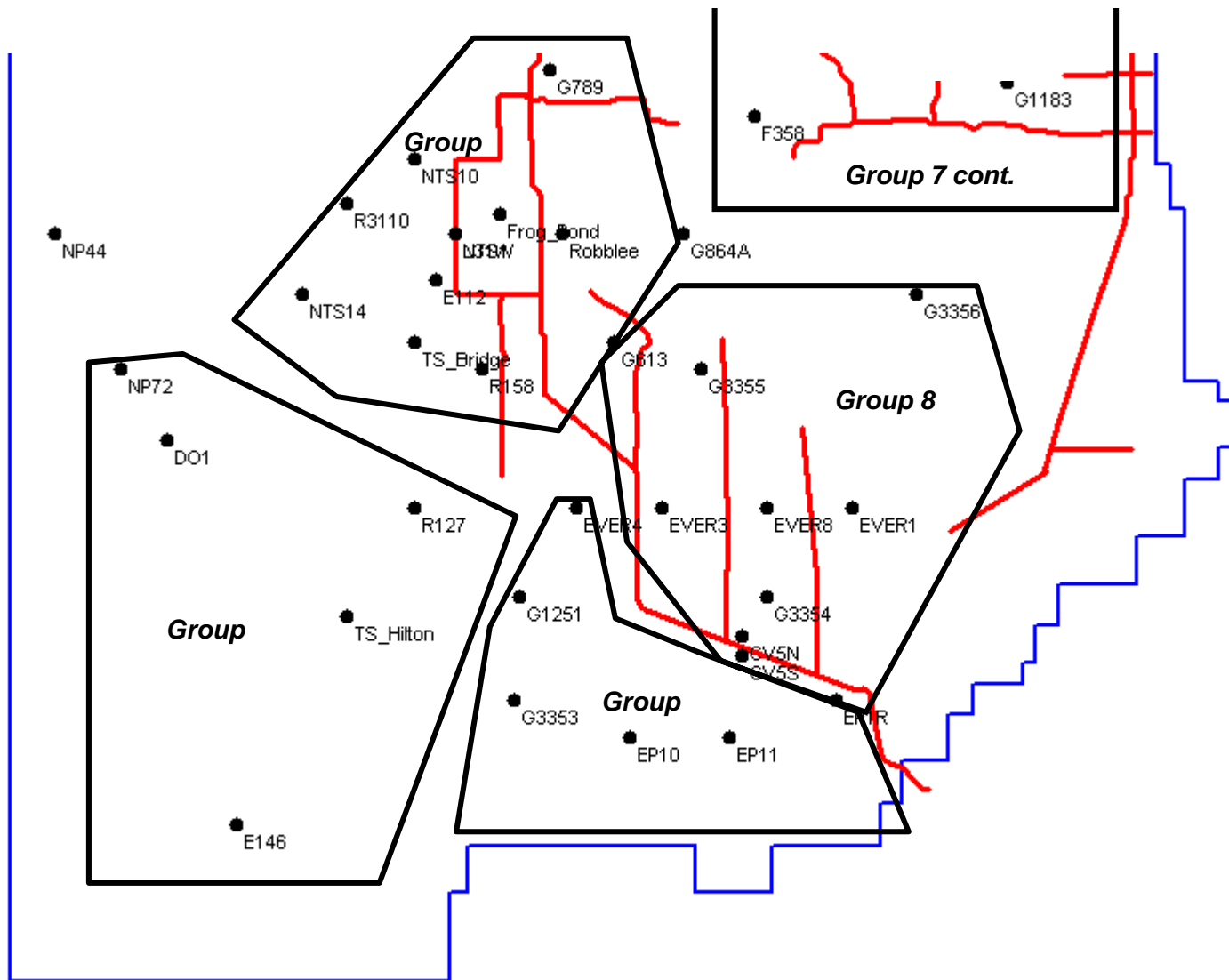


Figure 12b. Ground Water Observation Wells, South Model Domain.

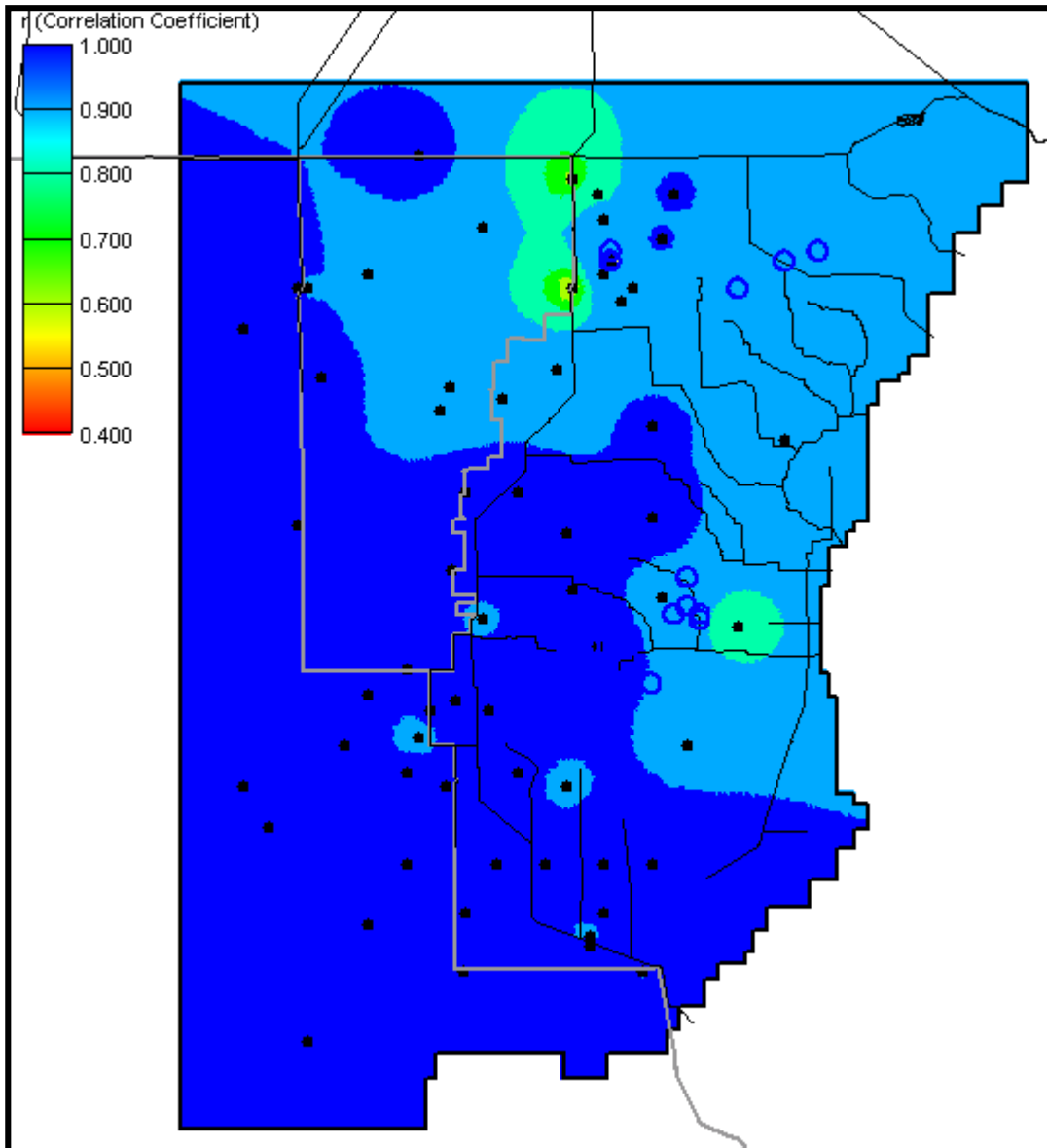


Figure 13a. Contours of Correlation Coefficient, Ground Water Observation Wells, MODBRANCH Results versus Field Data, 1995.

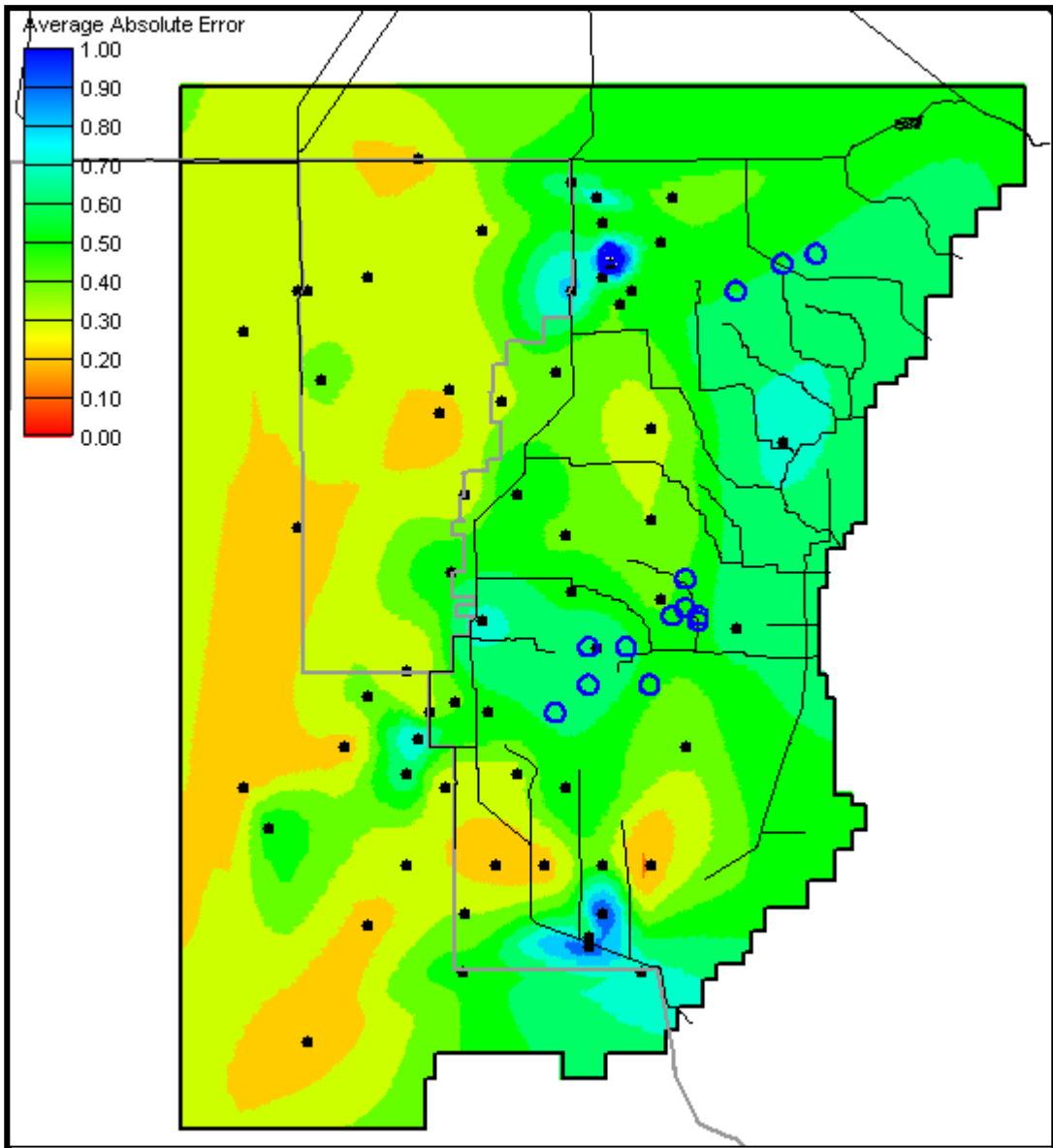


Figure 13b. Contours of Average Absolute Error (feet), Ground Water Observation Wells, MODBRANCH Results versus Field Data, 1995.

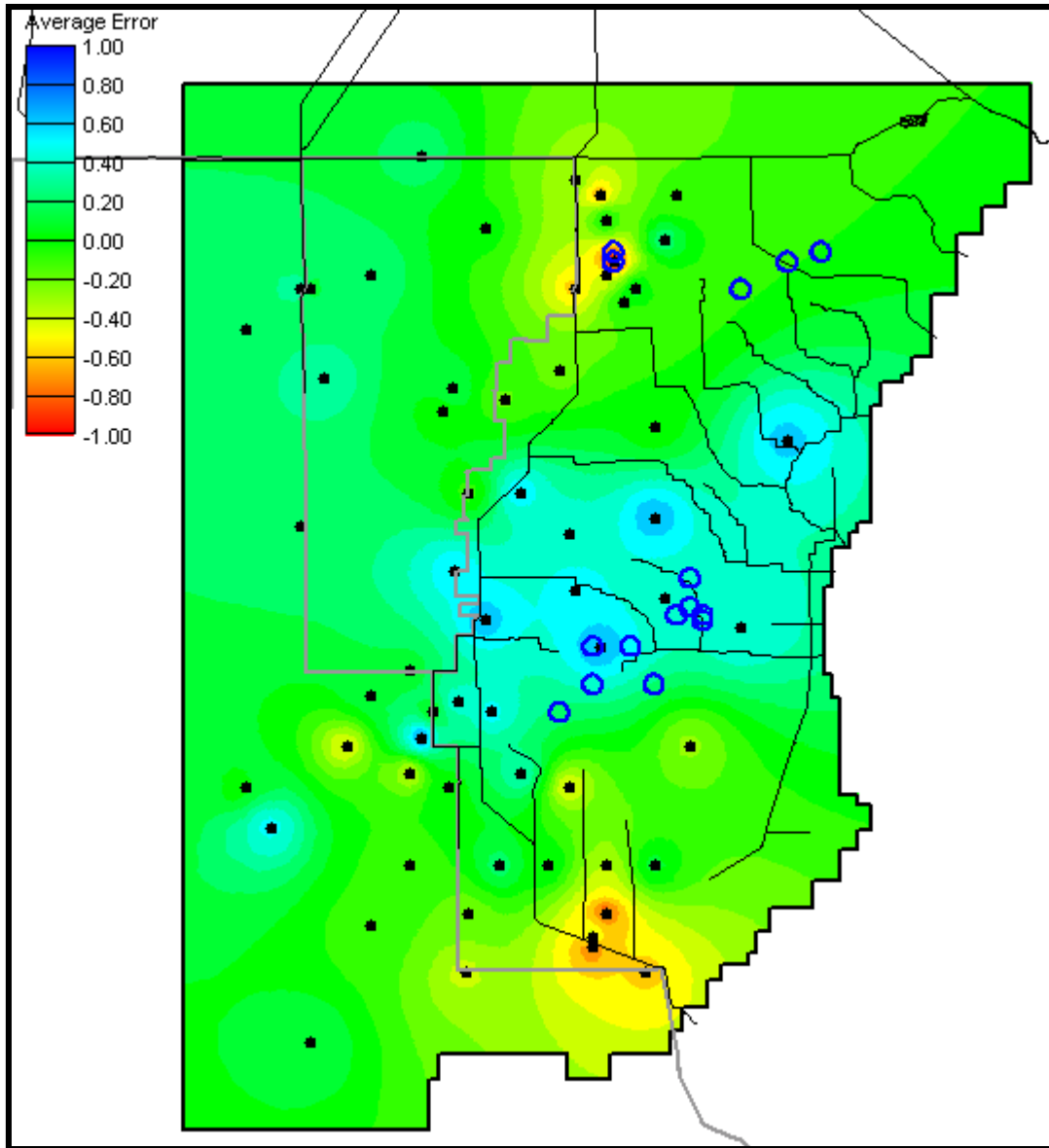


Figure 13c. Contours of Average Error (feet), Ground Water Observation Wells, MODBRANCH Results versus Field Data, 1995.

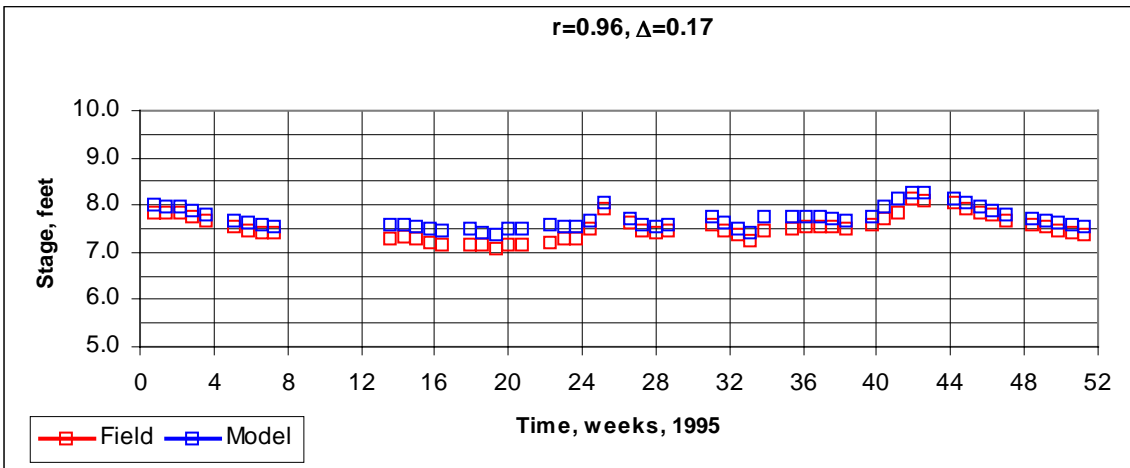
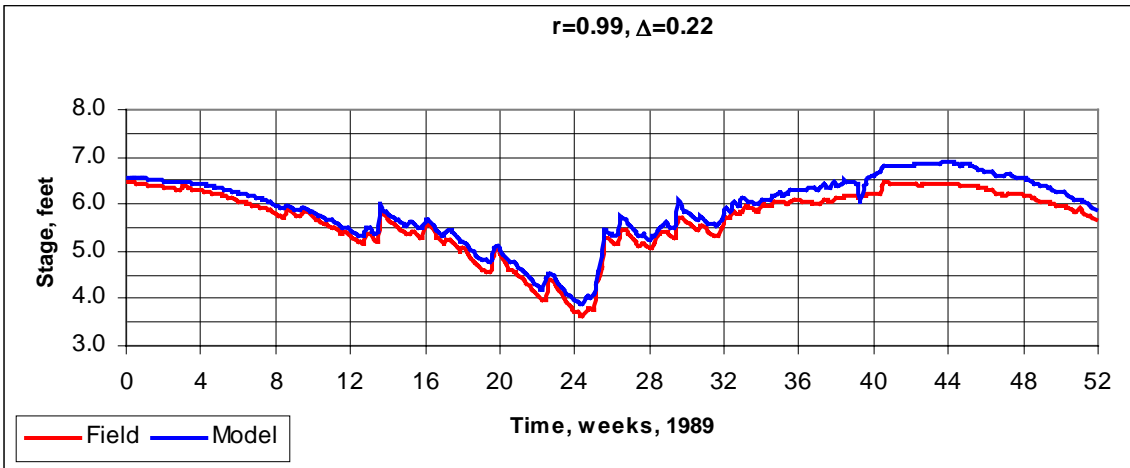
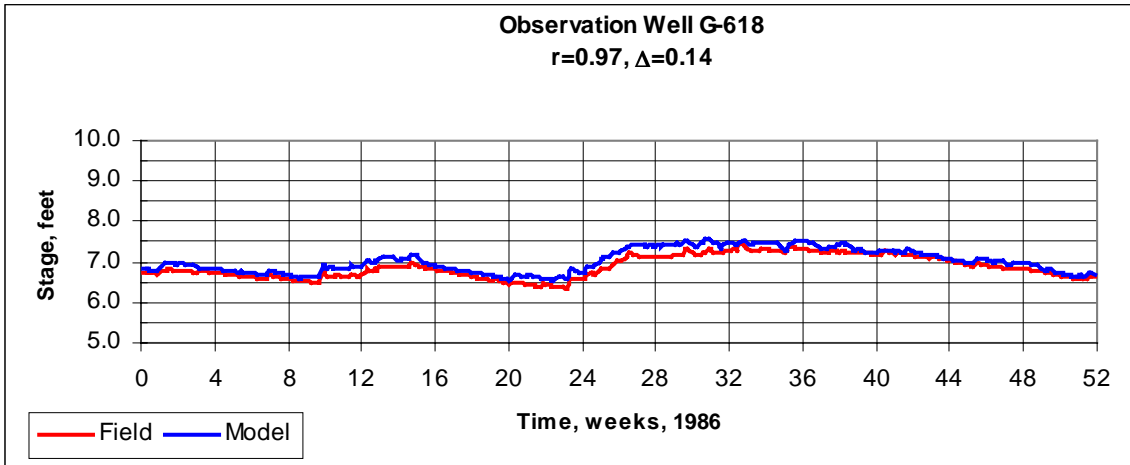


Figure 14: Observation Well G-618

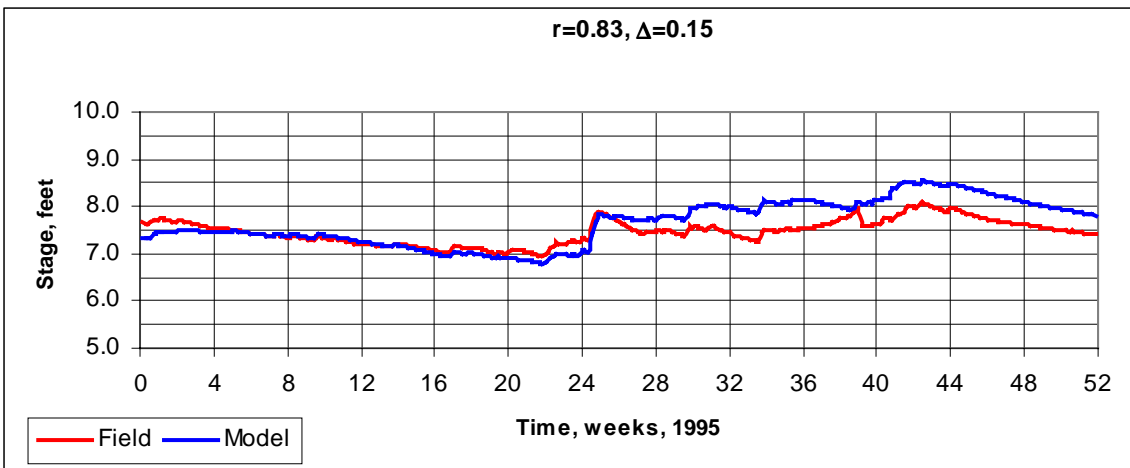
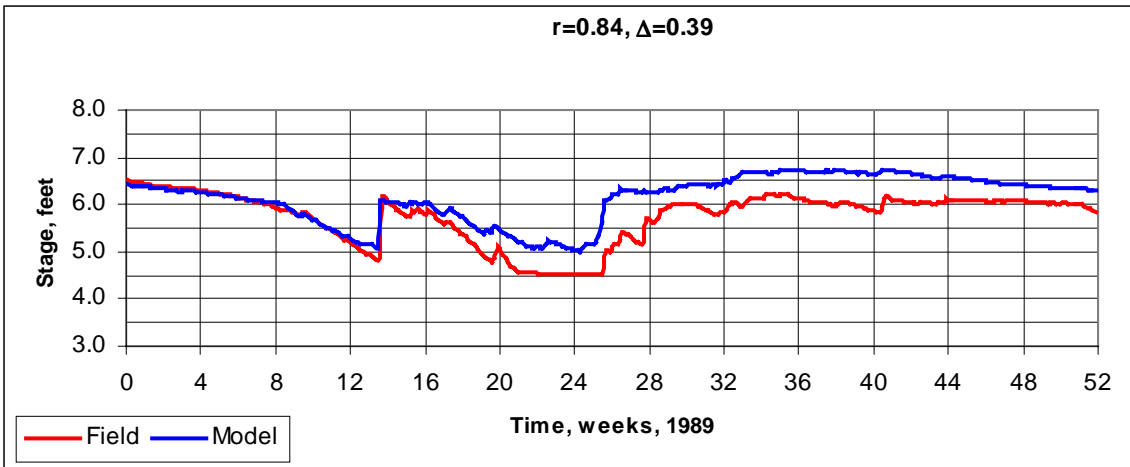
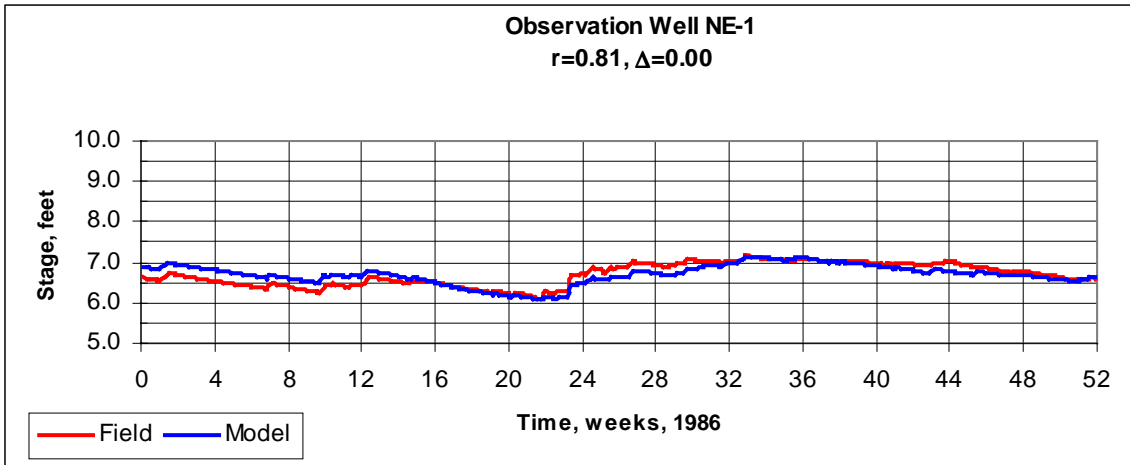


Figure 15: Observation Well NE-1

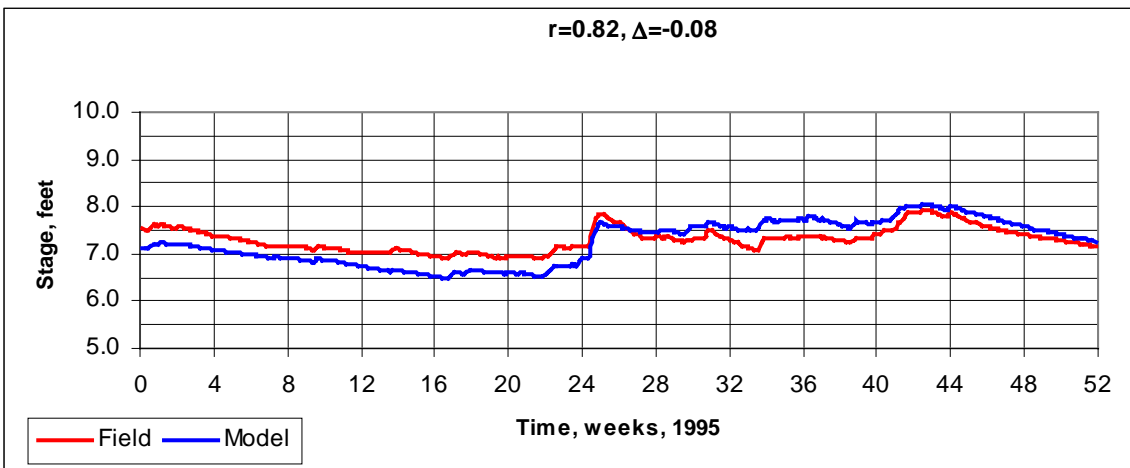
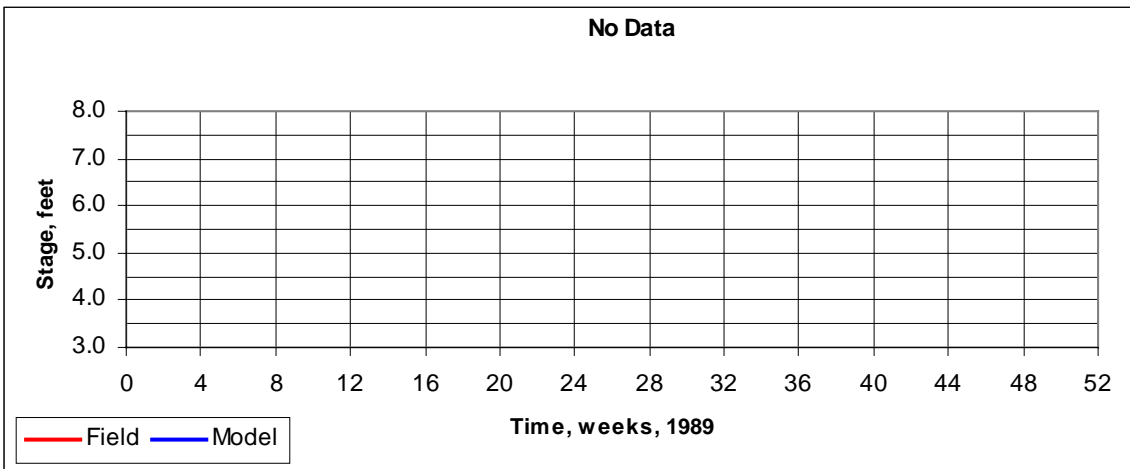
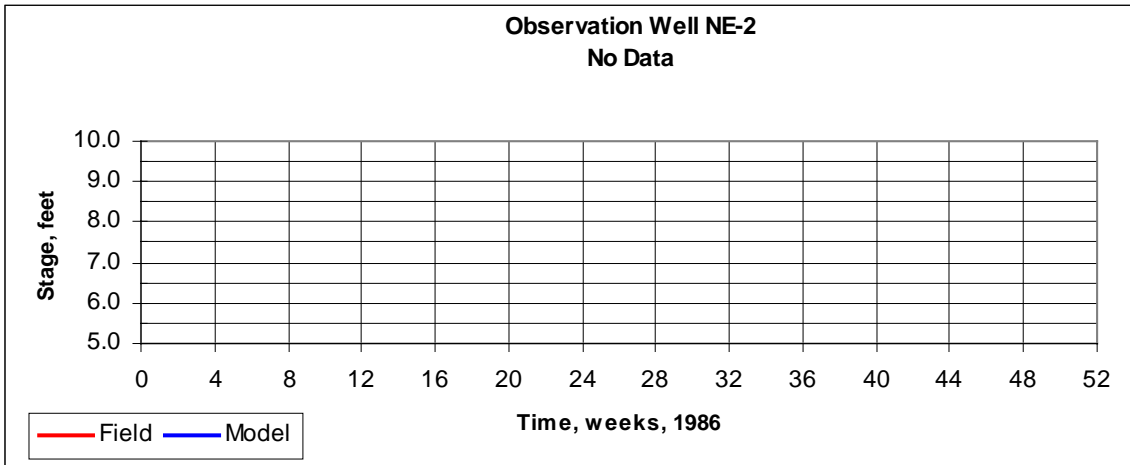


Figure 16: Observation Well NE-2

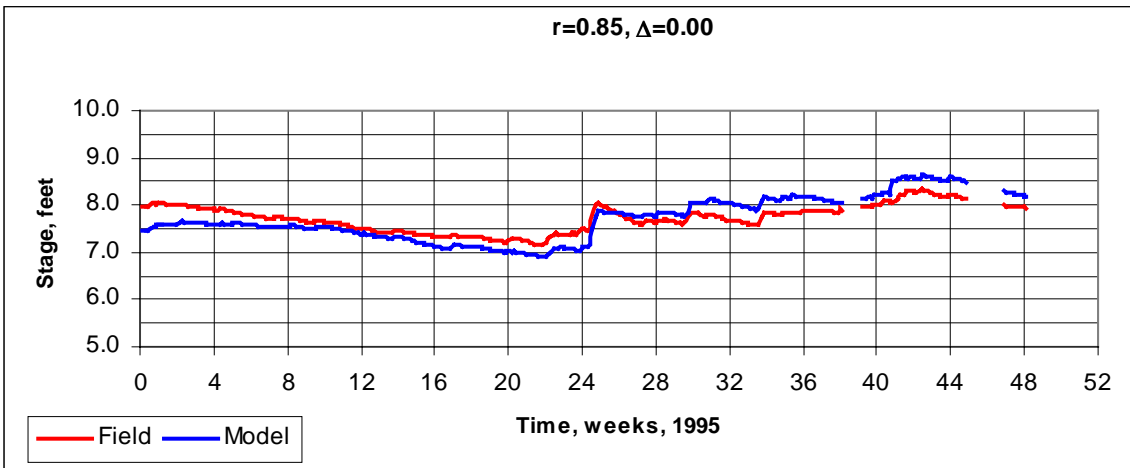
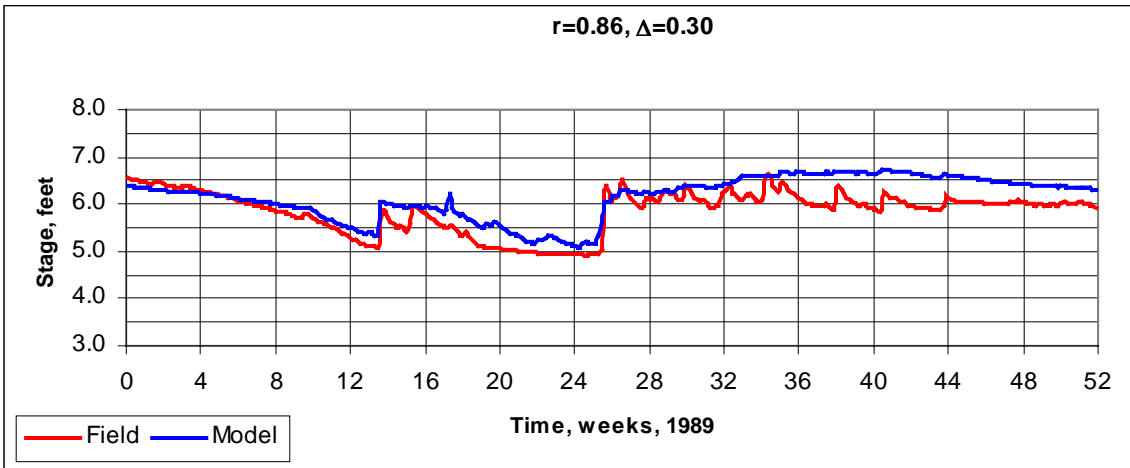
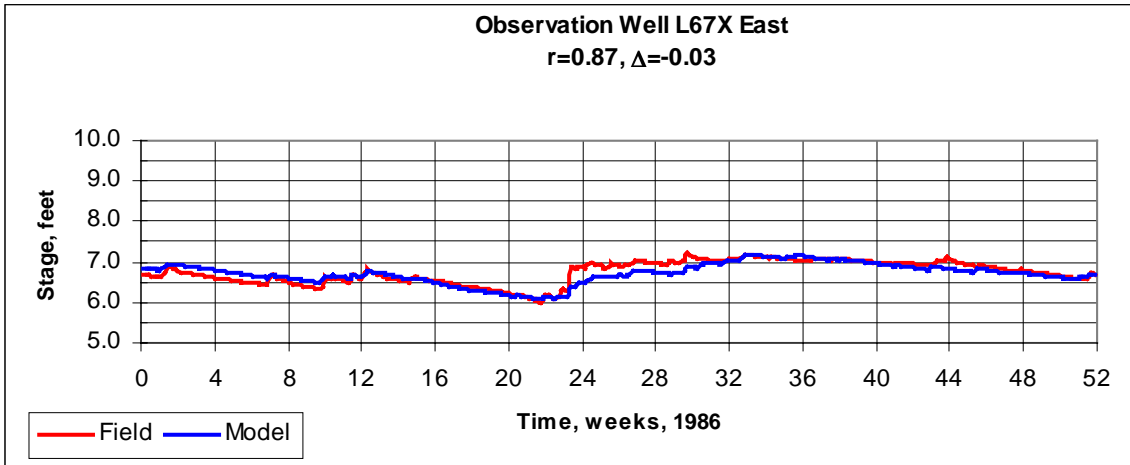


Figure 17: Observation Well L67X East

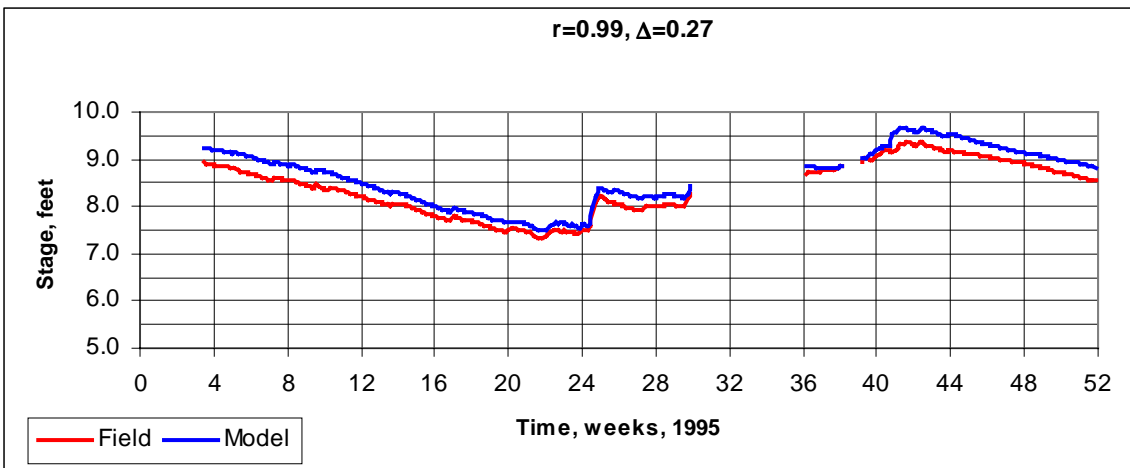
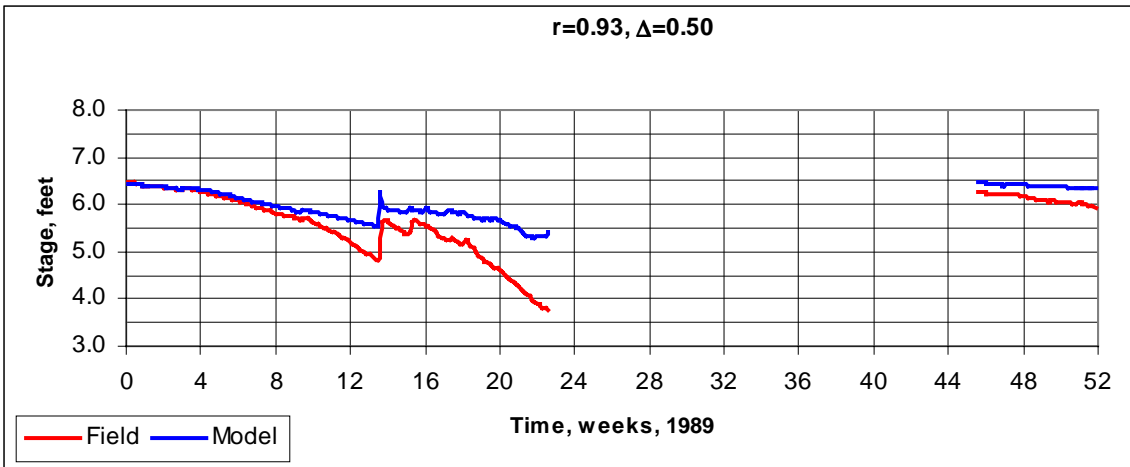
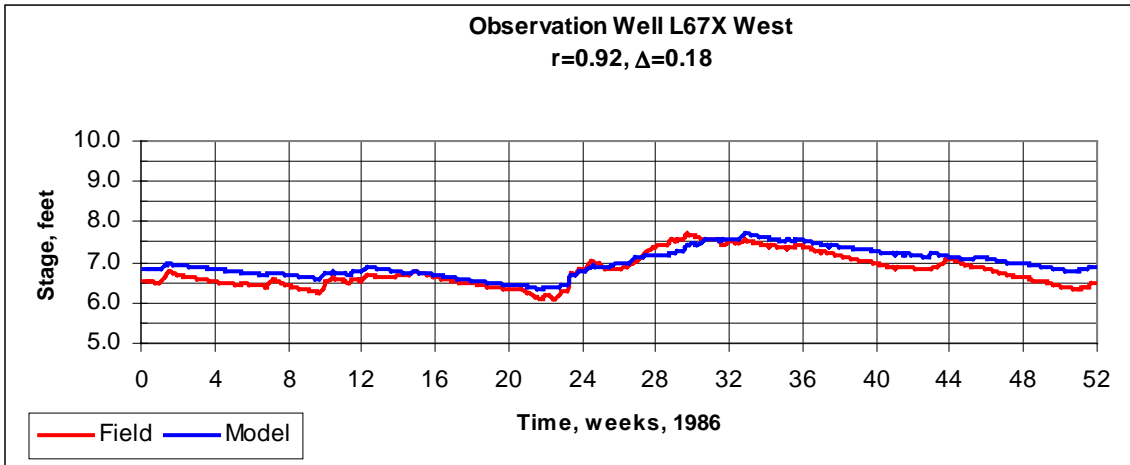


Figure 18: Observation Well L67X West

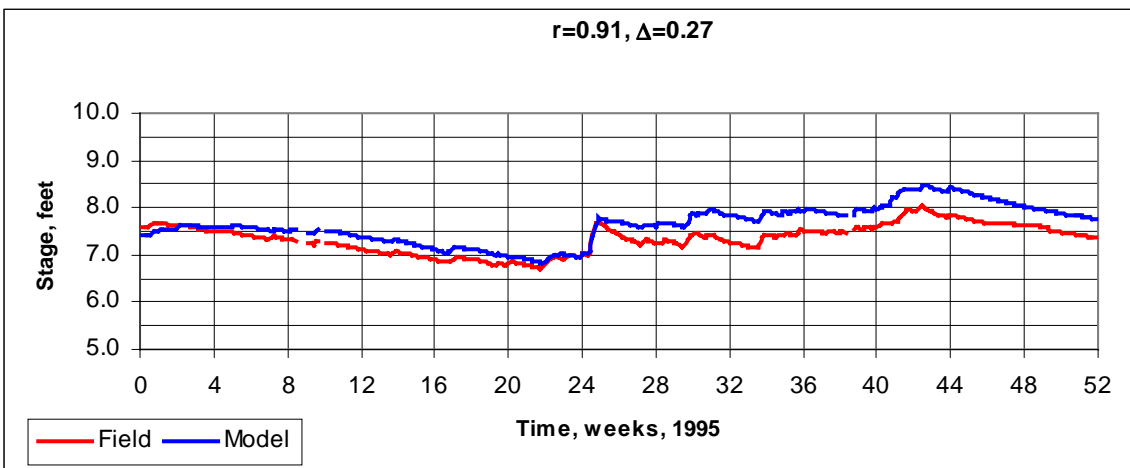
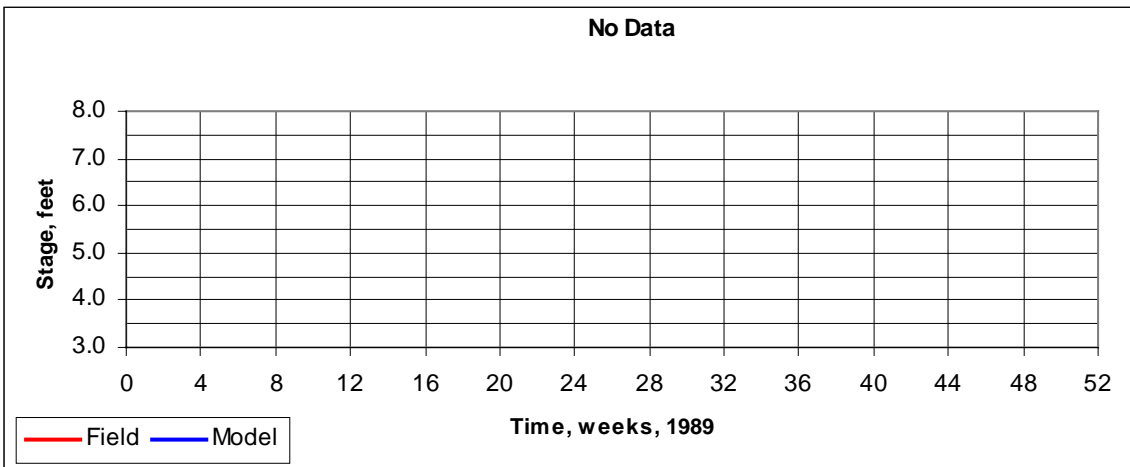
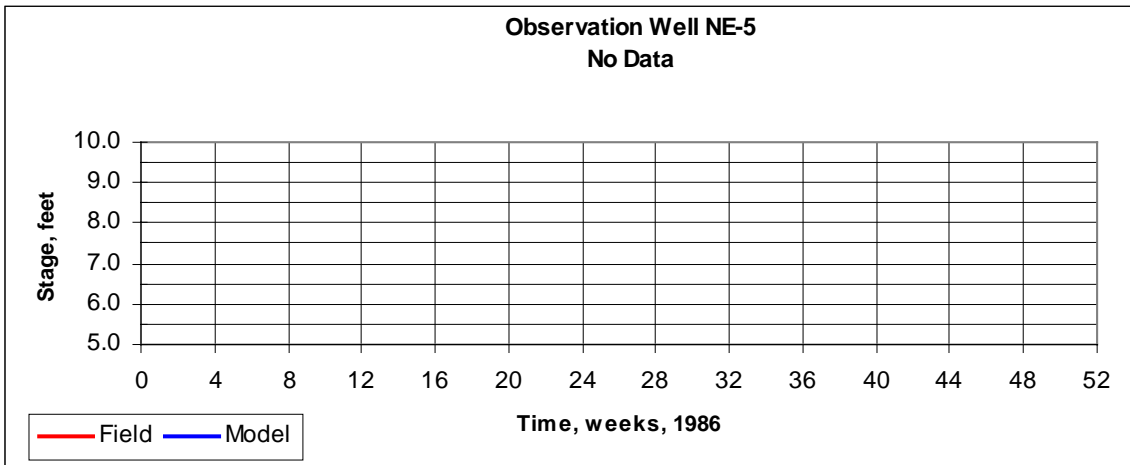


Figure 19: Observation Well NE-5

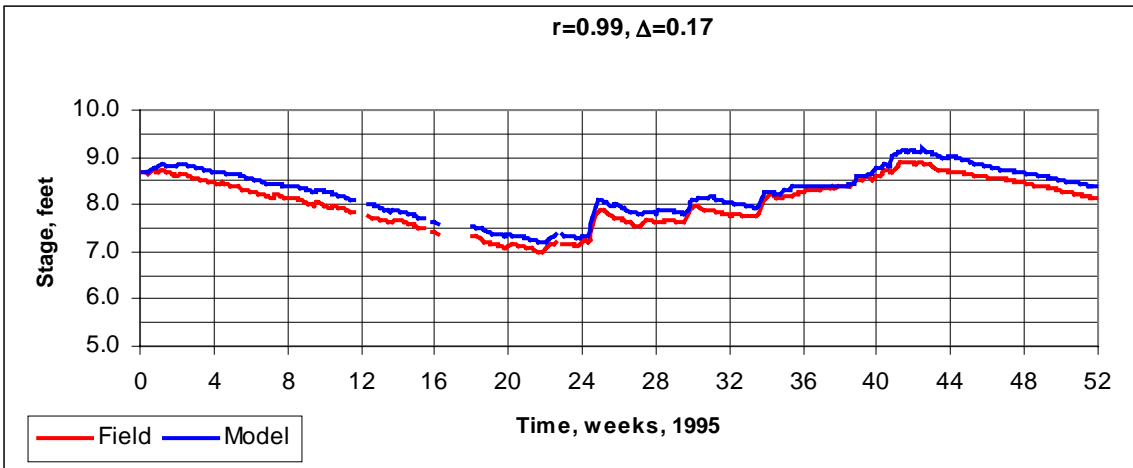
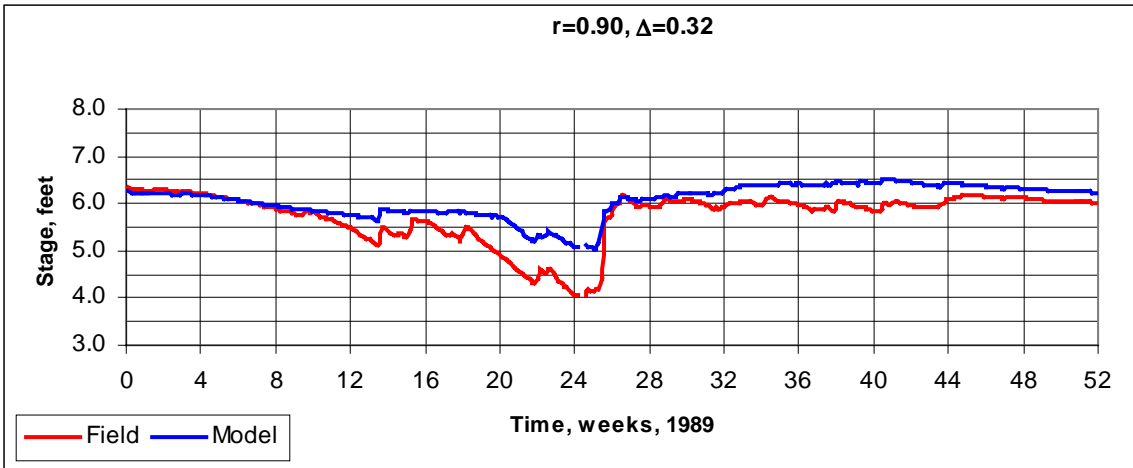
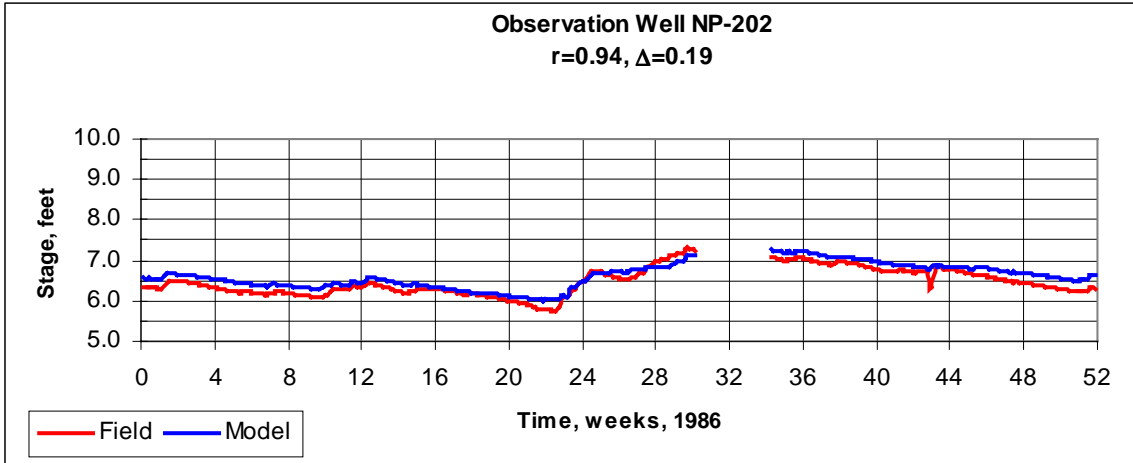


Figure 20: Observation Well NP-202

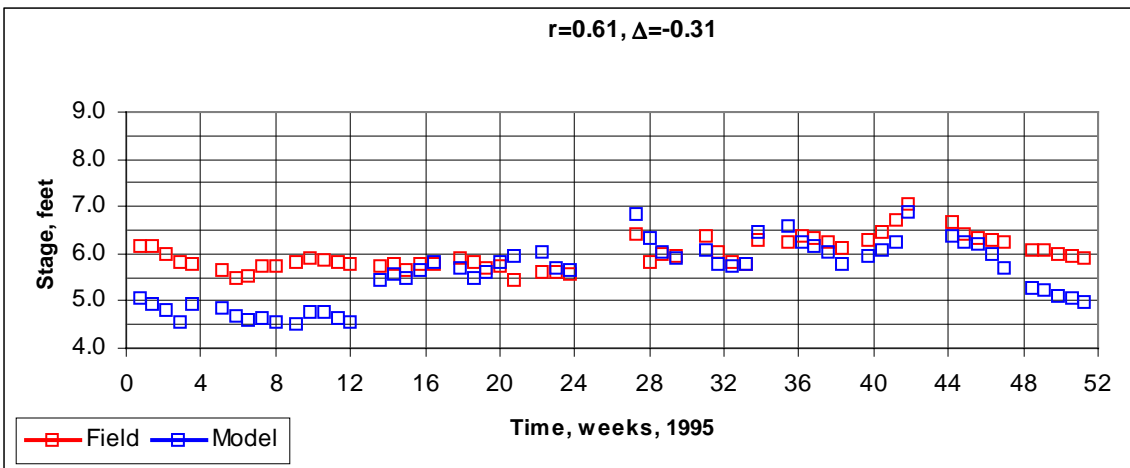
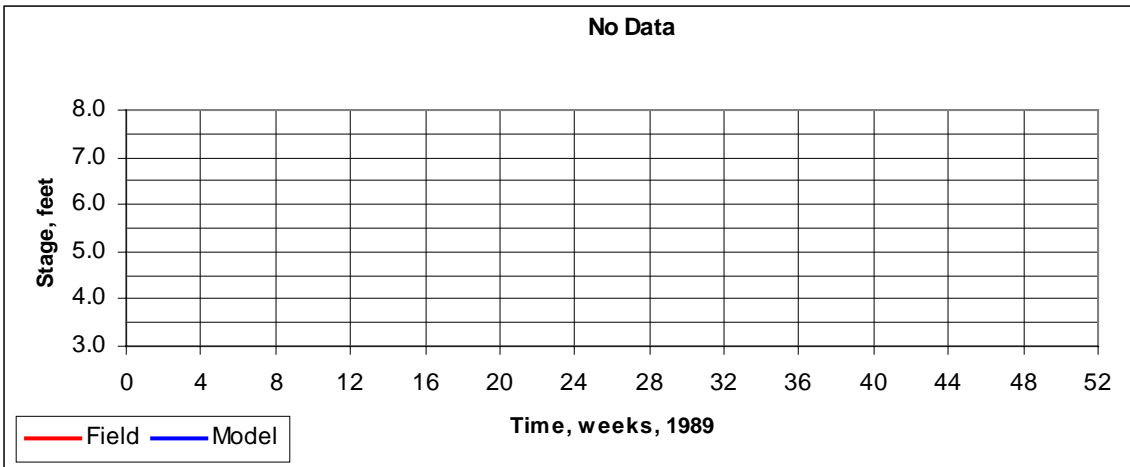
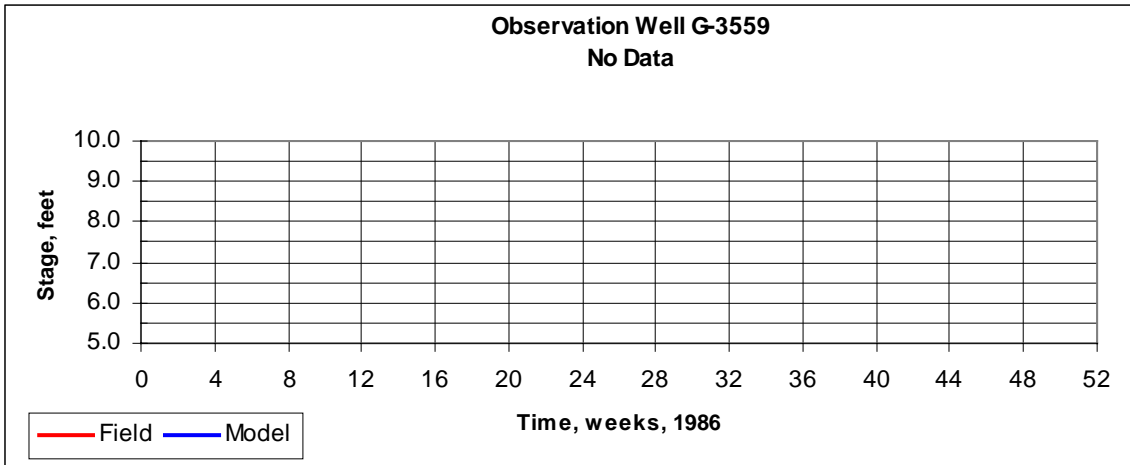


Figure 21 : Observation Well G-3559

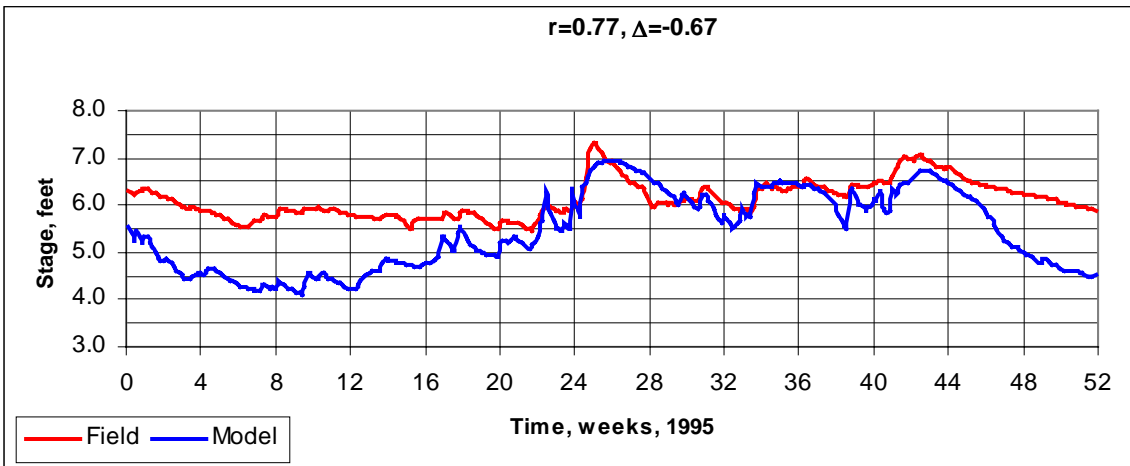
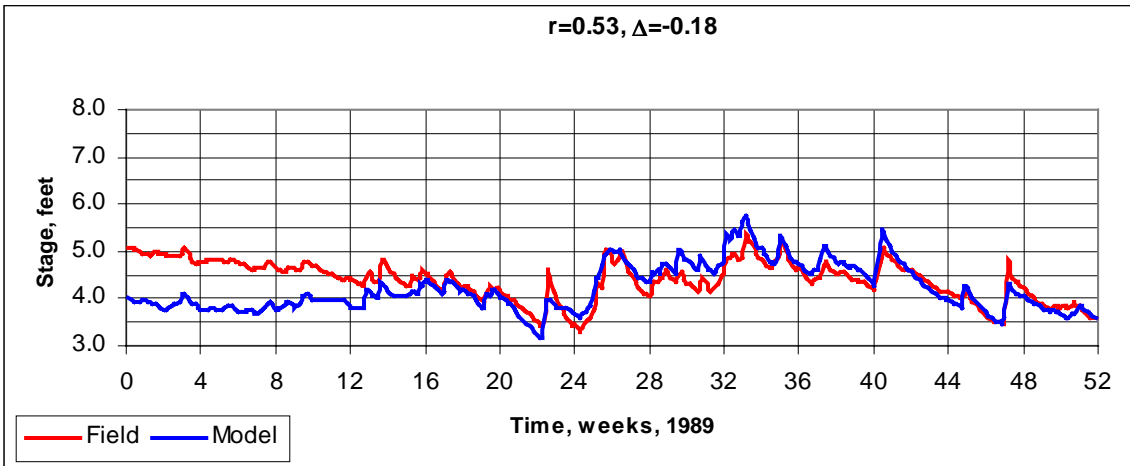
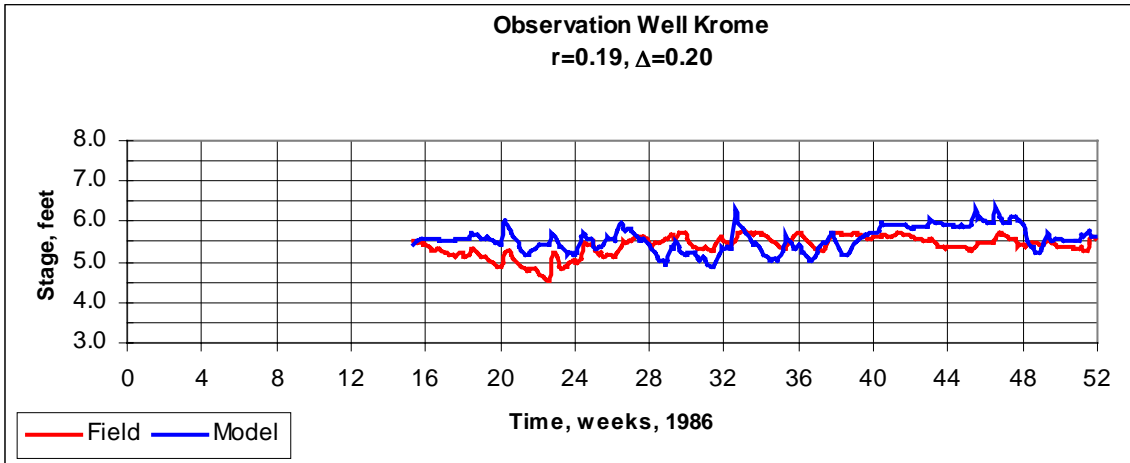


Figure 22: Observation Well: Krome

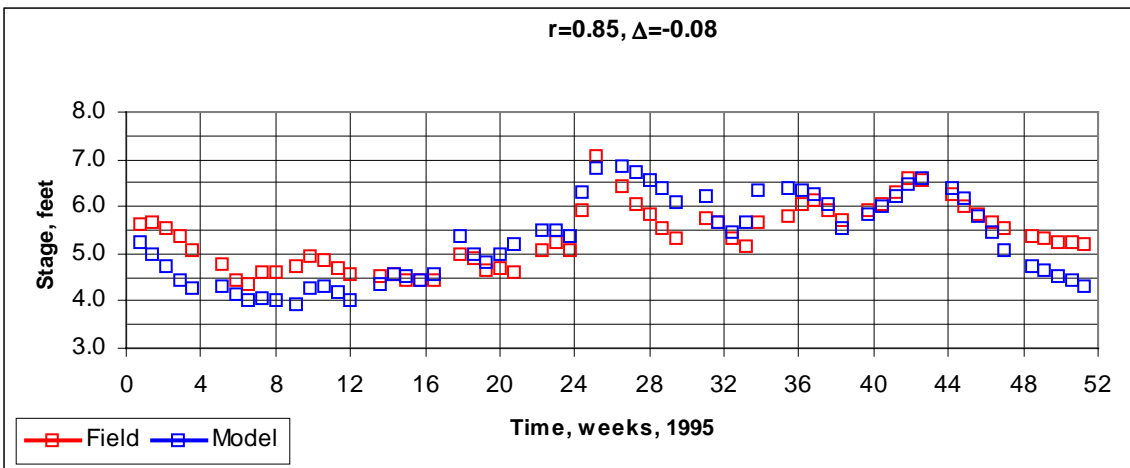
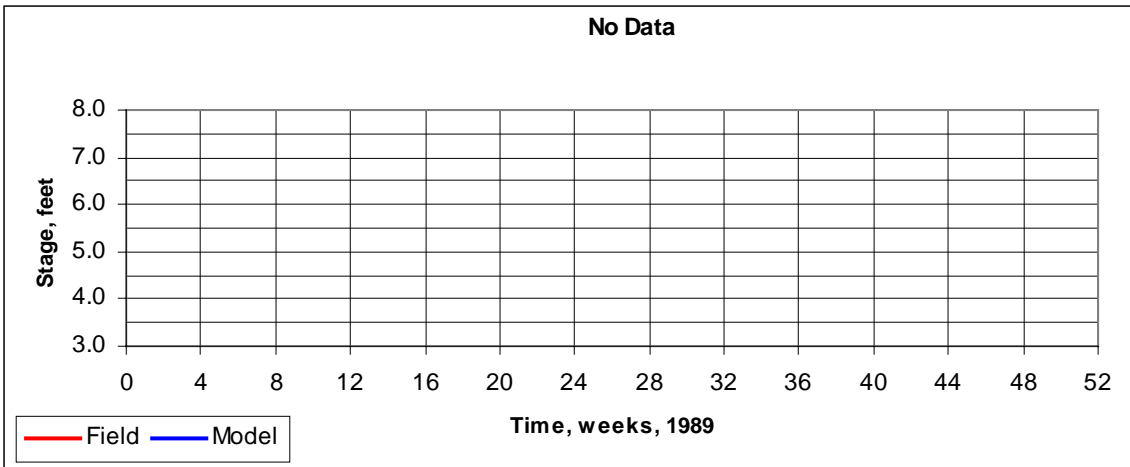
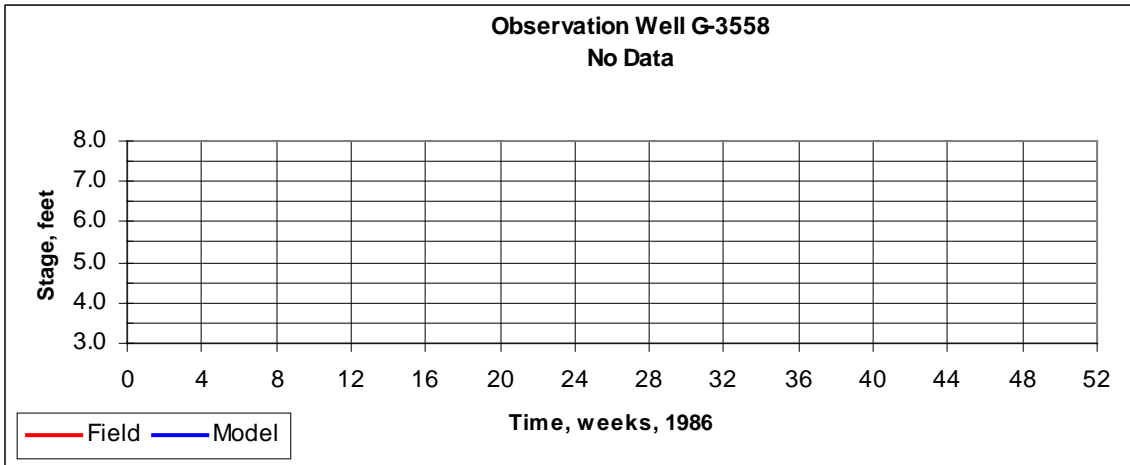


Figure 23: Observation Well G-3558

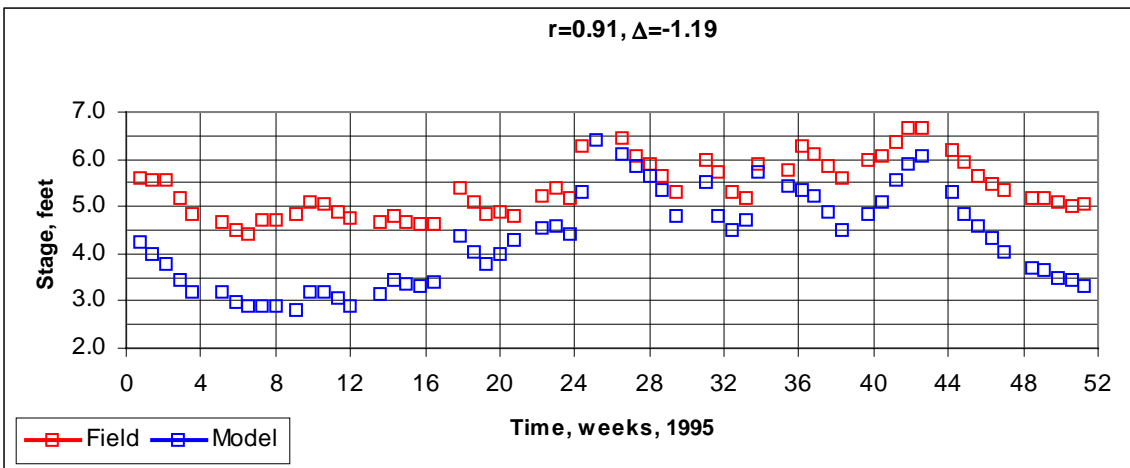
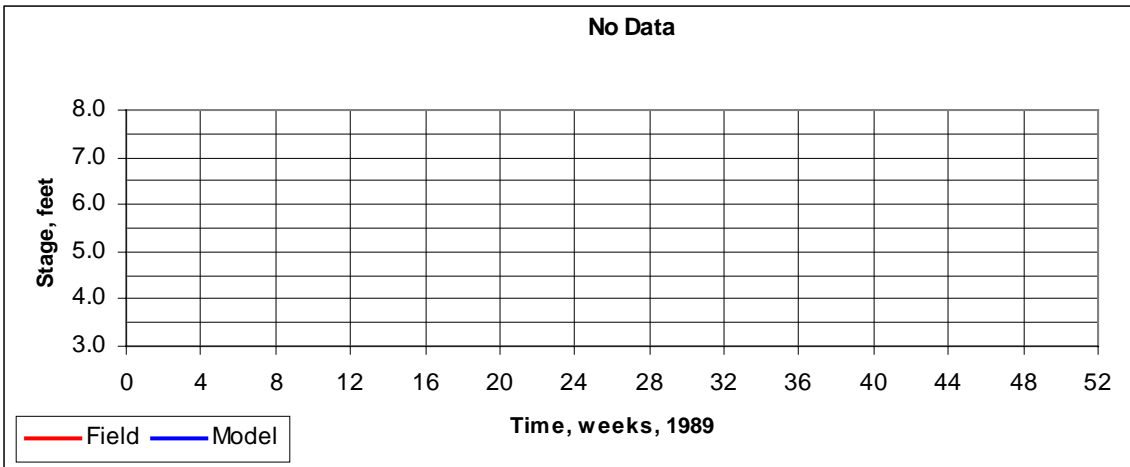
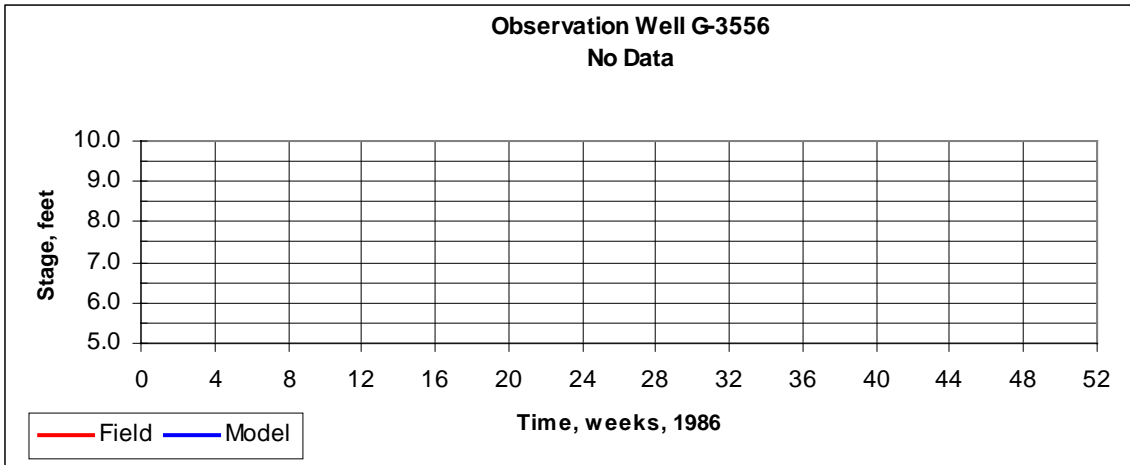


Figure 24: Observation Well: G-3556

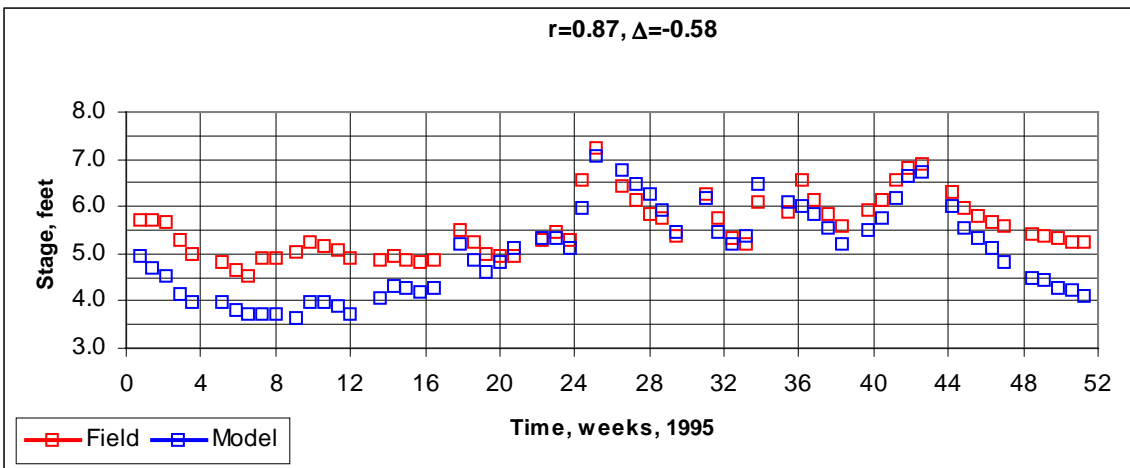
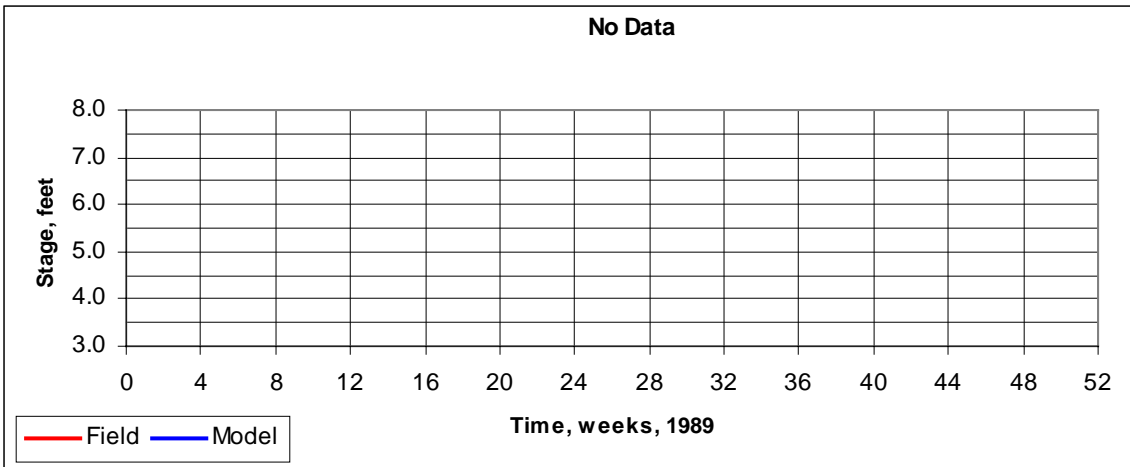
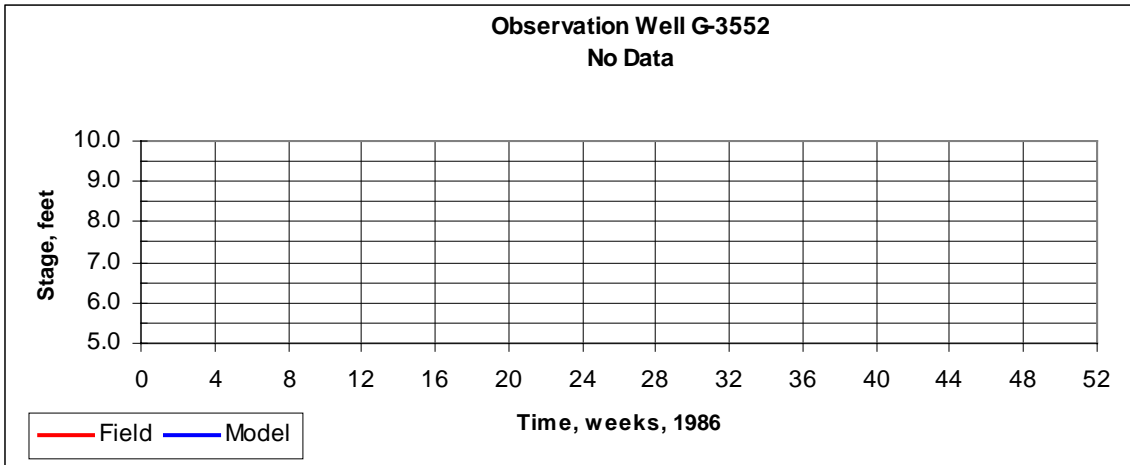


Figure 25: Observation Well G-3552

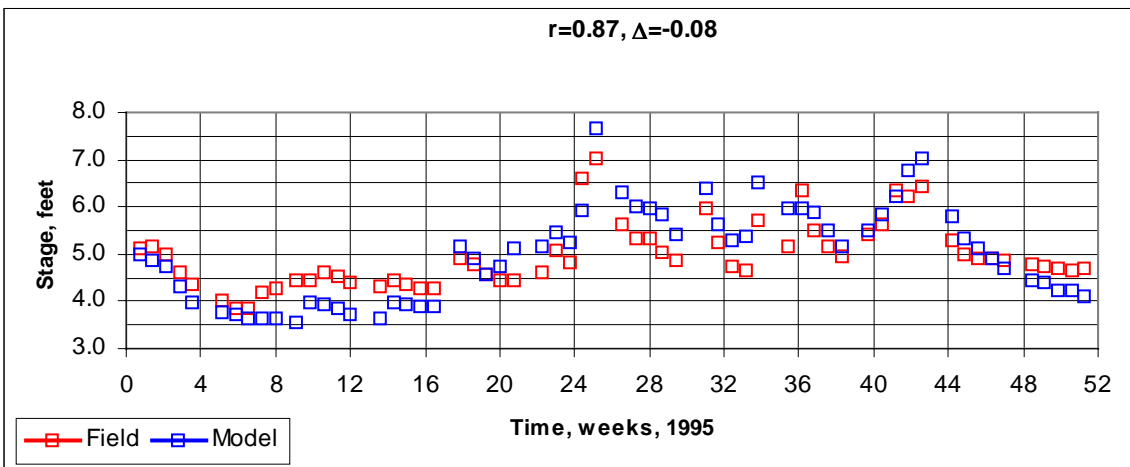
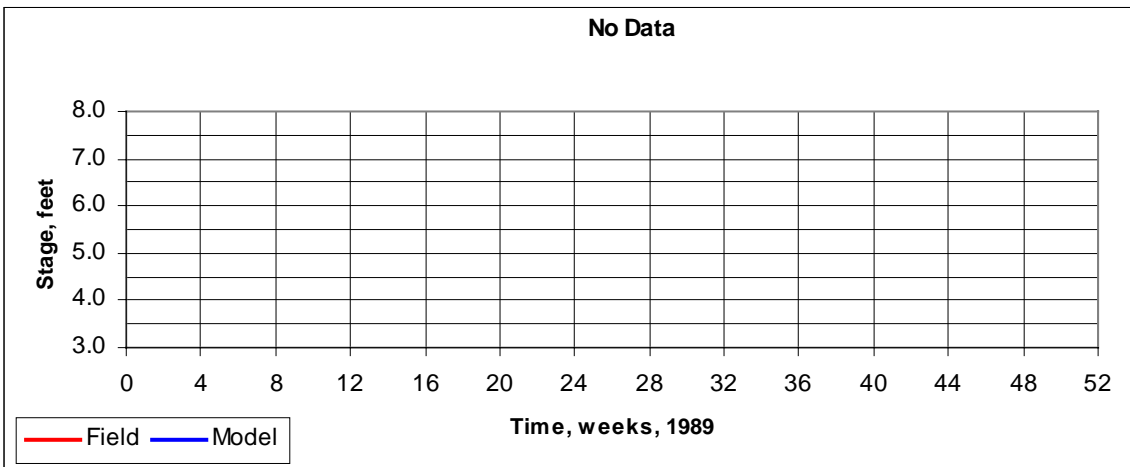
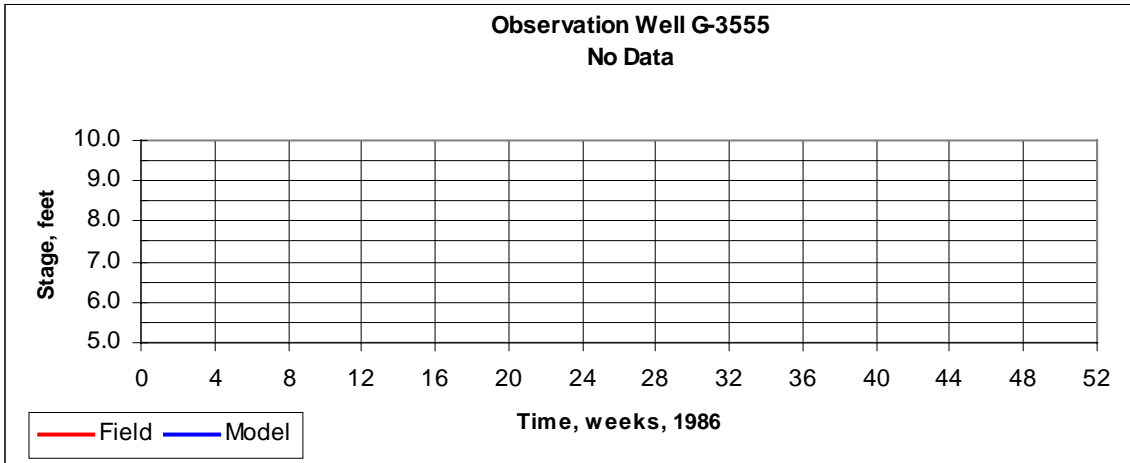


Figure 26: Observation Well G-3555

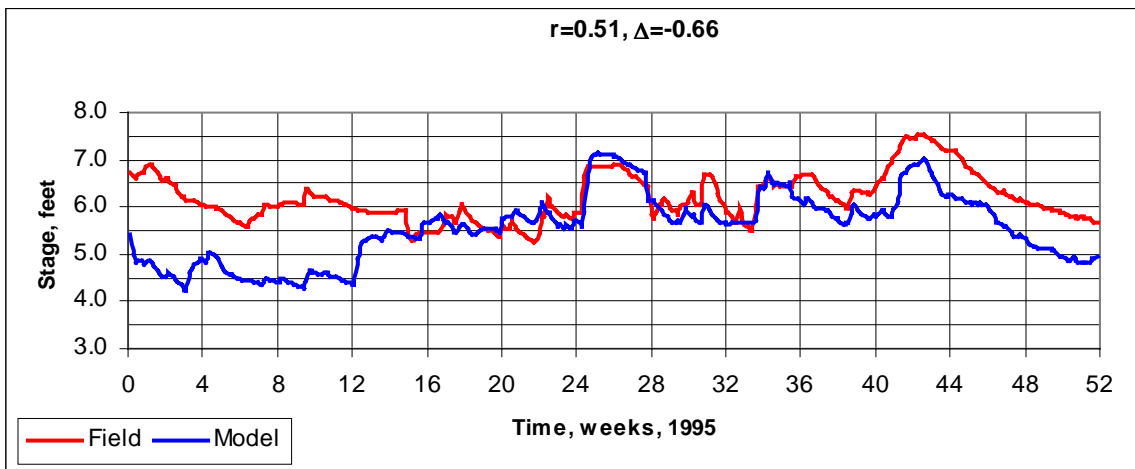
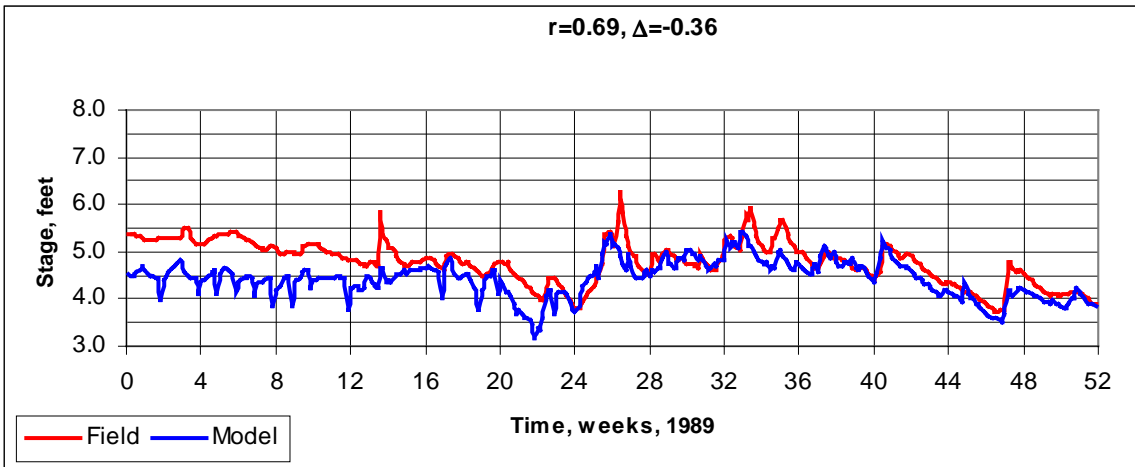
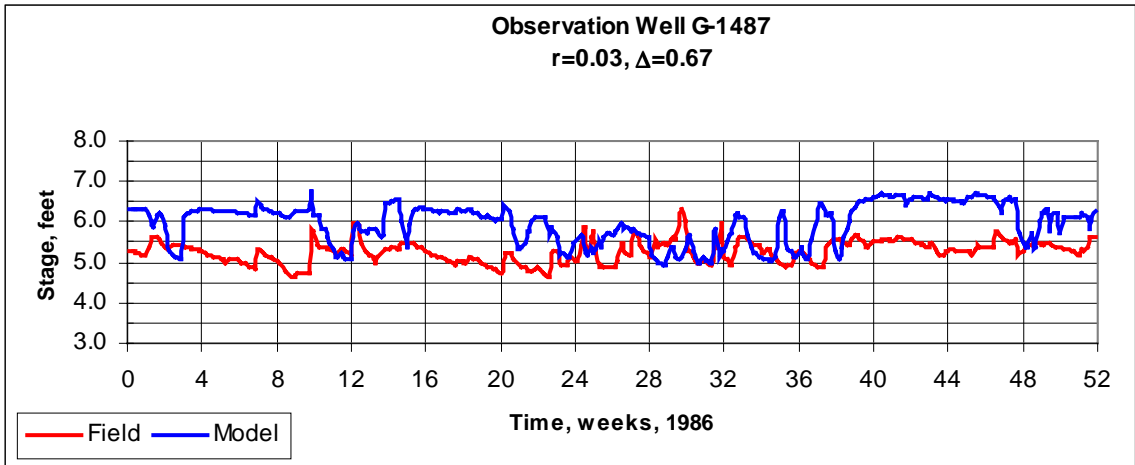


Figure 27: Observation Well G-1487

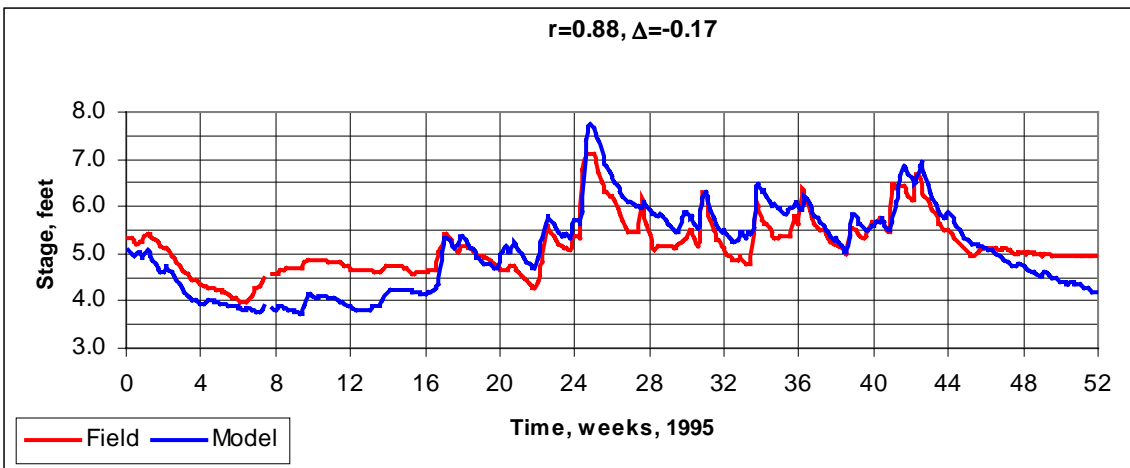
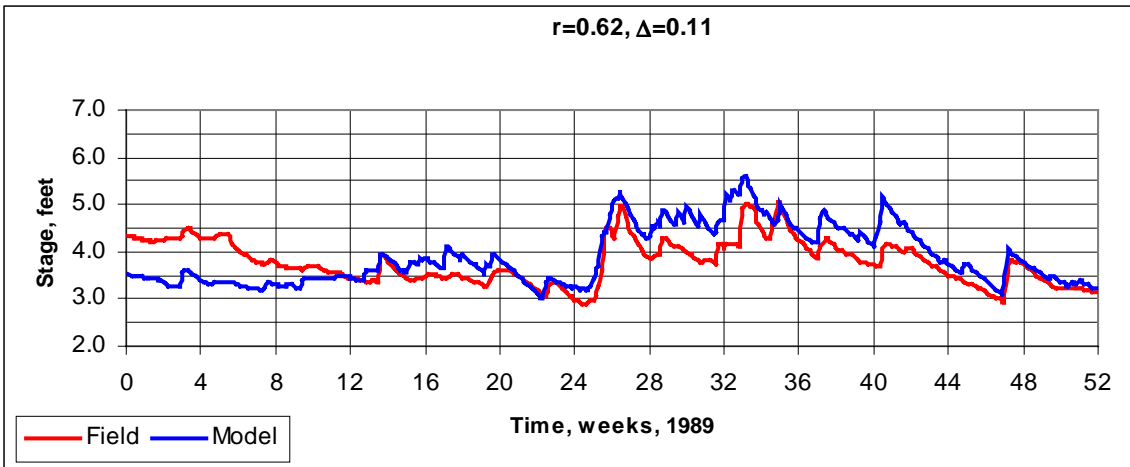
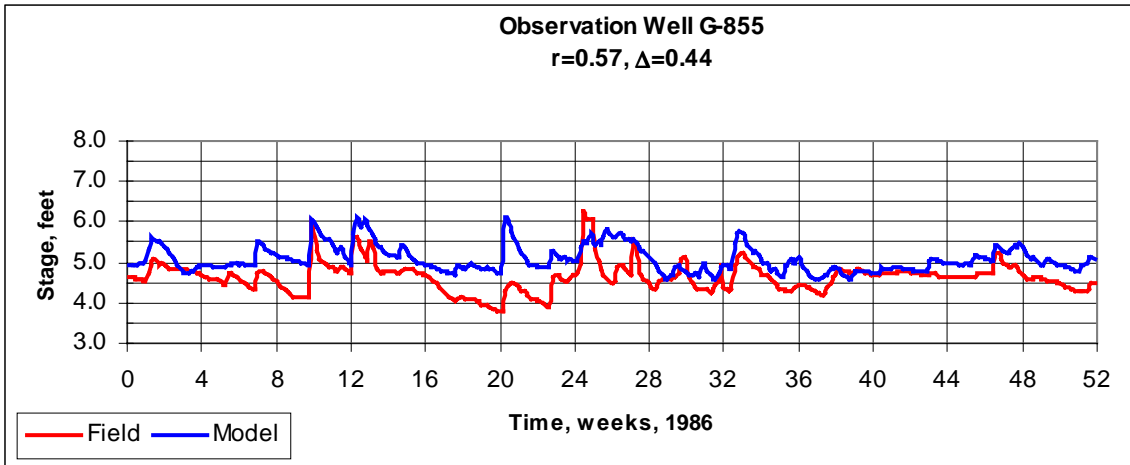


Figure 28: Observation Well G-855

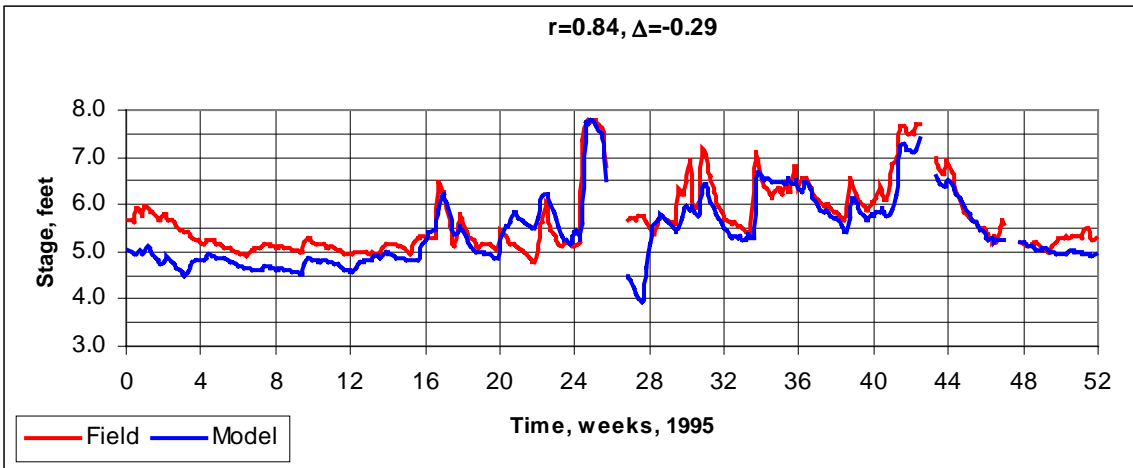
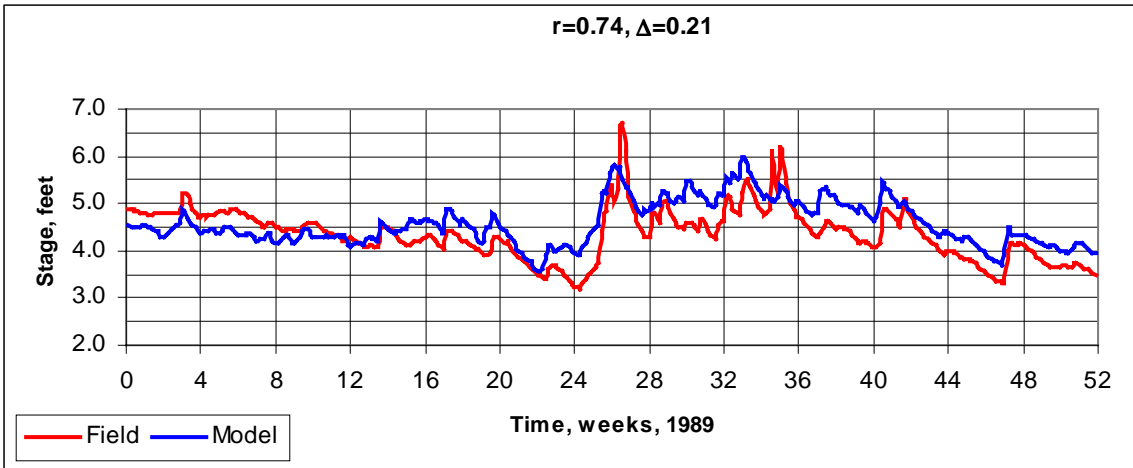
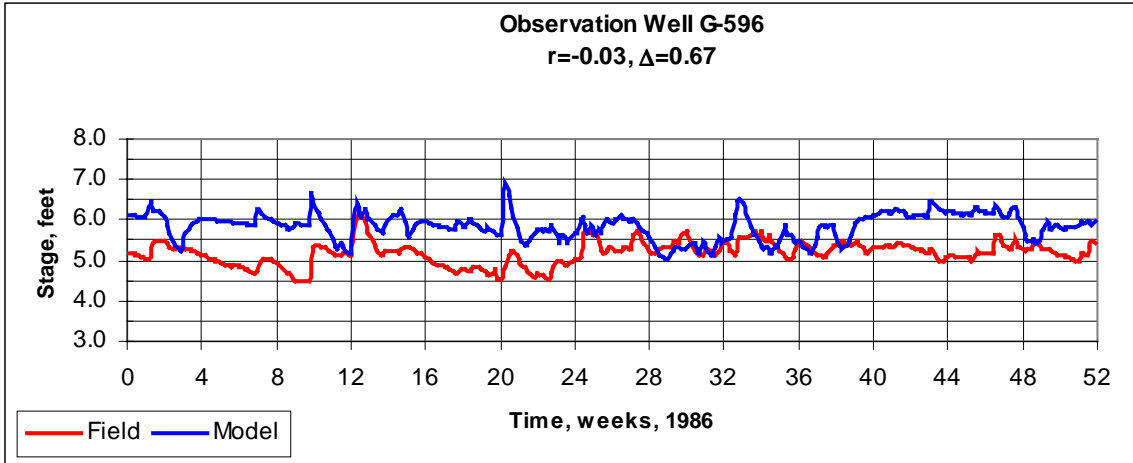


Figure 29 : Observation Well G-596

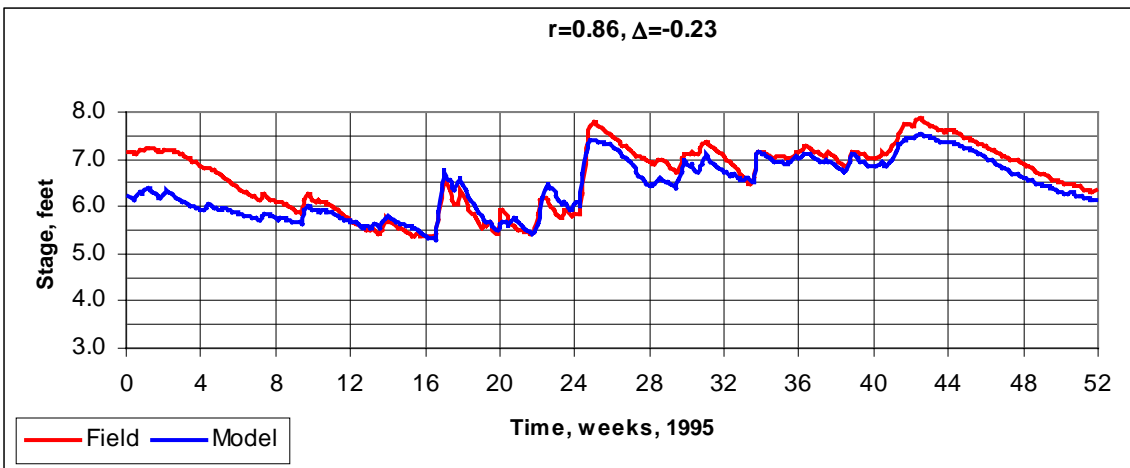
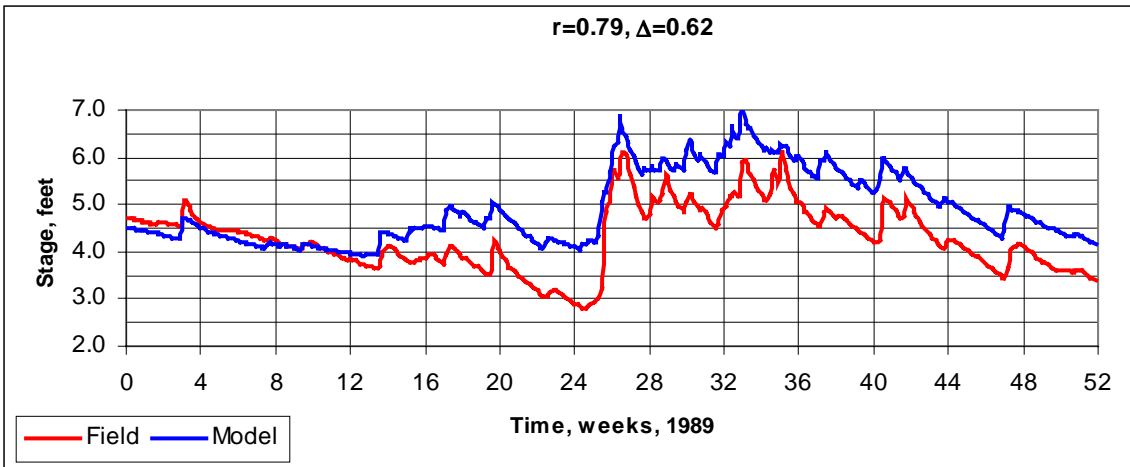
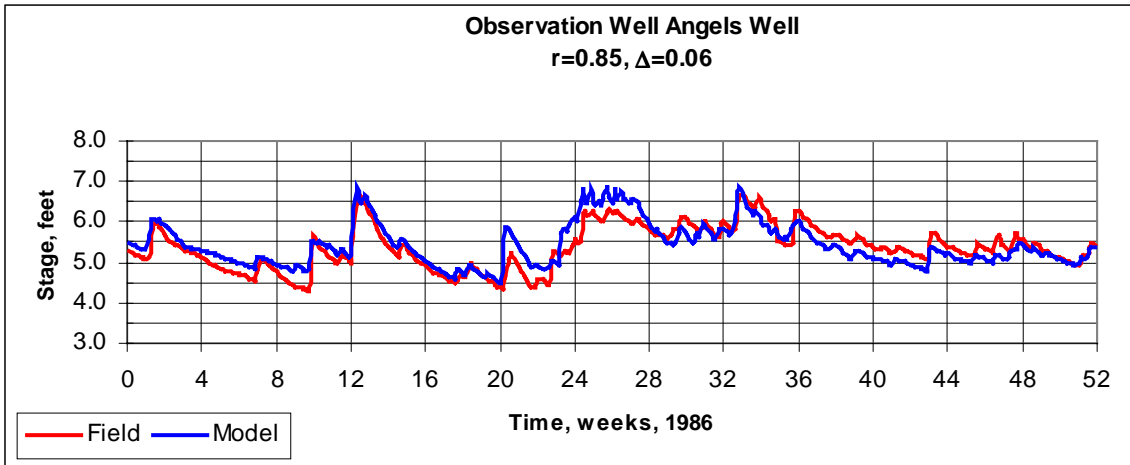


Figure 30: Observation Well Angels Well

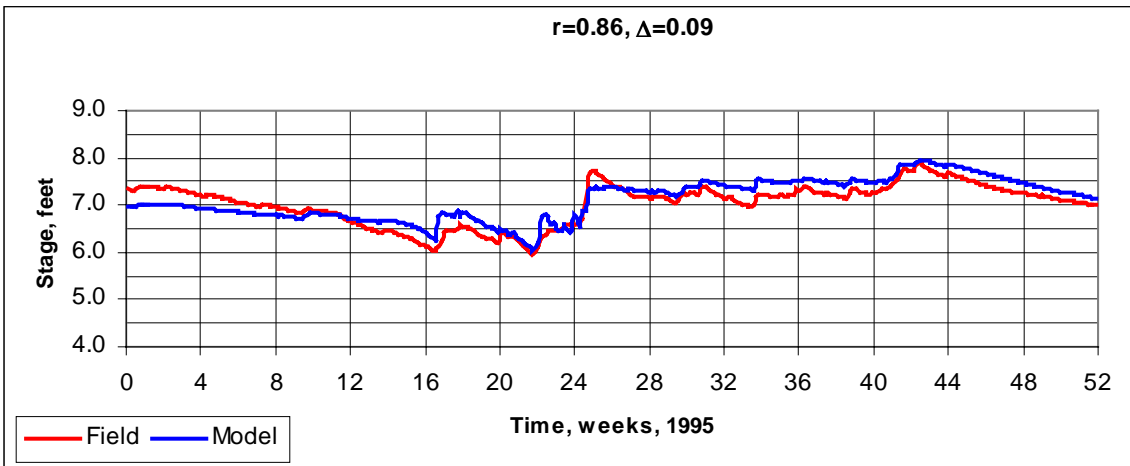
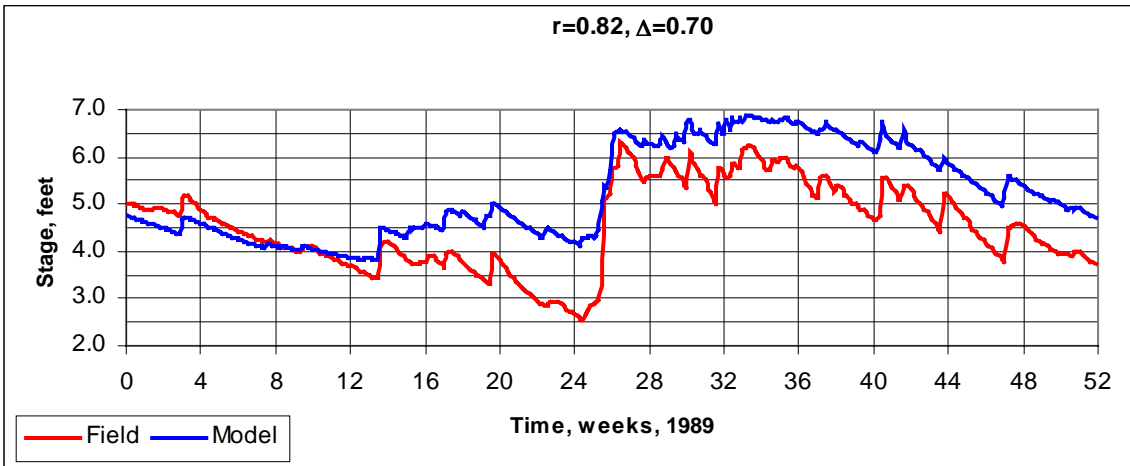
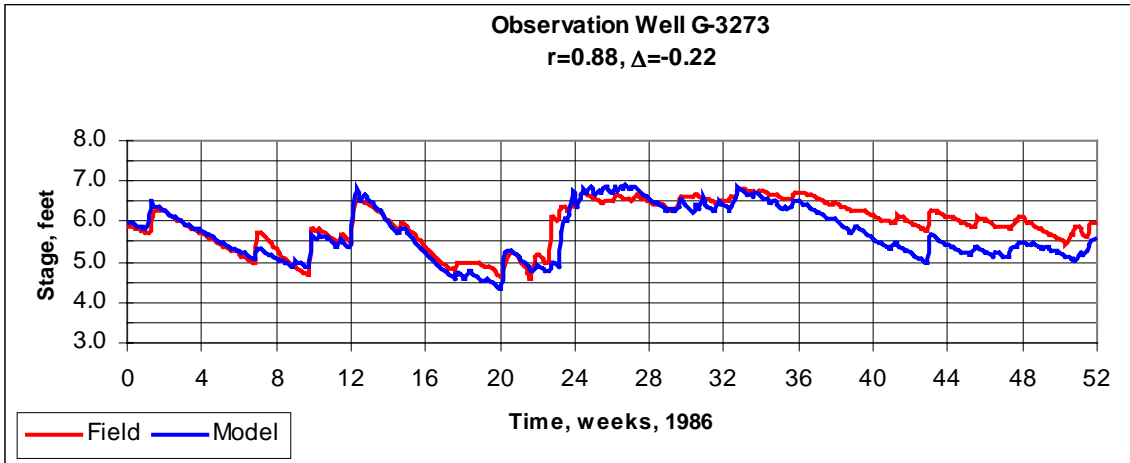


Figure 31: Observation Well G-3273

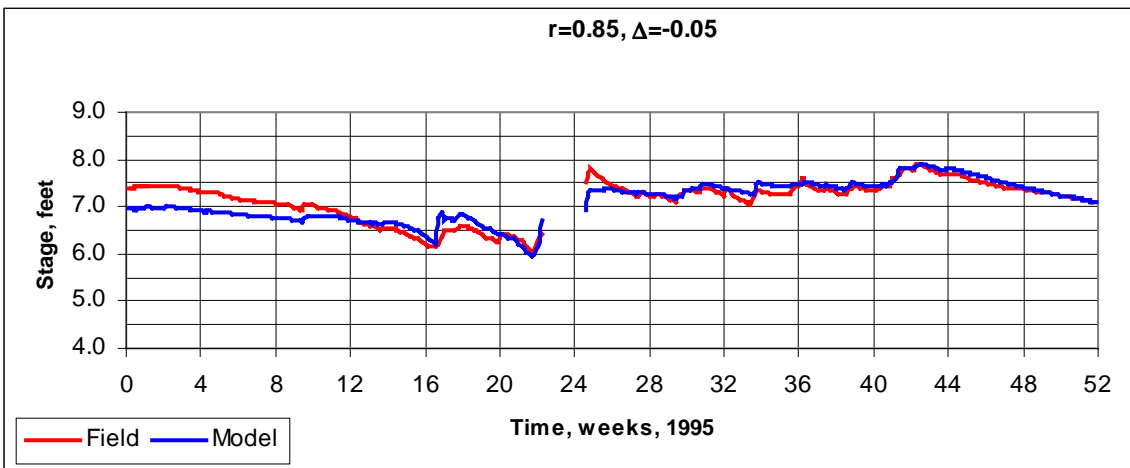
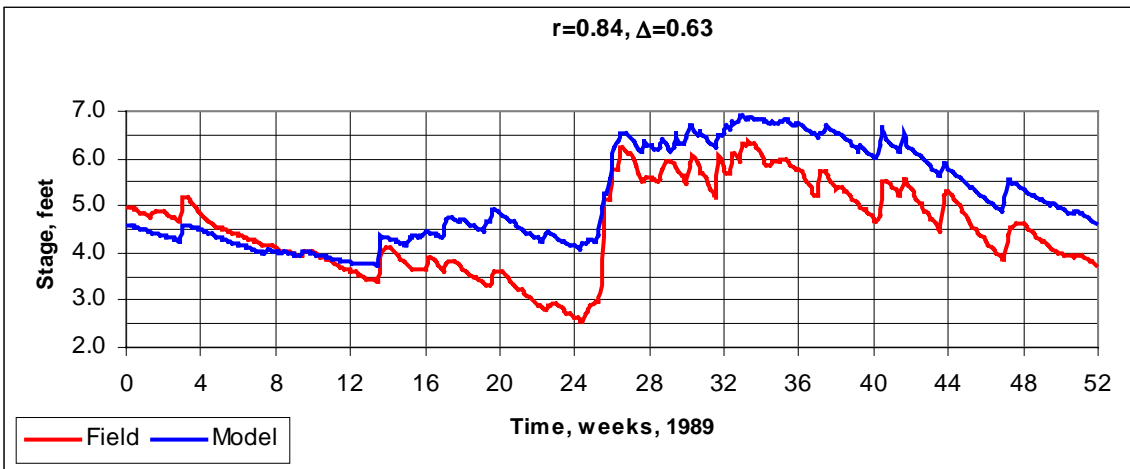
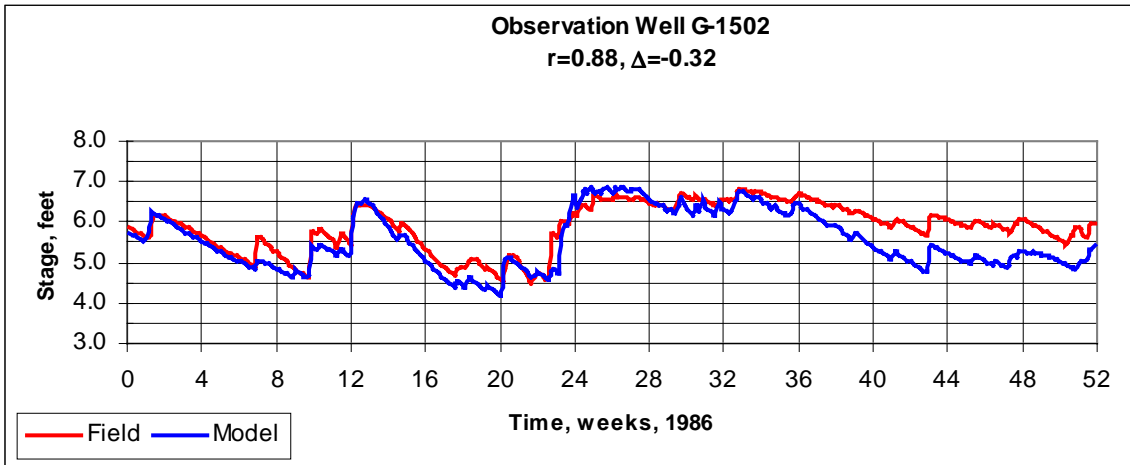


Figure 32: Observation Well G-1502

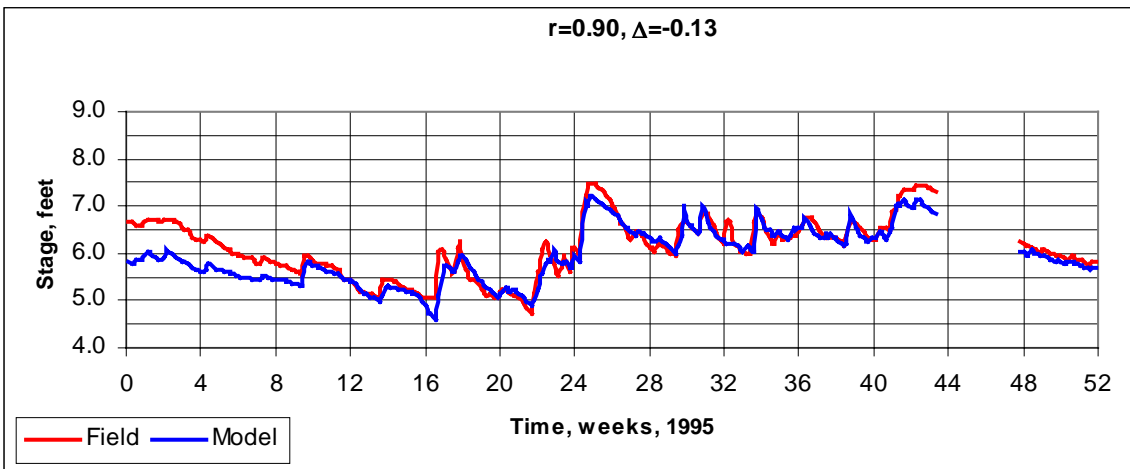
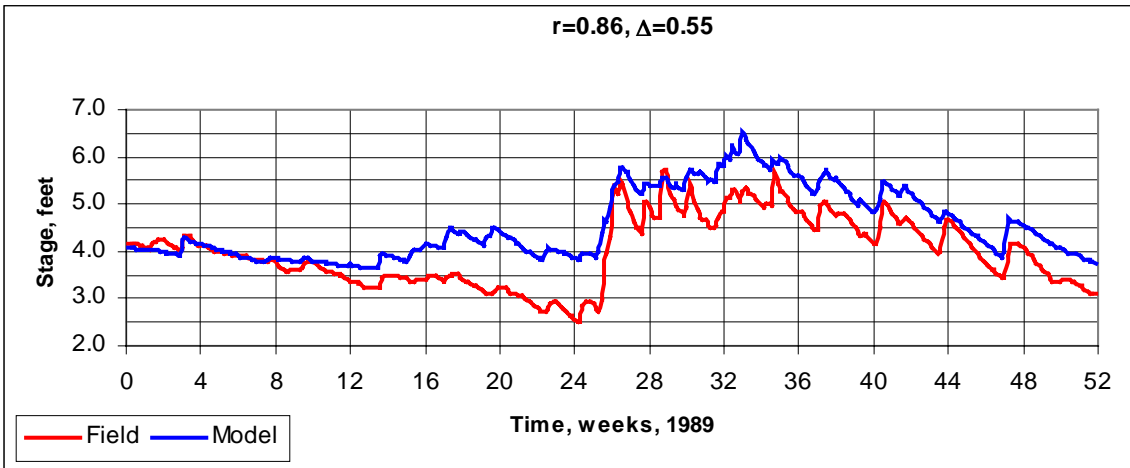
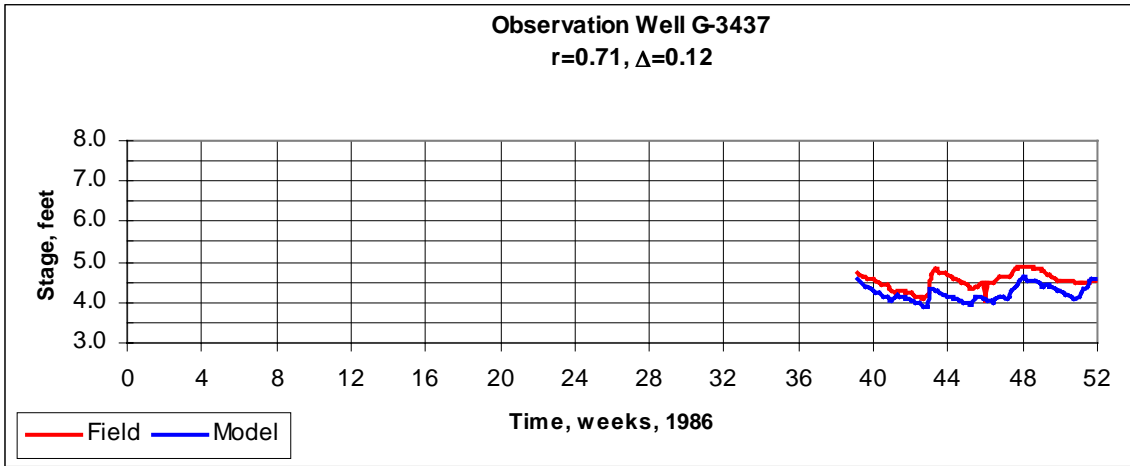


Figure 33: Observation Well G-3437

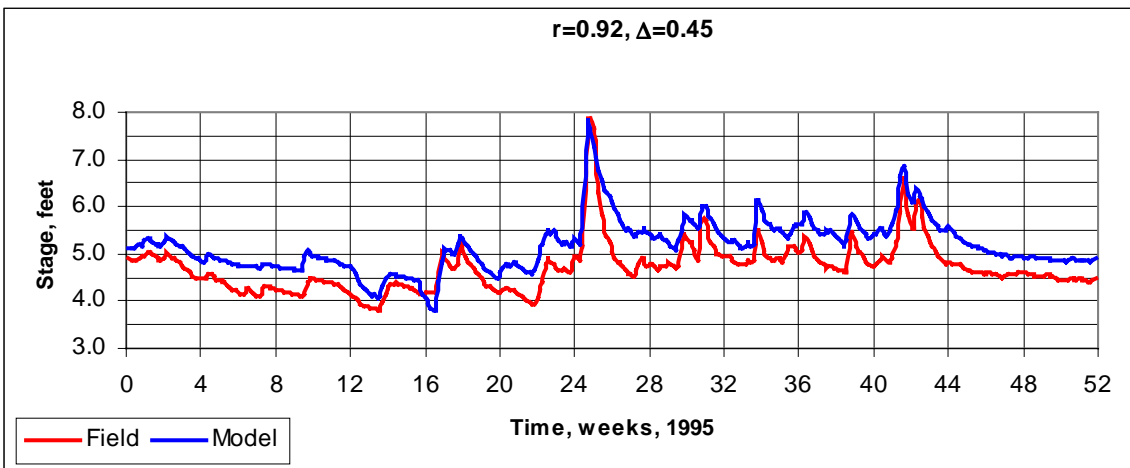
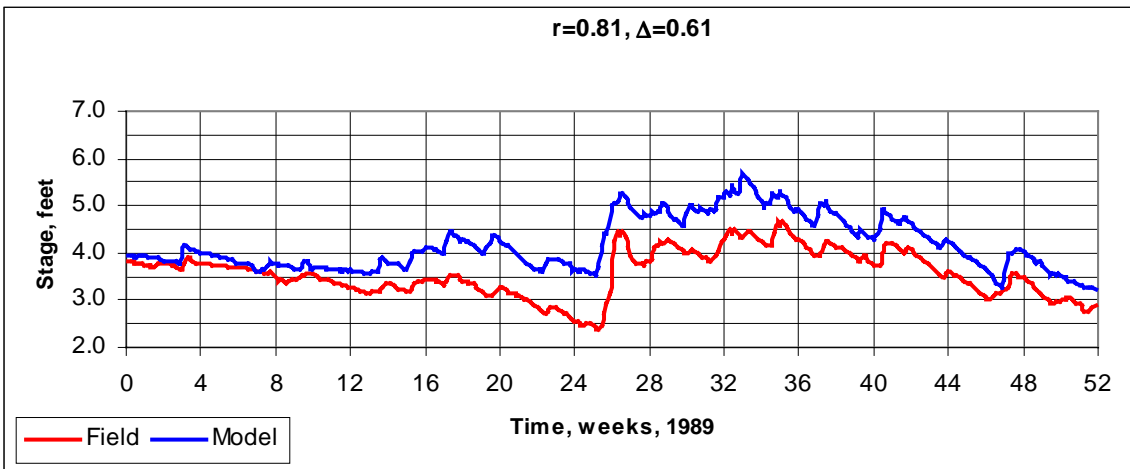
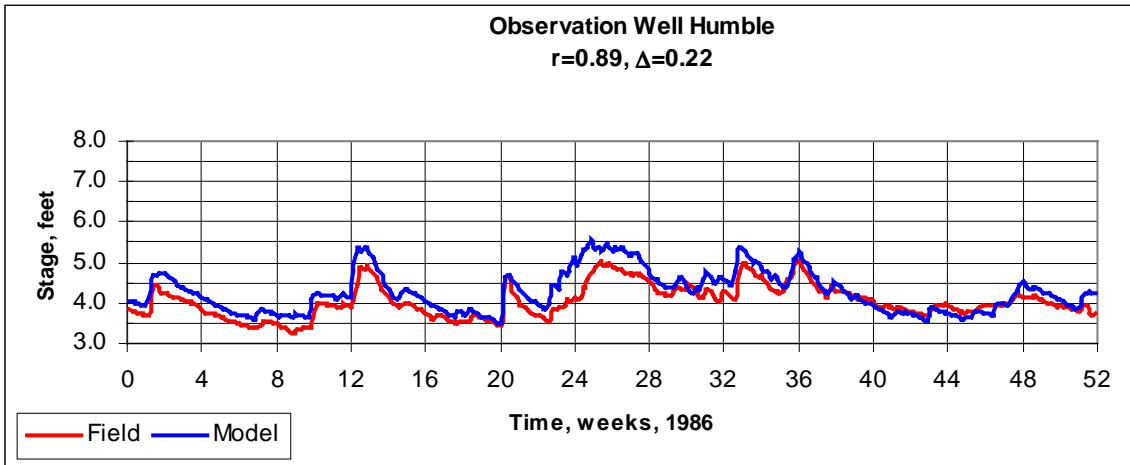


Figure 34: Observation Well Humble

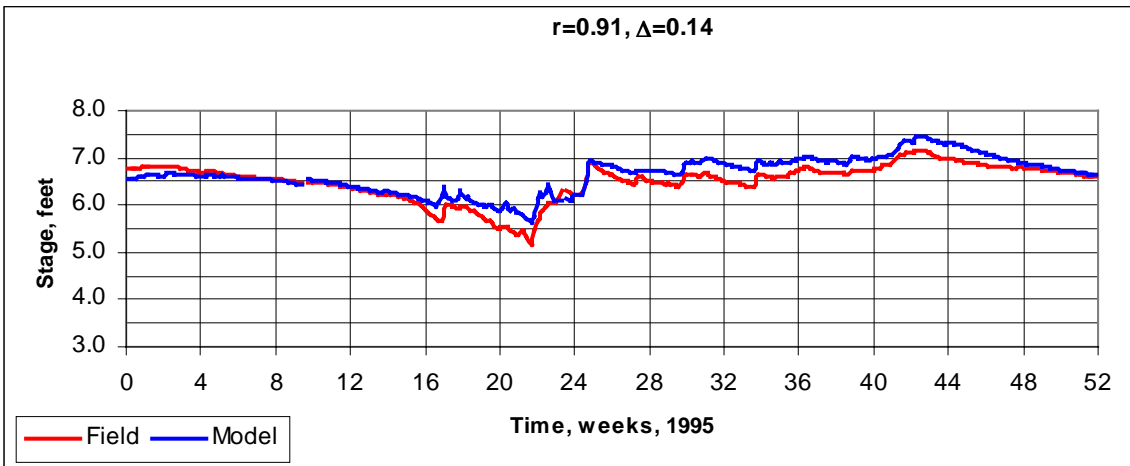
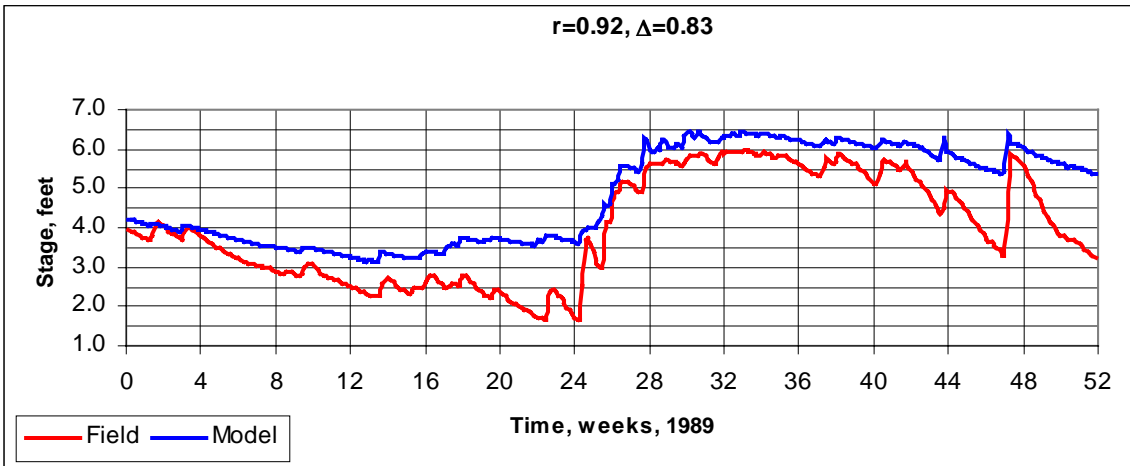
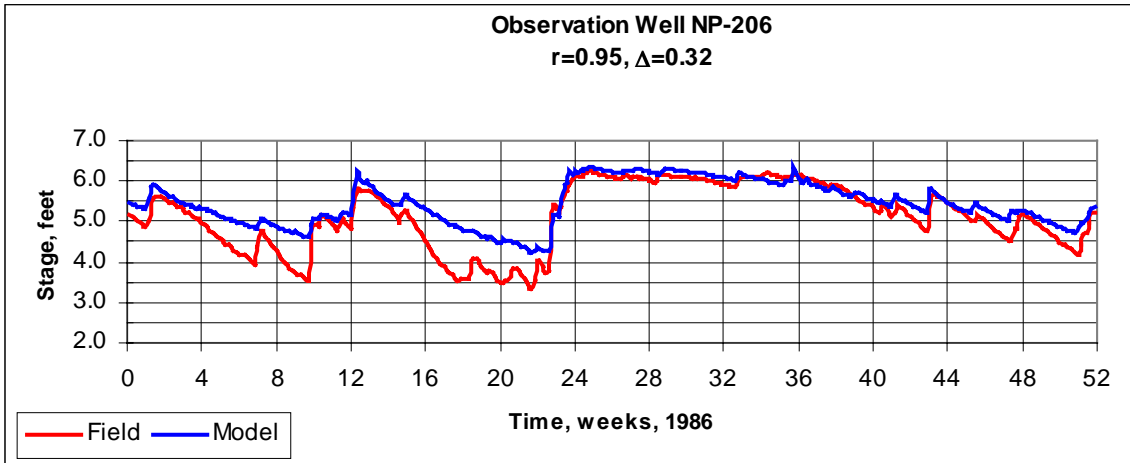


Figure 35: Observation Well NP-206

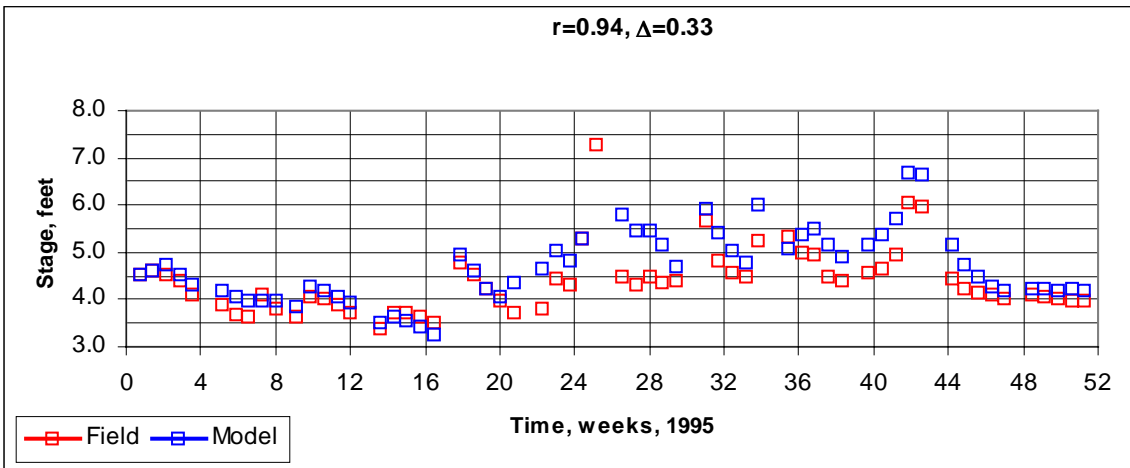
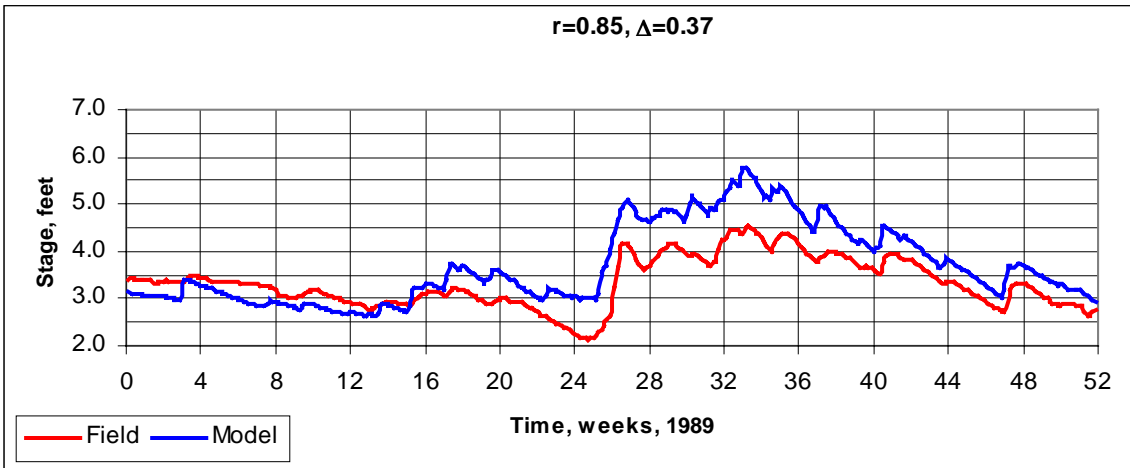
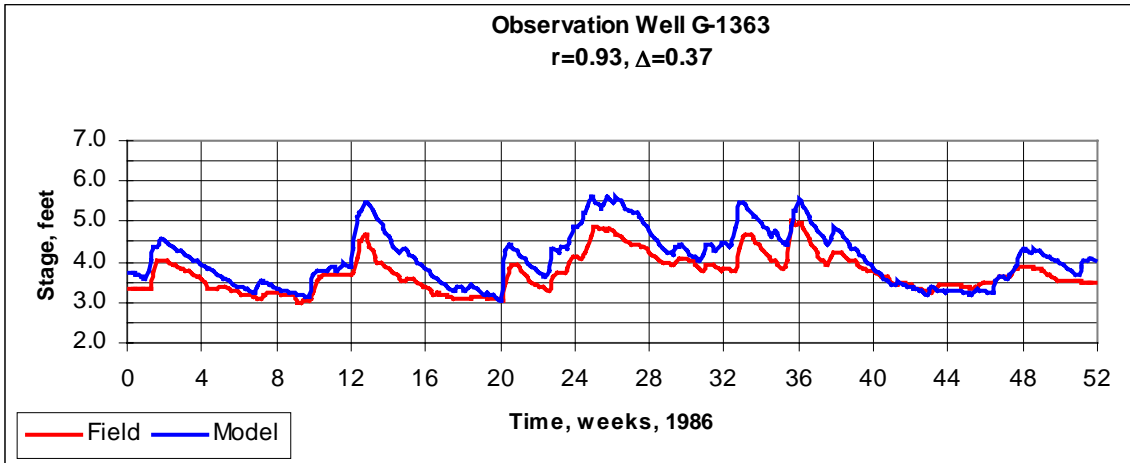


Figure 36: Observation Well G-1363

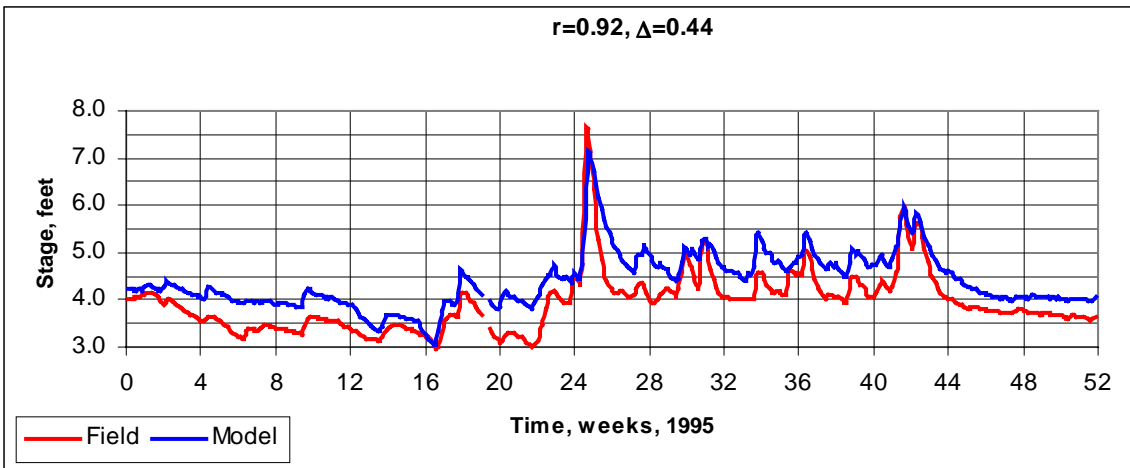
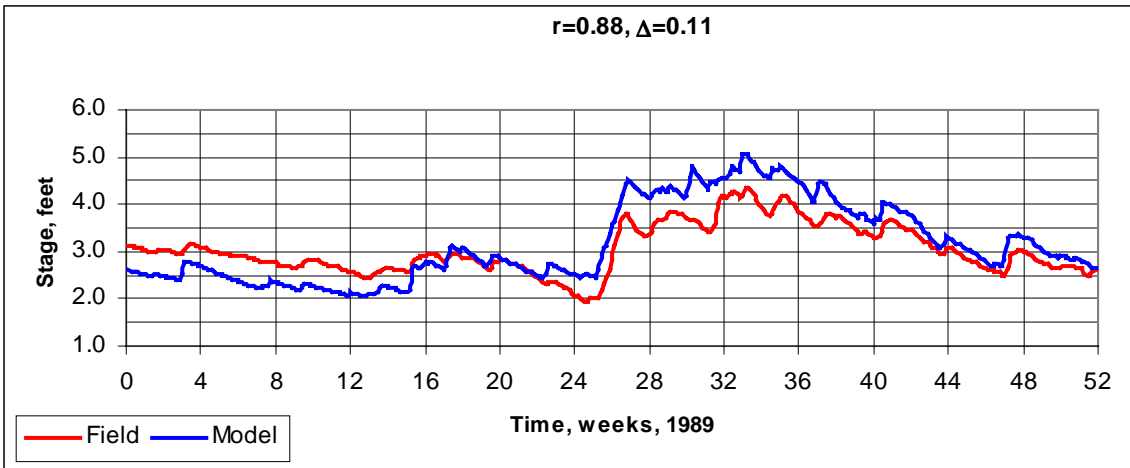
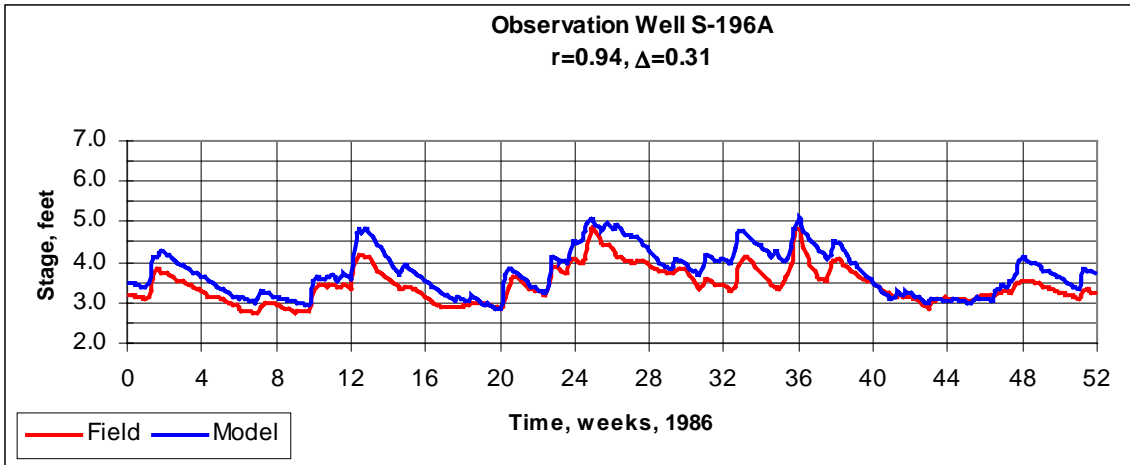


Figure 37: Observation Well S-196A

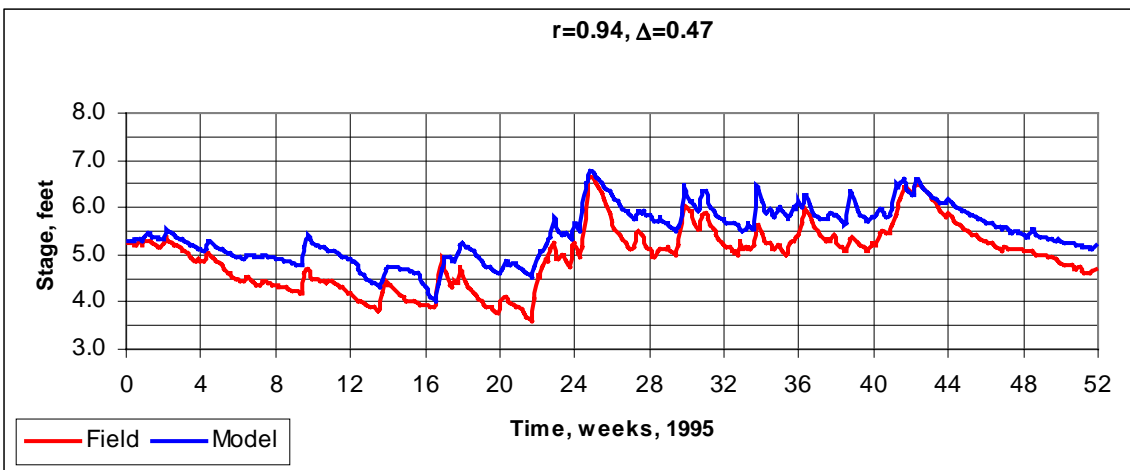
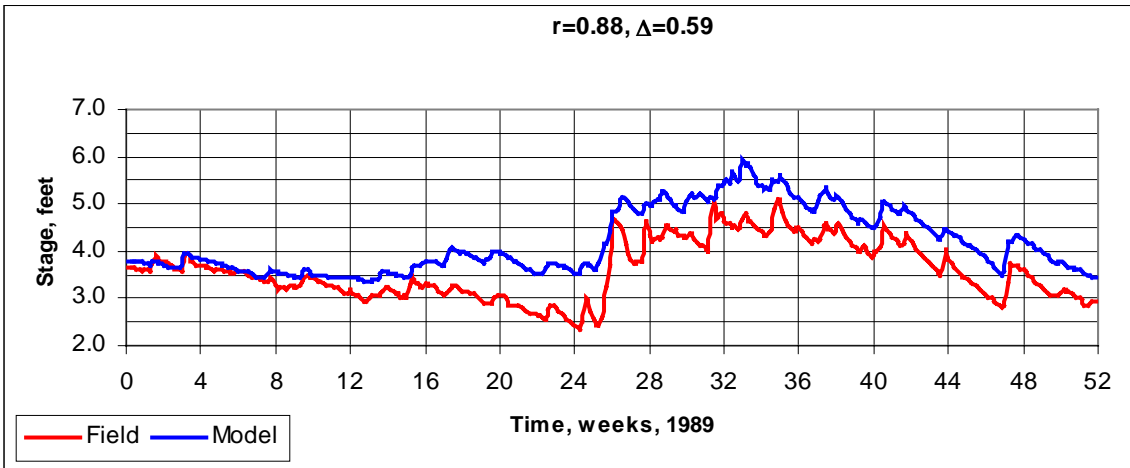
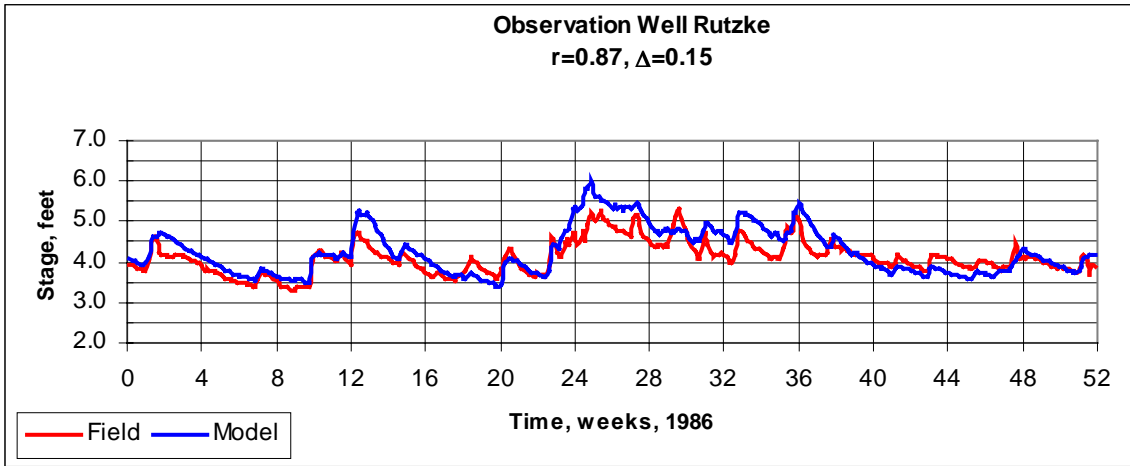


Figure 38: Observation Well Rutzke

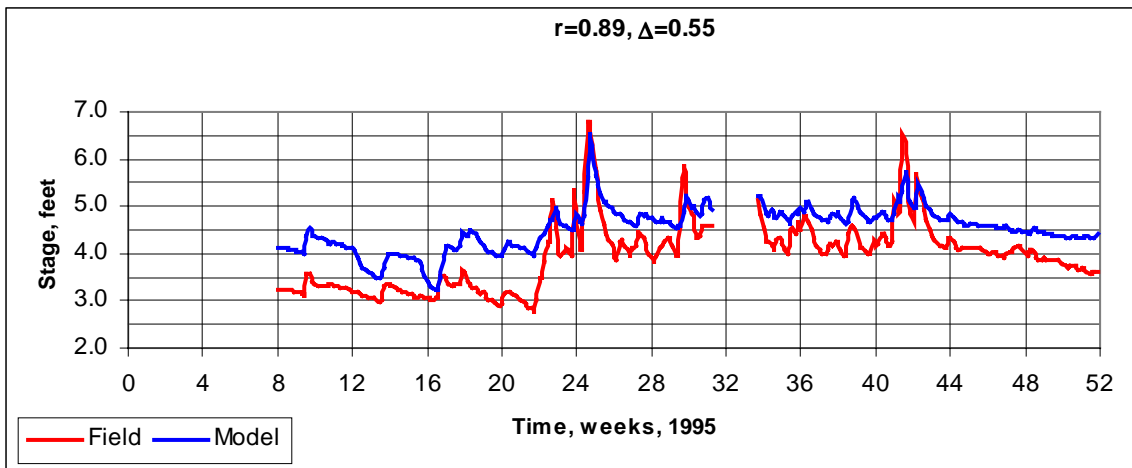
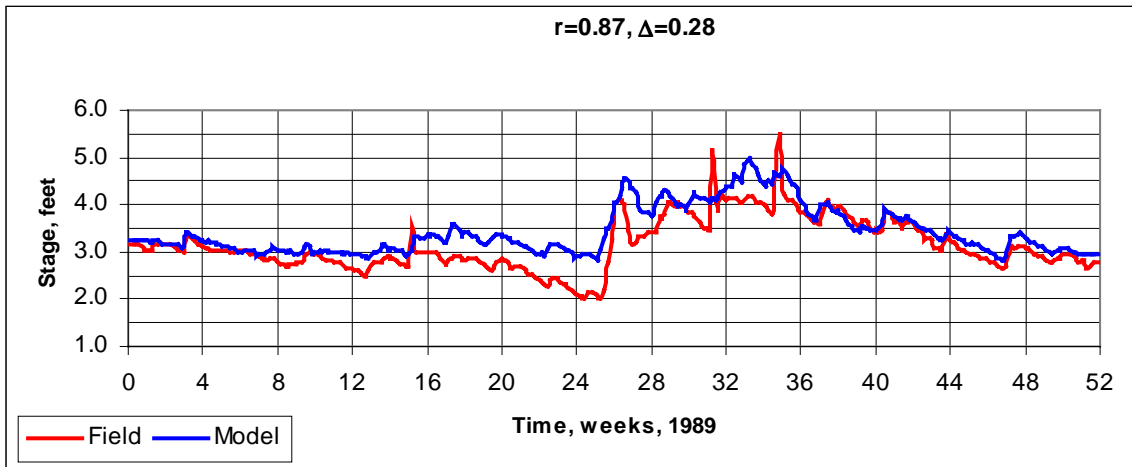
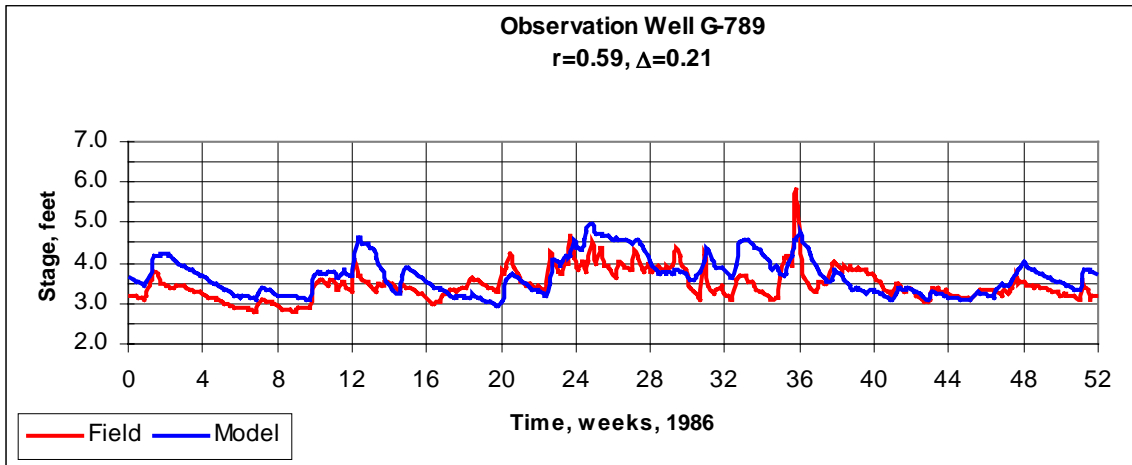


Figure 39 : Observation Well G-789

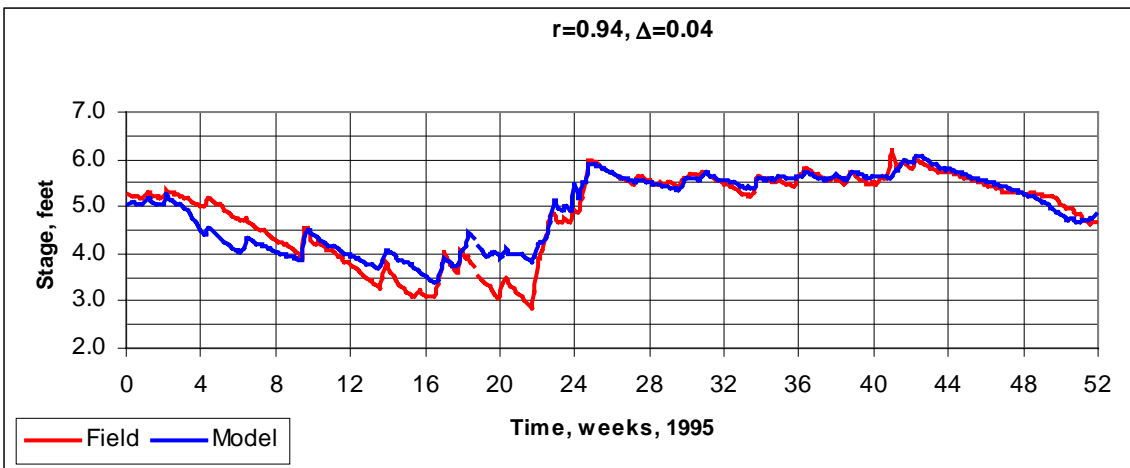
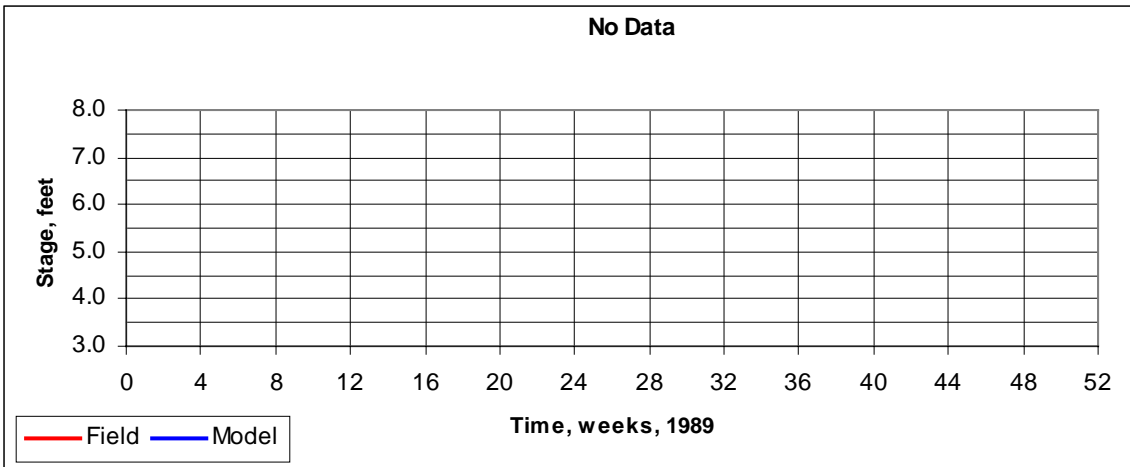
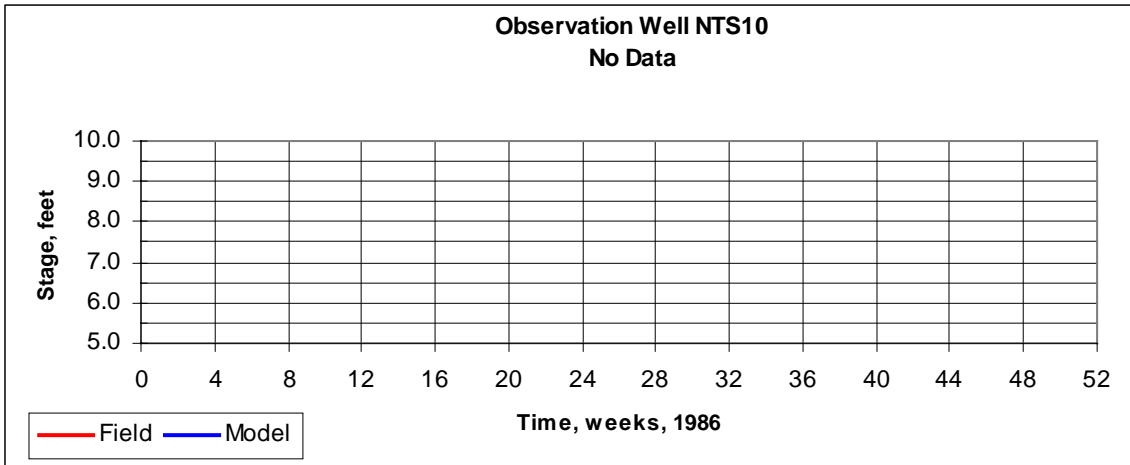


Figure 40: Observation Well NTS10

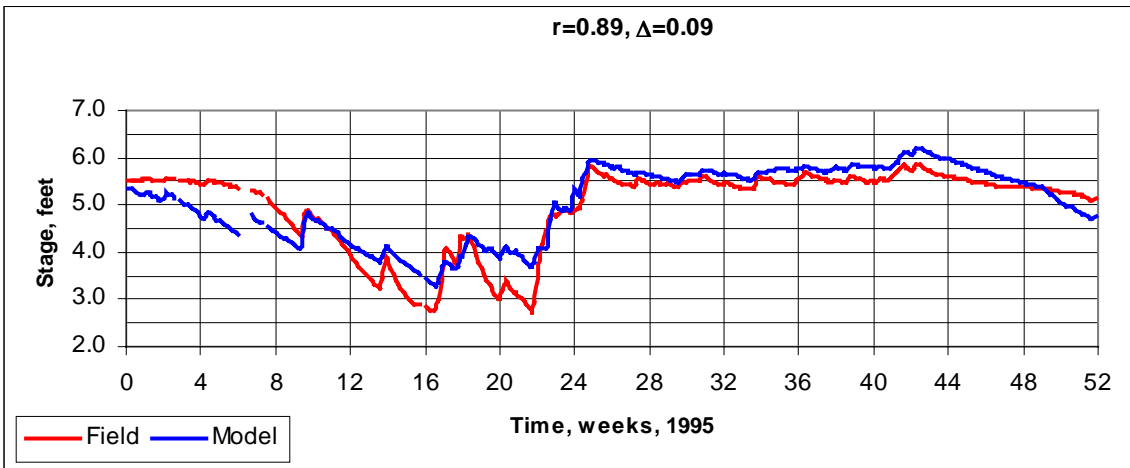
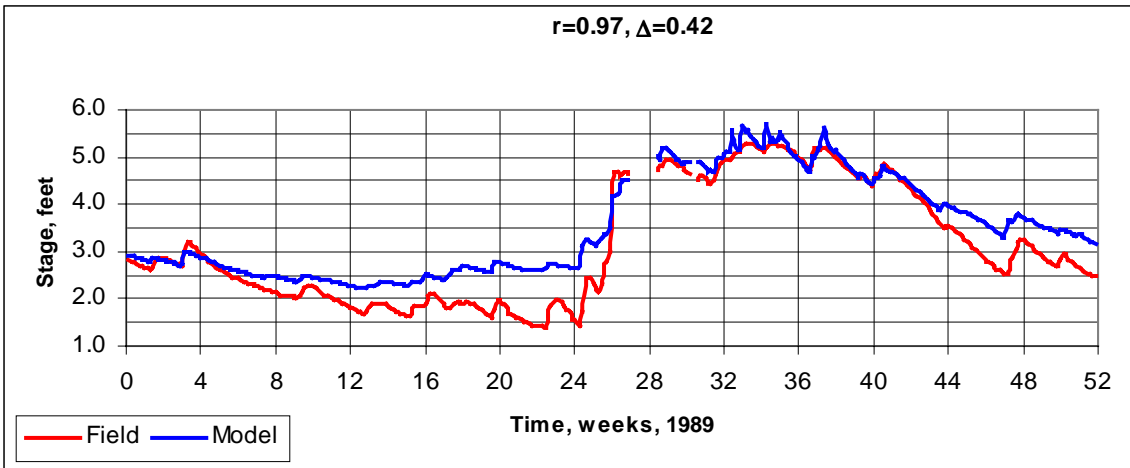
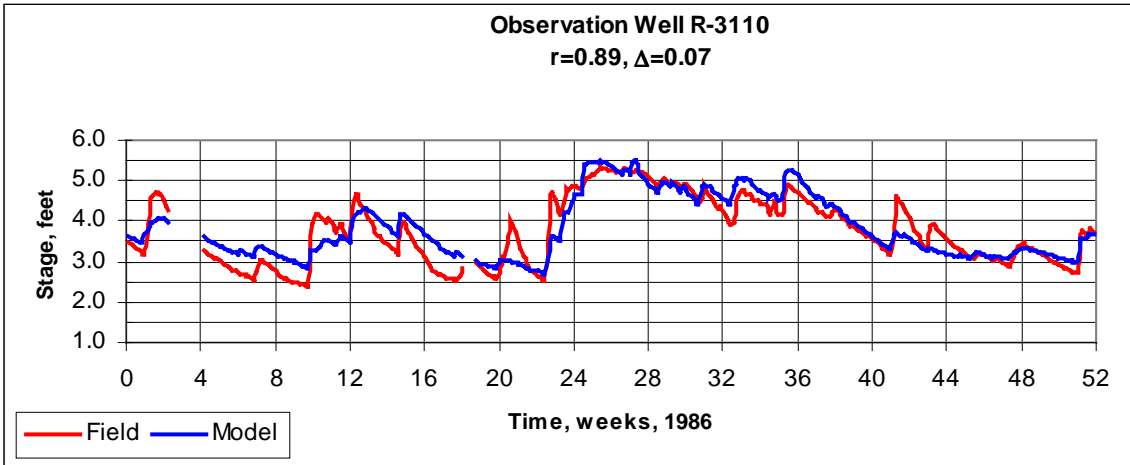


Figure 41: Observation Well R-3110

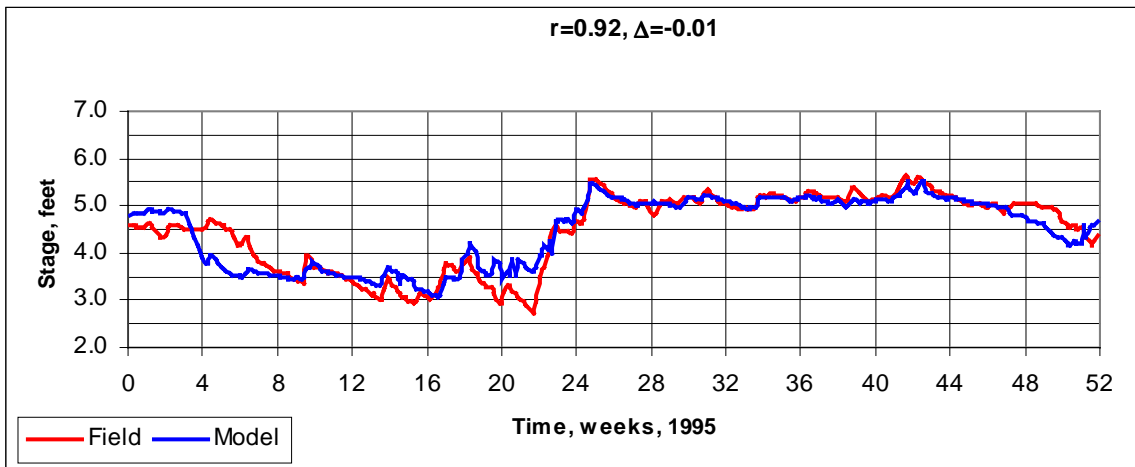
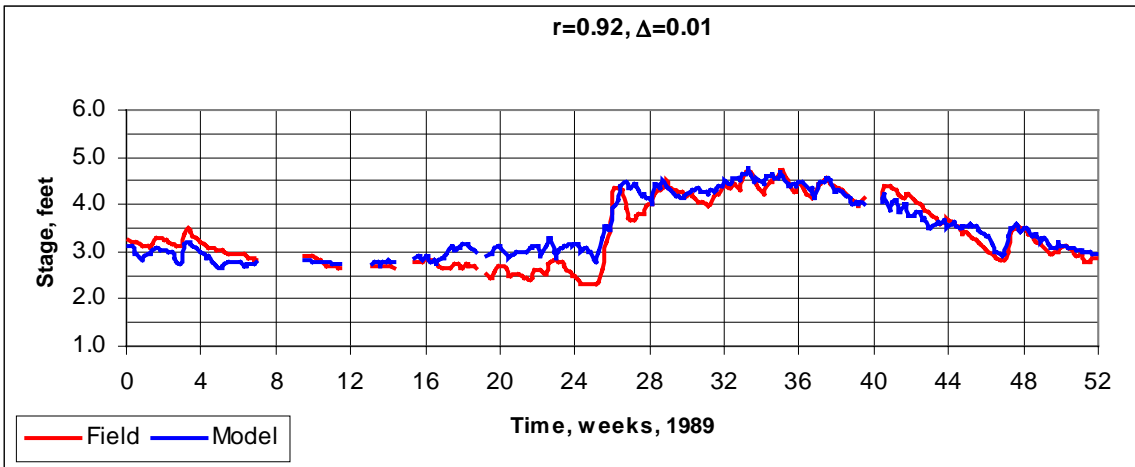
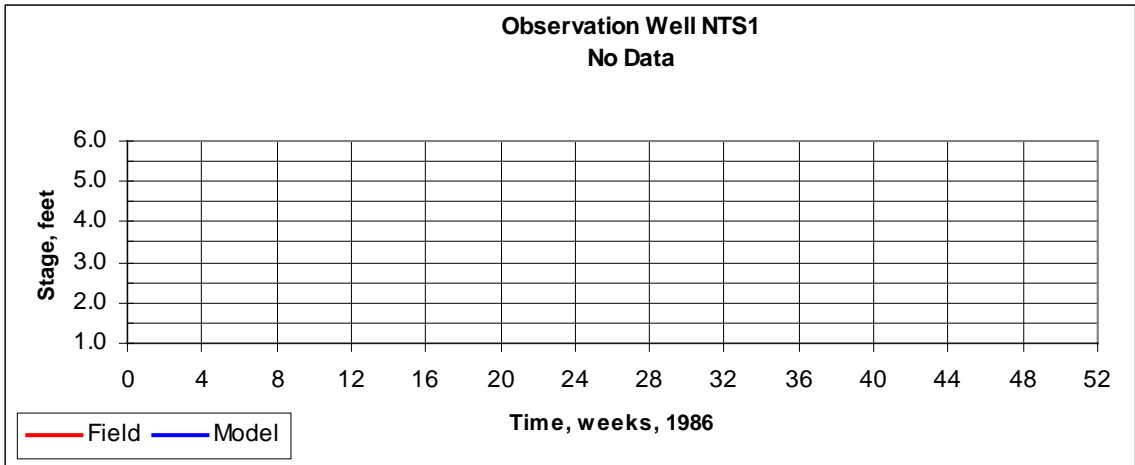


Figure 42: Observation Well NTS1

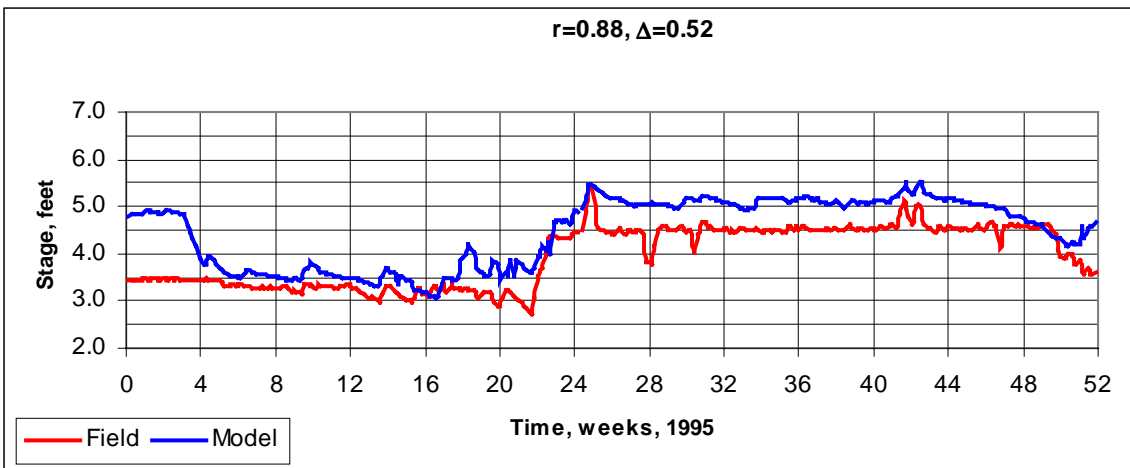
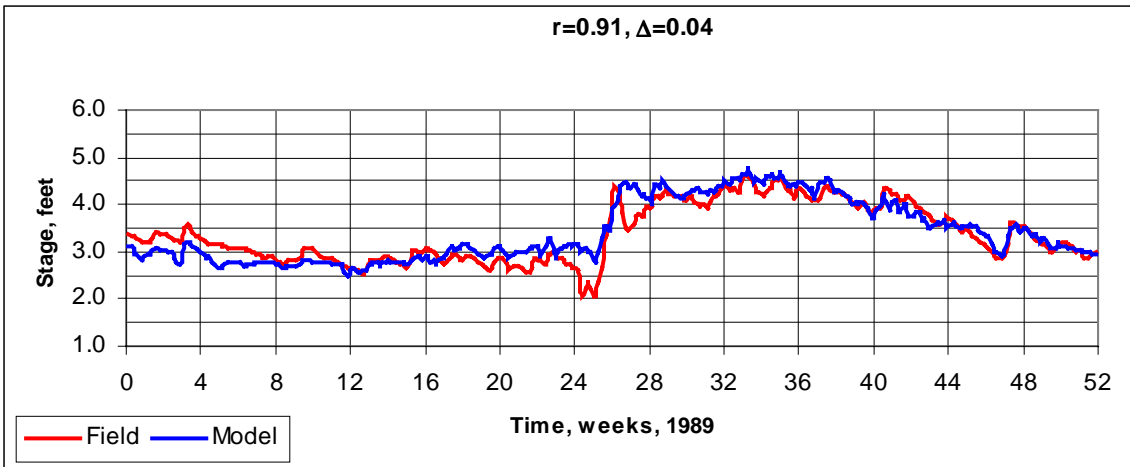
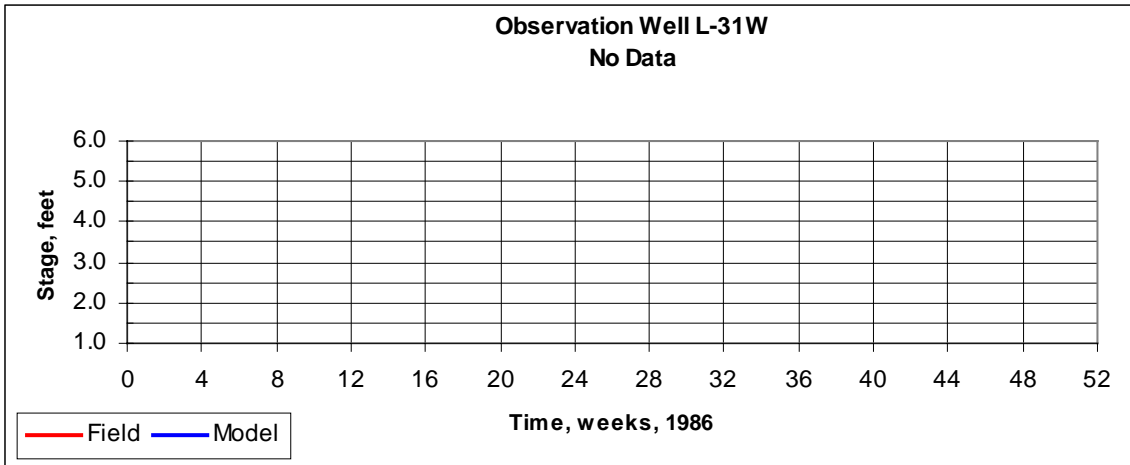


Figure 43: Observation Well L-31W

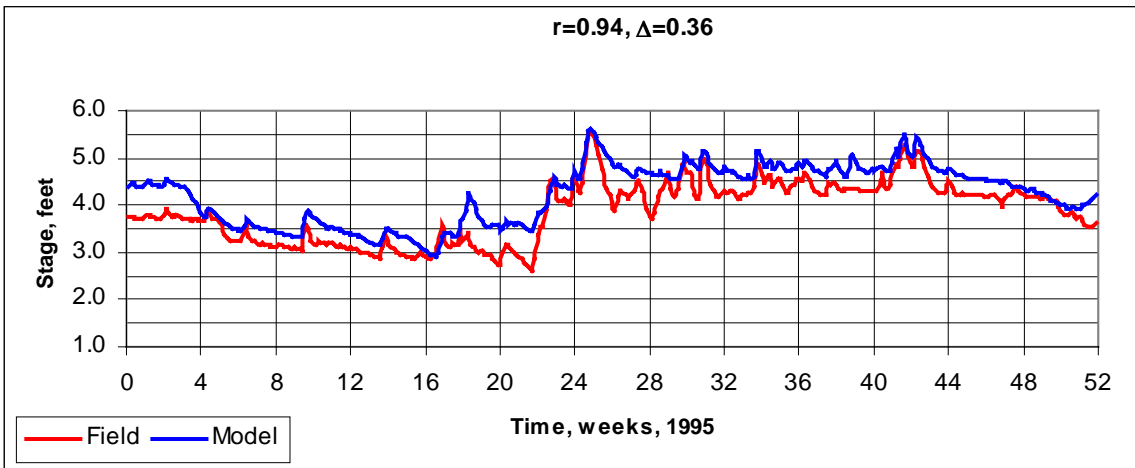
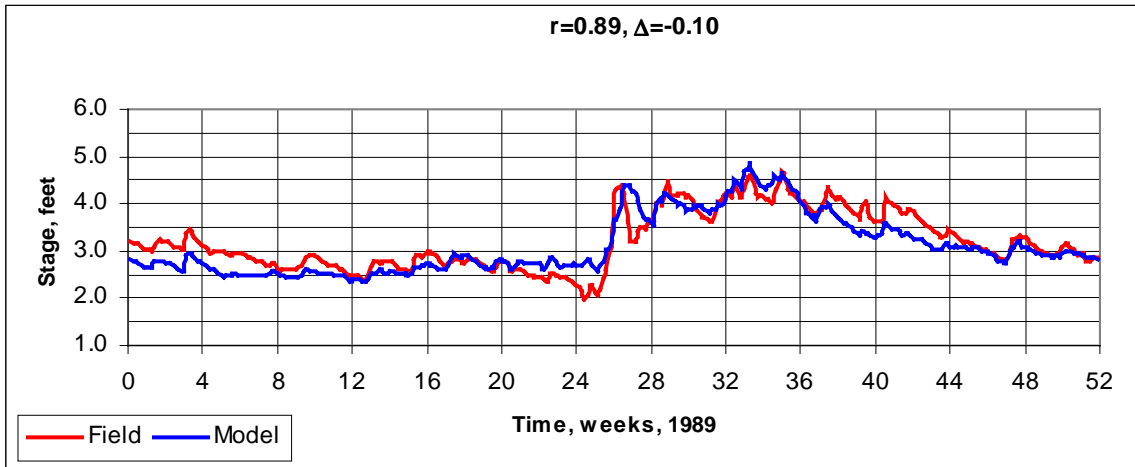
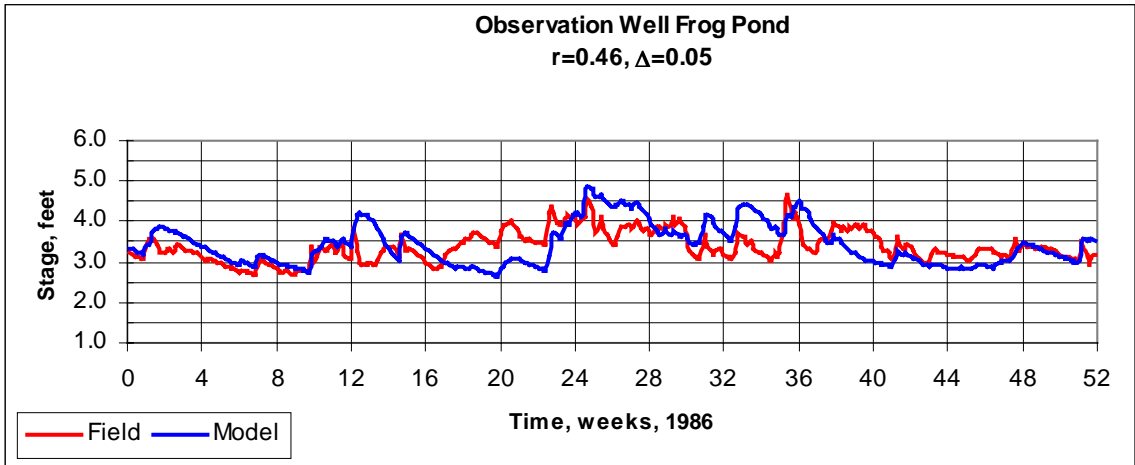


Figure 44: Observation Well Frog Pond

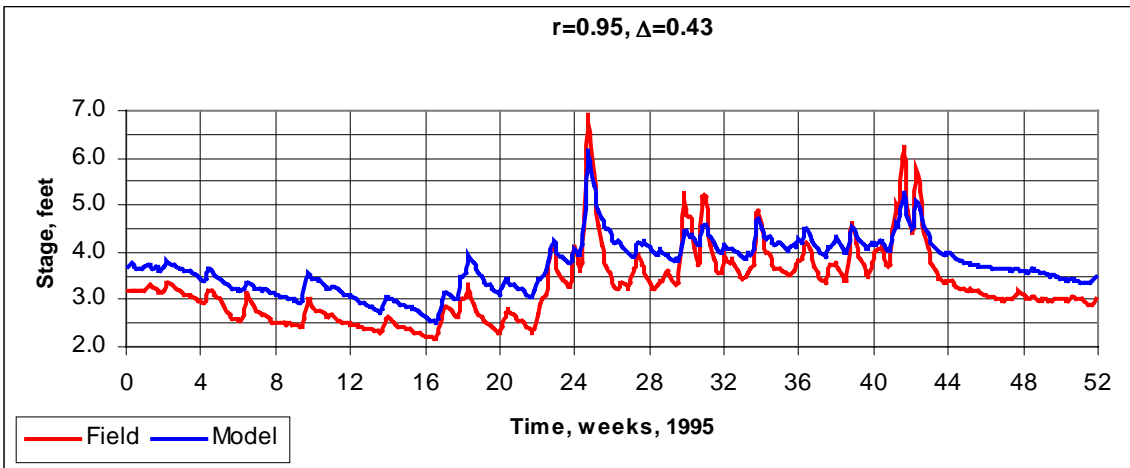
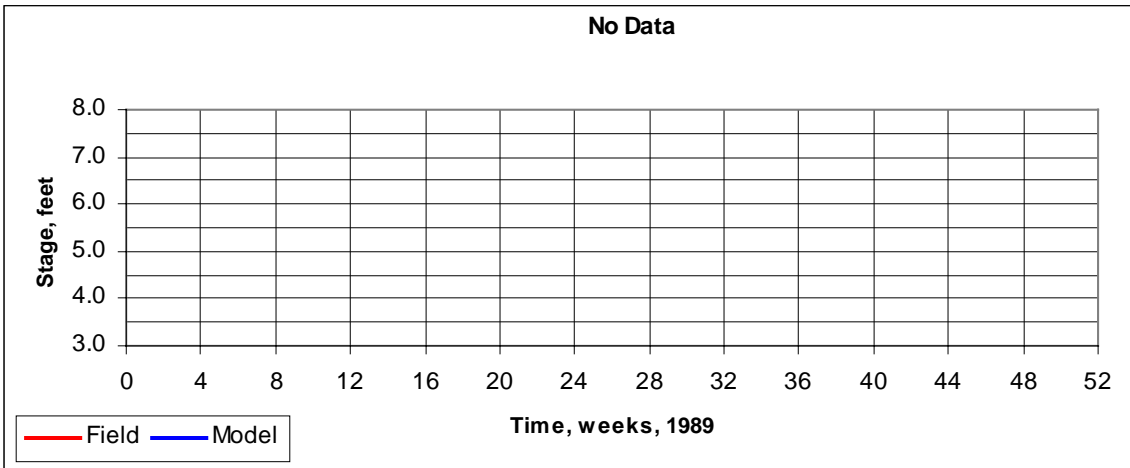
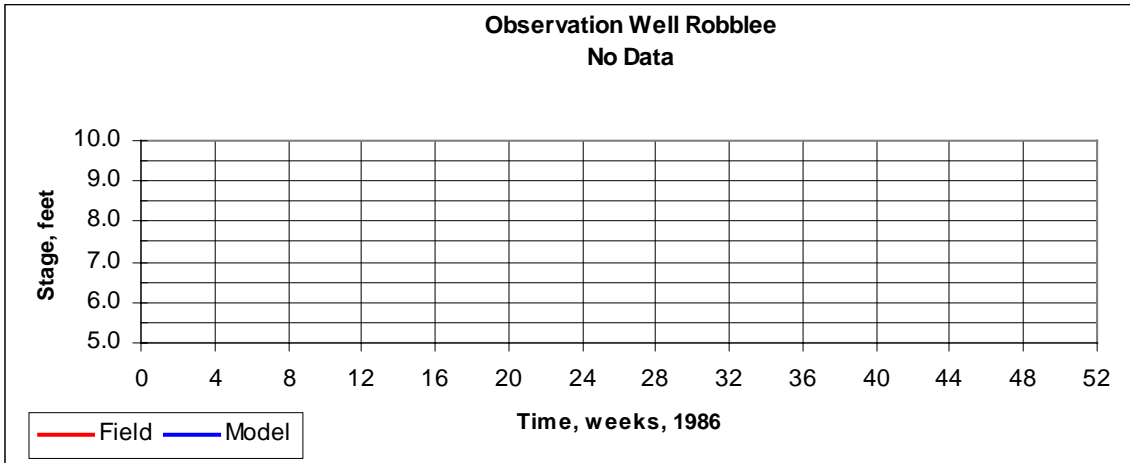


Figure 45: Observation Well Robblee

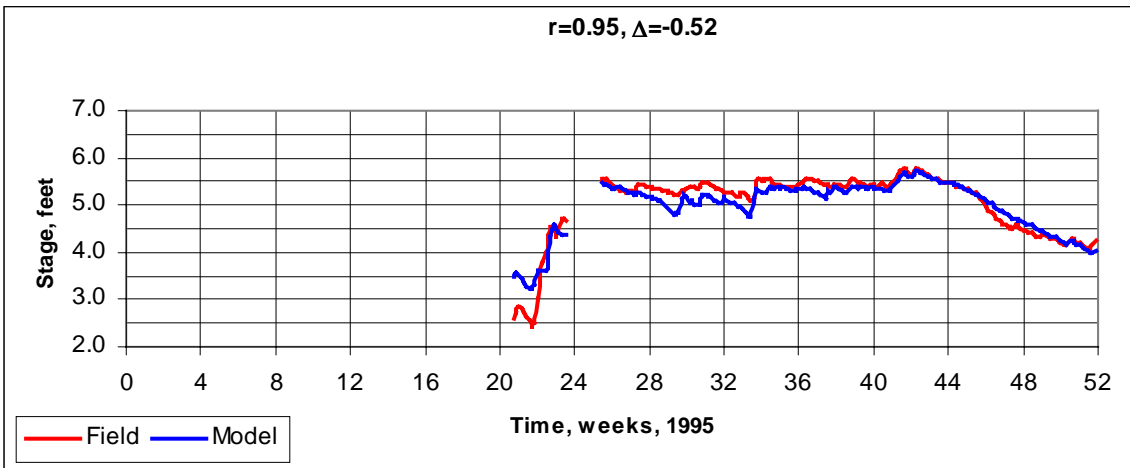
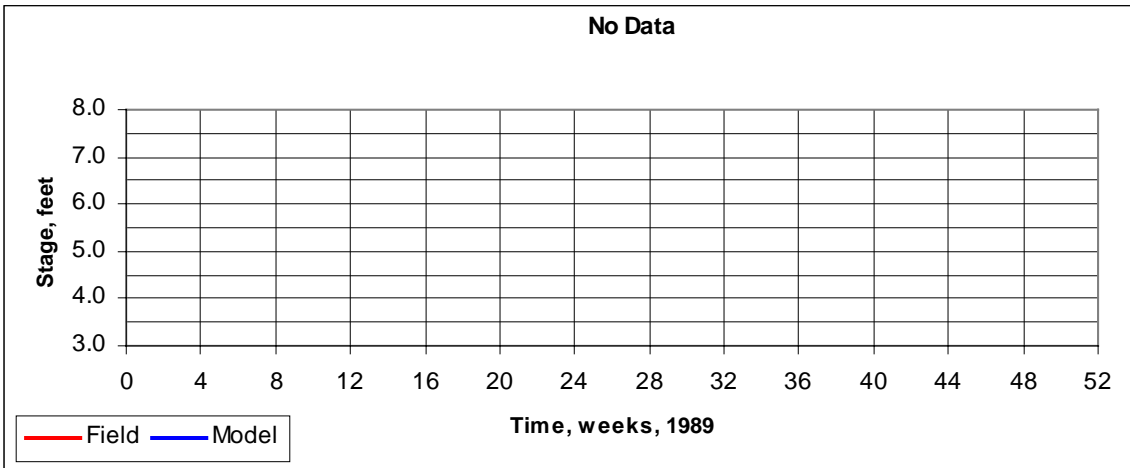
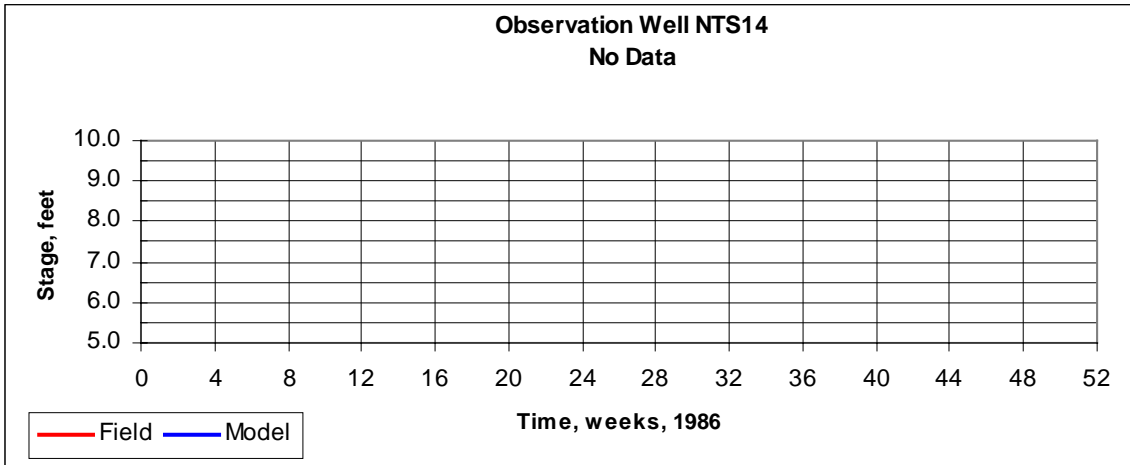


Figure 46: Observation Well NTS14

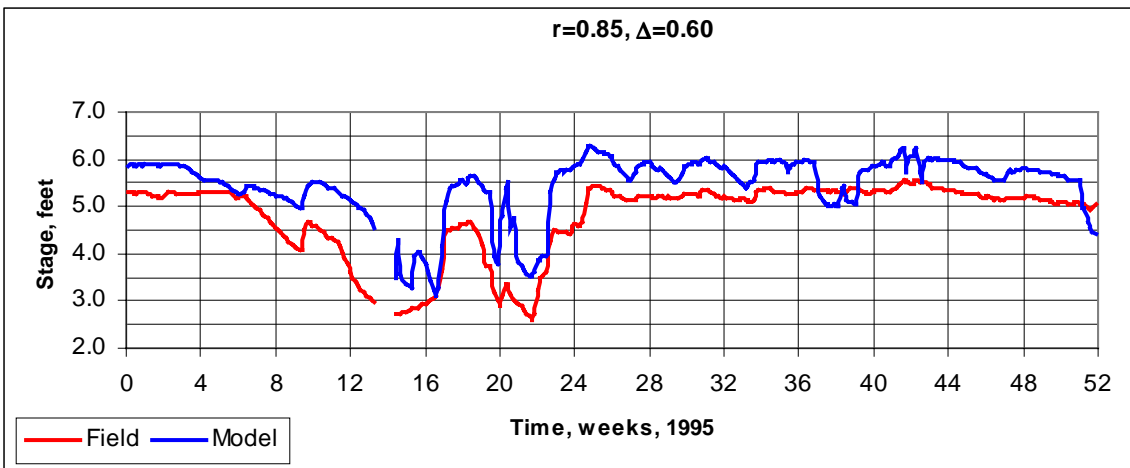
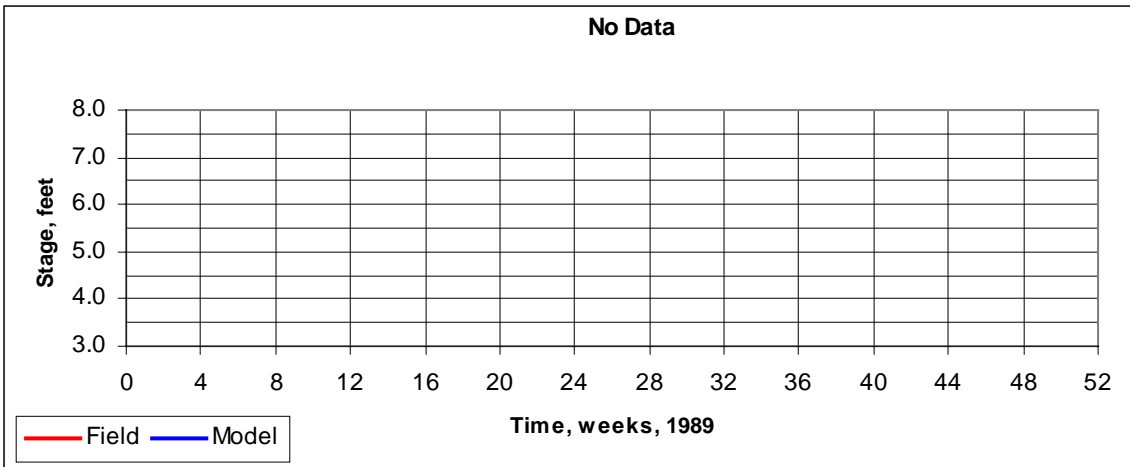
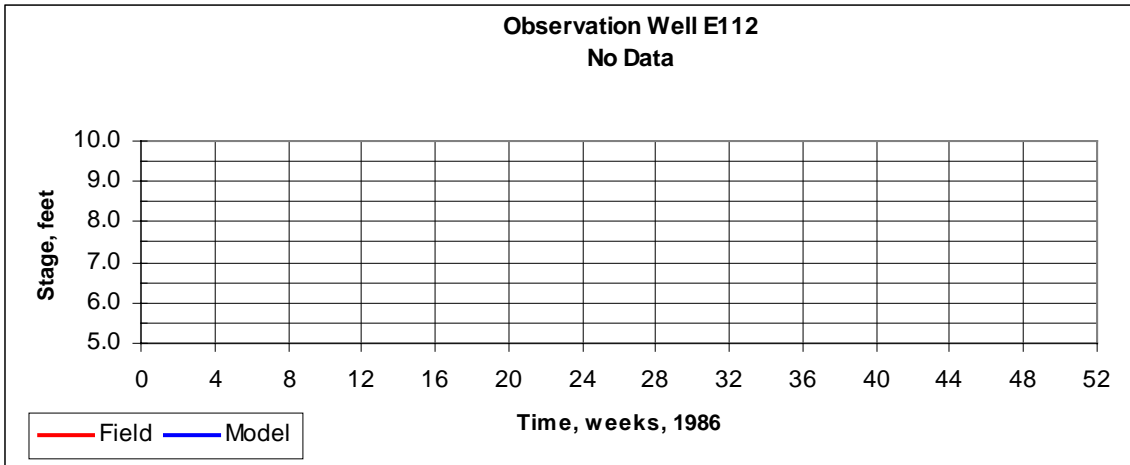


Figure 47: Observation Well E112

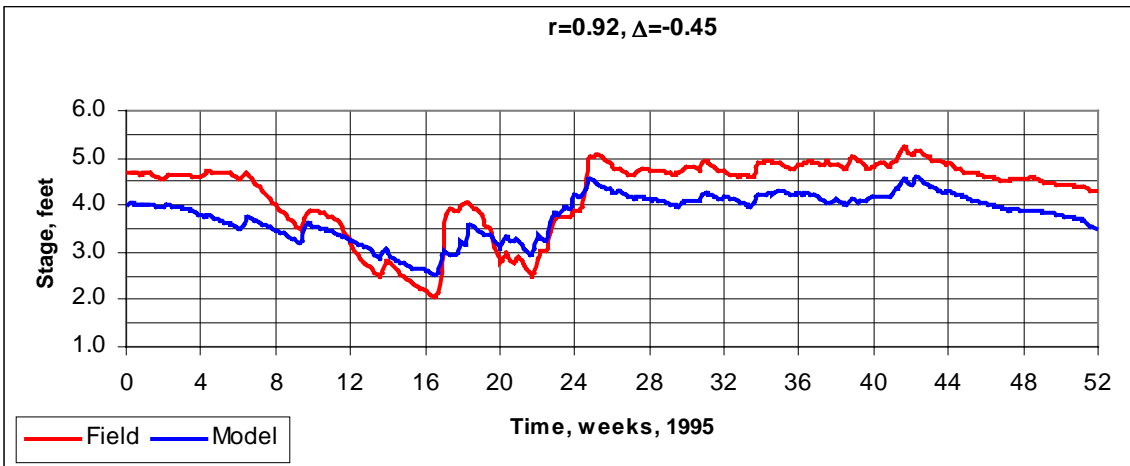
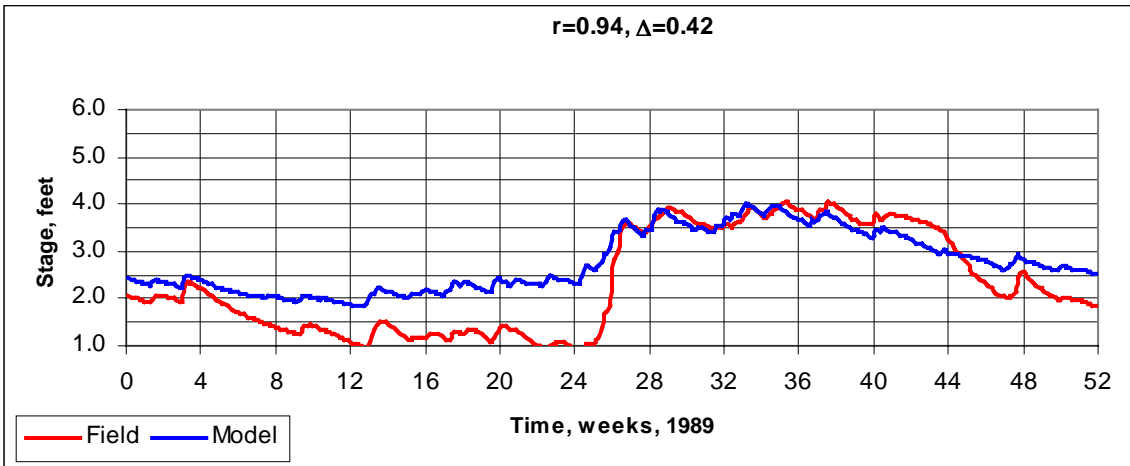
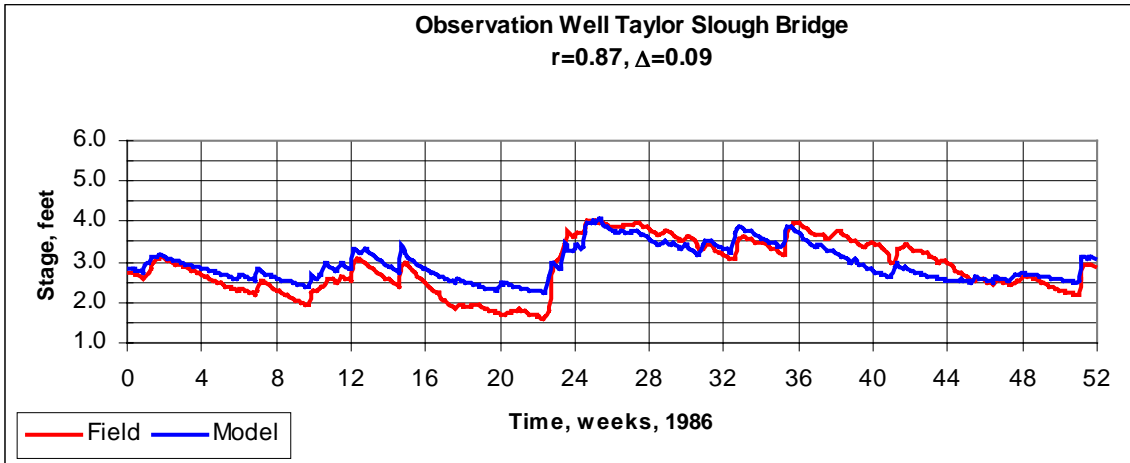


Figure 48: Observation Well Taylor Slough Bridge

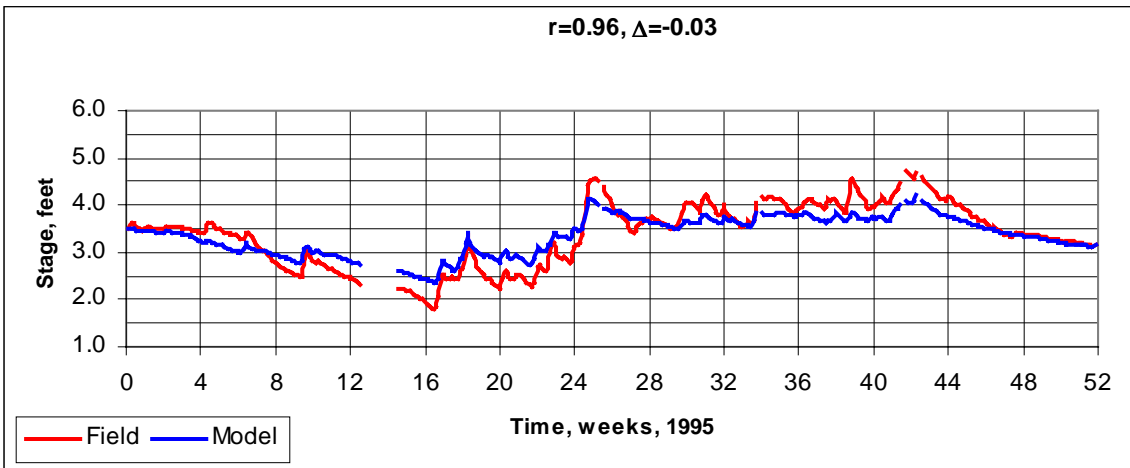
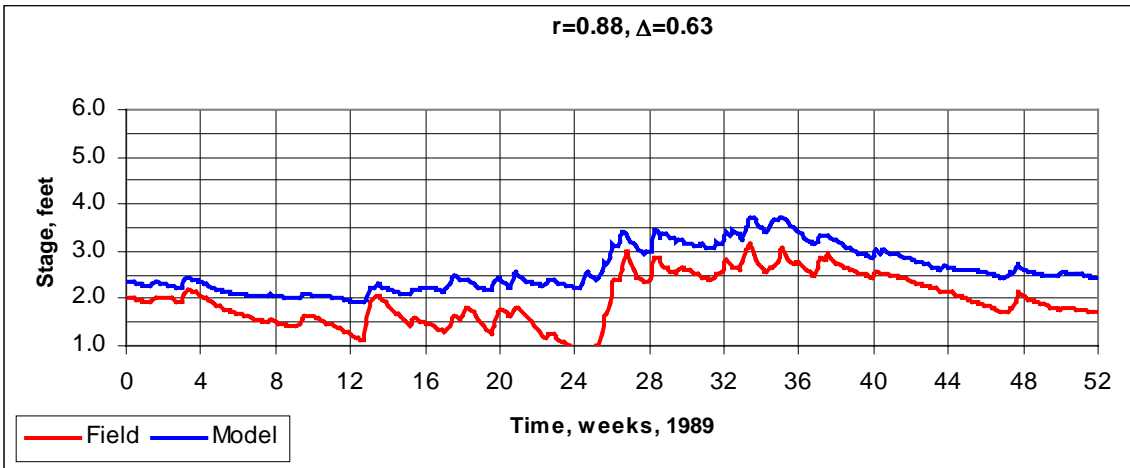
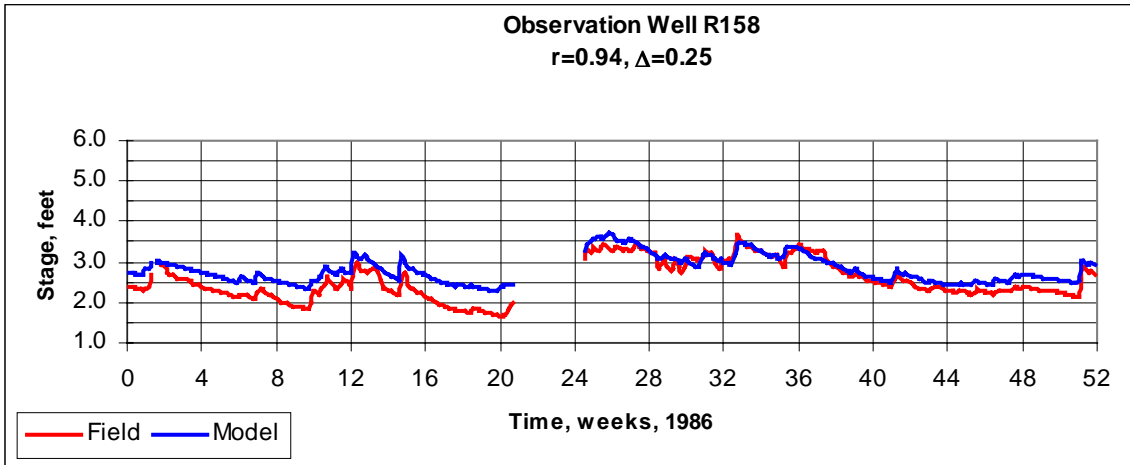


Figure 49: Observation Well R158

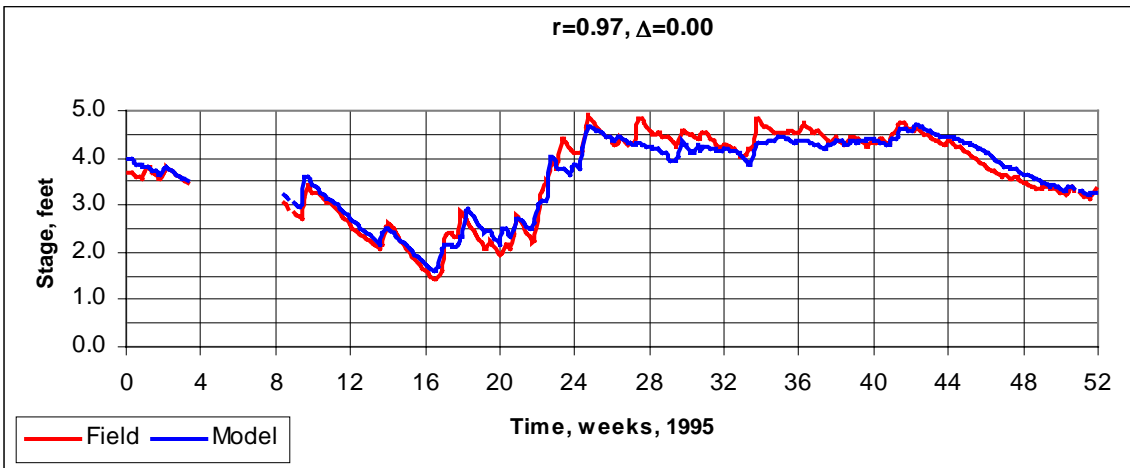
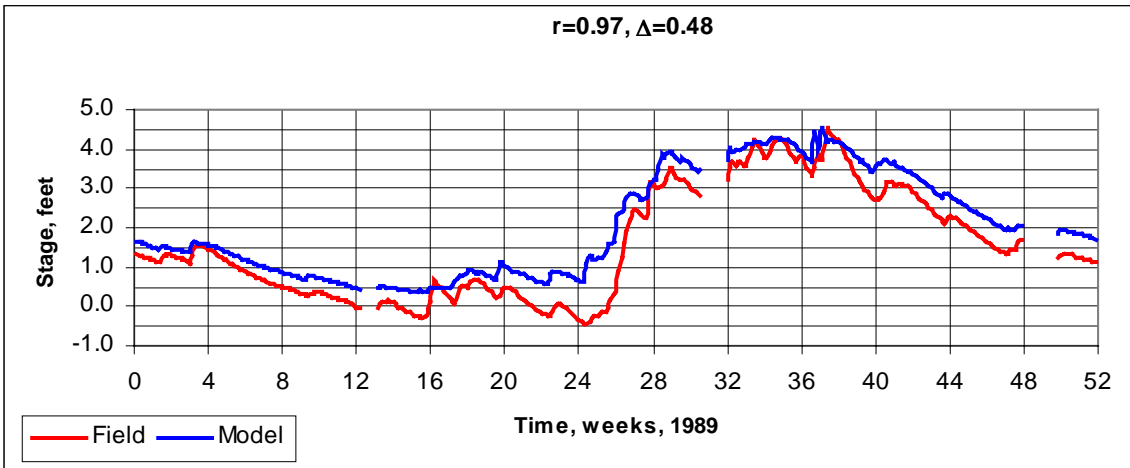
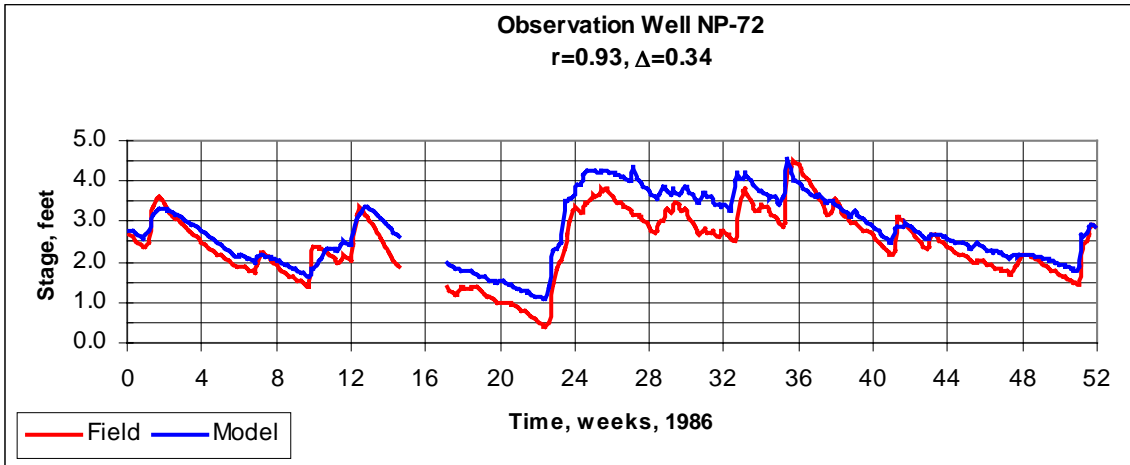


Figure 50: Observation Well NP-72

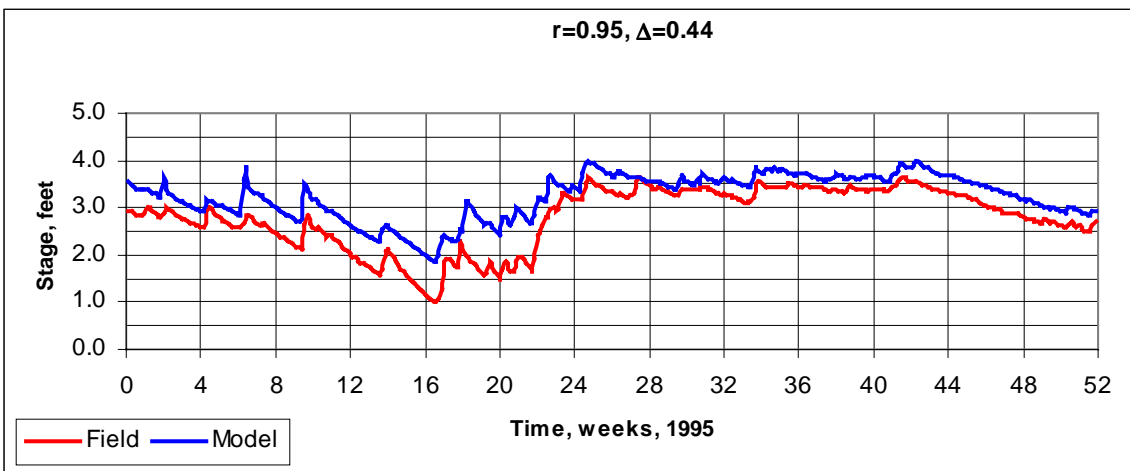
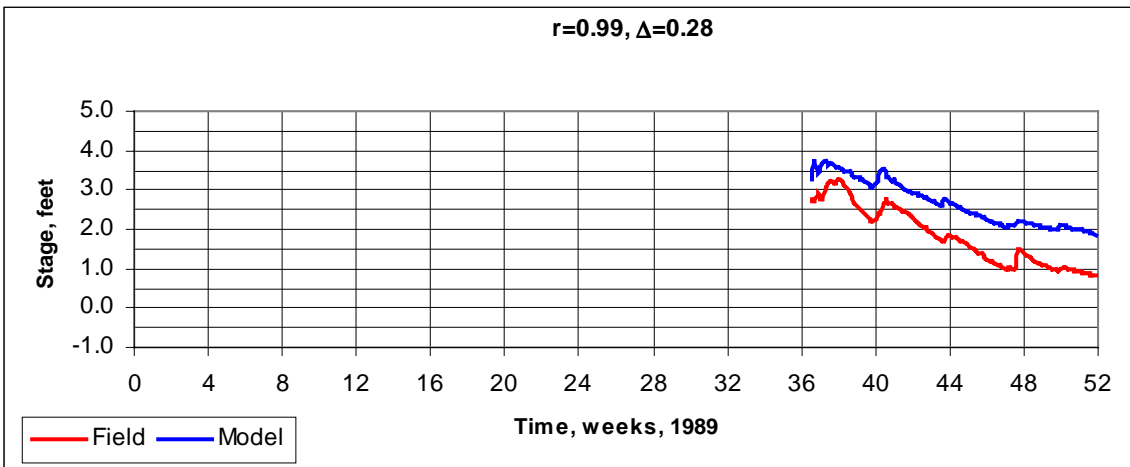
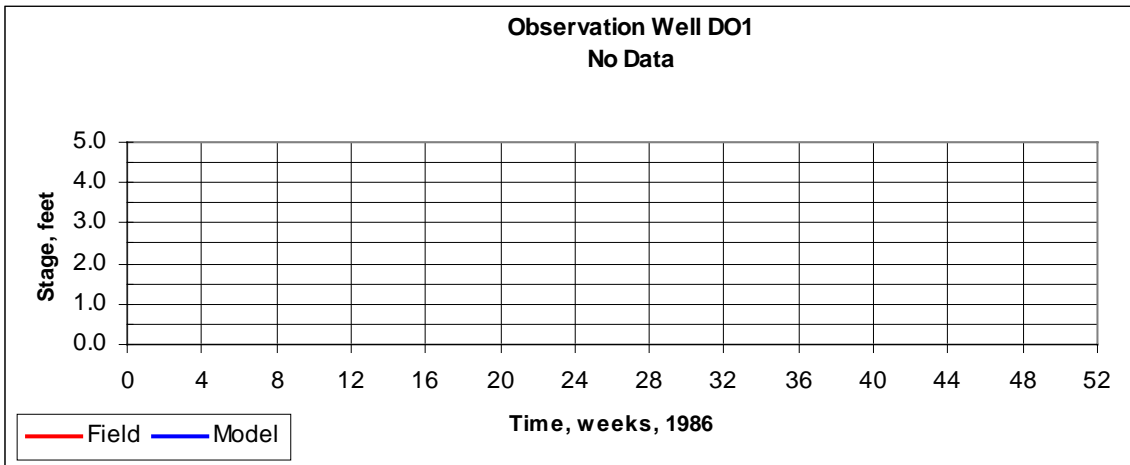


Figure 51: Observation Well DO1

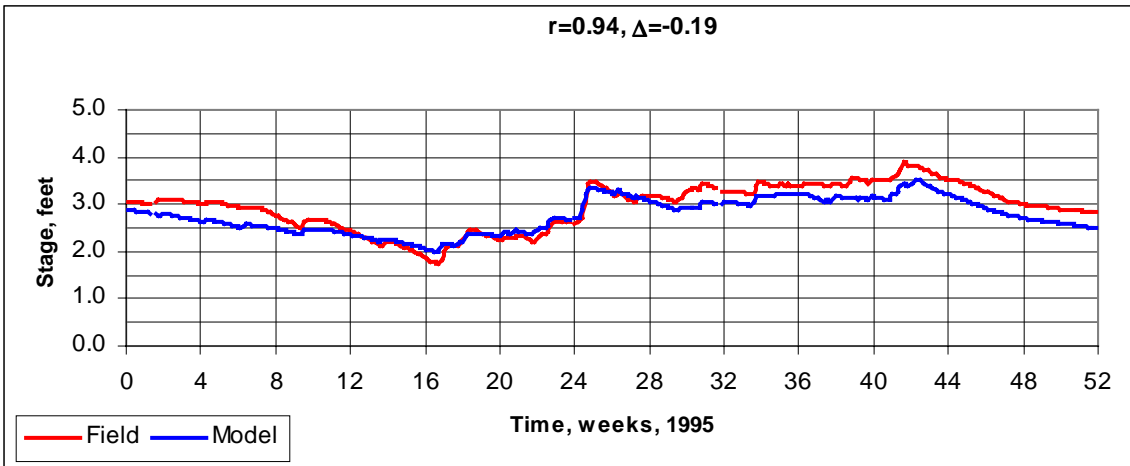
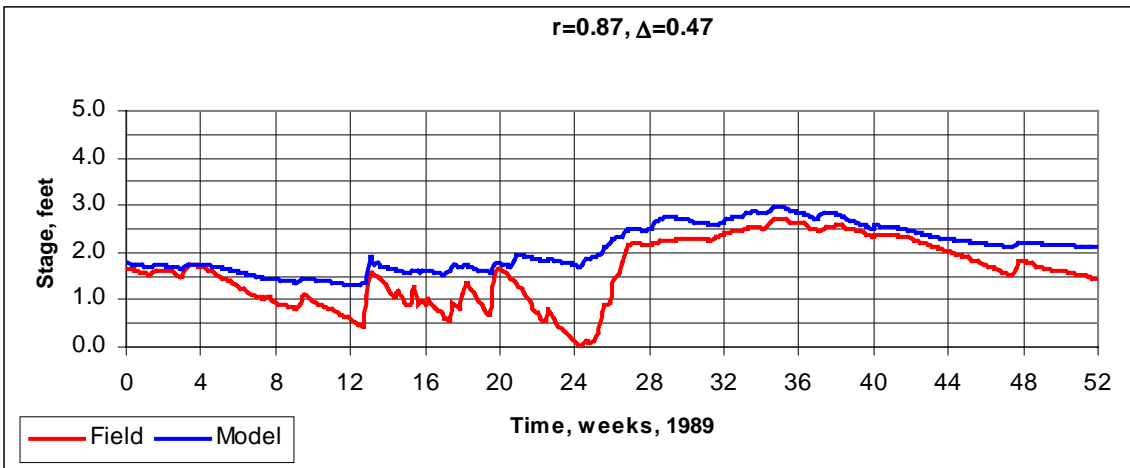
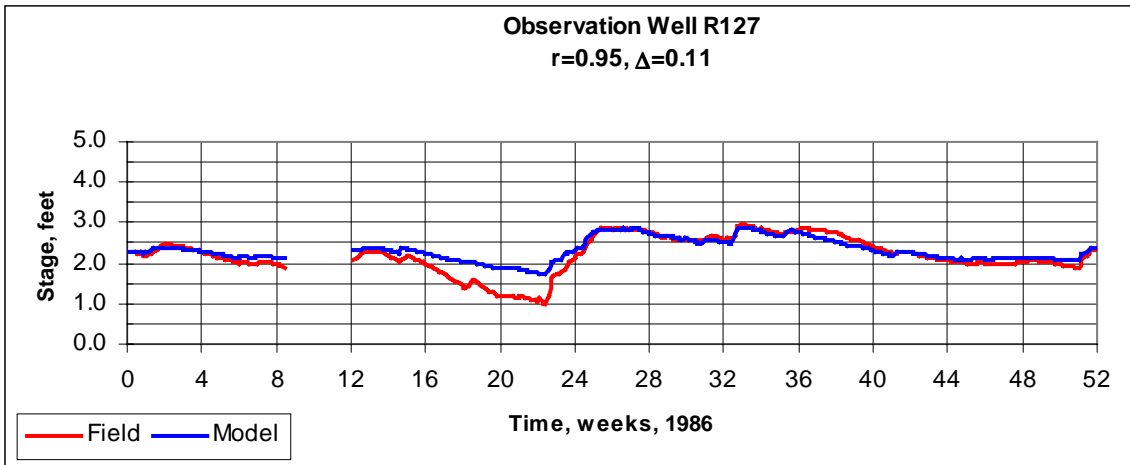


Figure 52: Observation Well R127

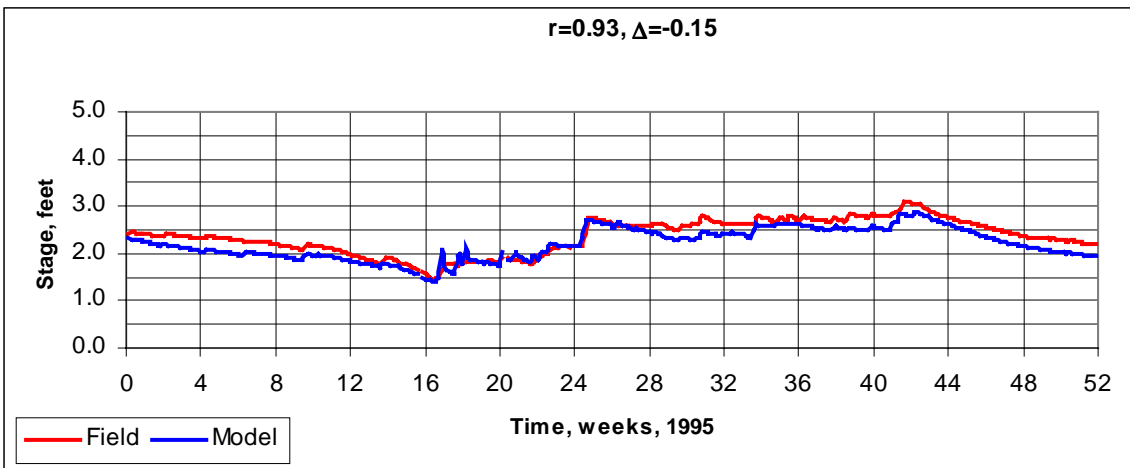
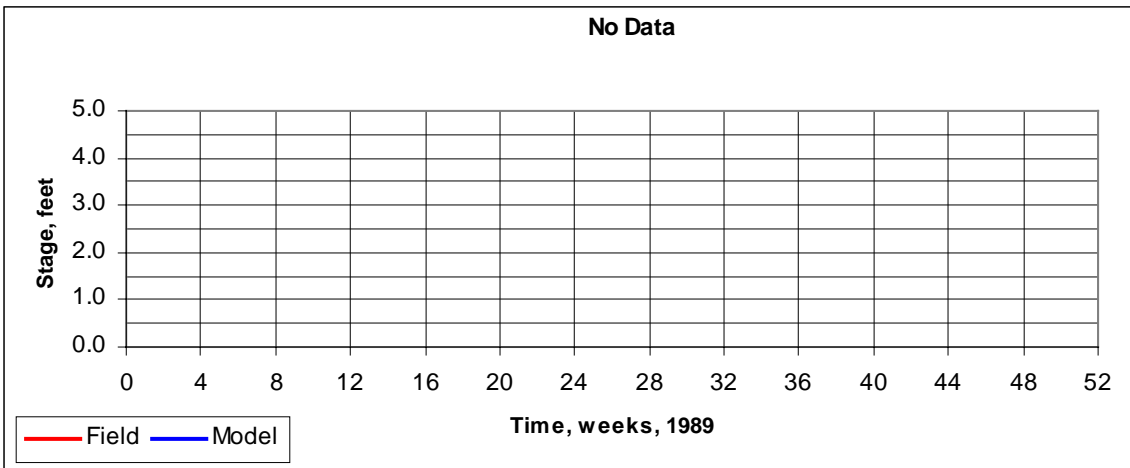
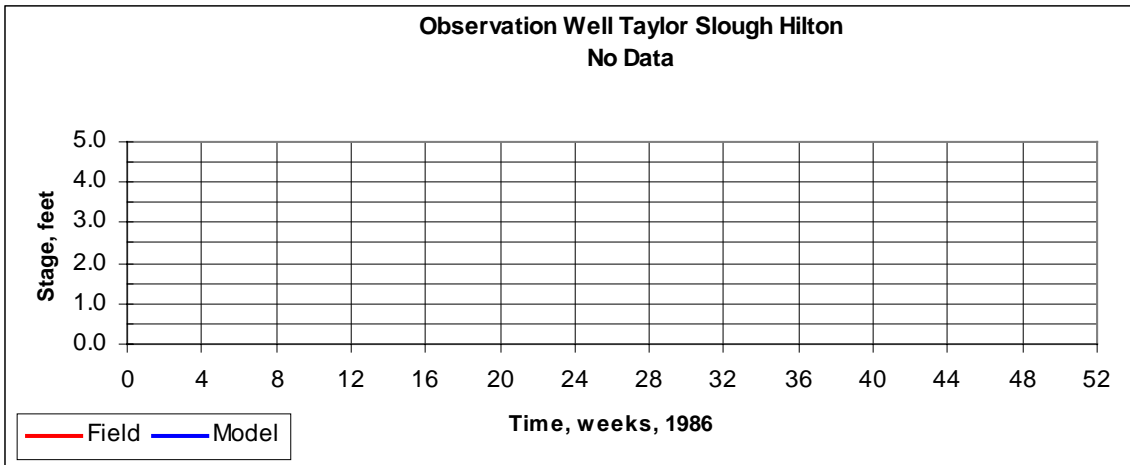


Figure 53: Observation Well Taylor Slough Hilton

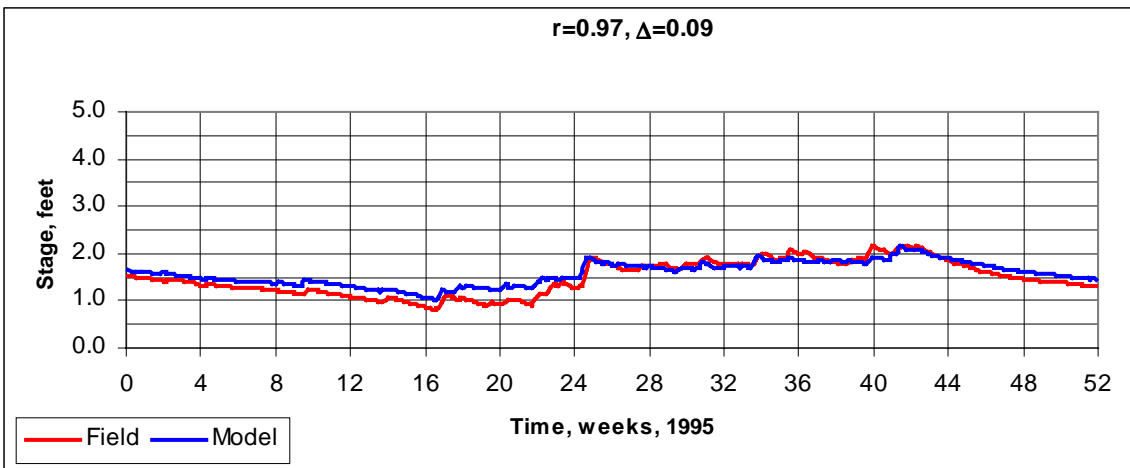
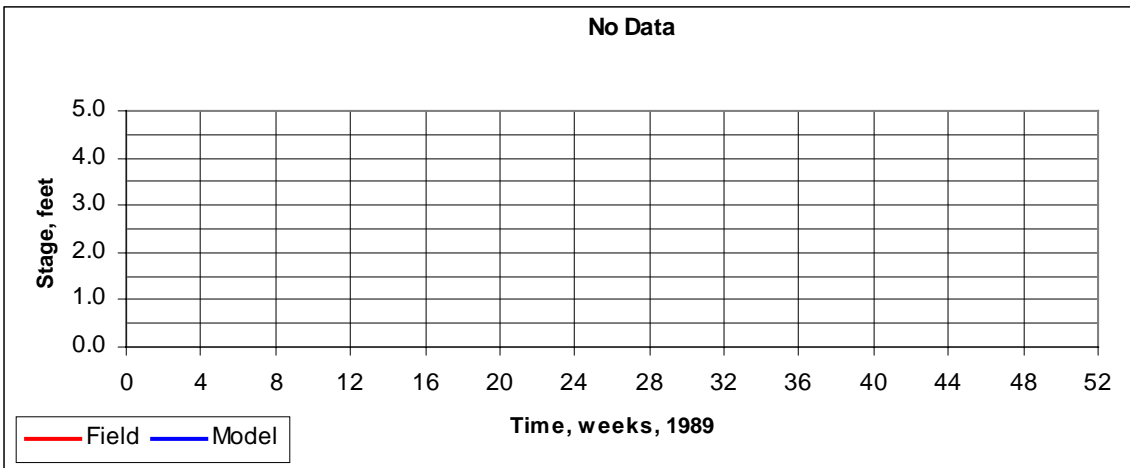
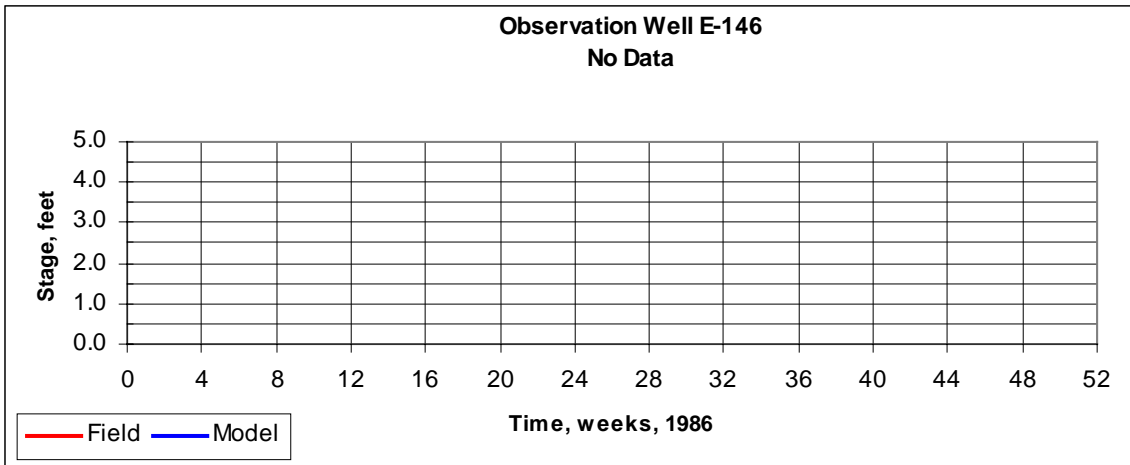


Figure 54: Observation Well E-146

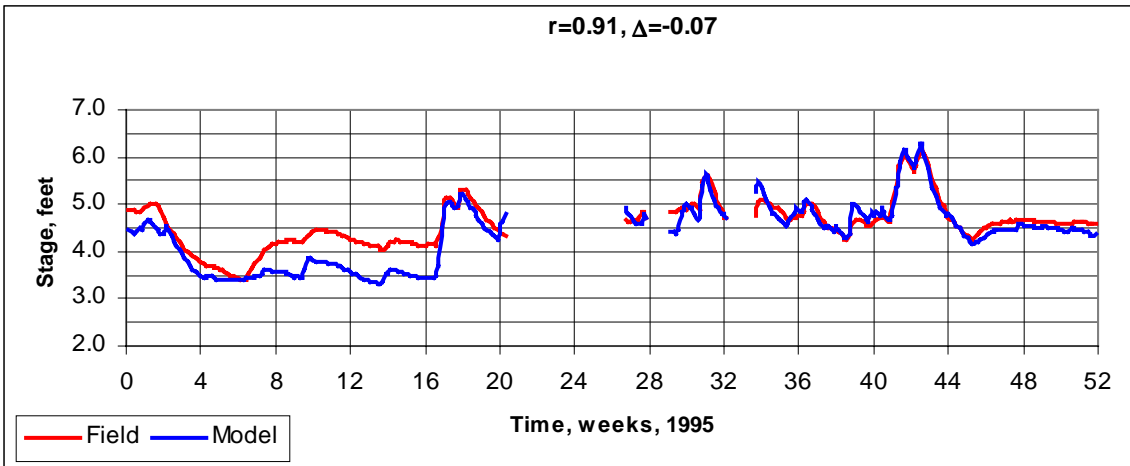
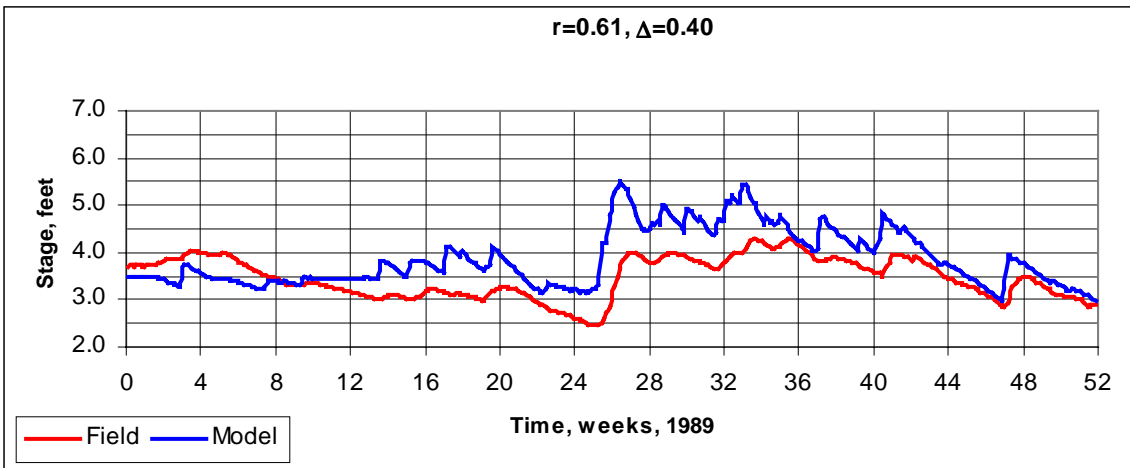
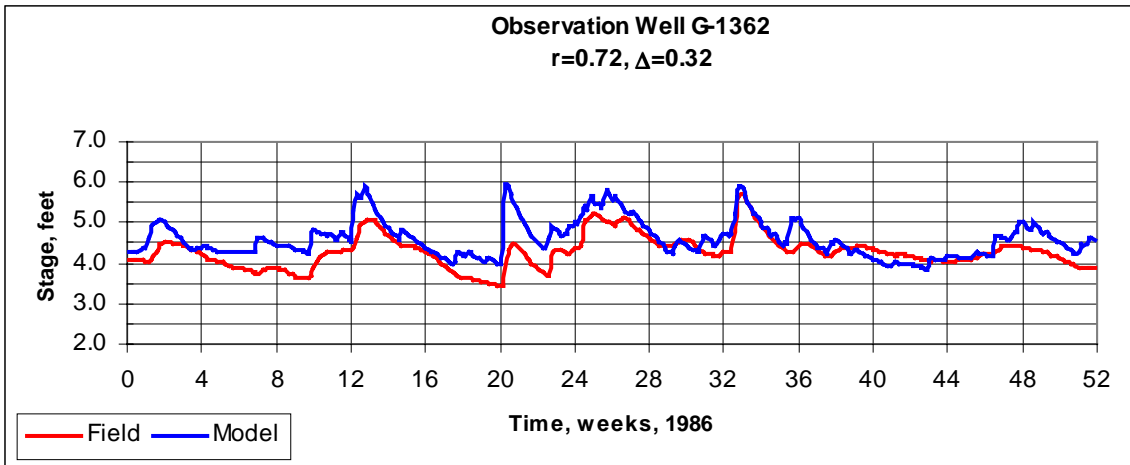


Figure 55: Observation Well G-1362

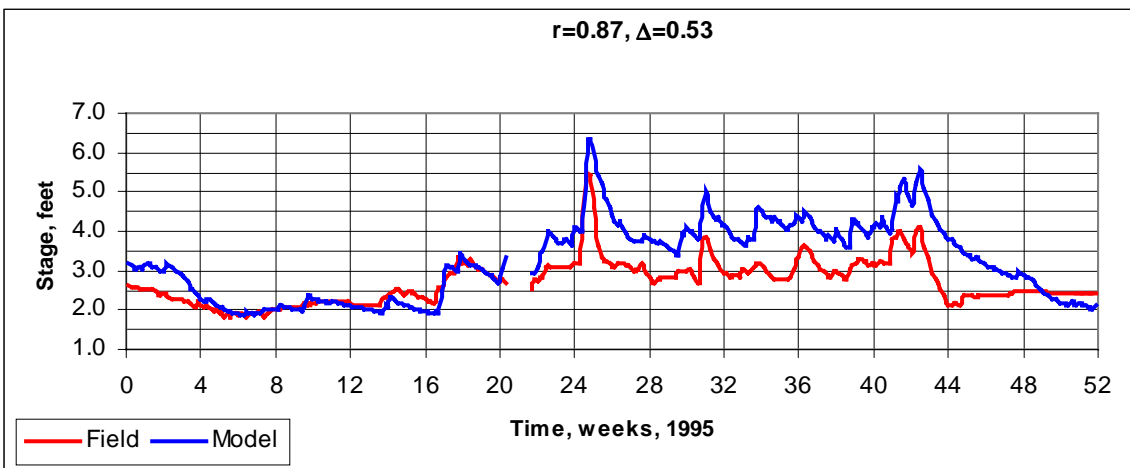
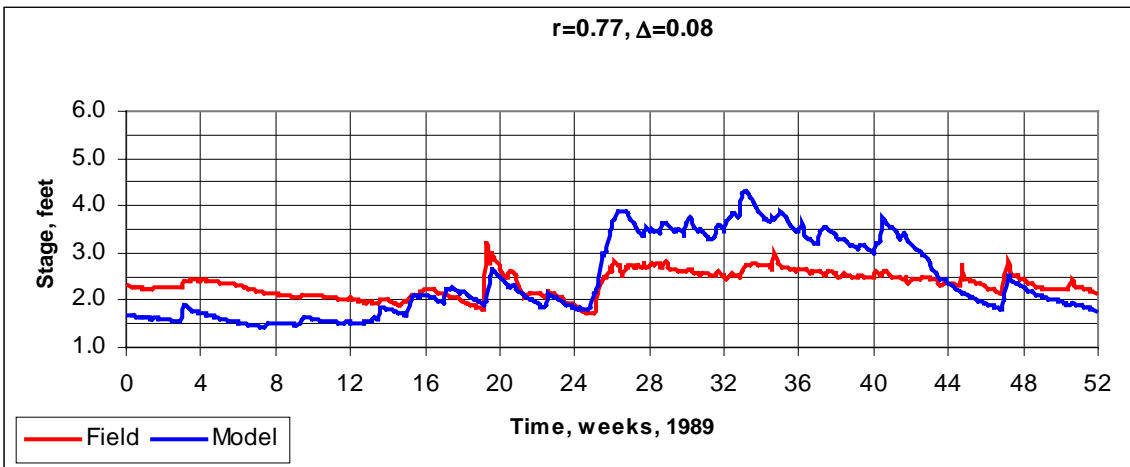
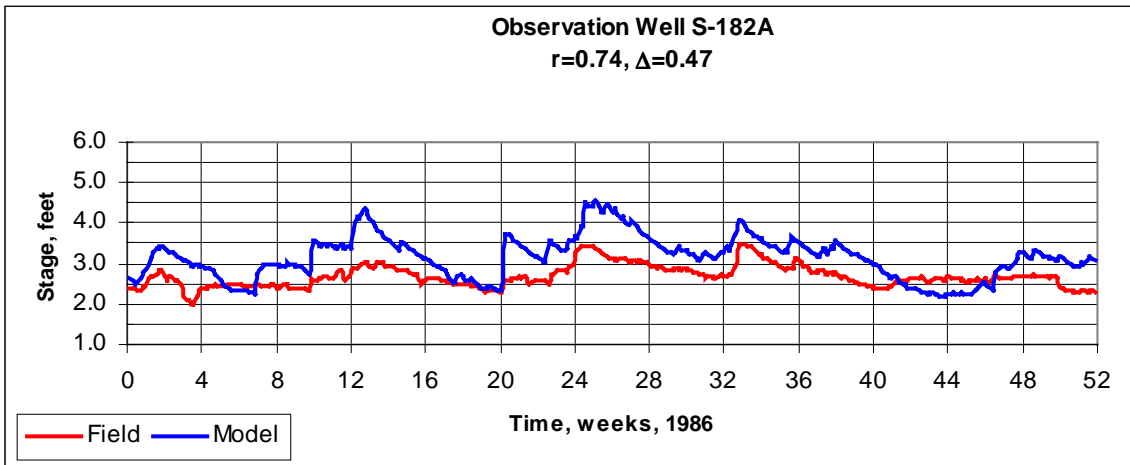


Figure 56: Observation Well S-182A

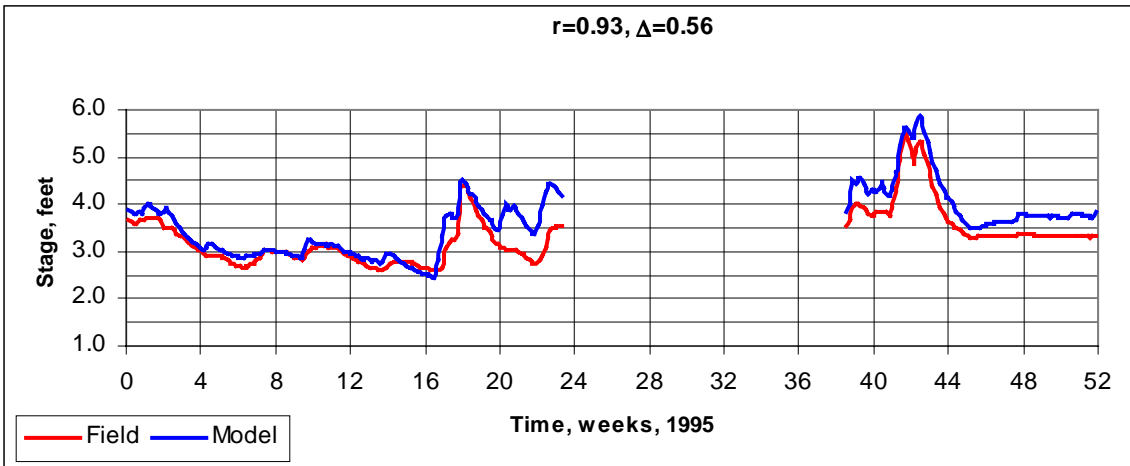
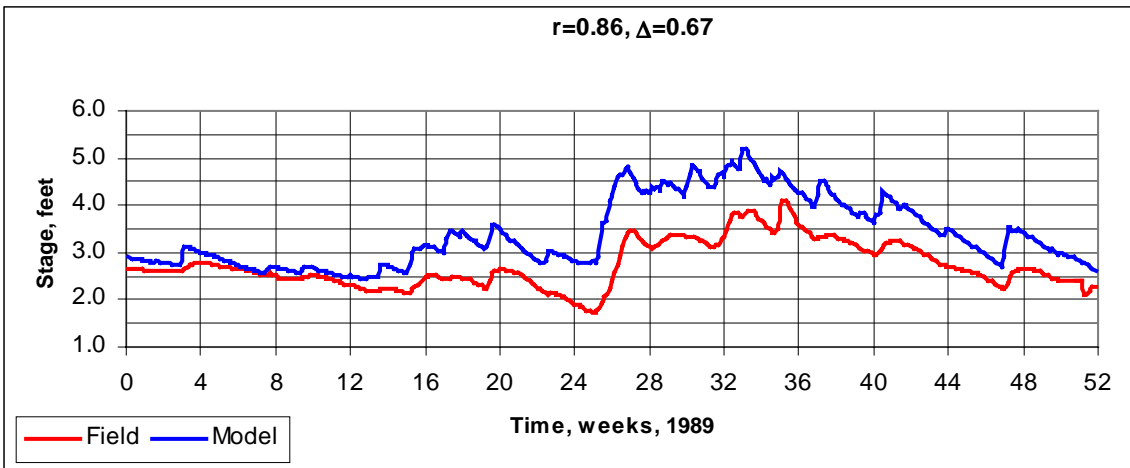
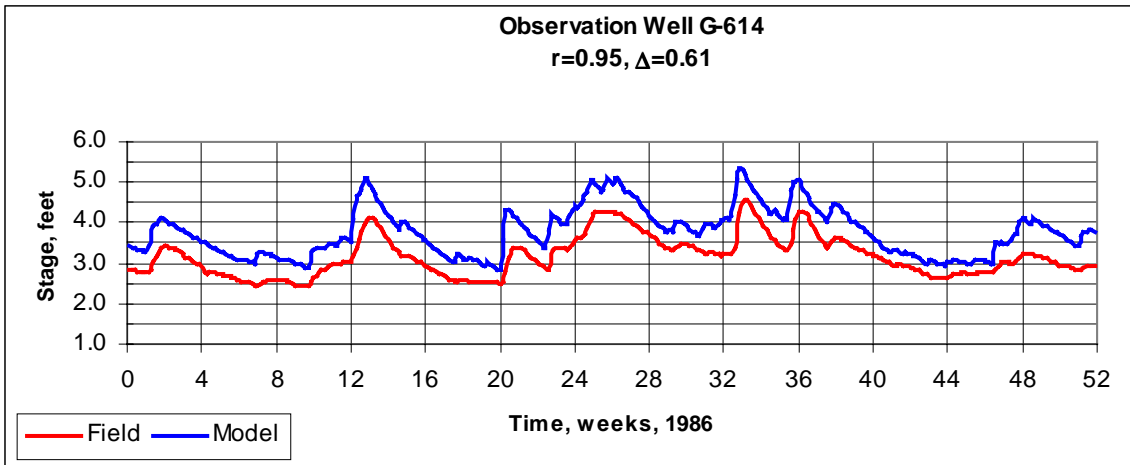


Figure 57: Observation Well G-614

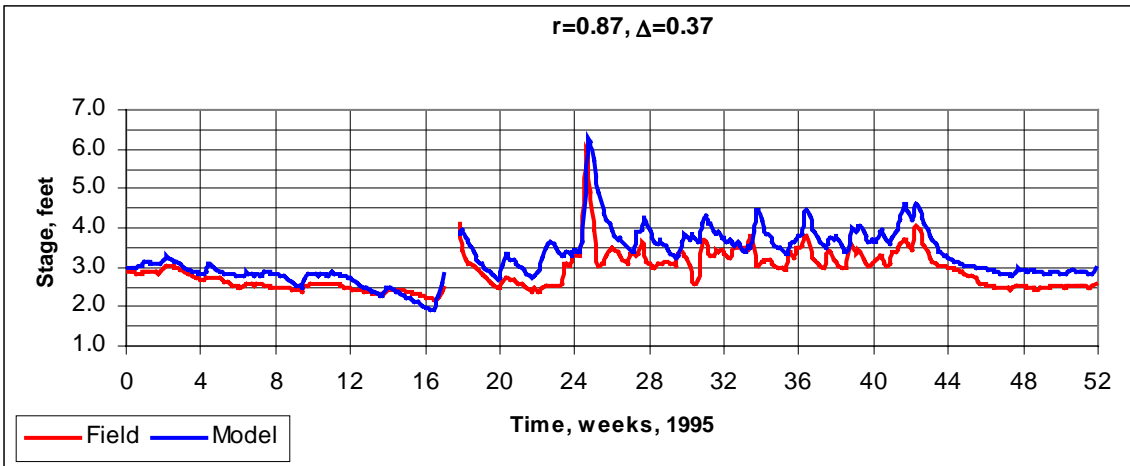
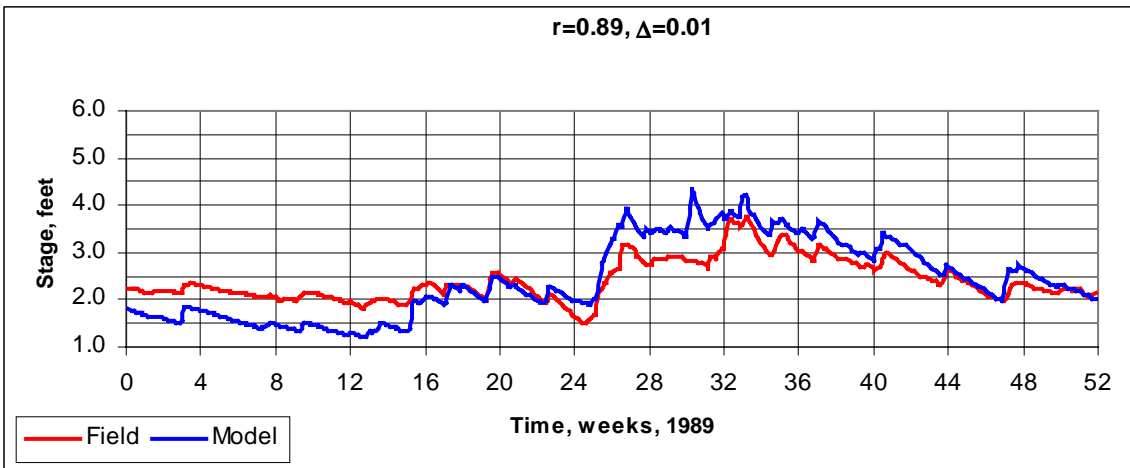
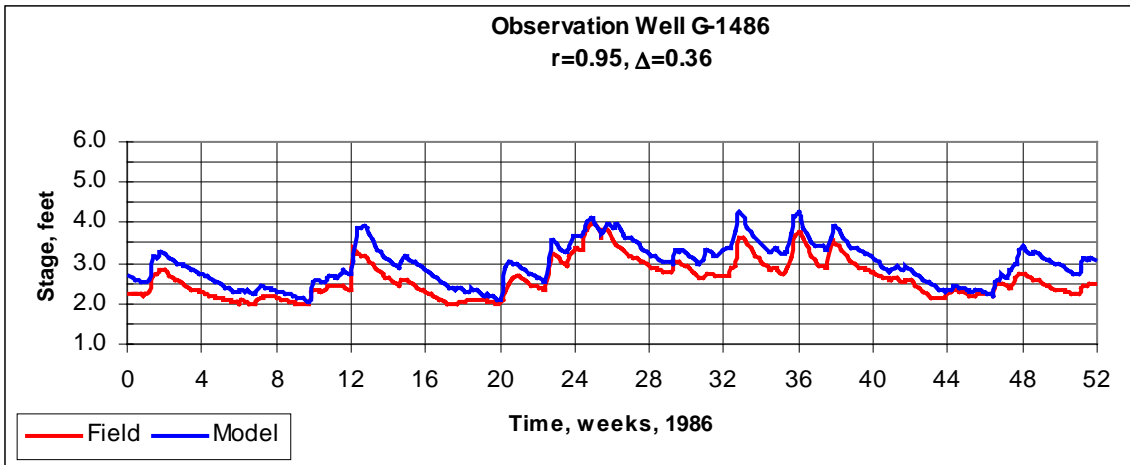


Figure 58: Observation Well G-1486

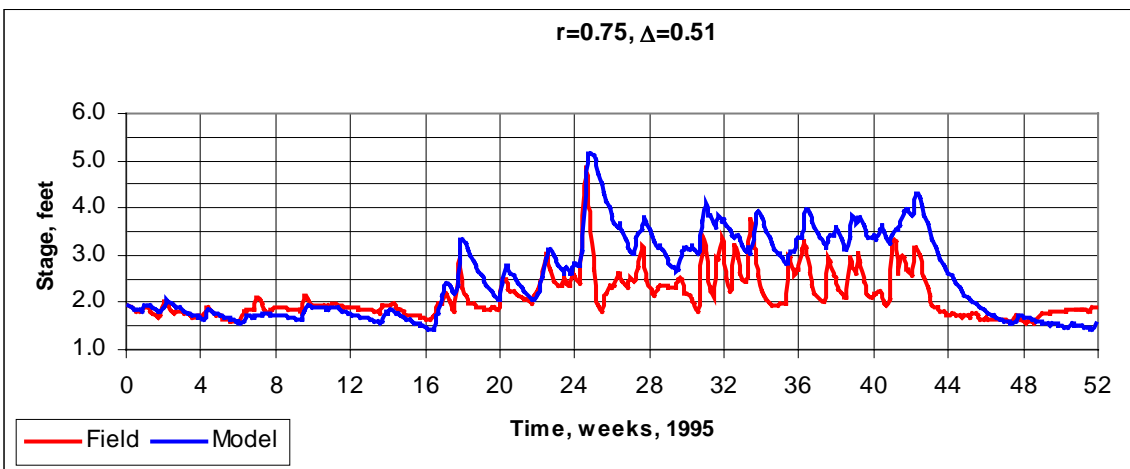
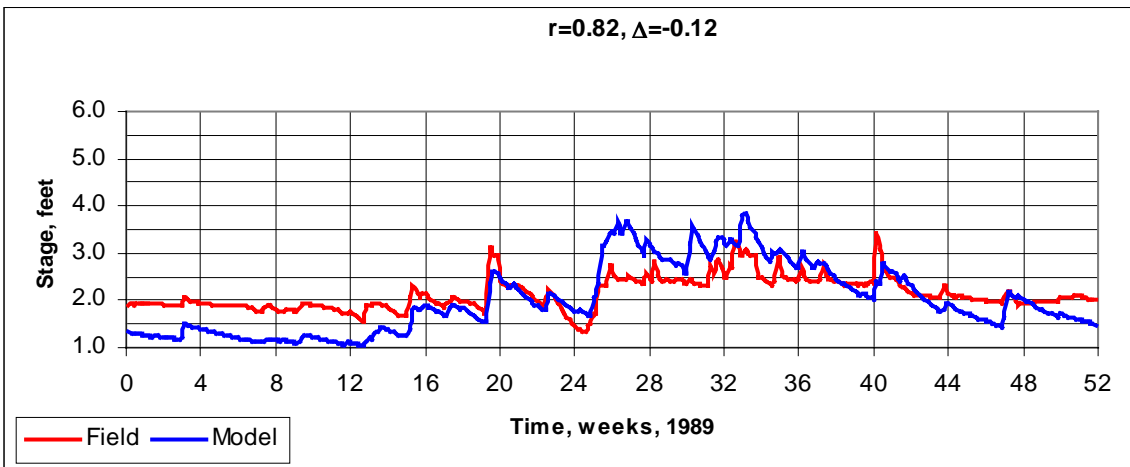
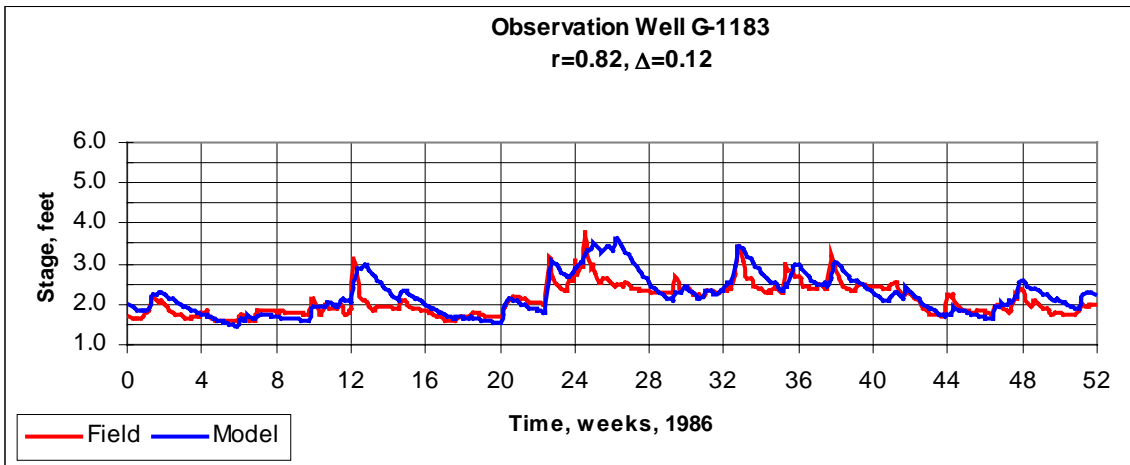


Figure 59: Observation Well G-1183

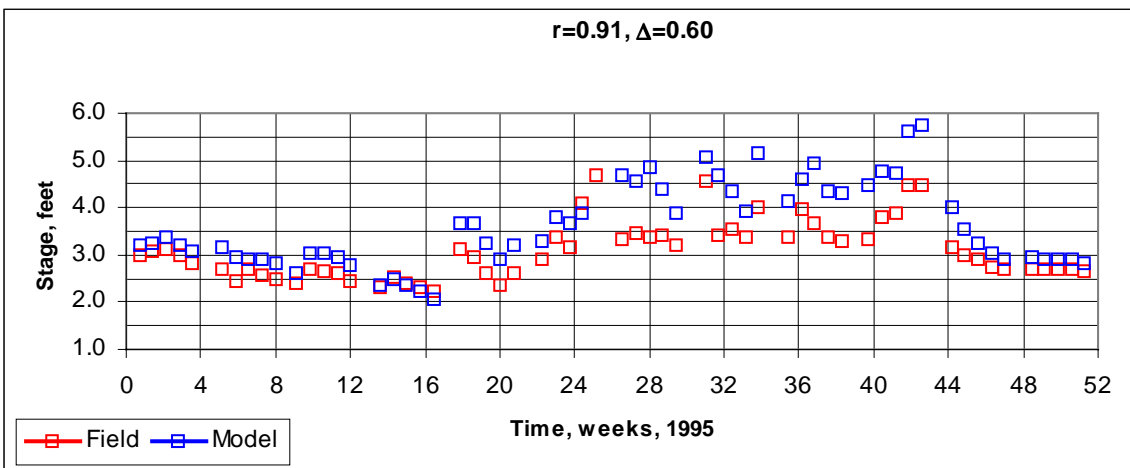
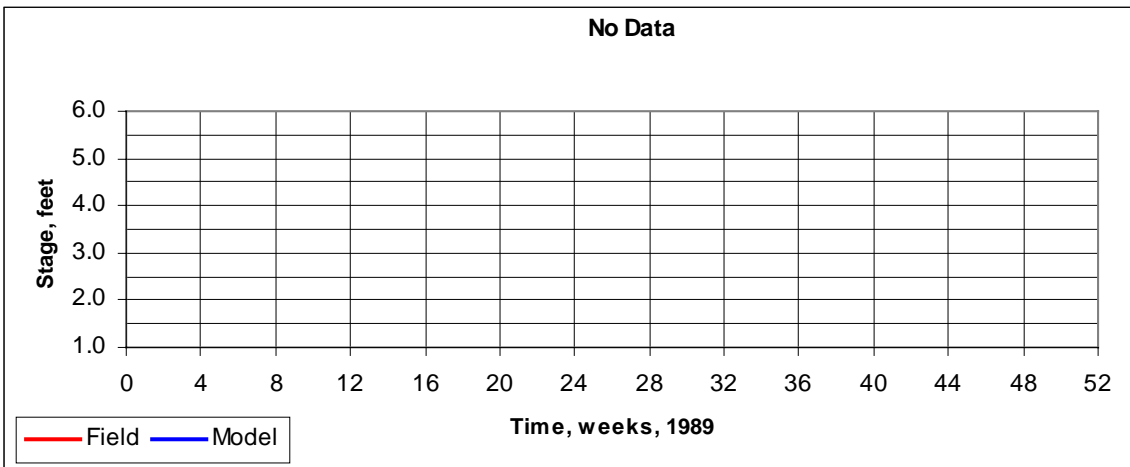
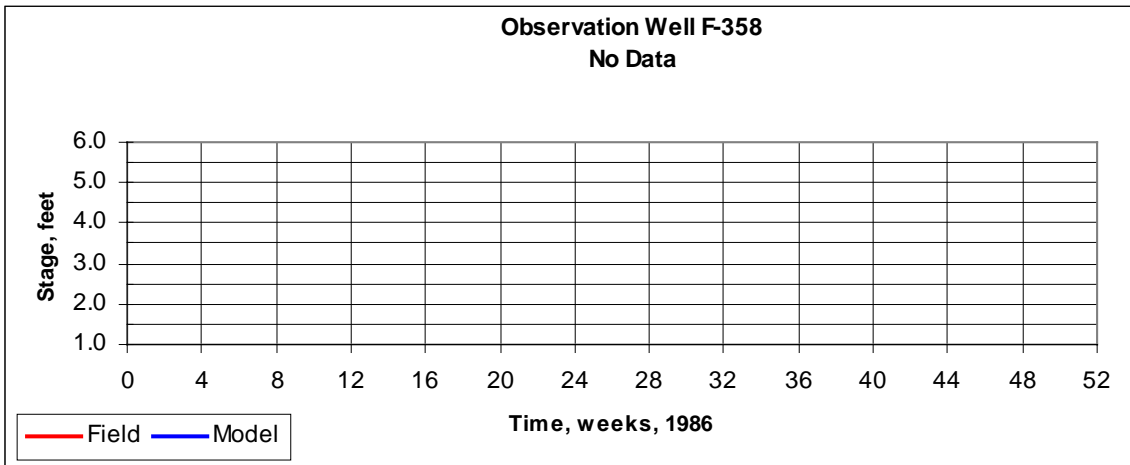


Figure 60 : Observation Well F-358

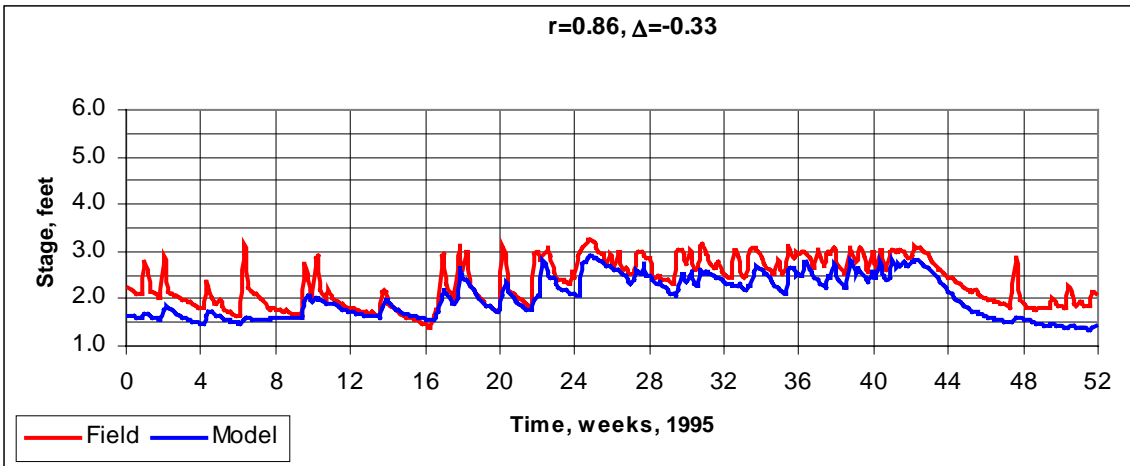
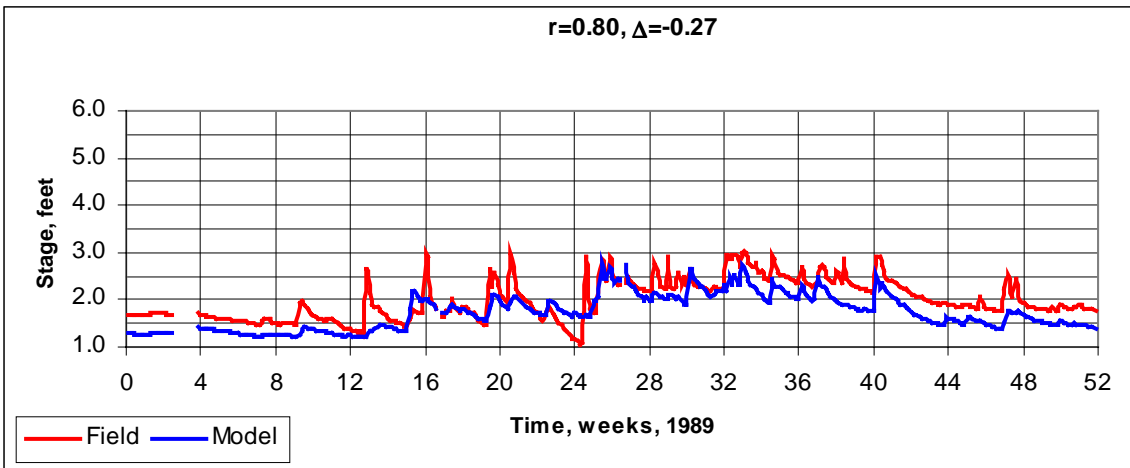
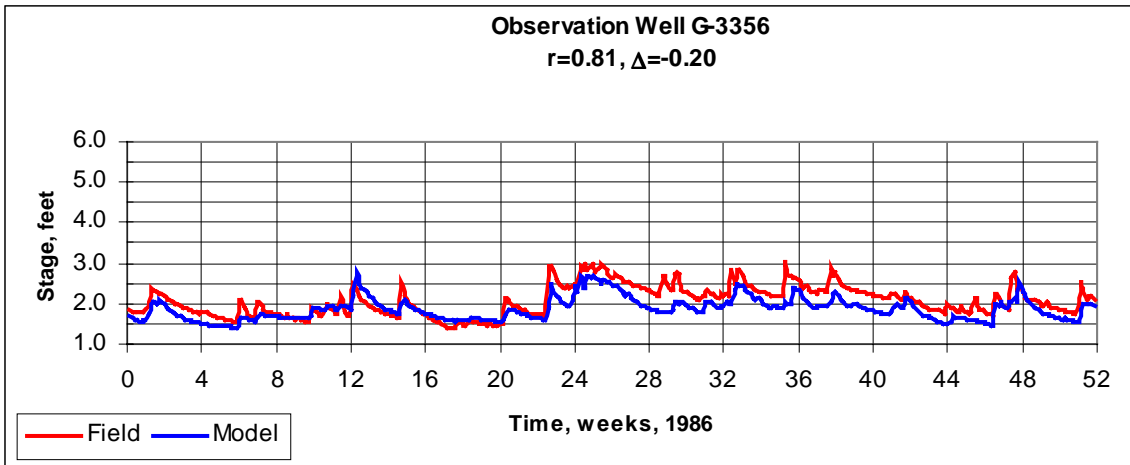


Figure 61: Observation Well G-3356

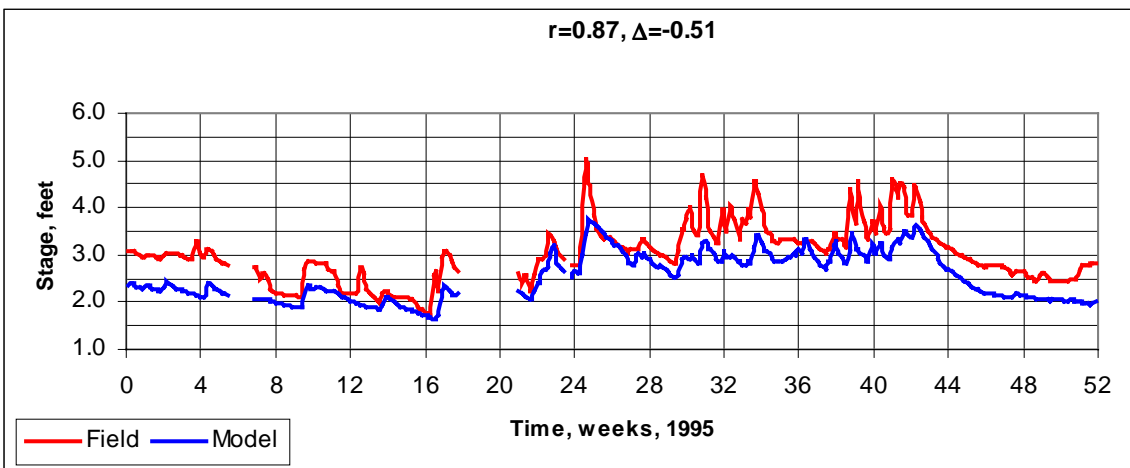
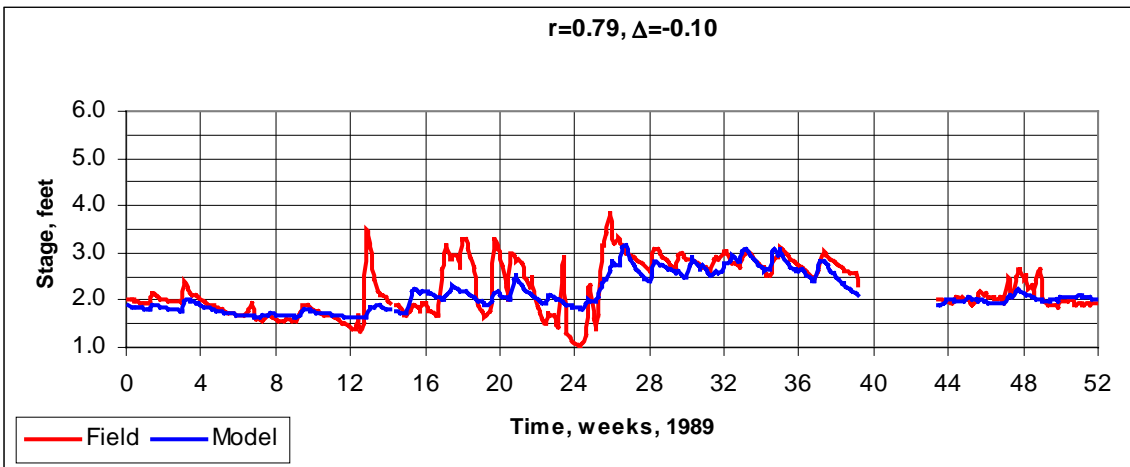
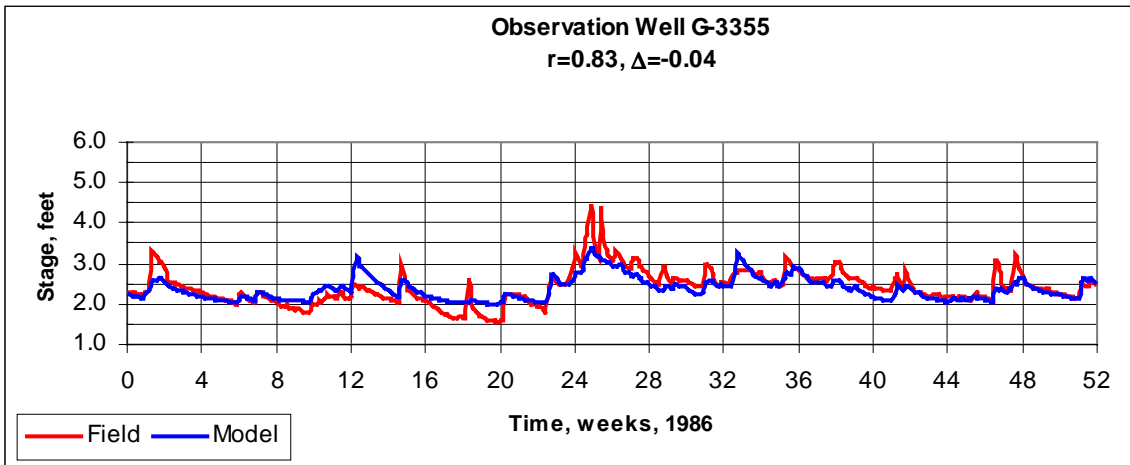


Figure 62: Observation Well G-3355

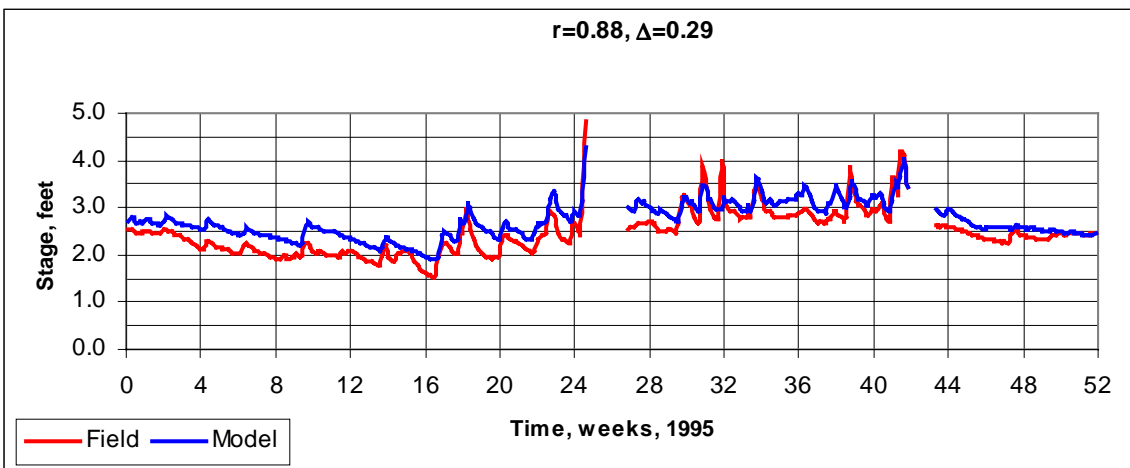
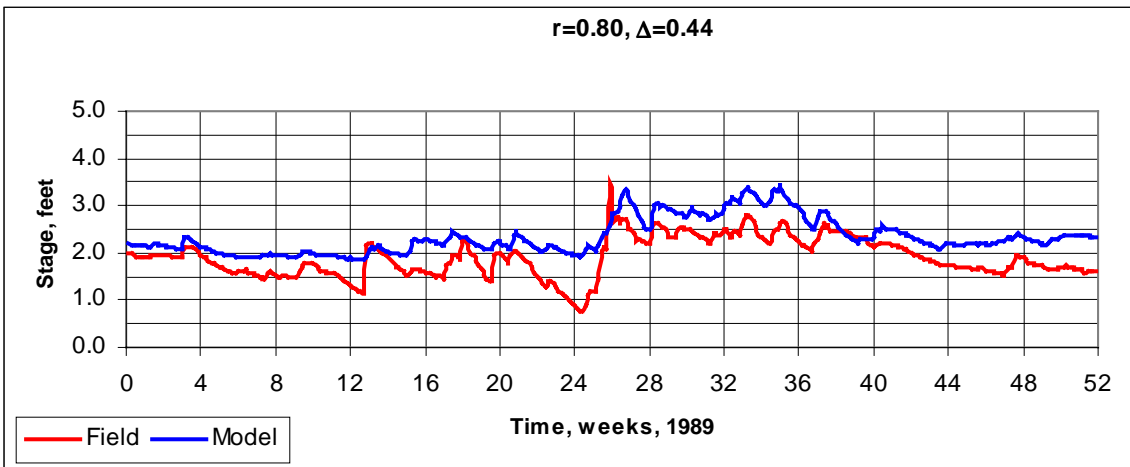
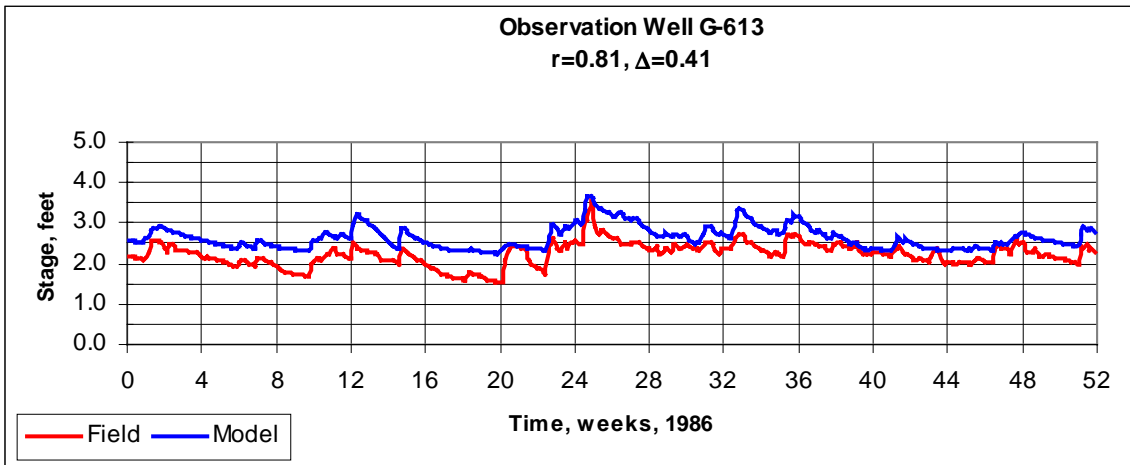


Figure 63: Observation Well G-613

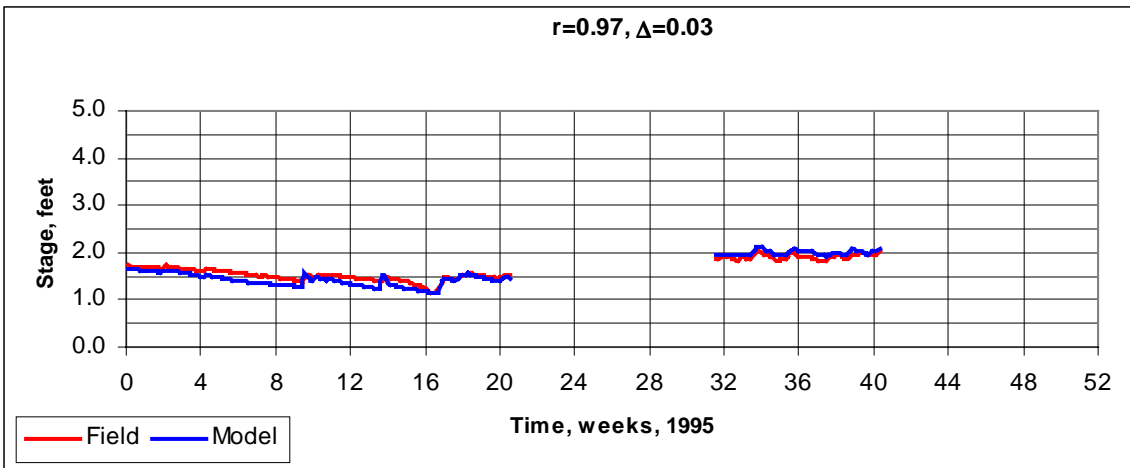
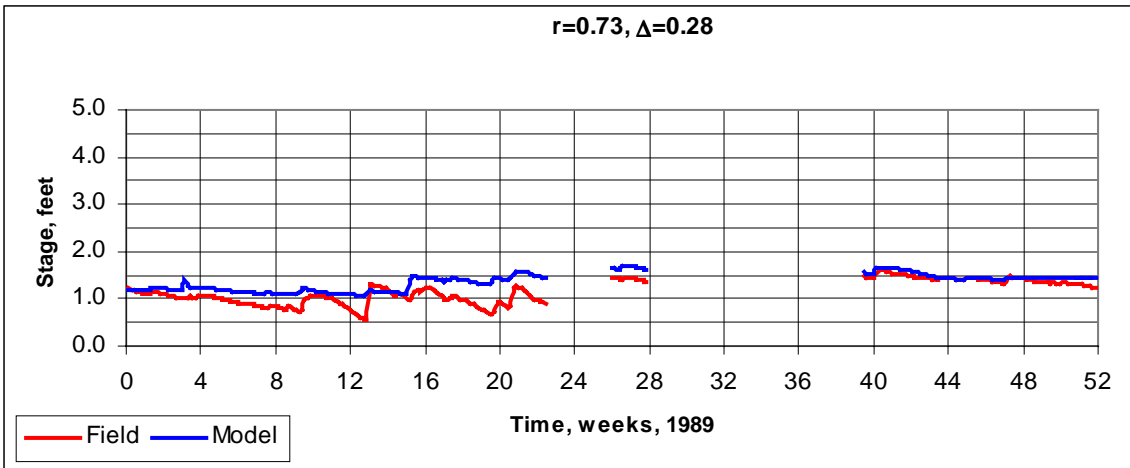
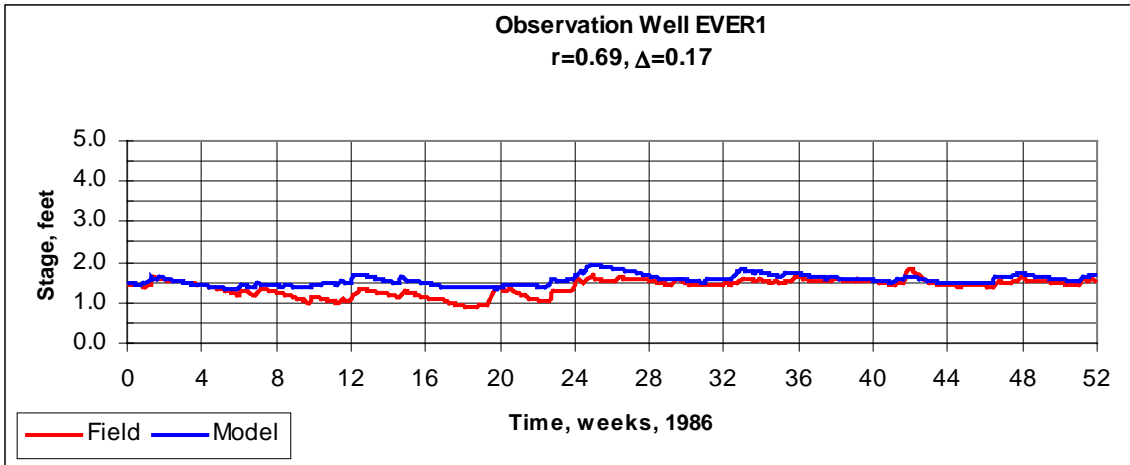


Figure 64: Observation Well EVER1

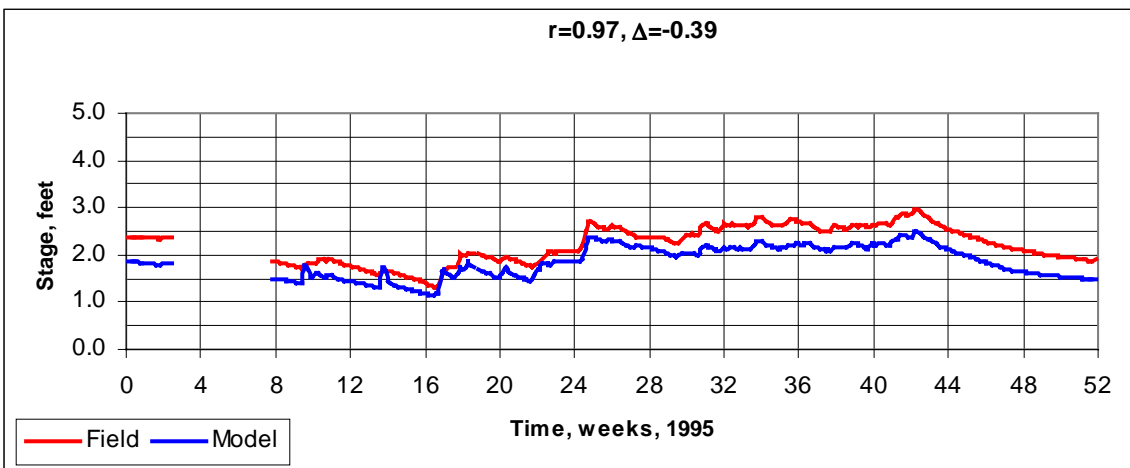
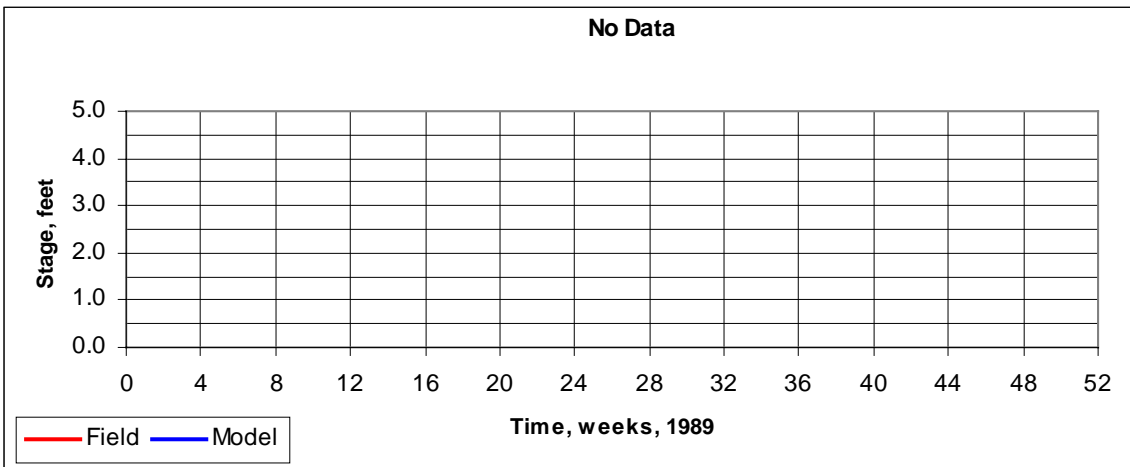
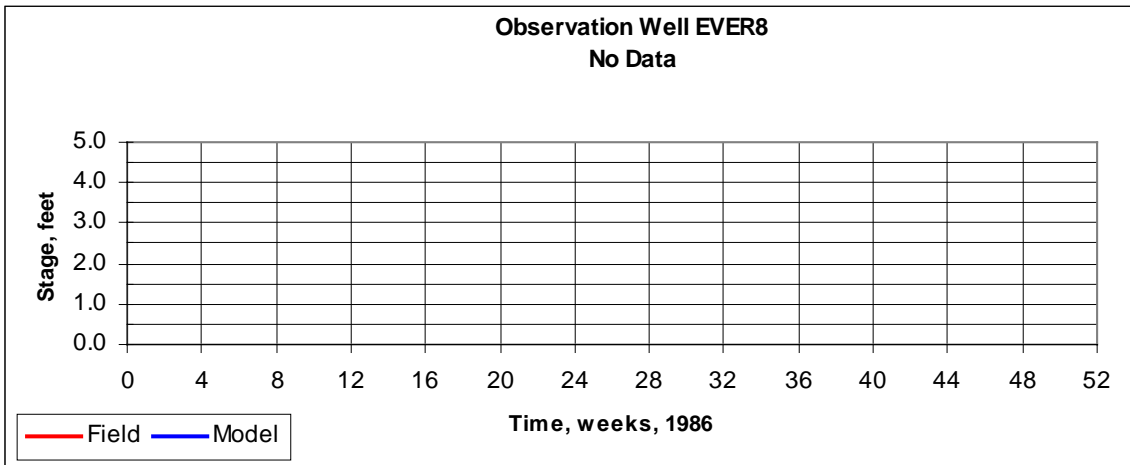


Figure 65: Observation Well EVER8

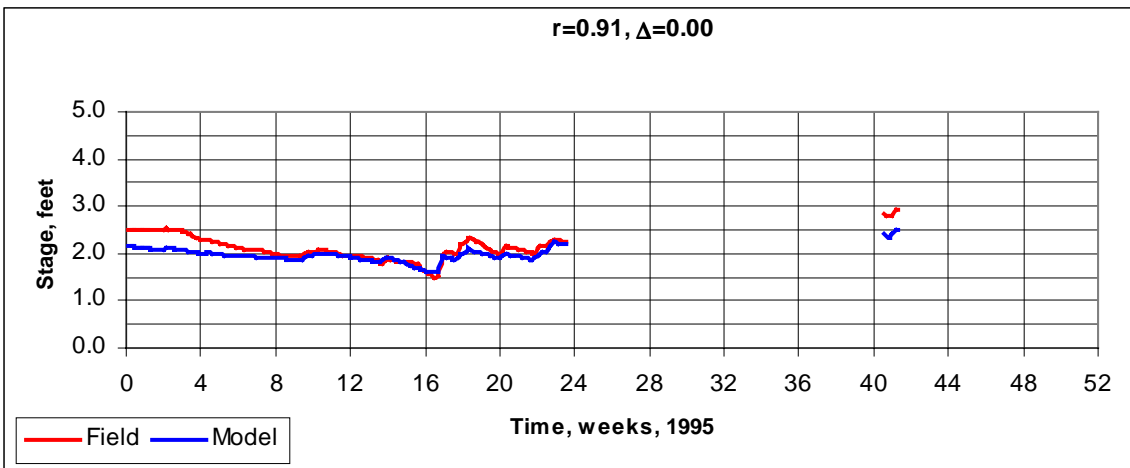
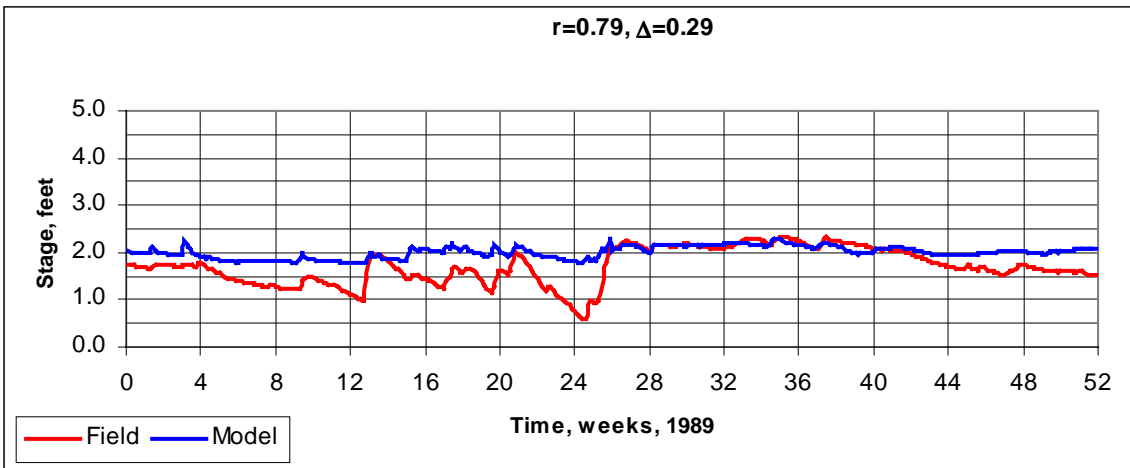
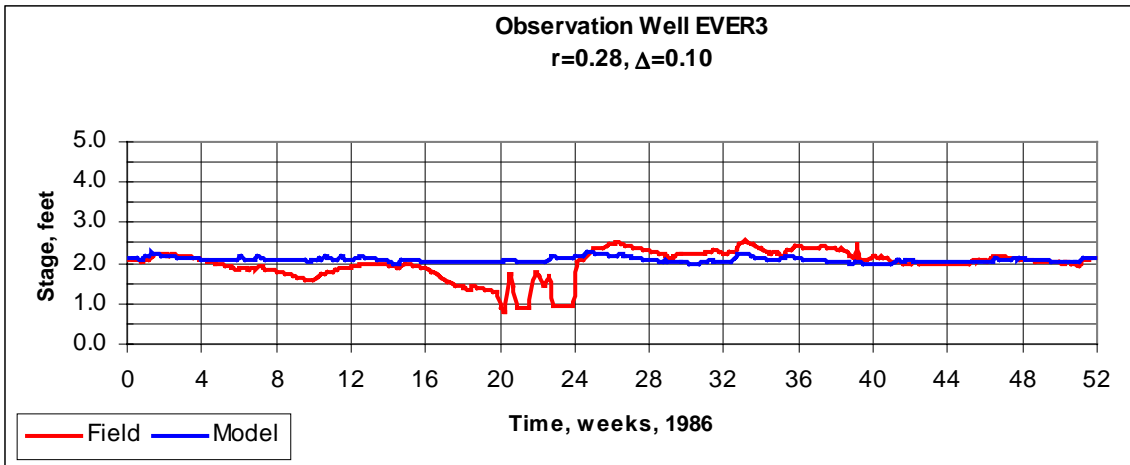


Figure 66: Observation Well EVER3

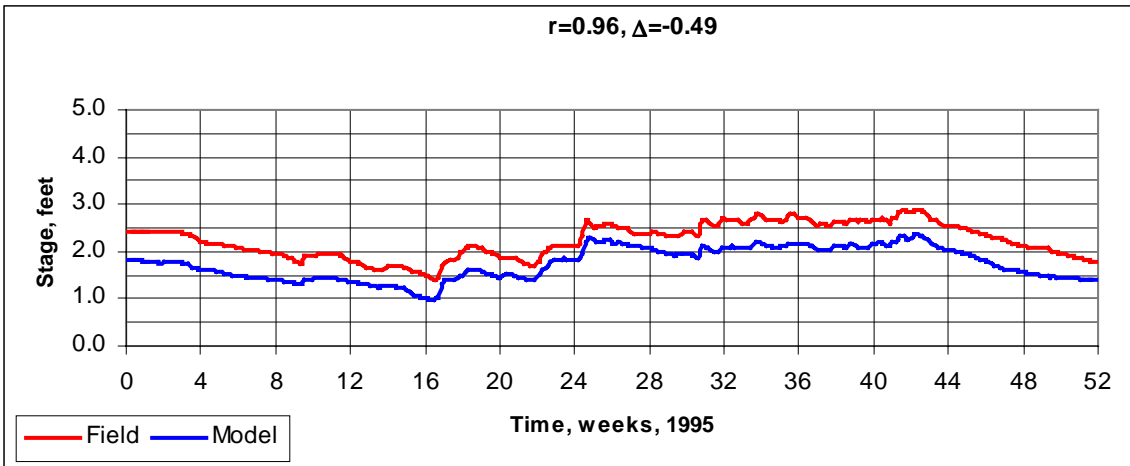
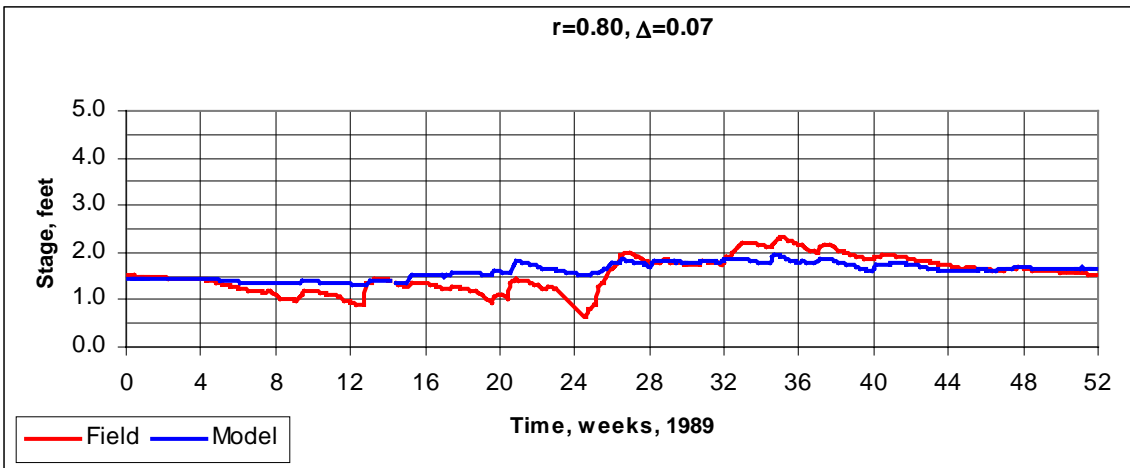
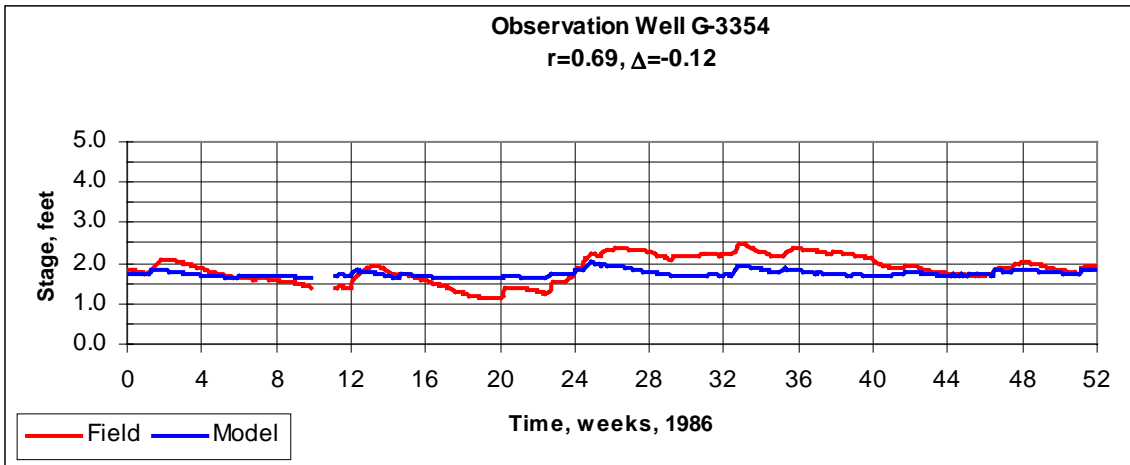


Figure 67: Observation Well G-3354

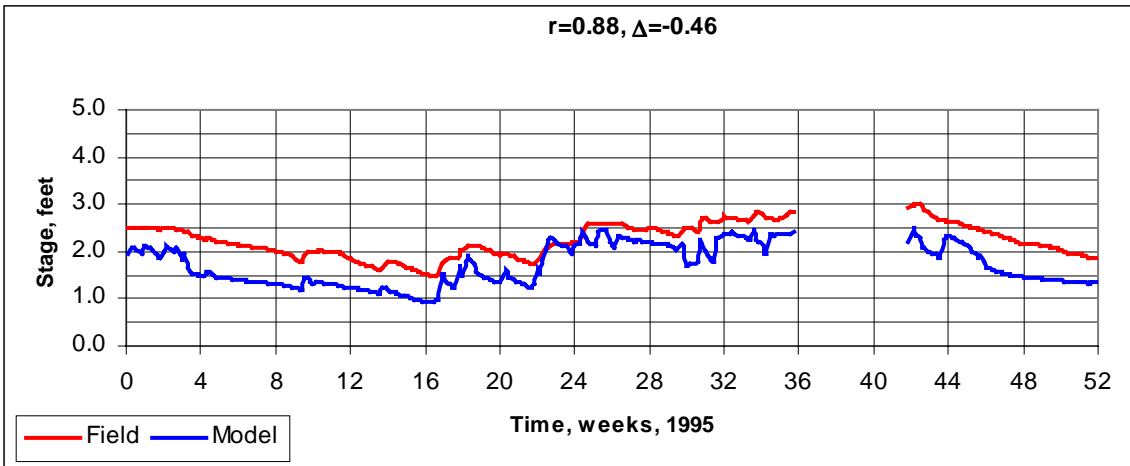
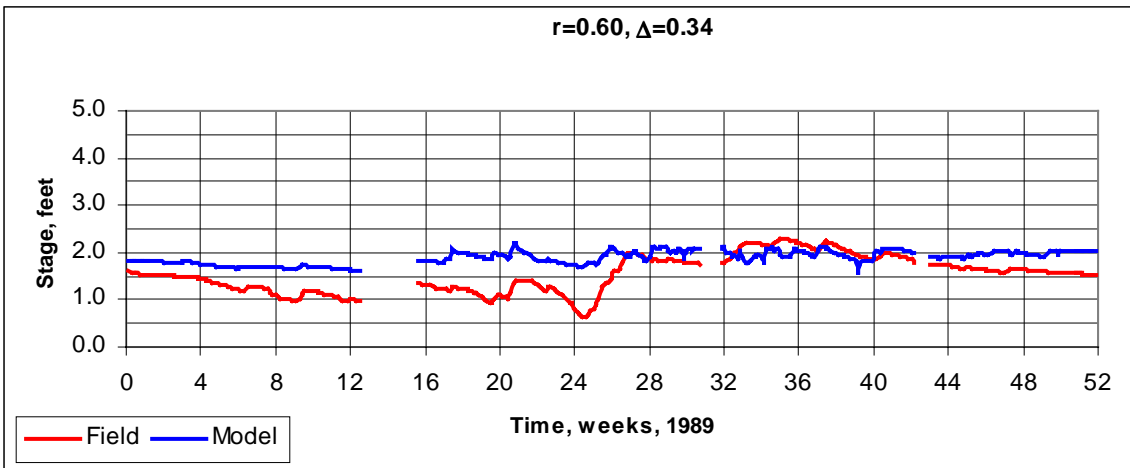
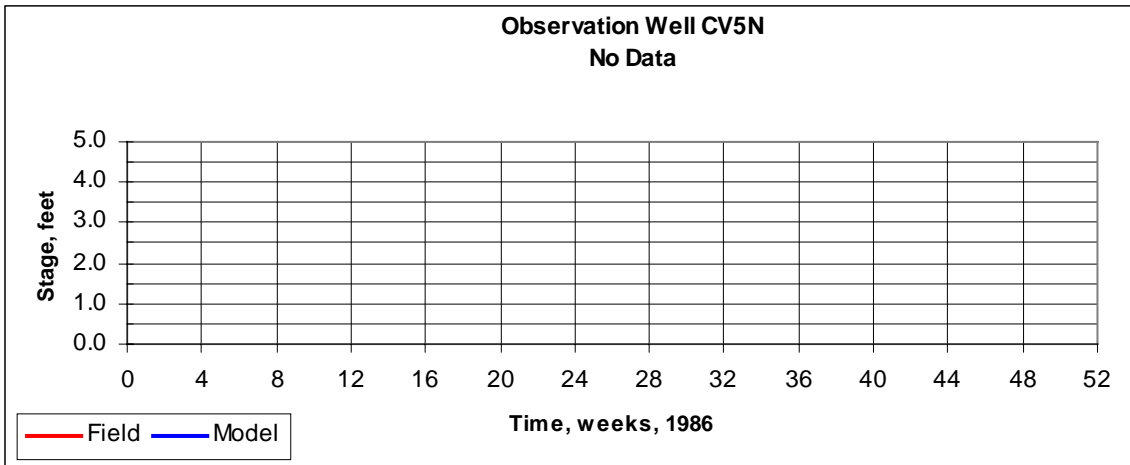


Figure 68: Observation Well CV5N

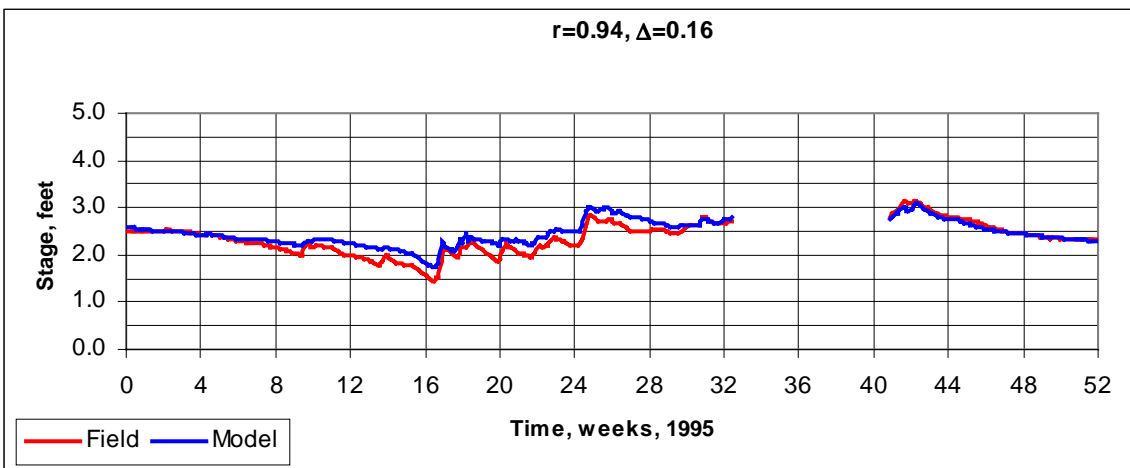
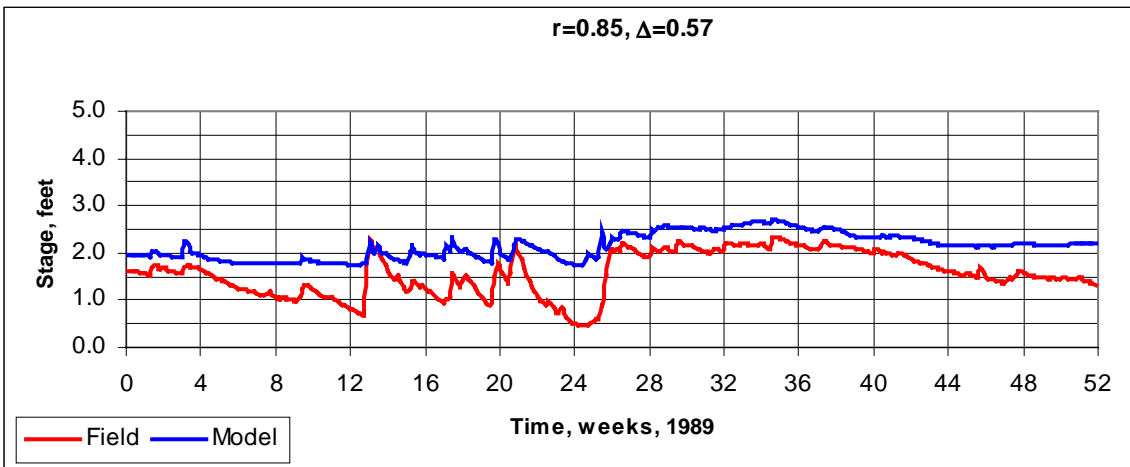
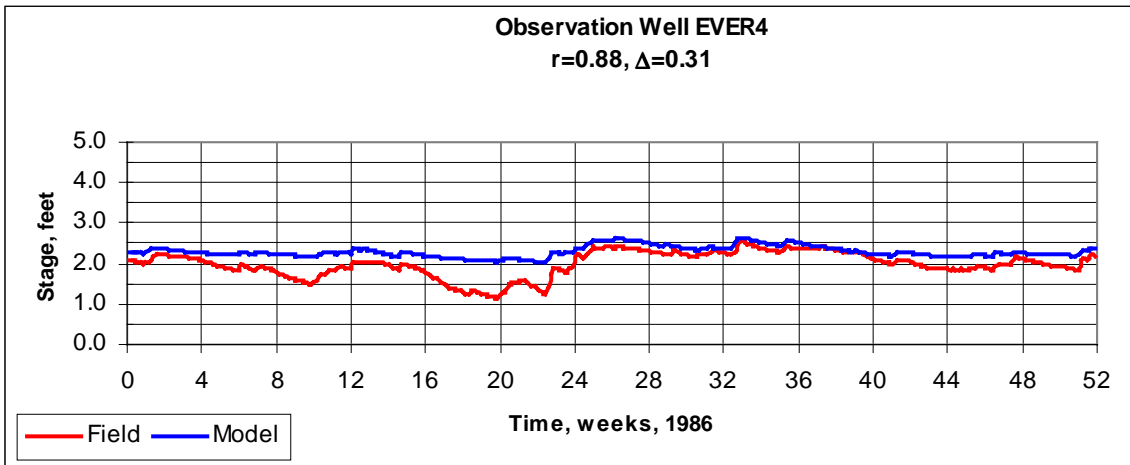


Figure 69: Observation Well EVER4

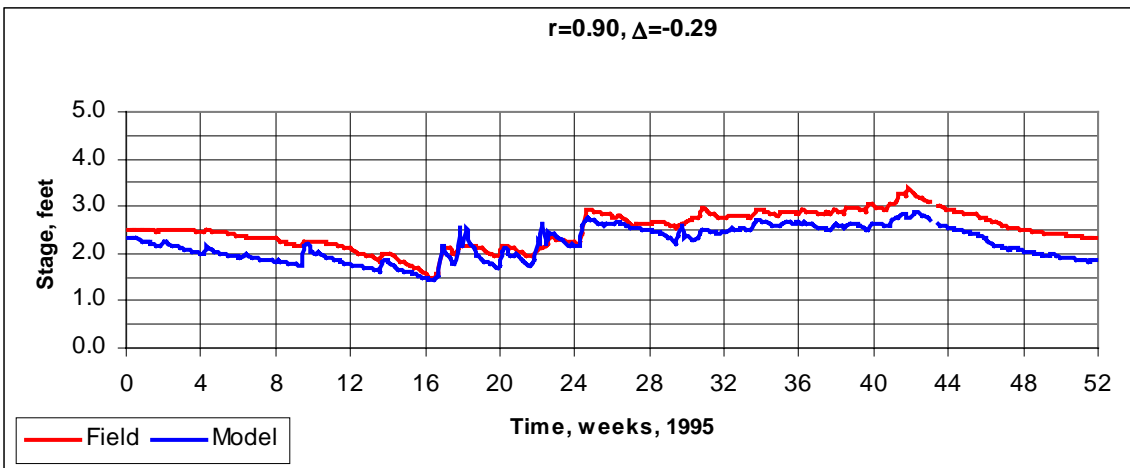
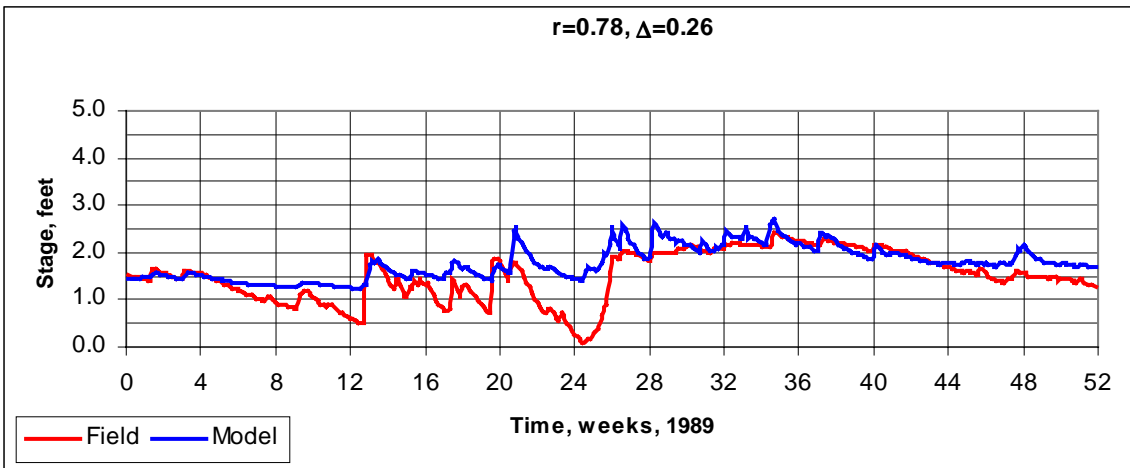
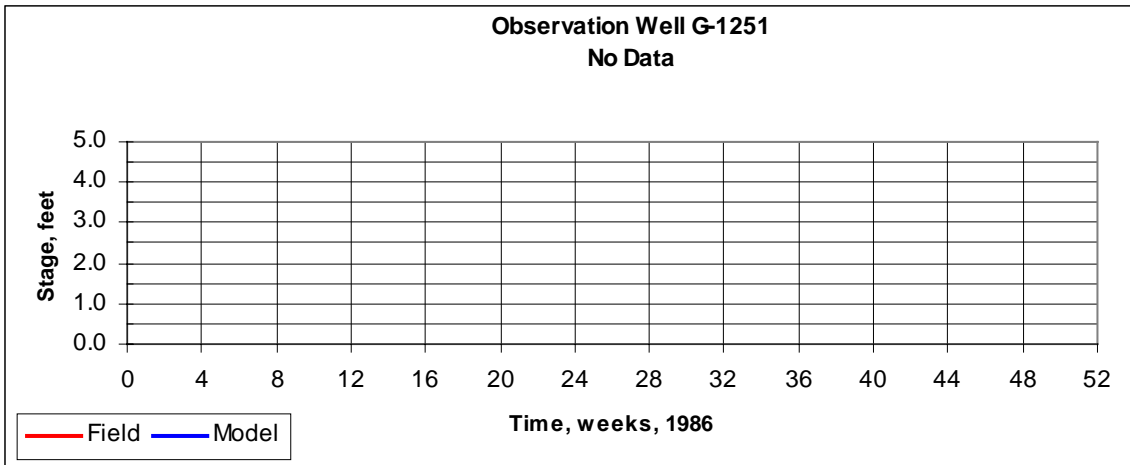


Figure 70: Observation Well G-1251

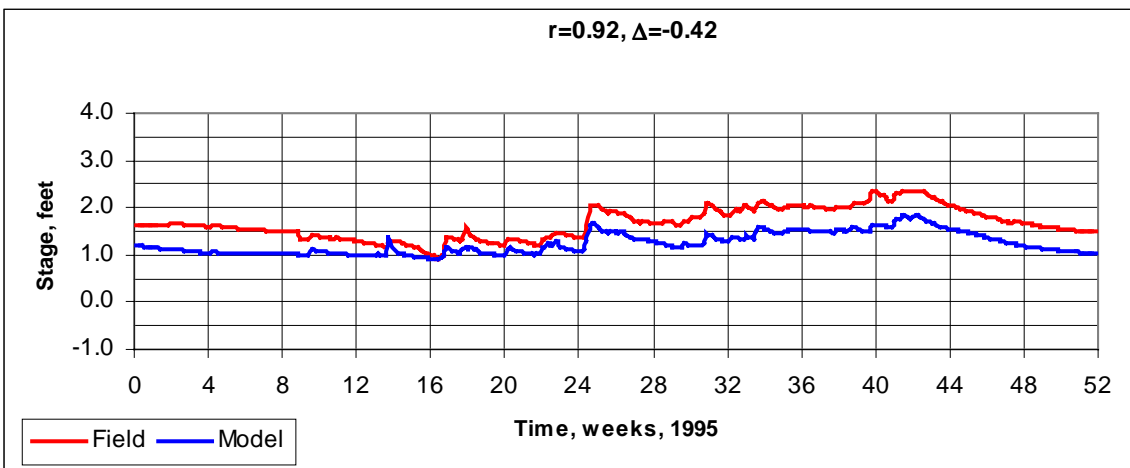
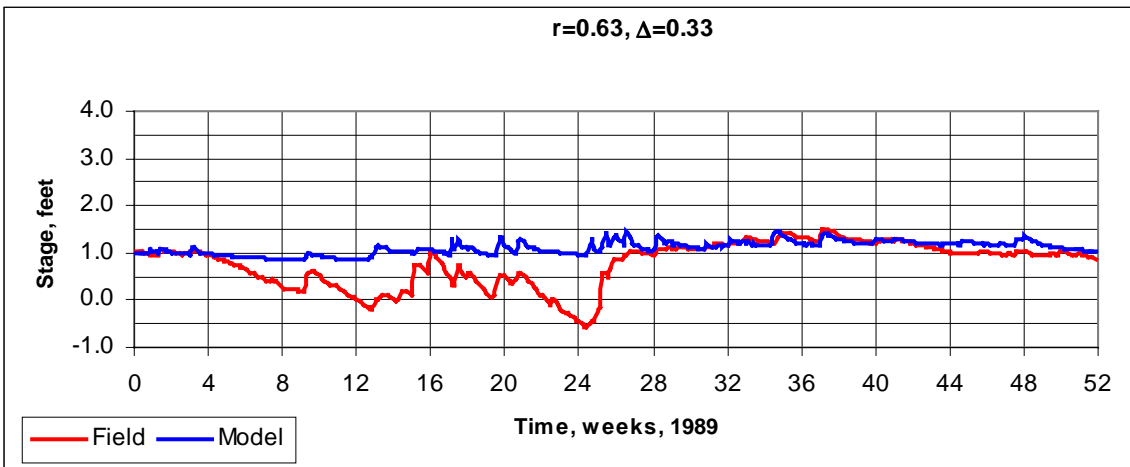
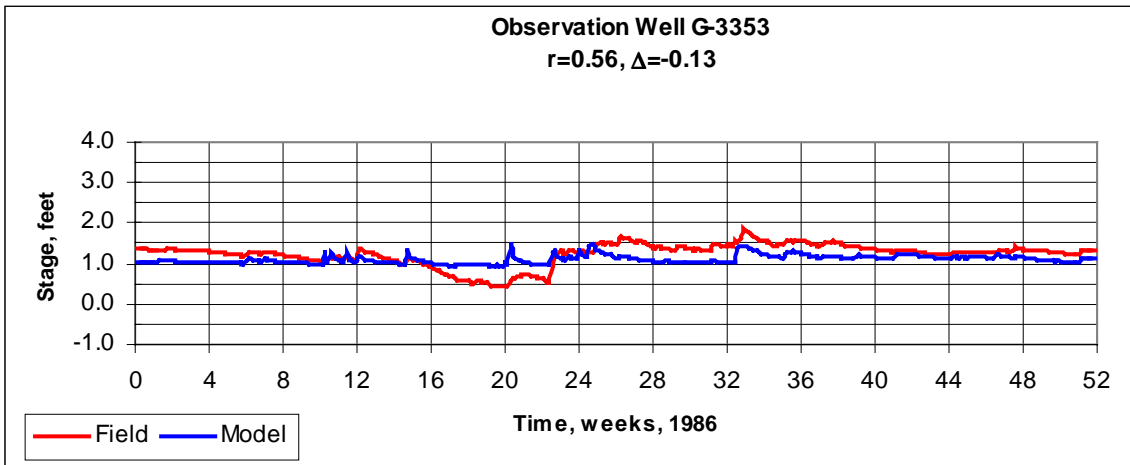


Figure 71: Observation Well G-3353

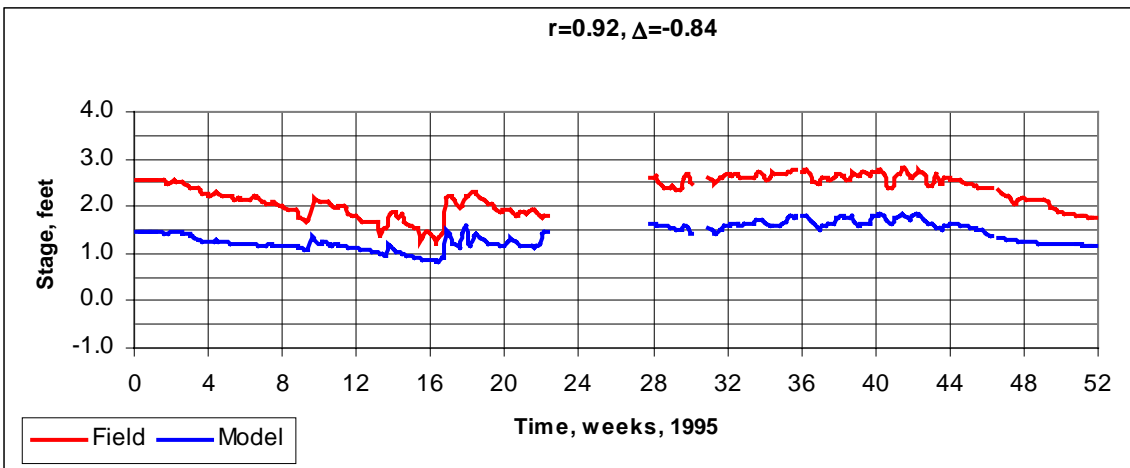
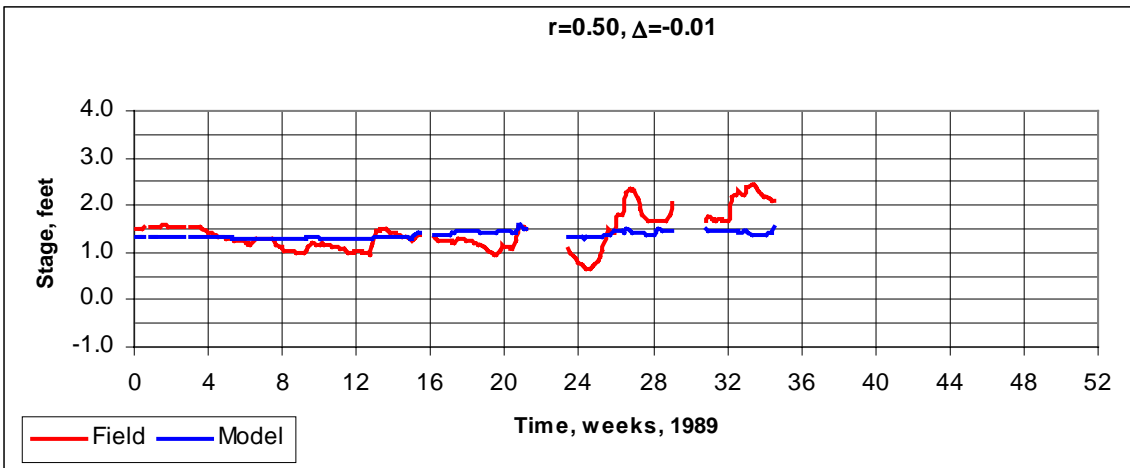
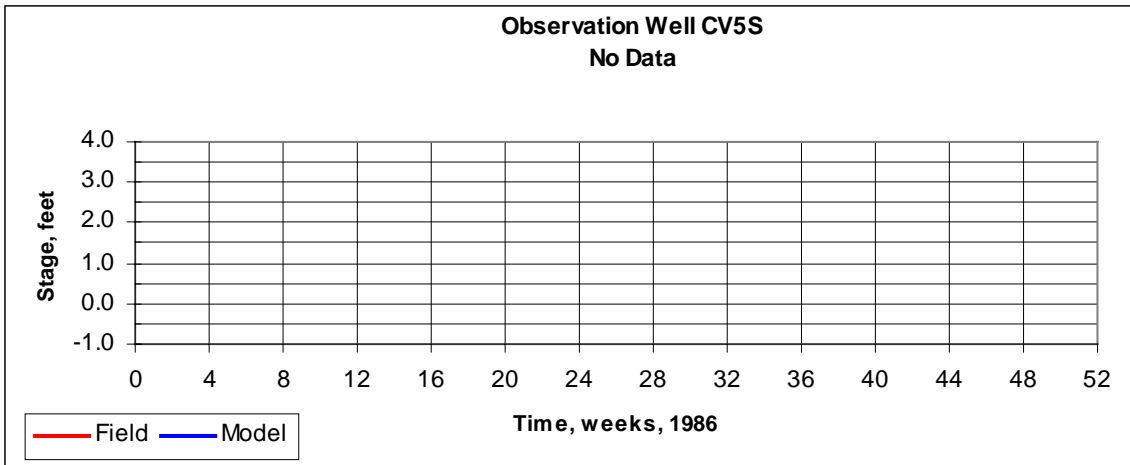


Figure 72: Observation Well CV5S

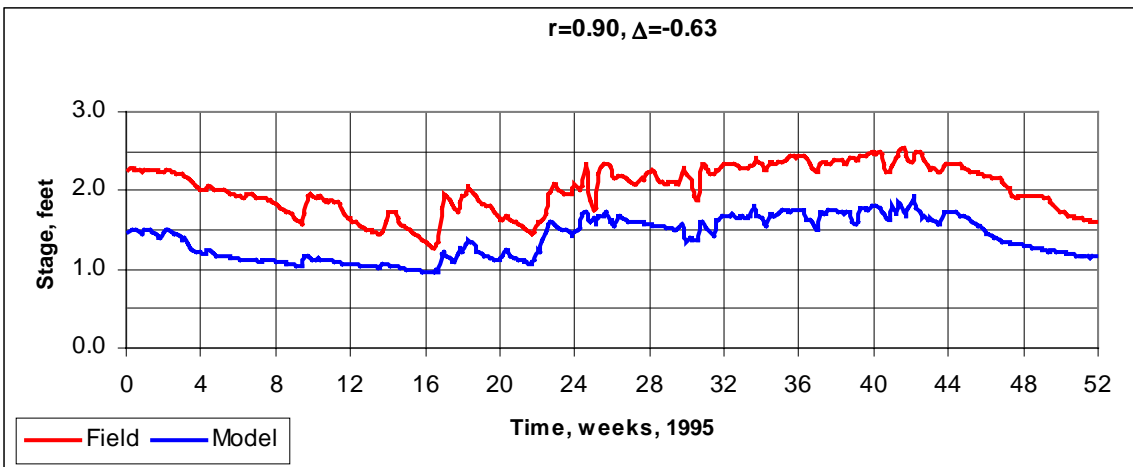
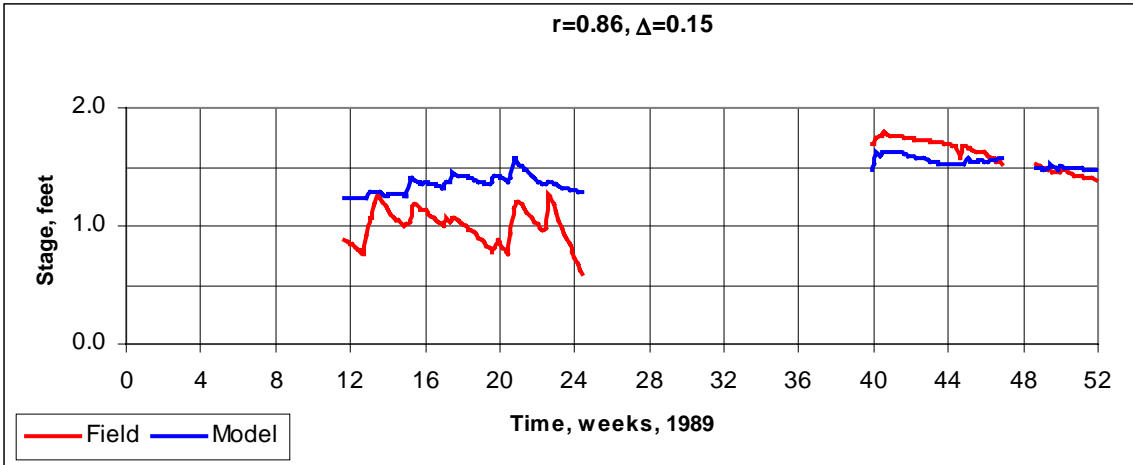
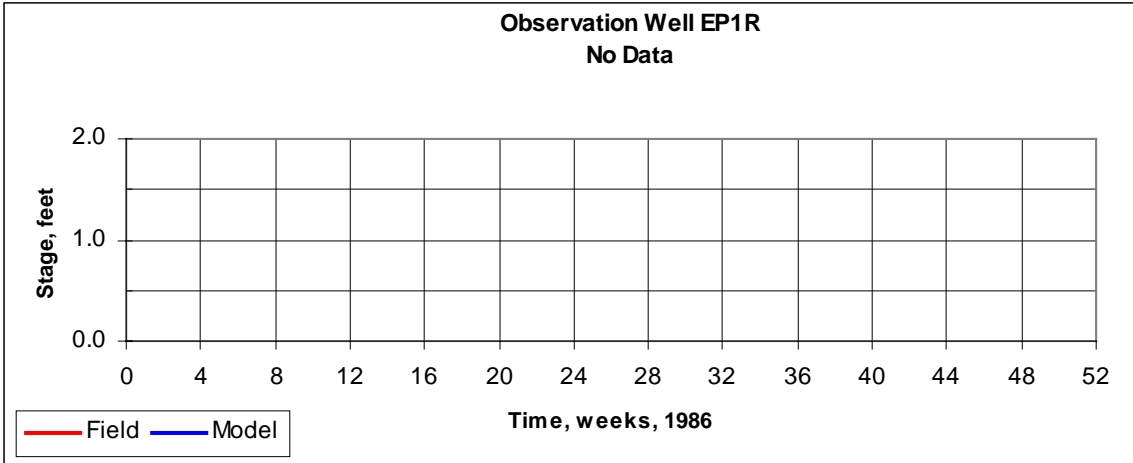


Figure 73: Observation Well EP1R

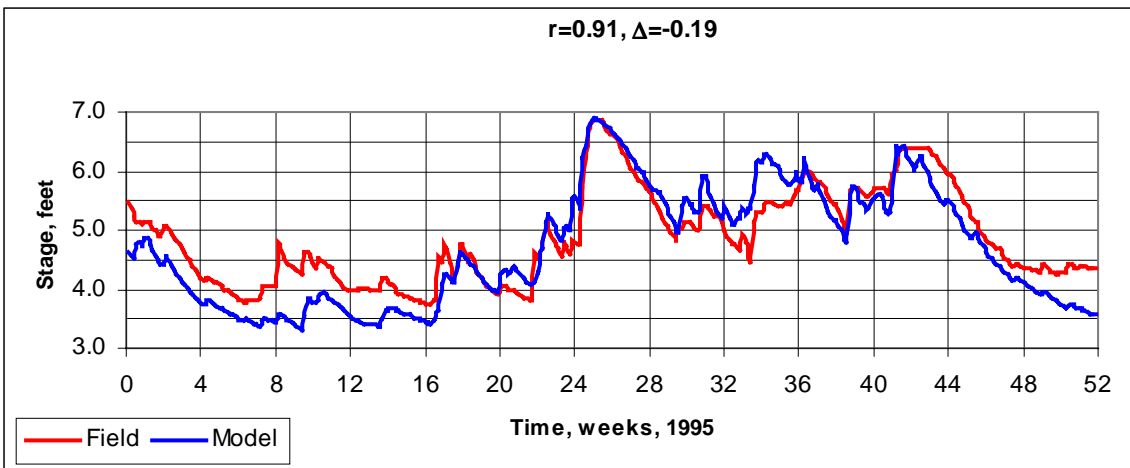
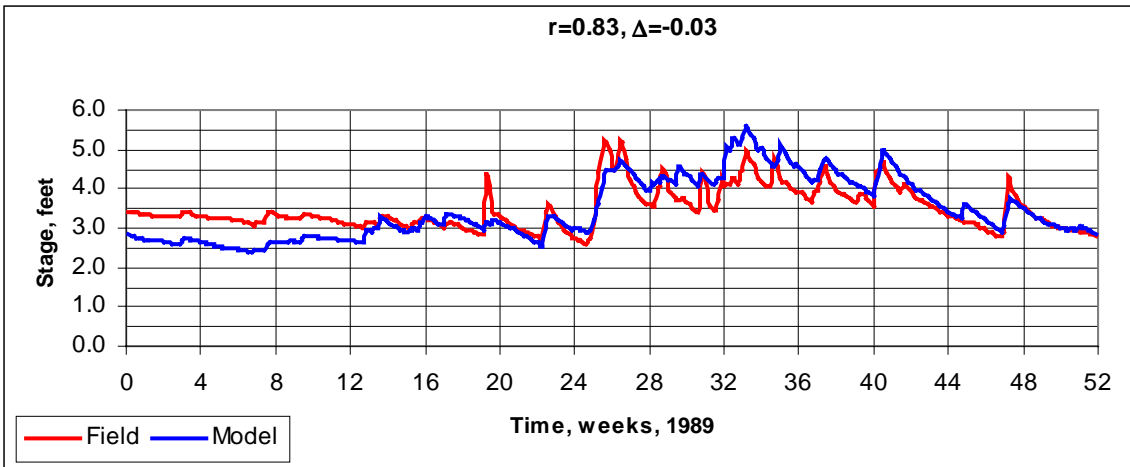
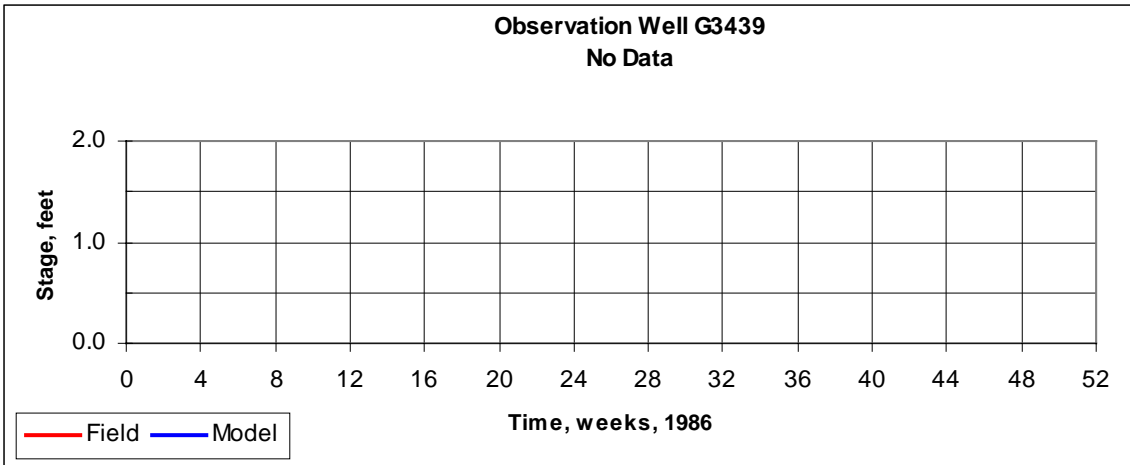


Figure 74: Observation Well G-3439

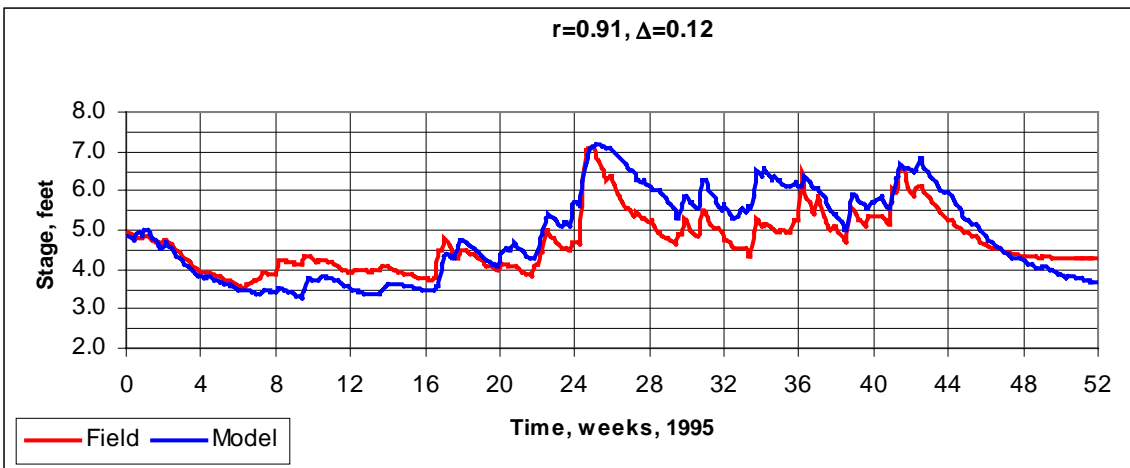
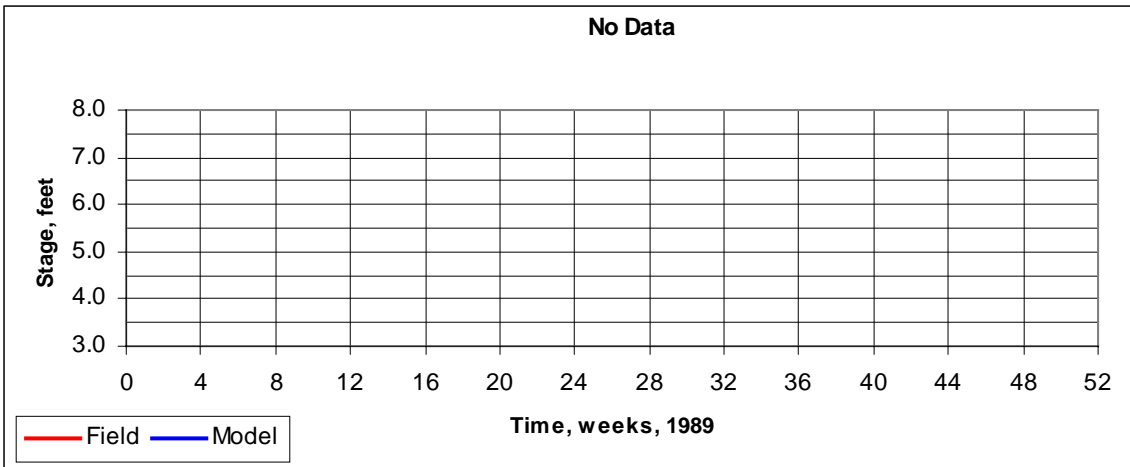
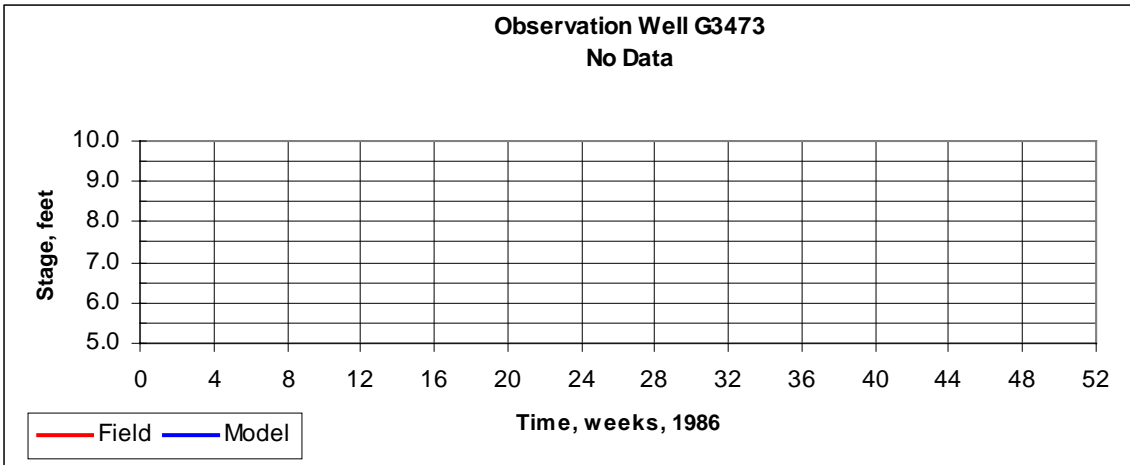


Figure 75: Observation Well G-3473

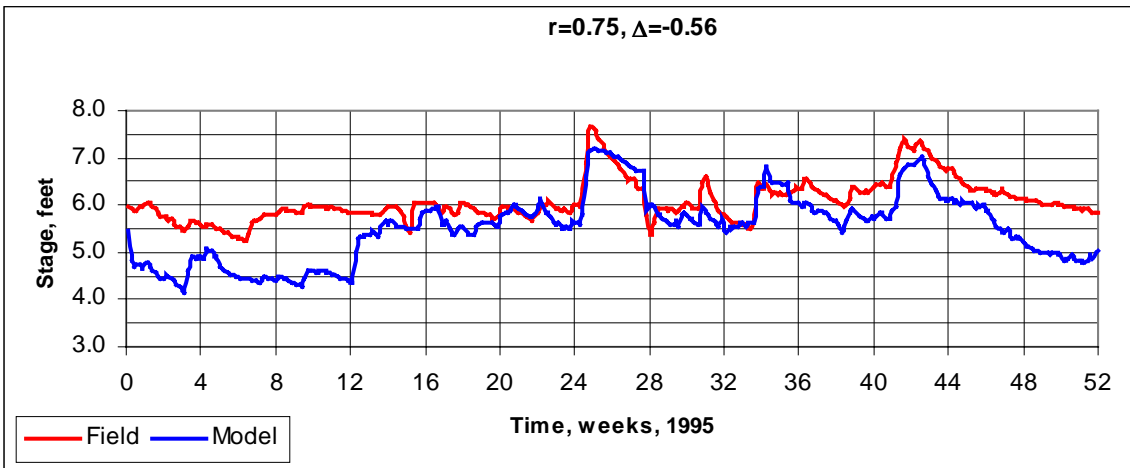
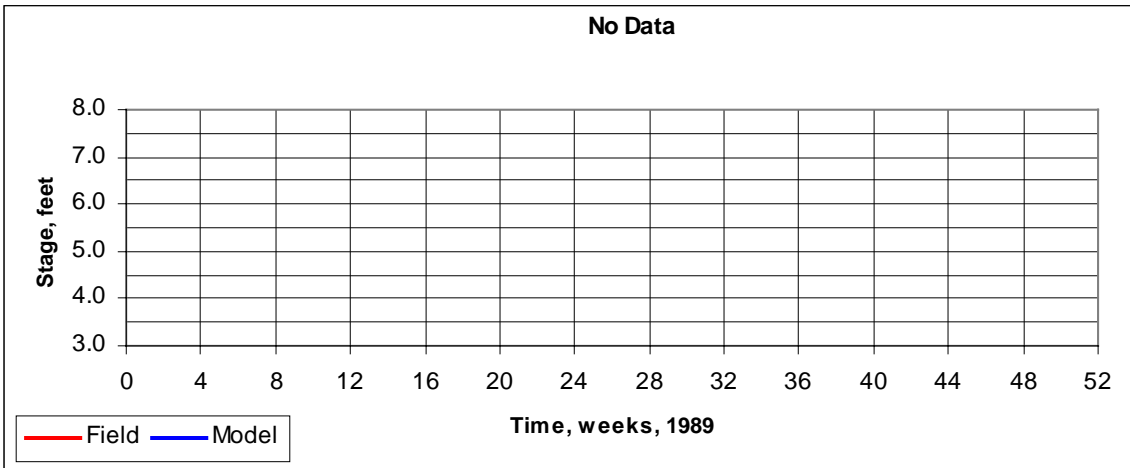
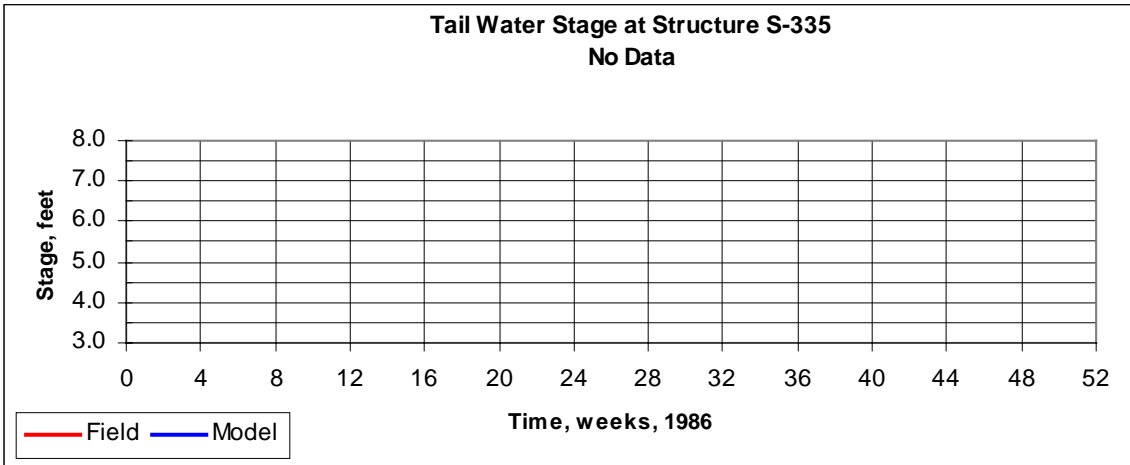


Figure 76: Tail Water Stage at S-335

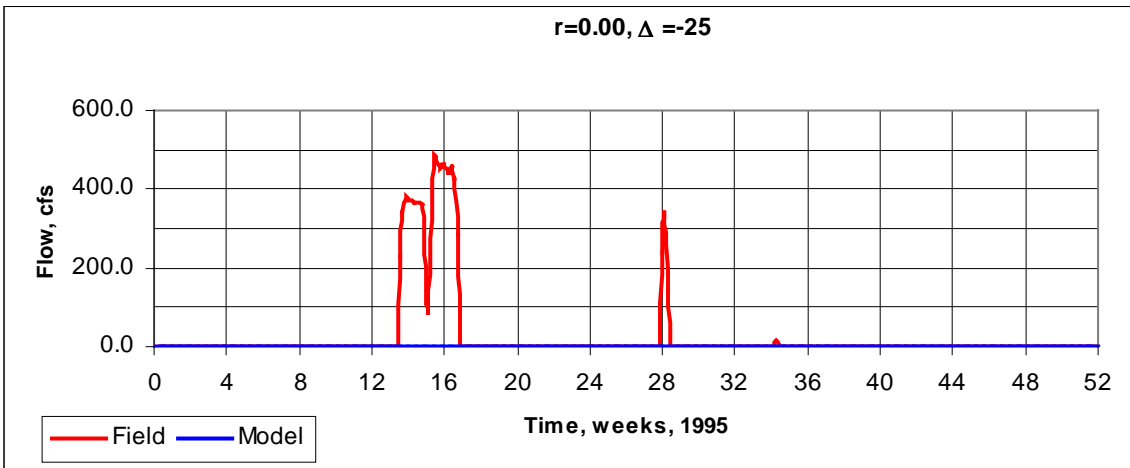
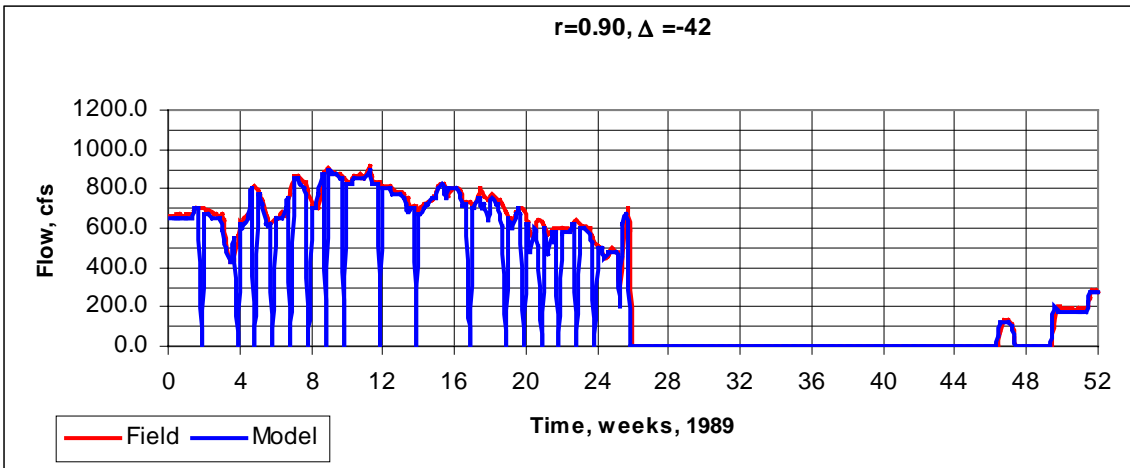
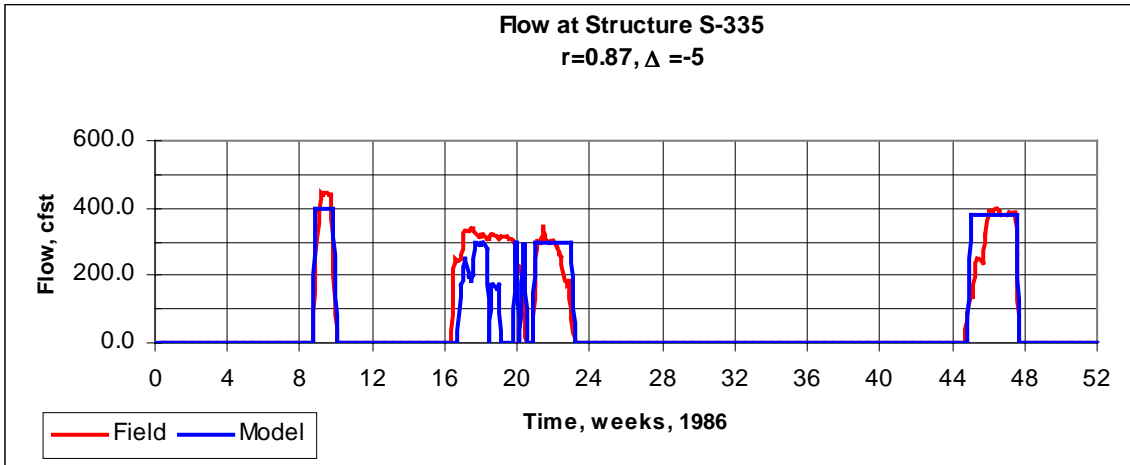


Figure 77: Flow at S-335

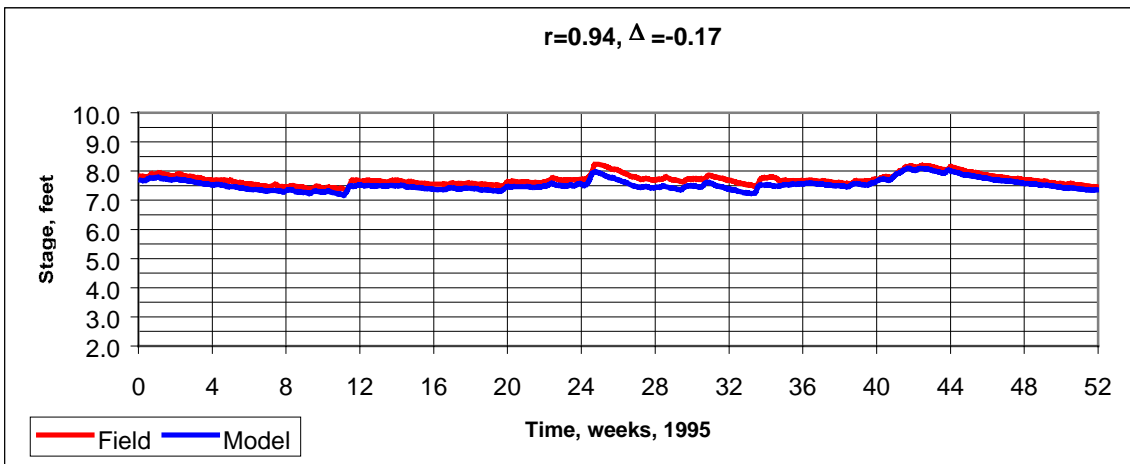
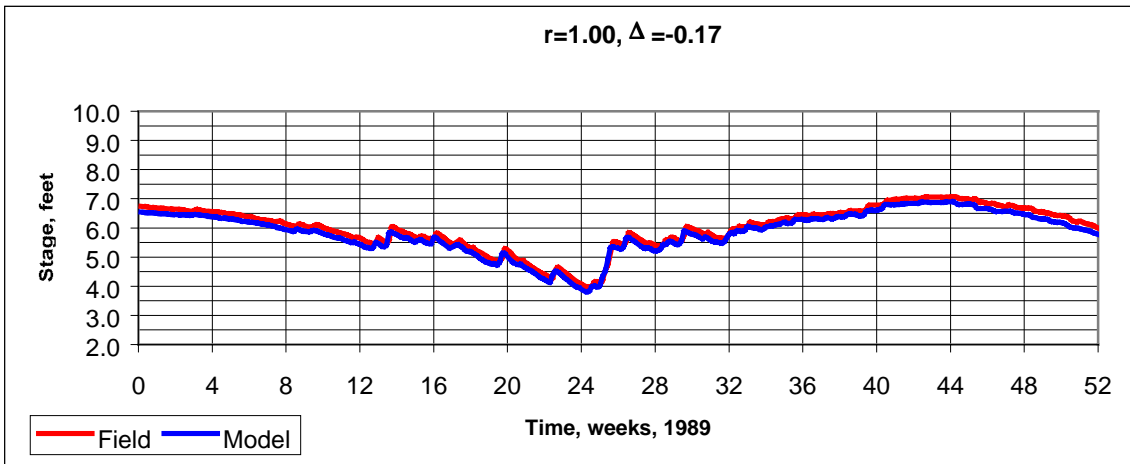
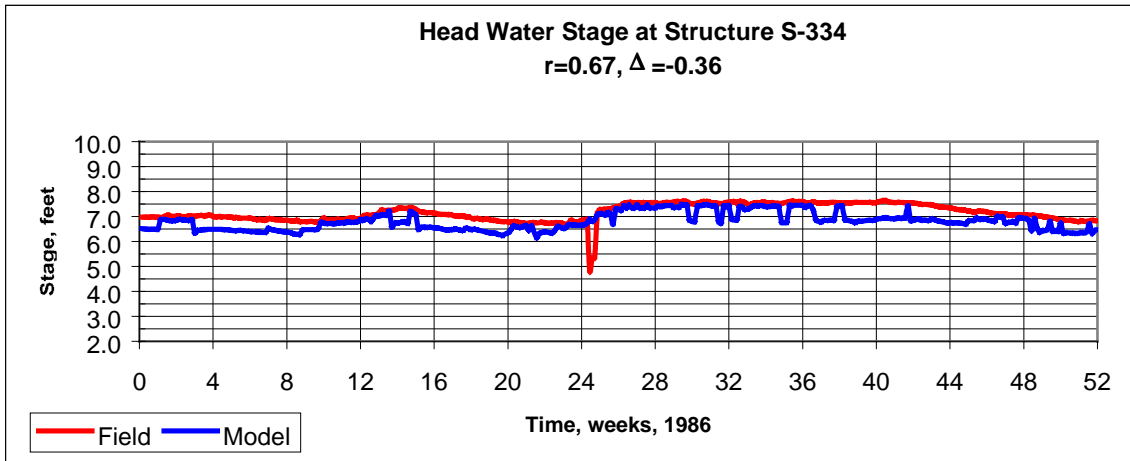


Figure 78: Head Water Stage at S-334

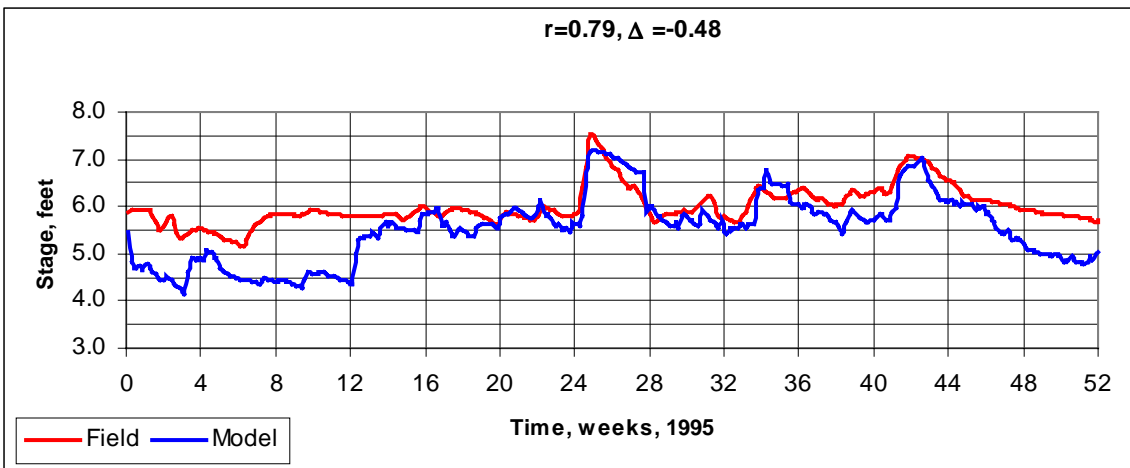
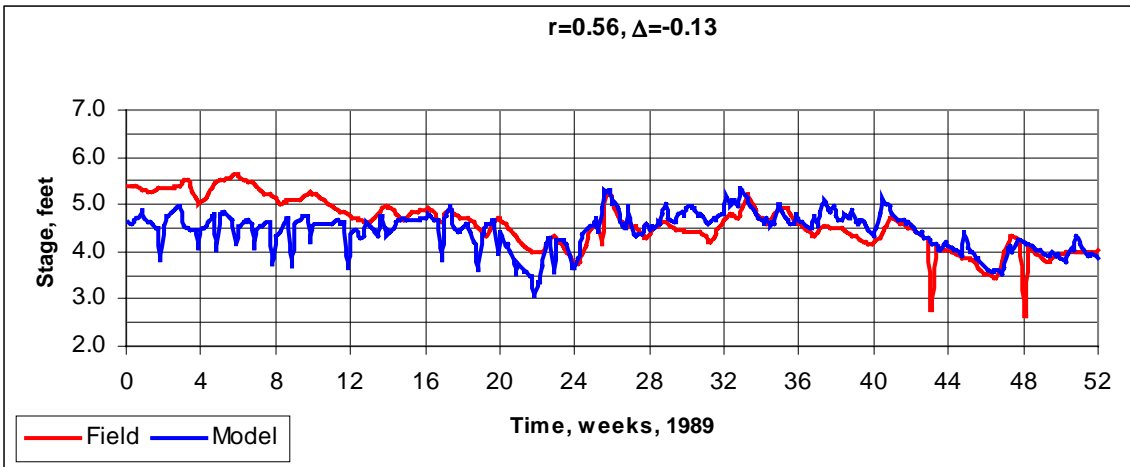
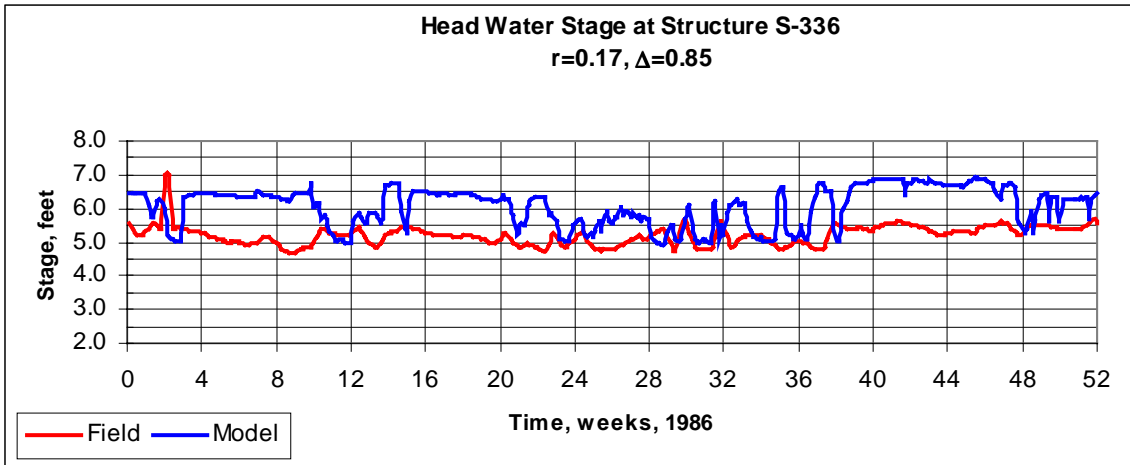


Figure 79: Head Water Stage at S-336

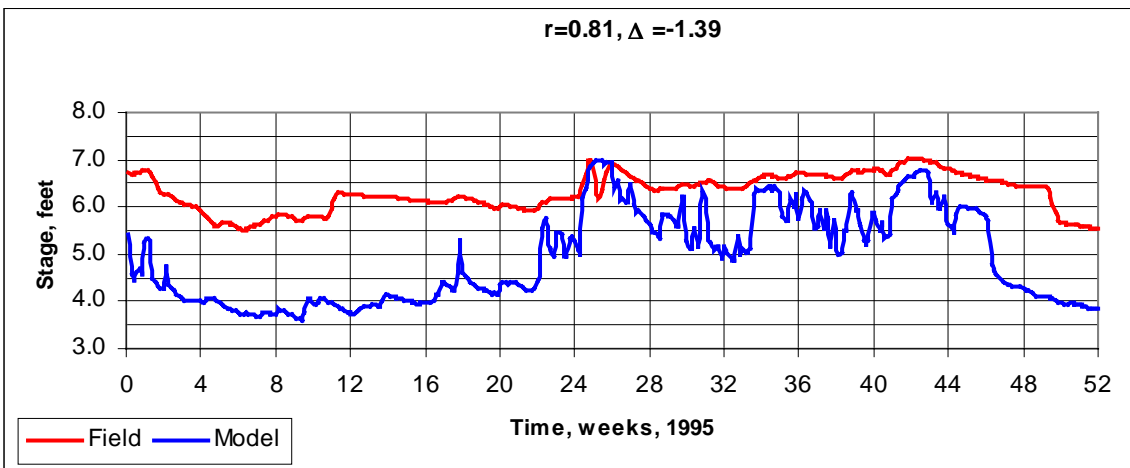
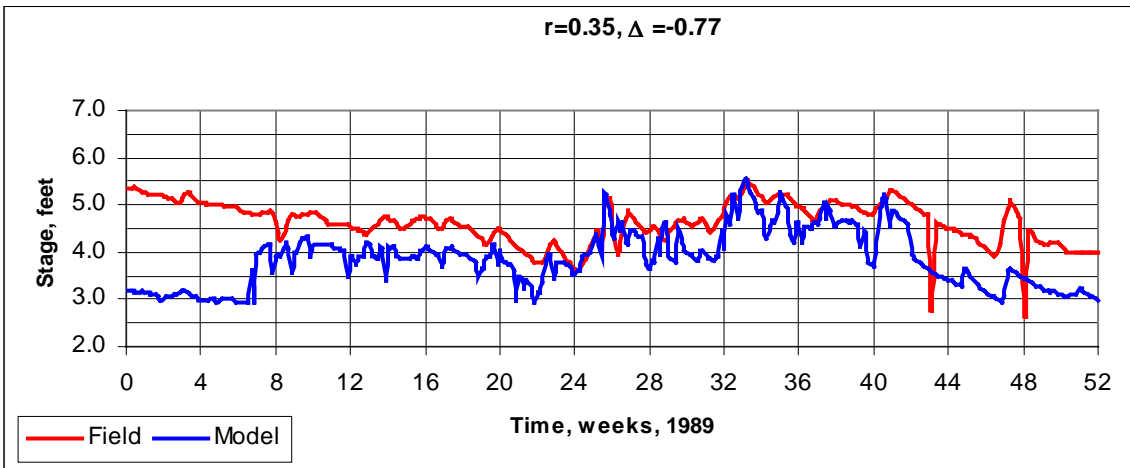
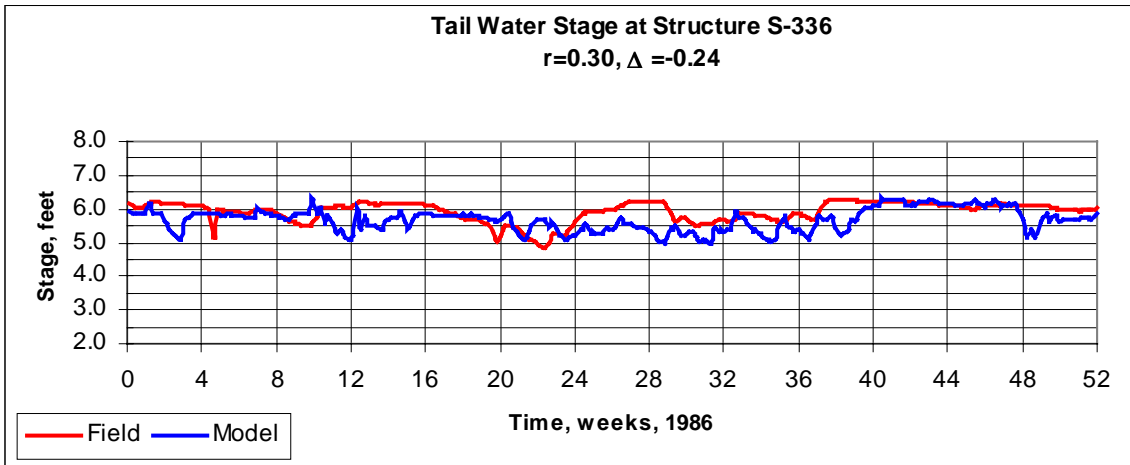


Figure 80: Tail Water Stage at S-336

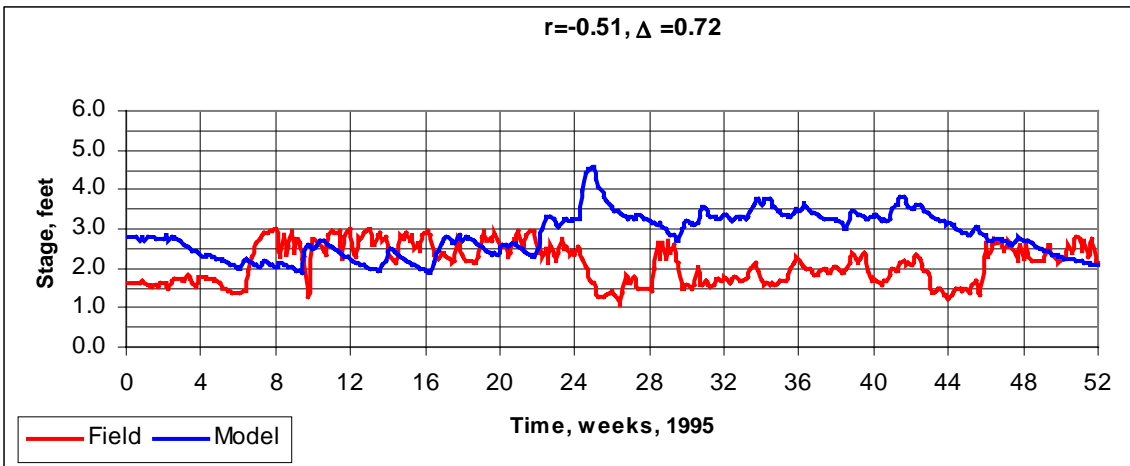
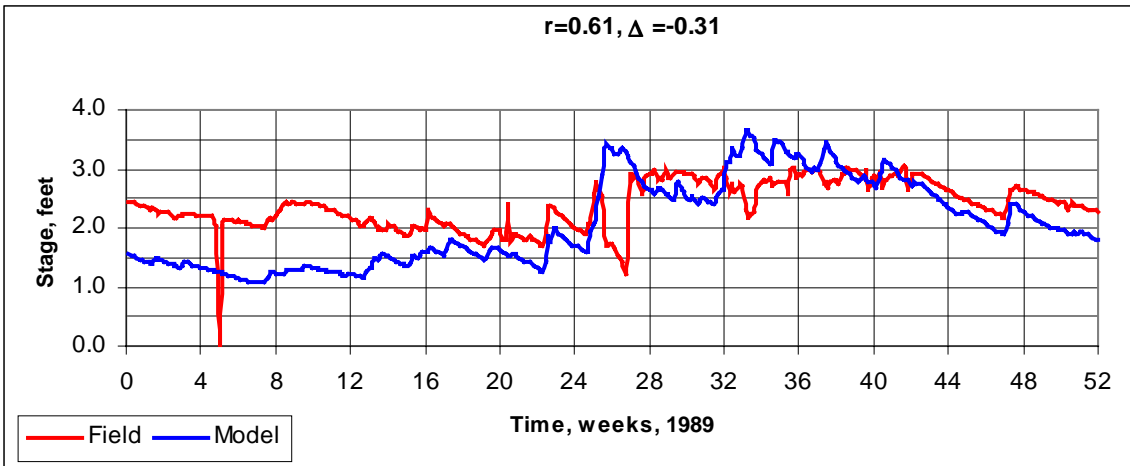
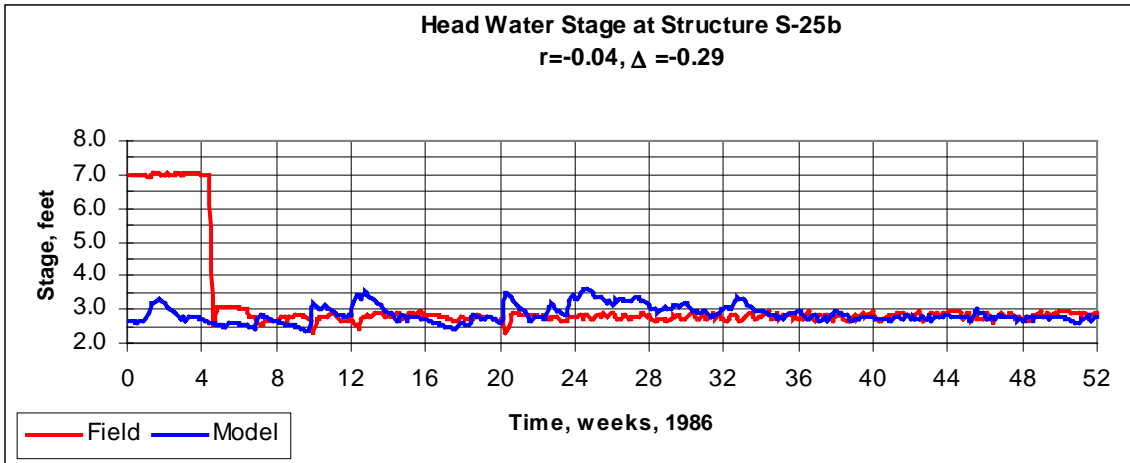


Figure 81: Head Water Stage at S-25b

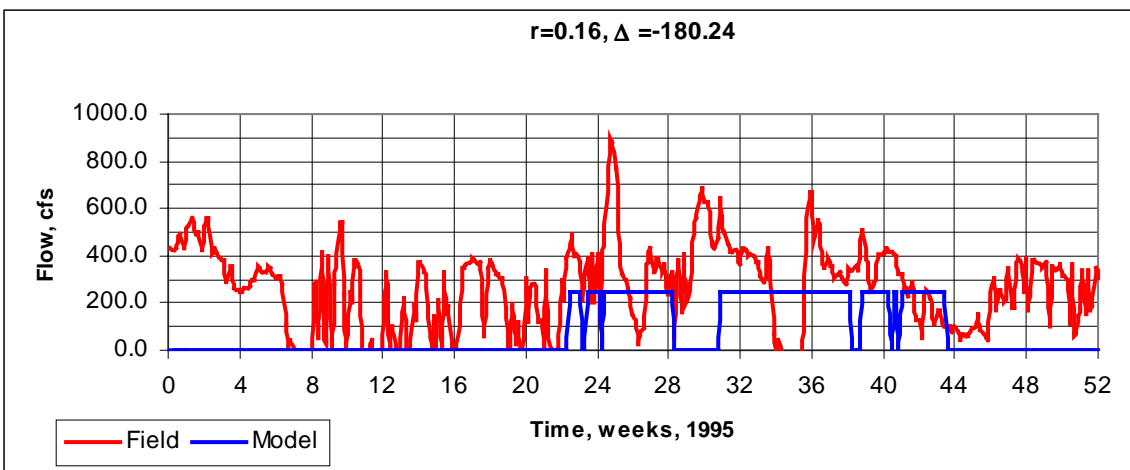
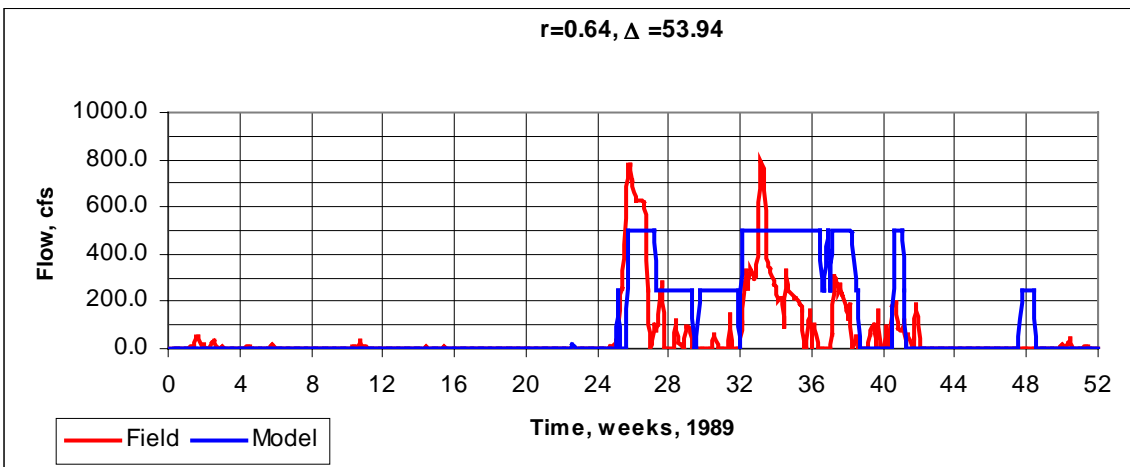
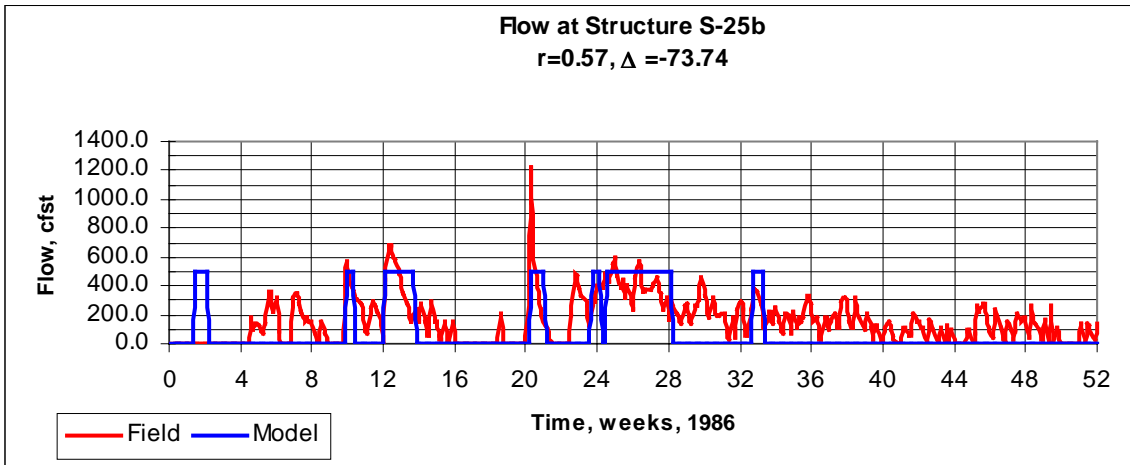


Figure 82: Flow at S-25b

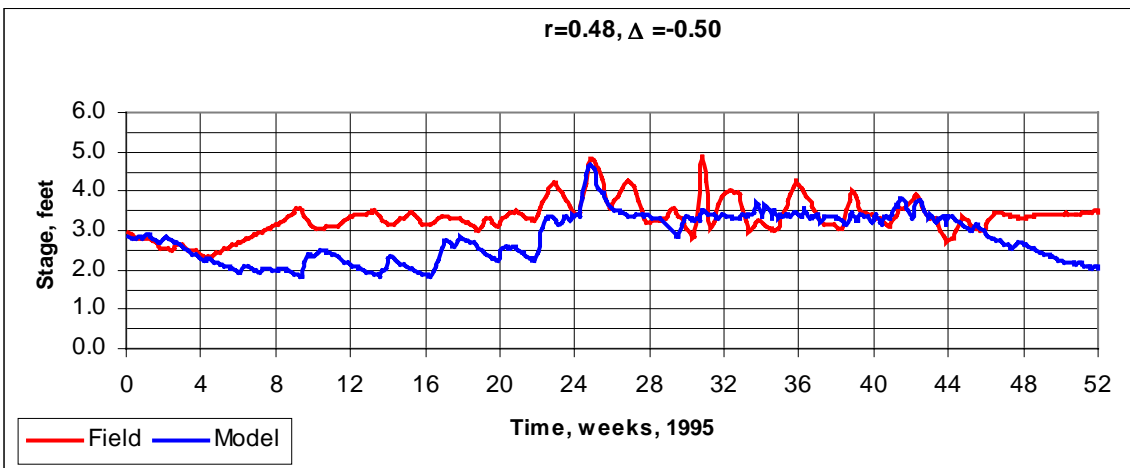
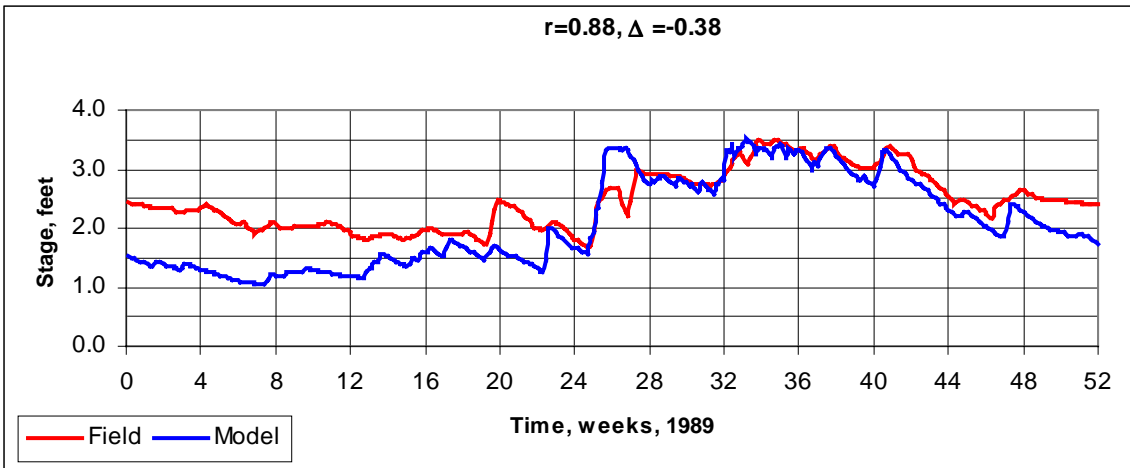
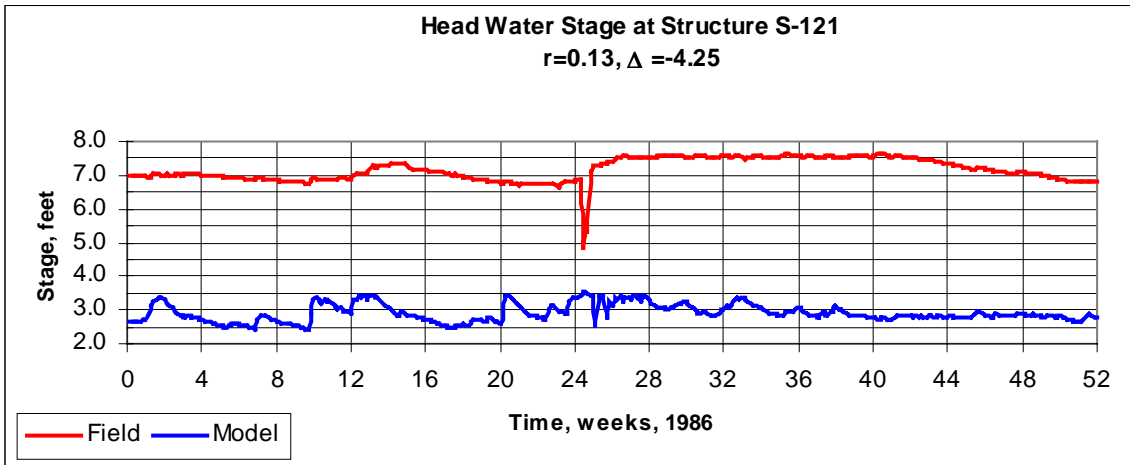


Figure 83: Head Water Stage at S-121

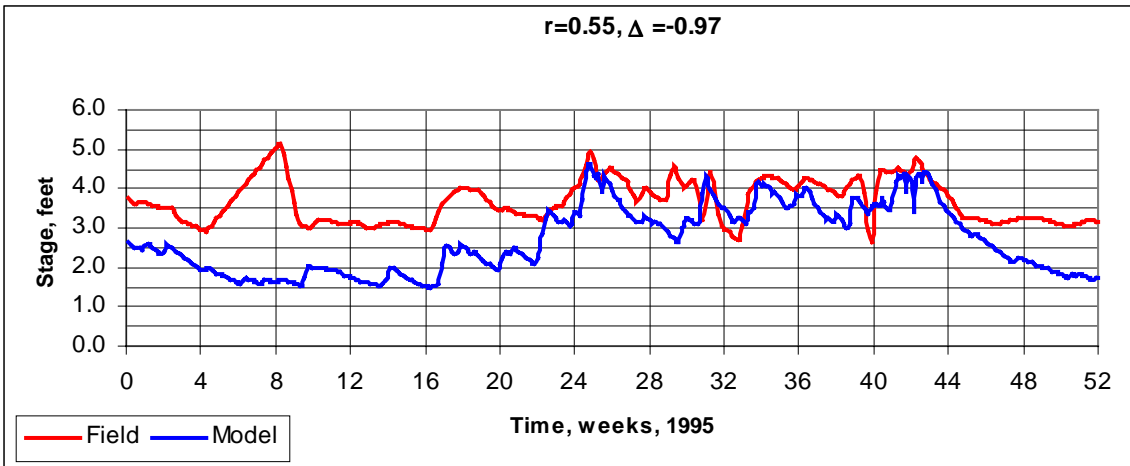
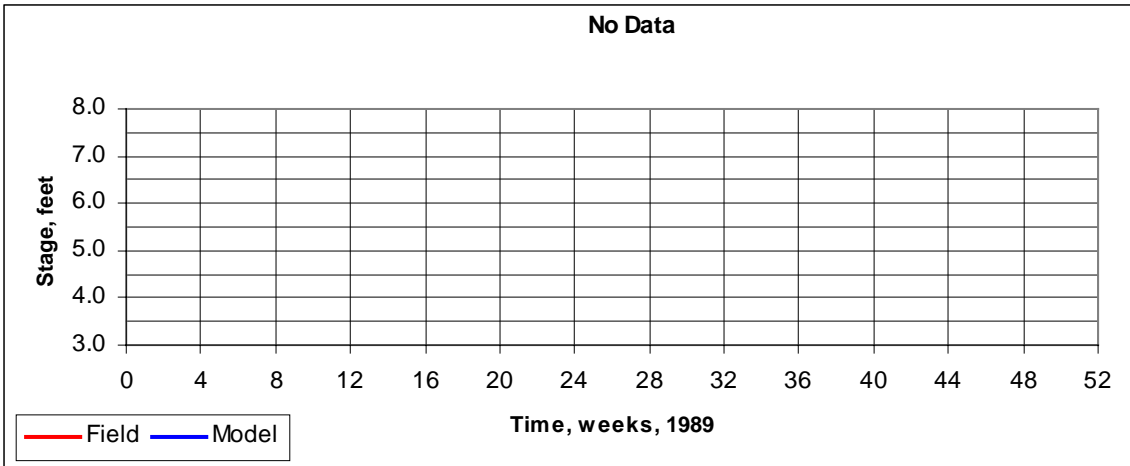
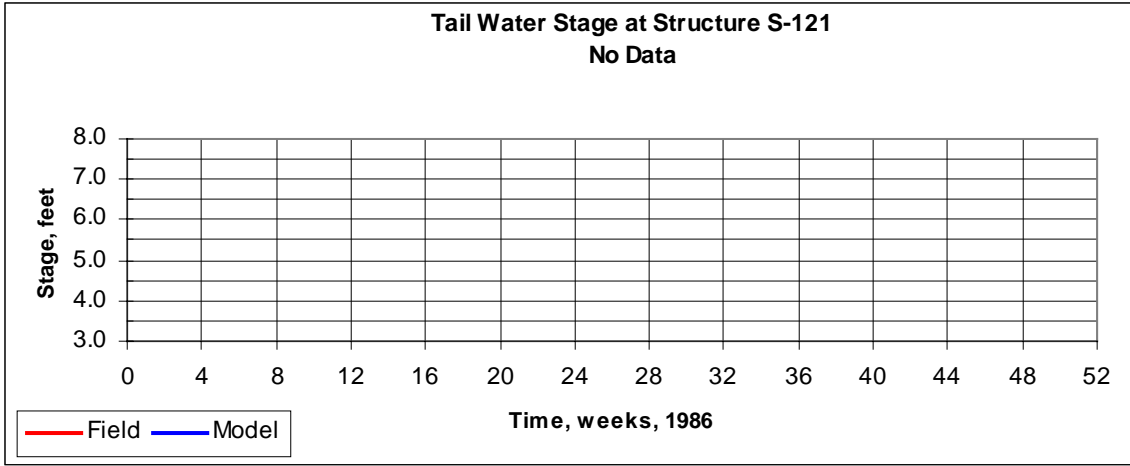


Figure 84: Tail Water Stage at S-121

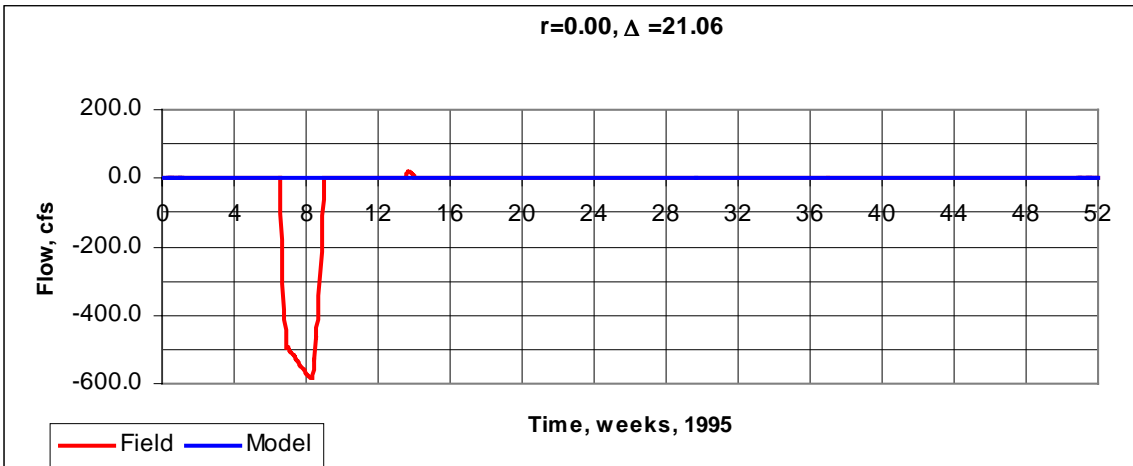
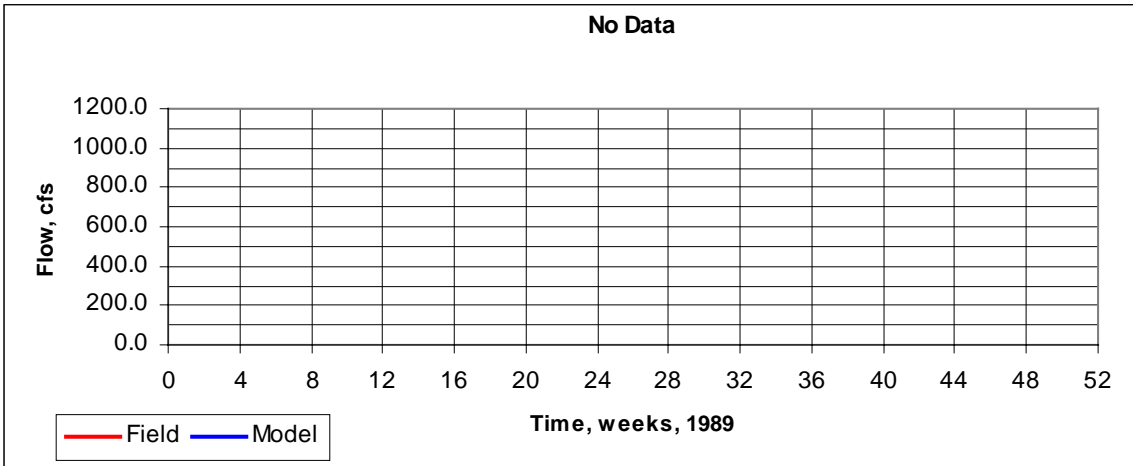
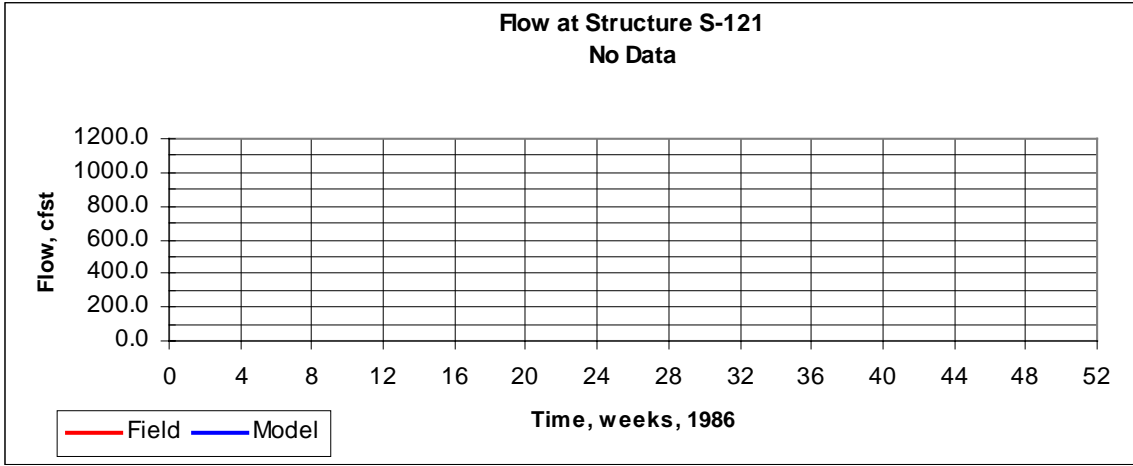


Figure 85: Flow at S-121

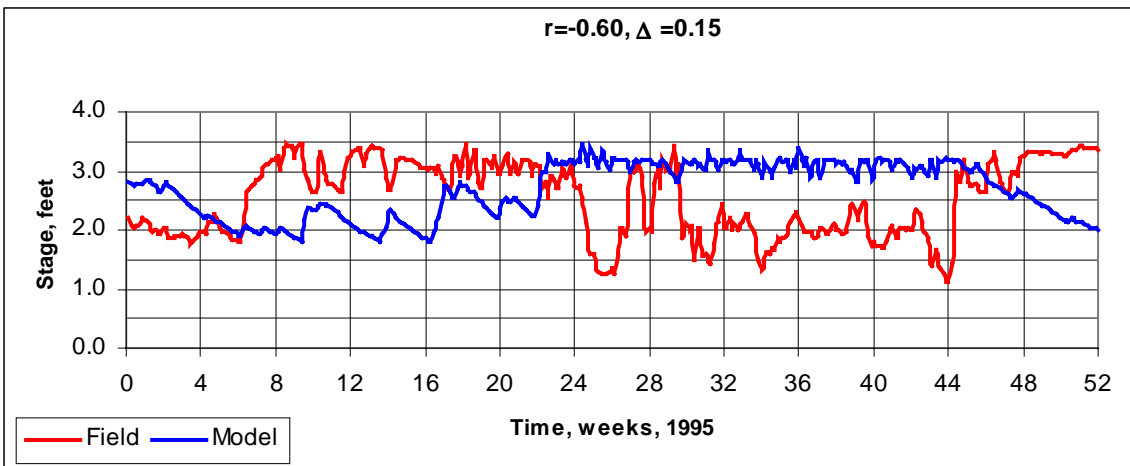
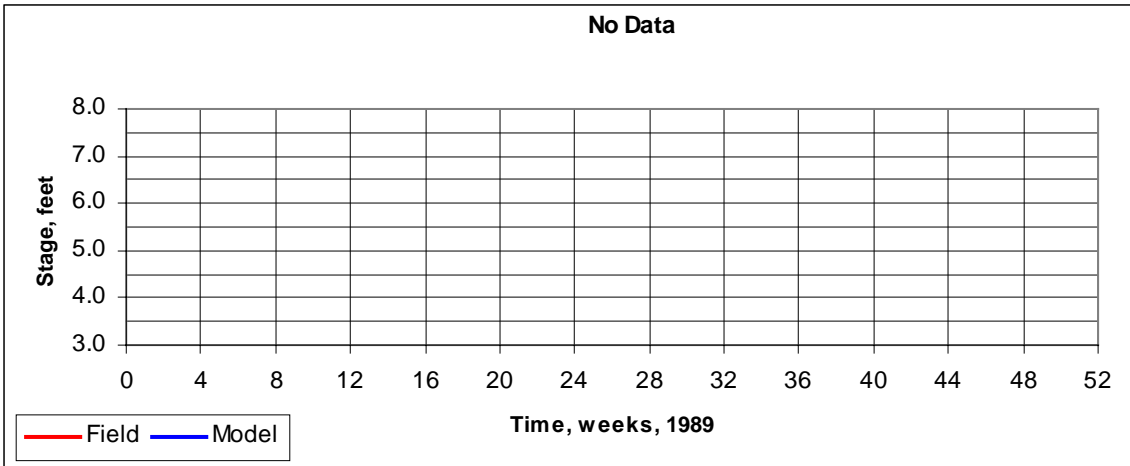
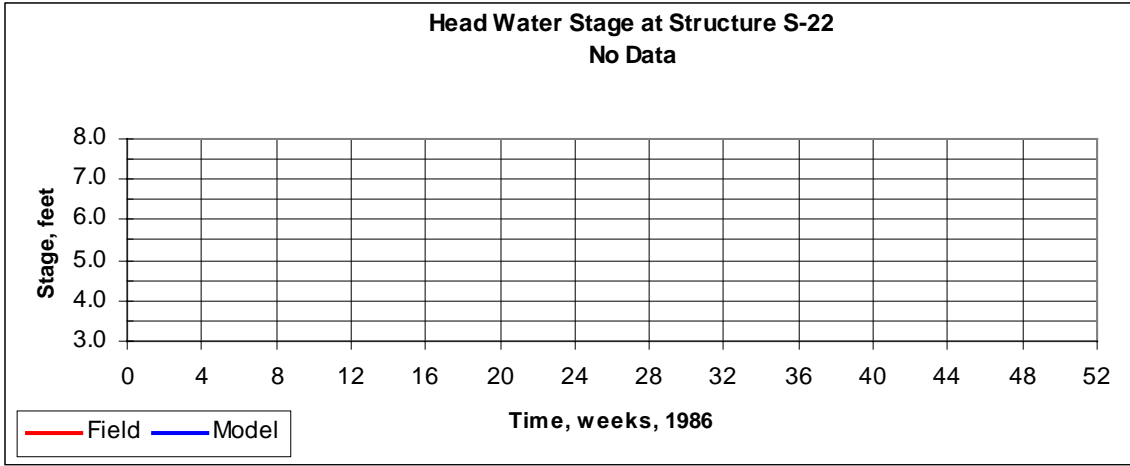


Figure 86: Head Water Stage at S-22

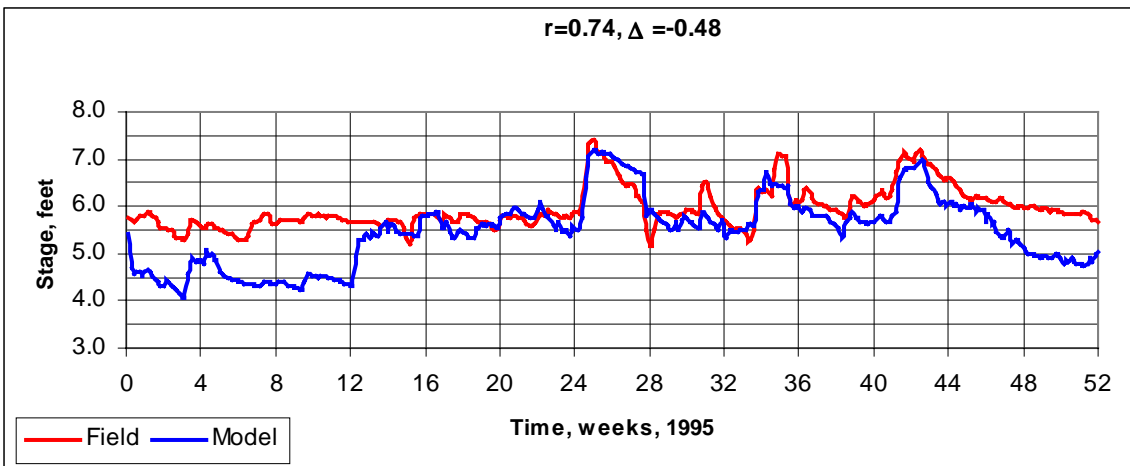
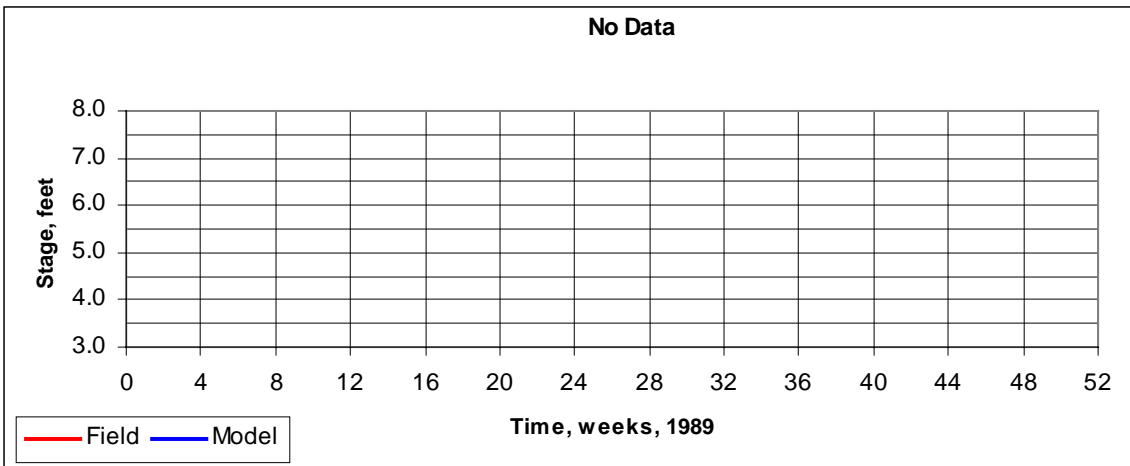
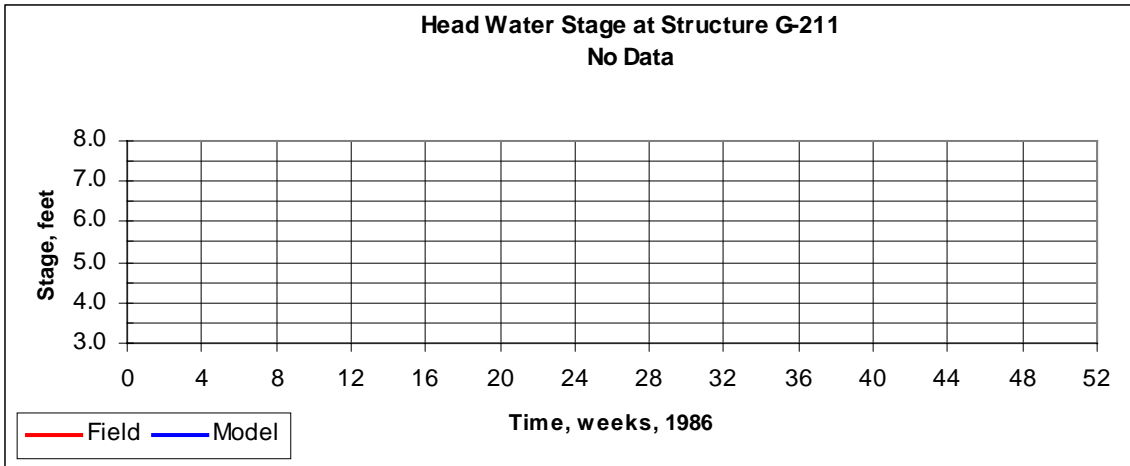


Figure 87: Head Water Stage at G-211

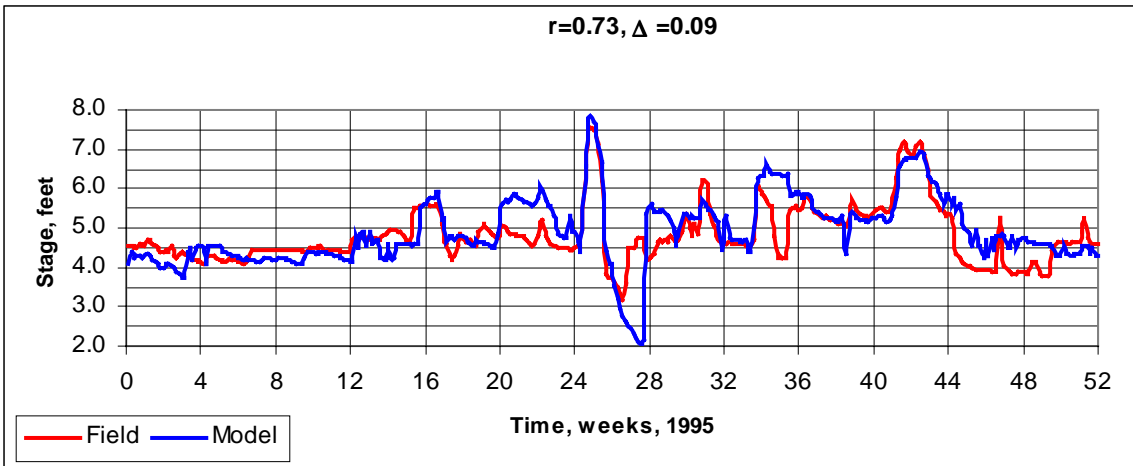
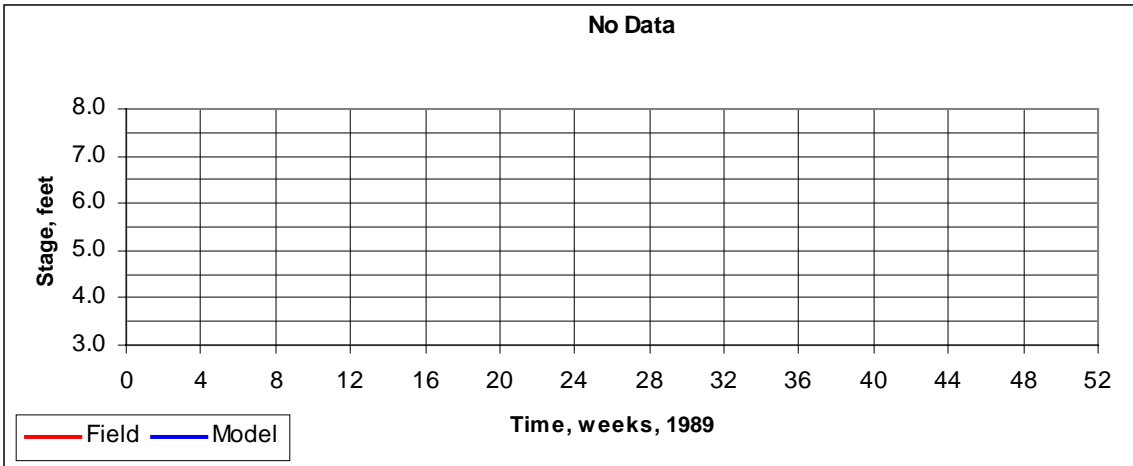
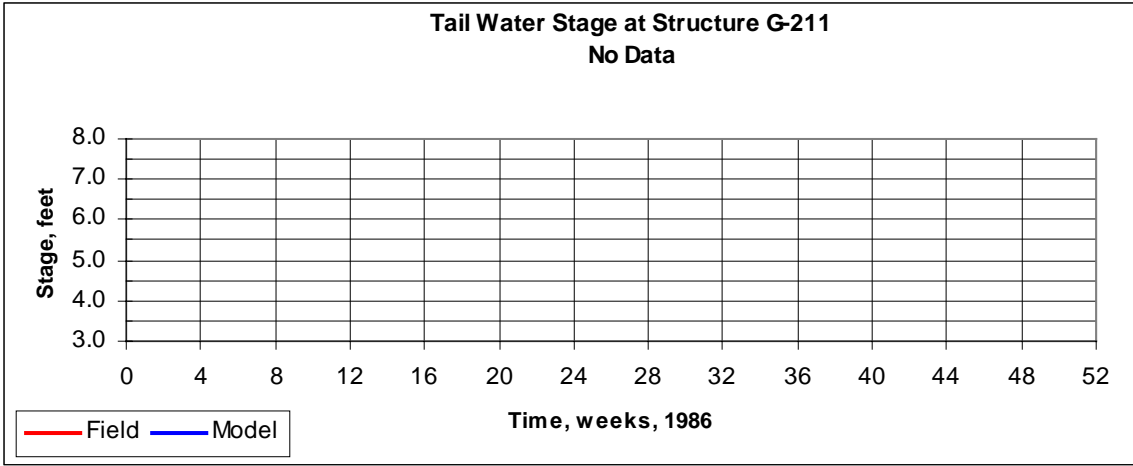


Figure 88: Tail Water Stage at G-211

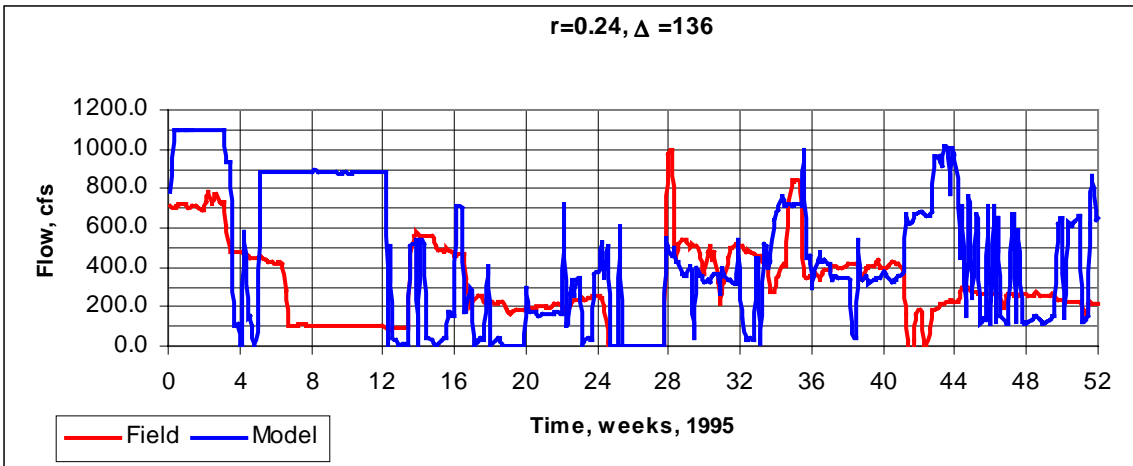
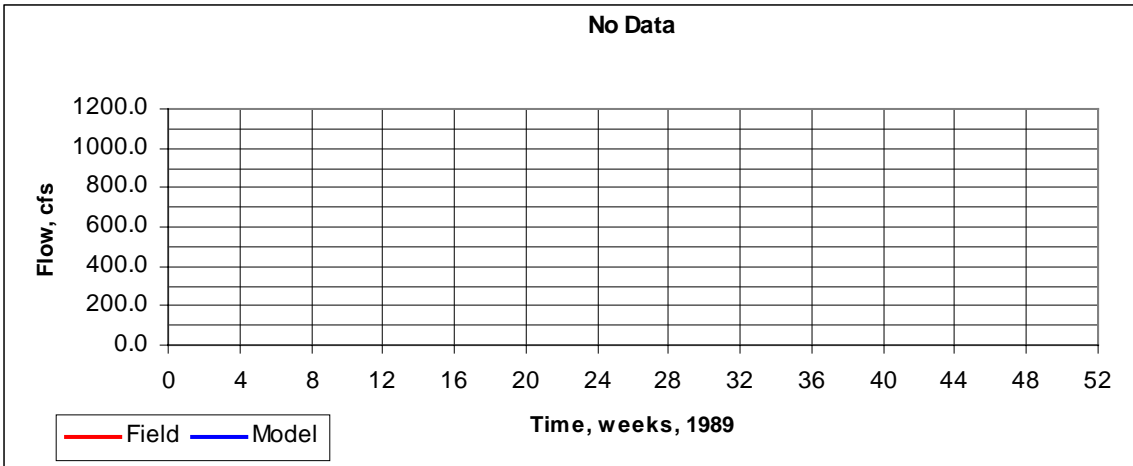
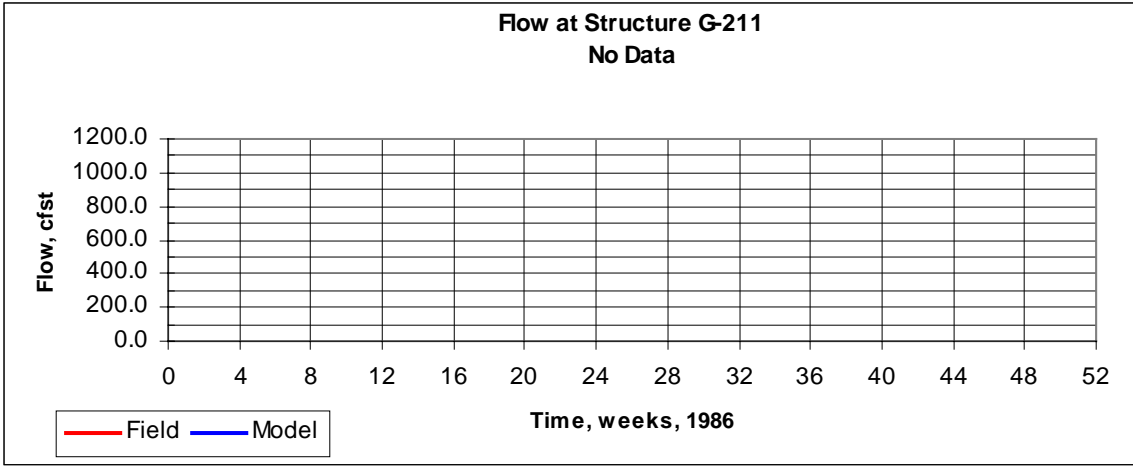


Figure 89: Flow at Structure G-211

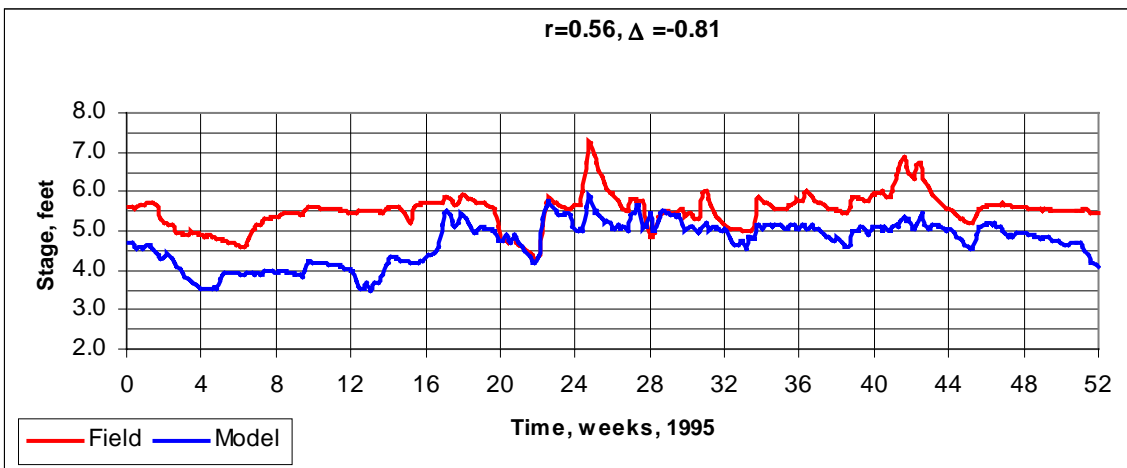
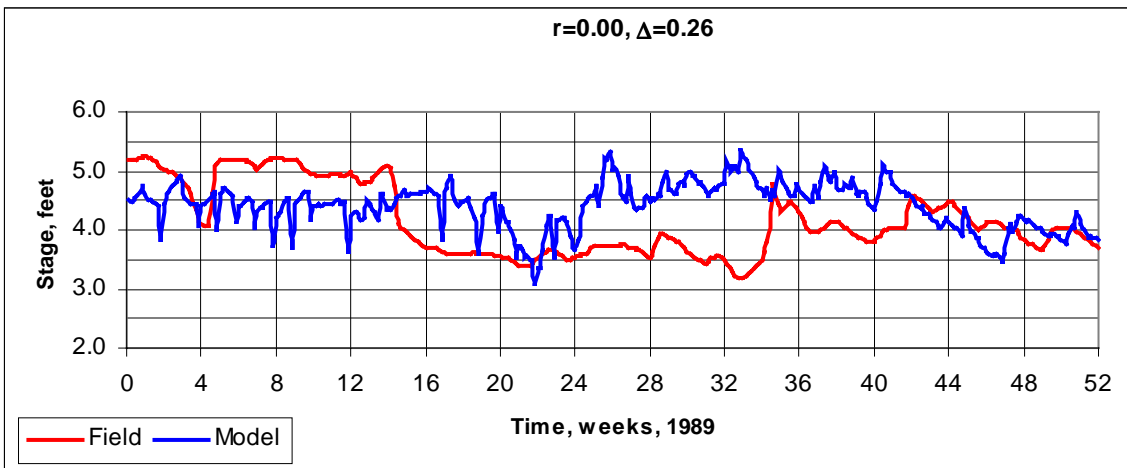
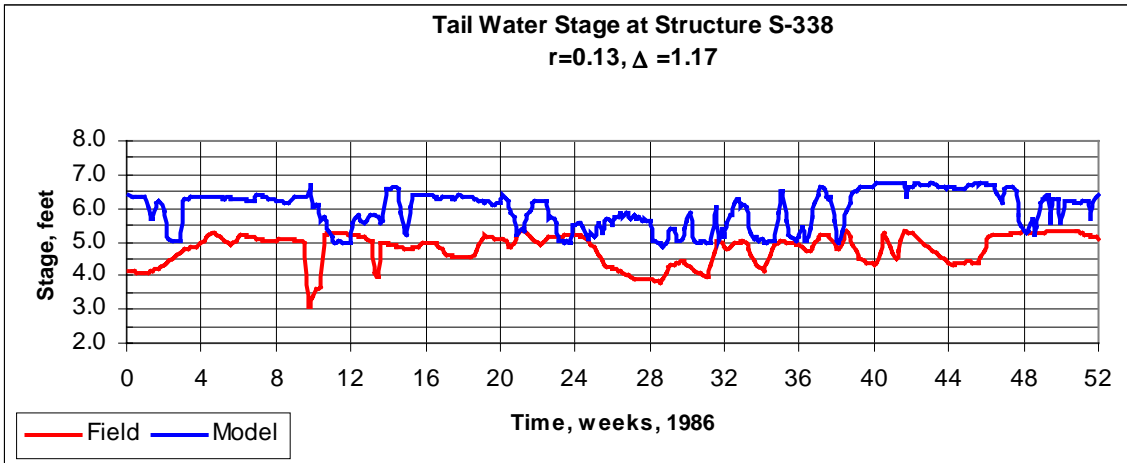


Figure 90: Tail Water Stage at S-338

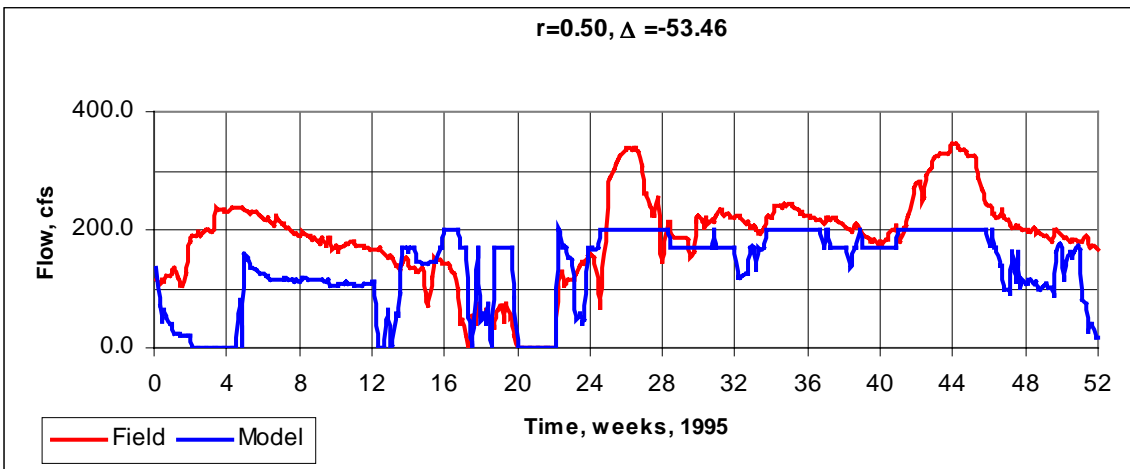
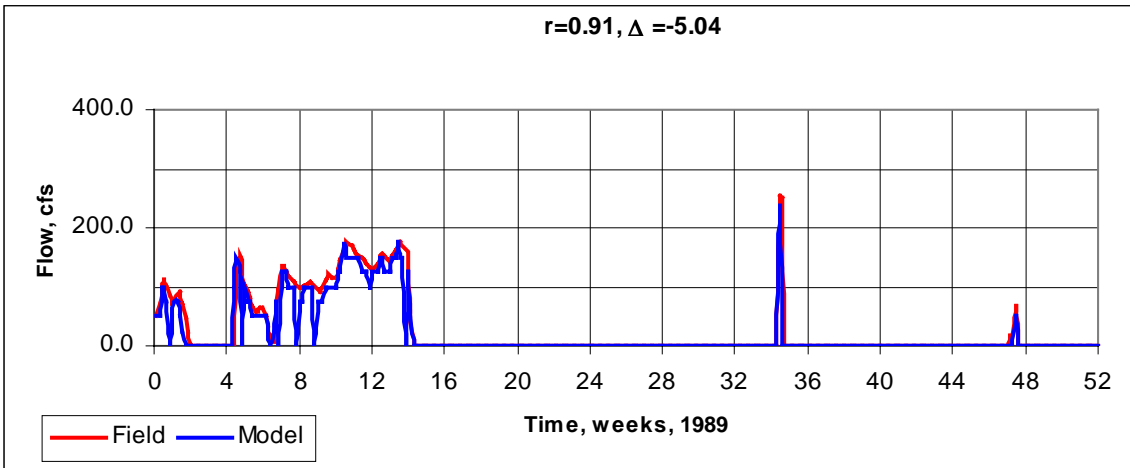
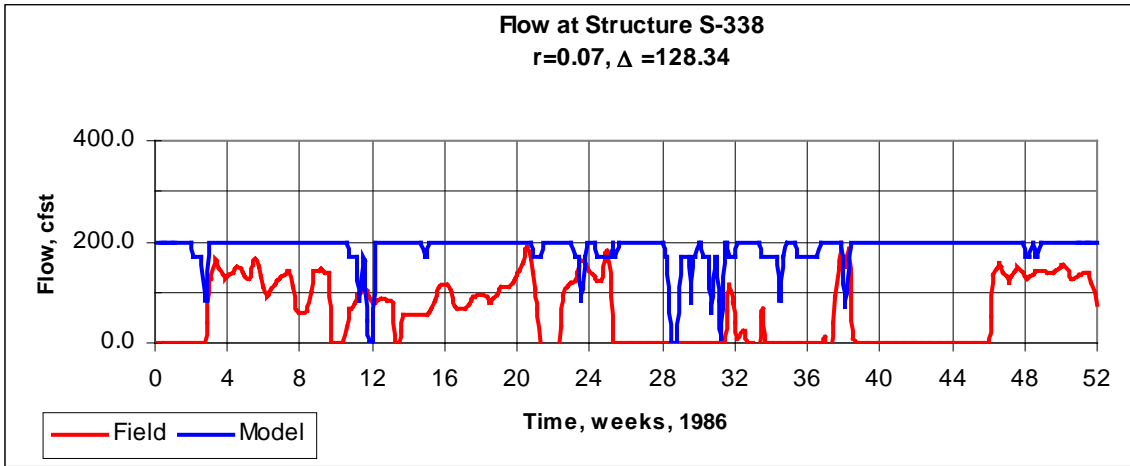


Figure 91: Flow at S-338

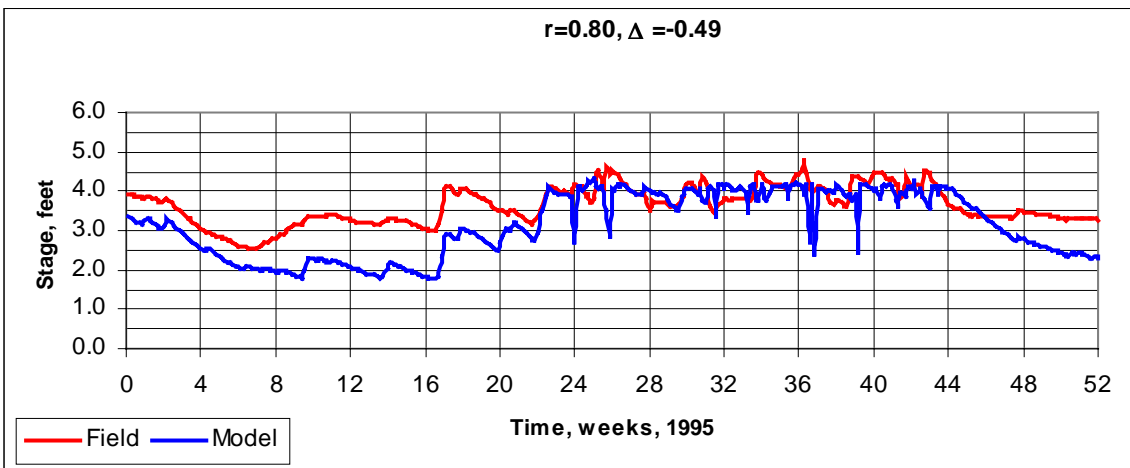
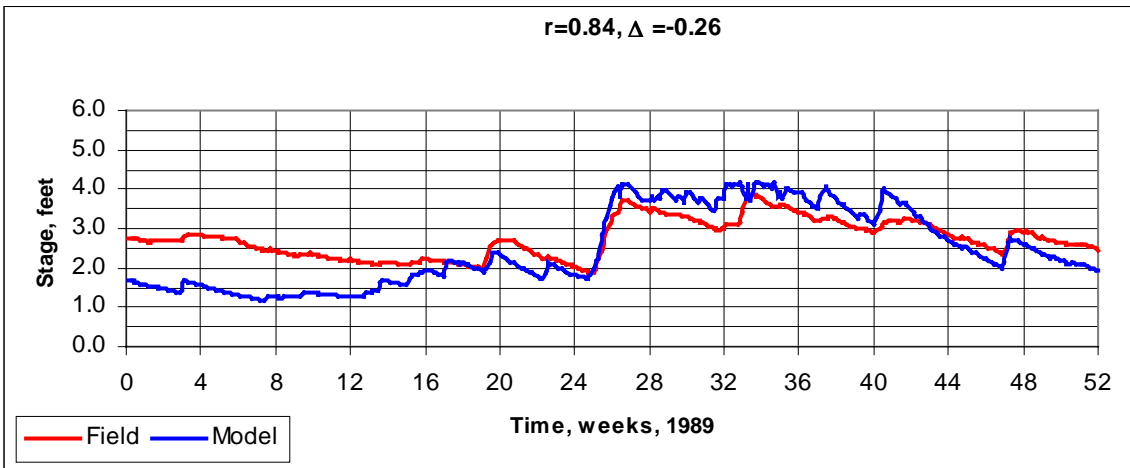
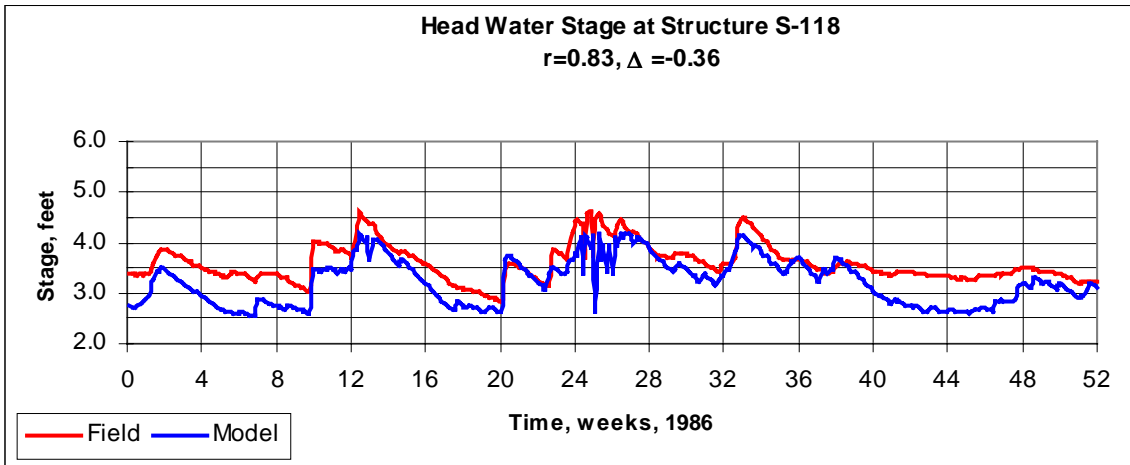


Figure 92: Head Water Stage at S-118

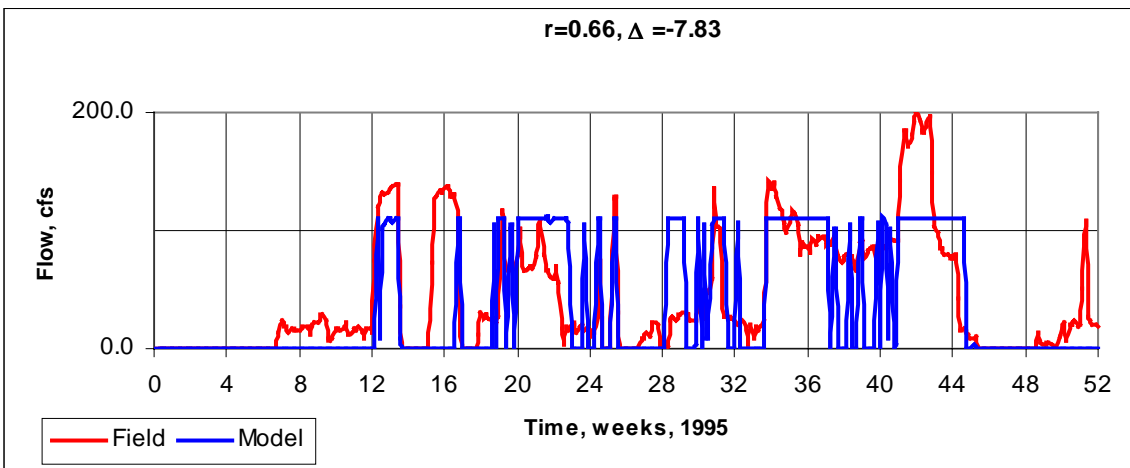
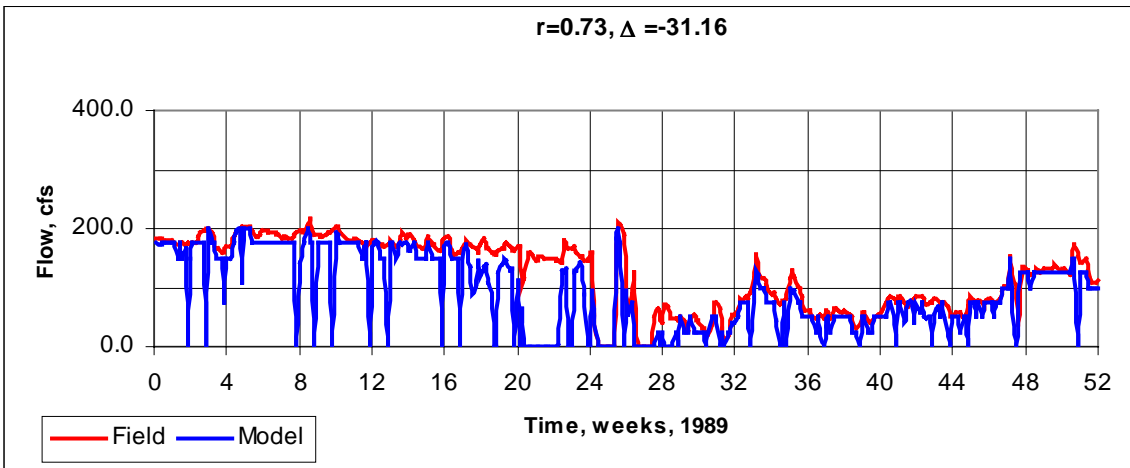
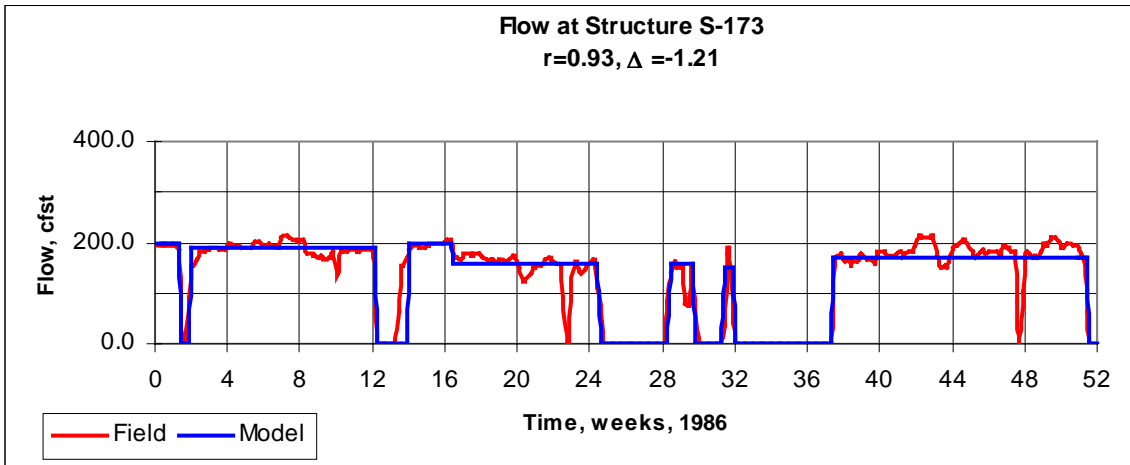


Figure 93: Flow at S-173

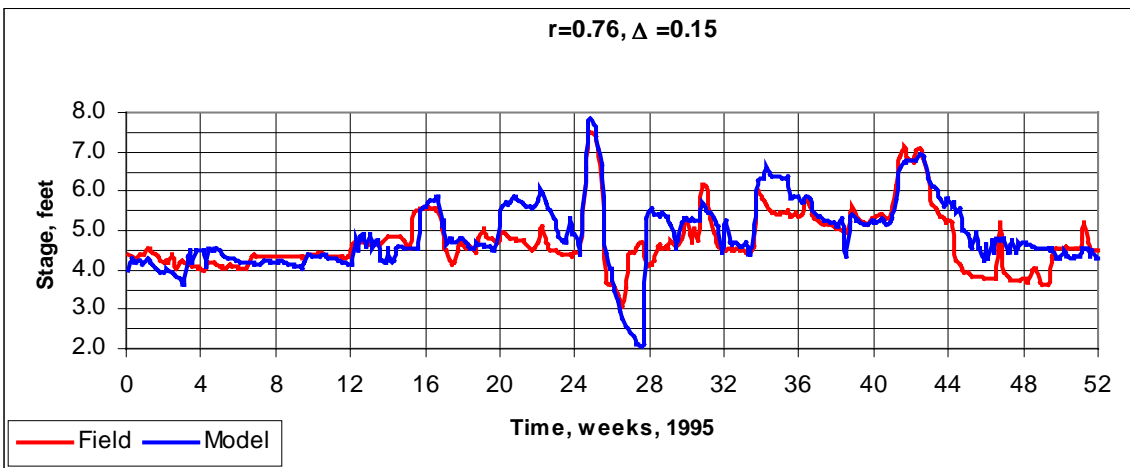
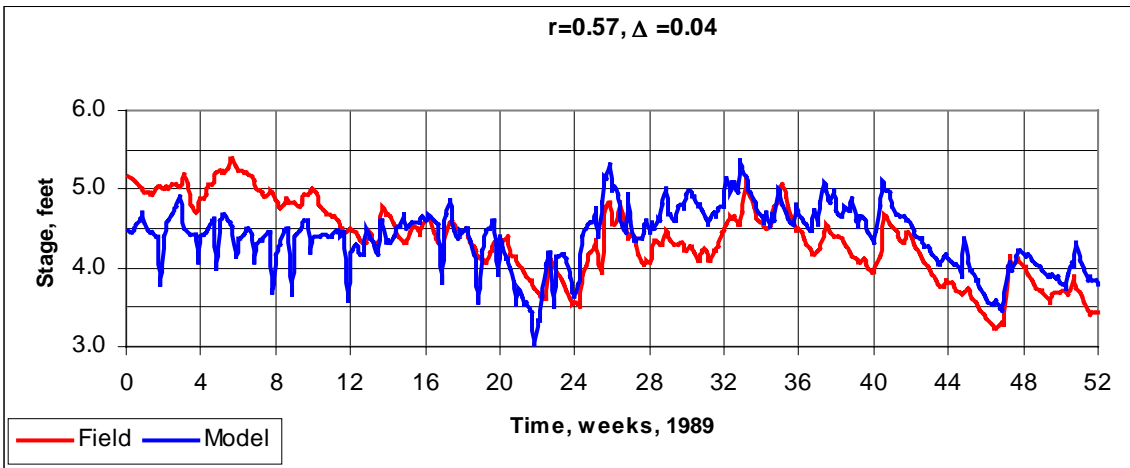
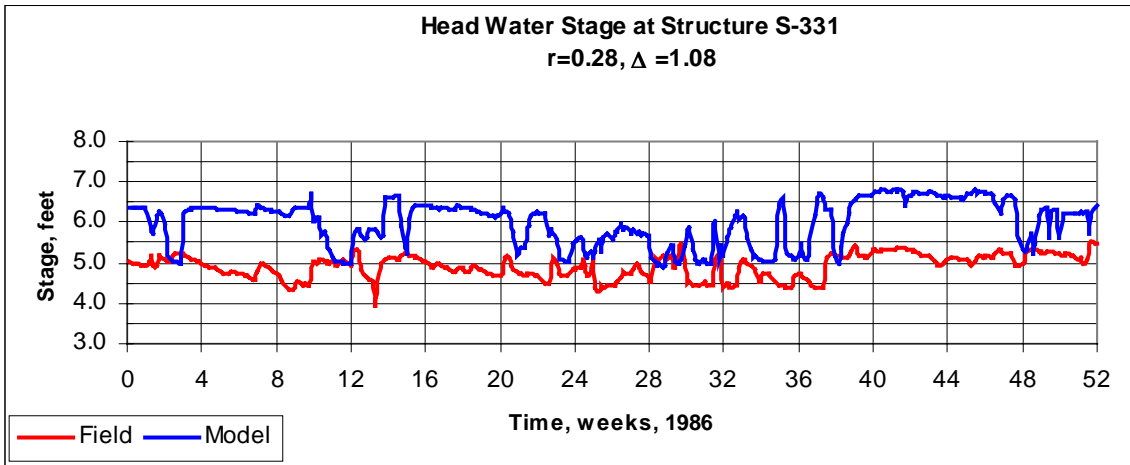


Figure 94: Head Water Stage at S-331

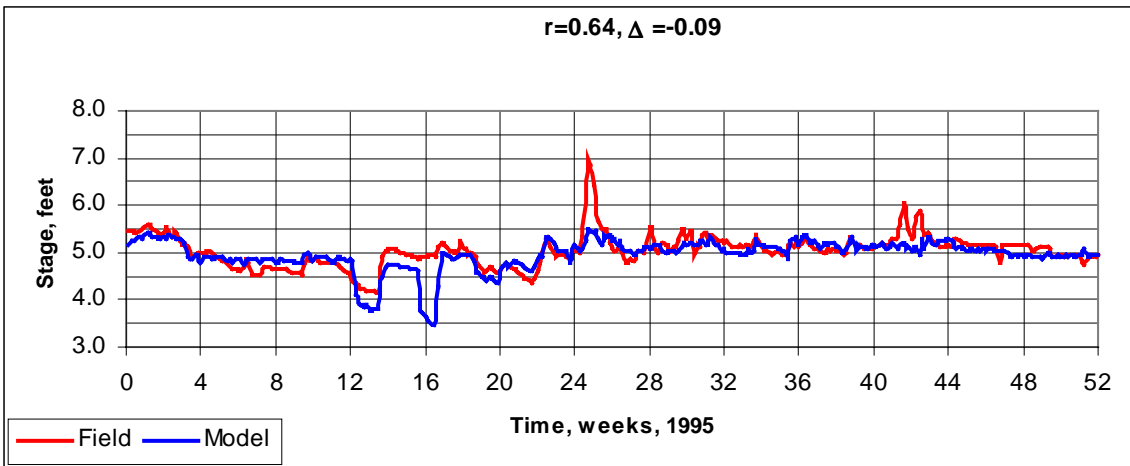
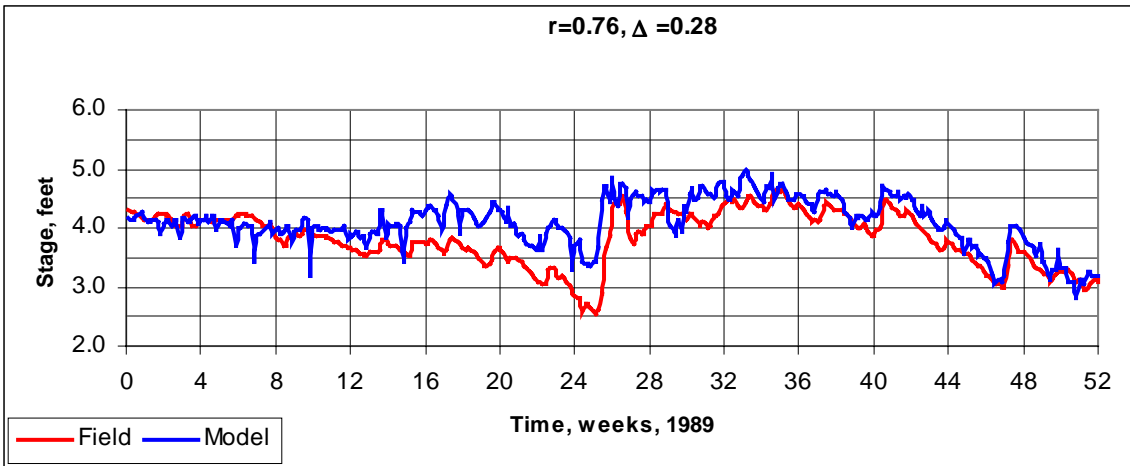
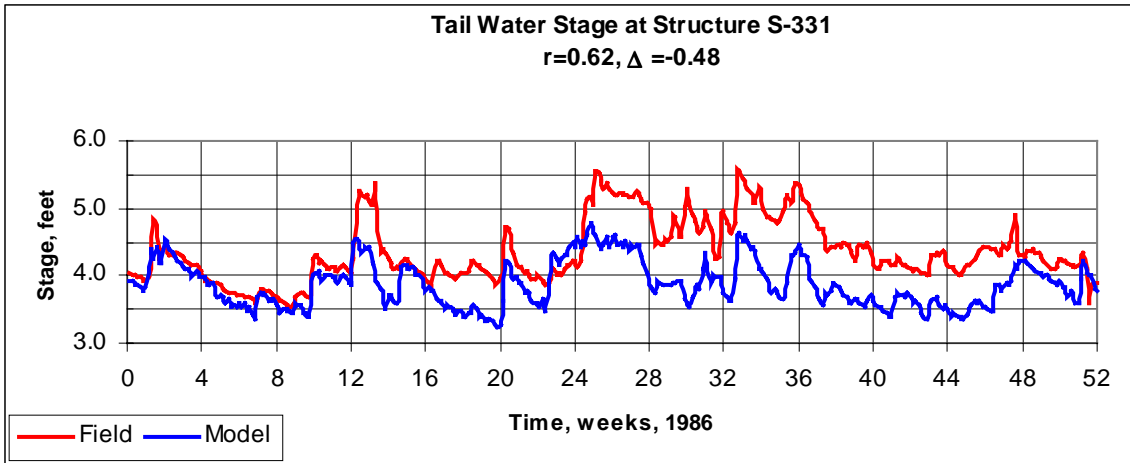


Figure 95: Tail Water Stage at S-331

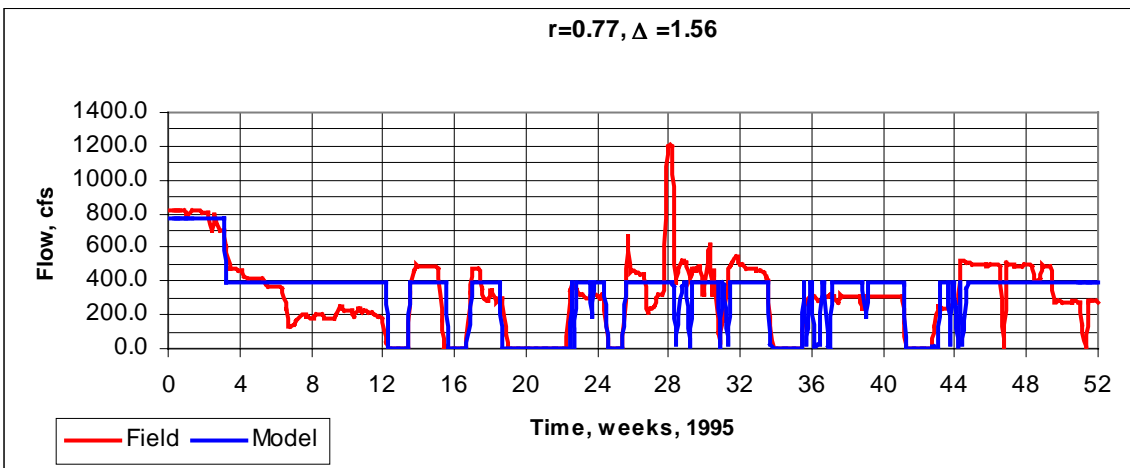
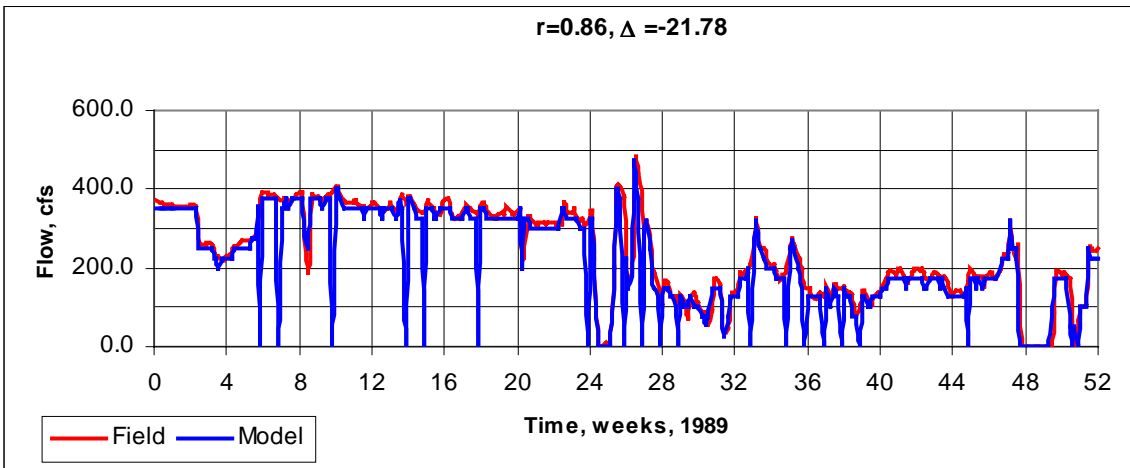
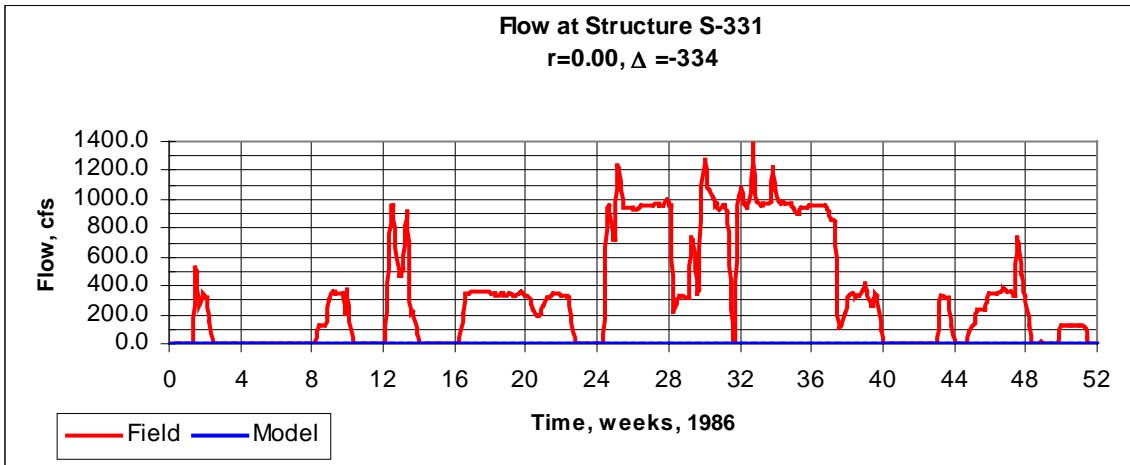


Figure 96: Flow at S-331

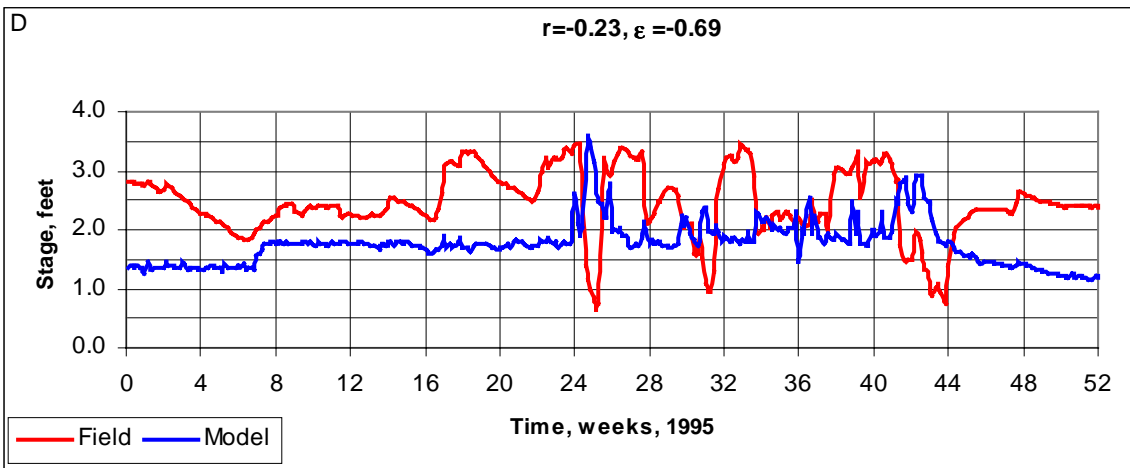
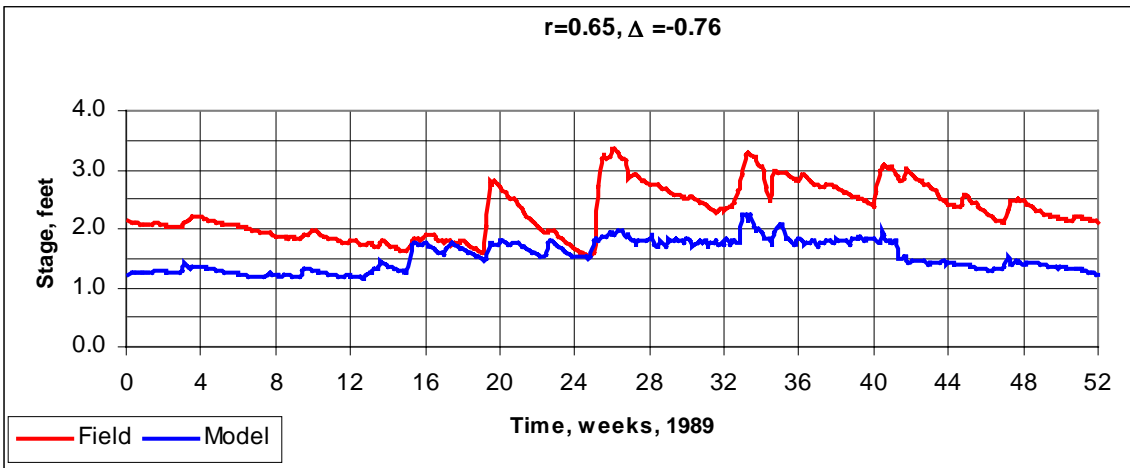
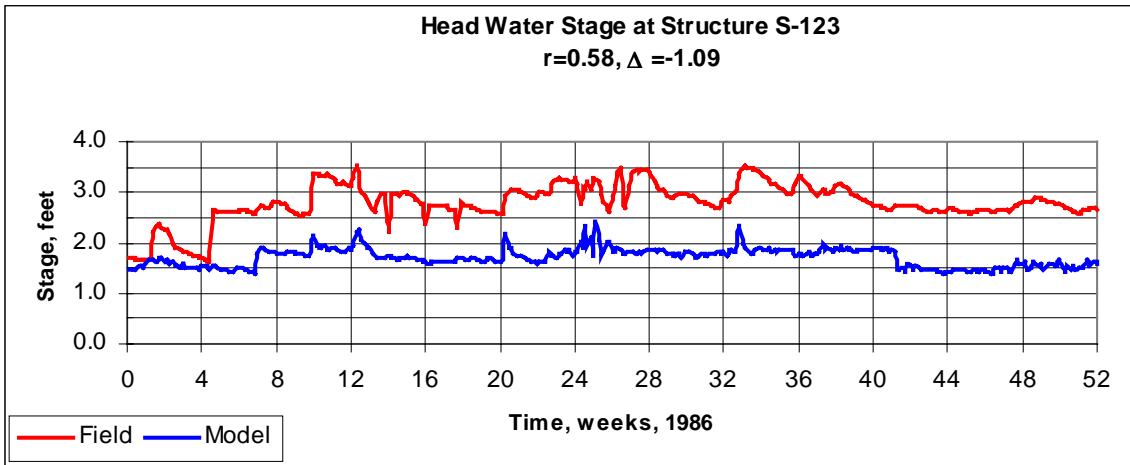


Figure 97: Head Water Stage at S-123

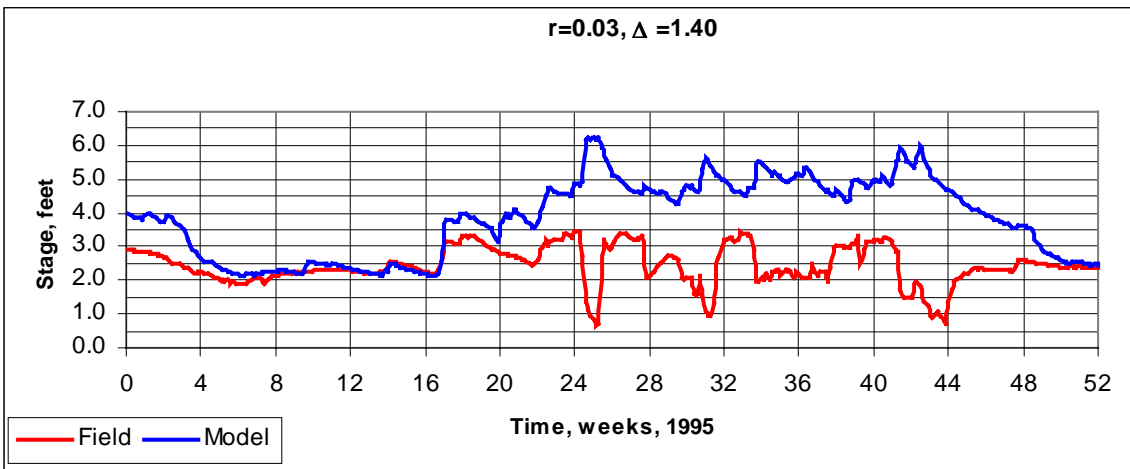
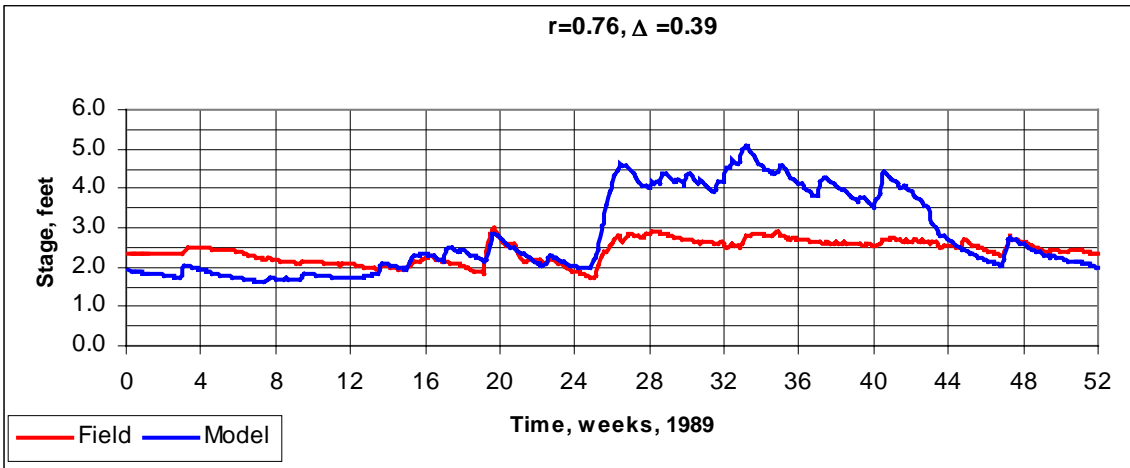
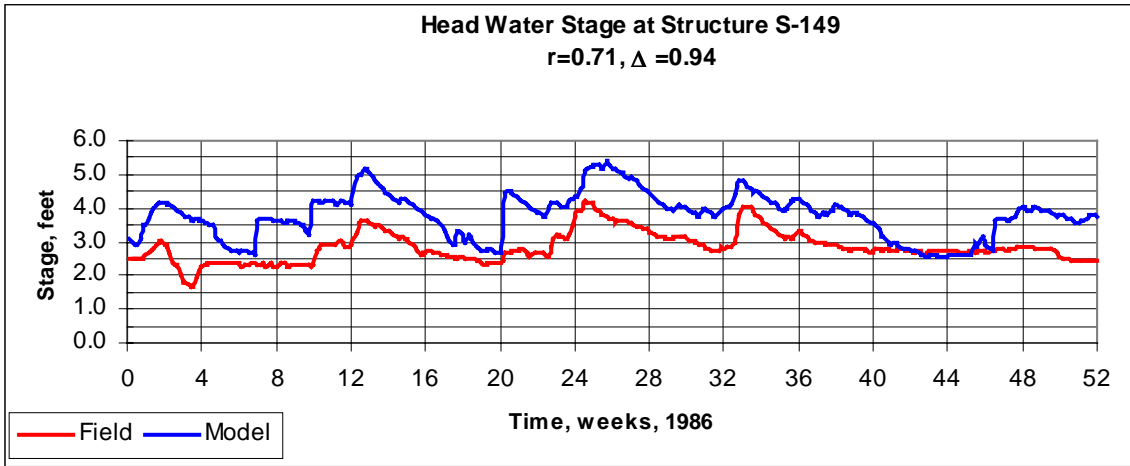


Figure 98: Head Water Stage at S-149

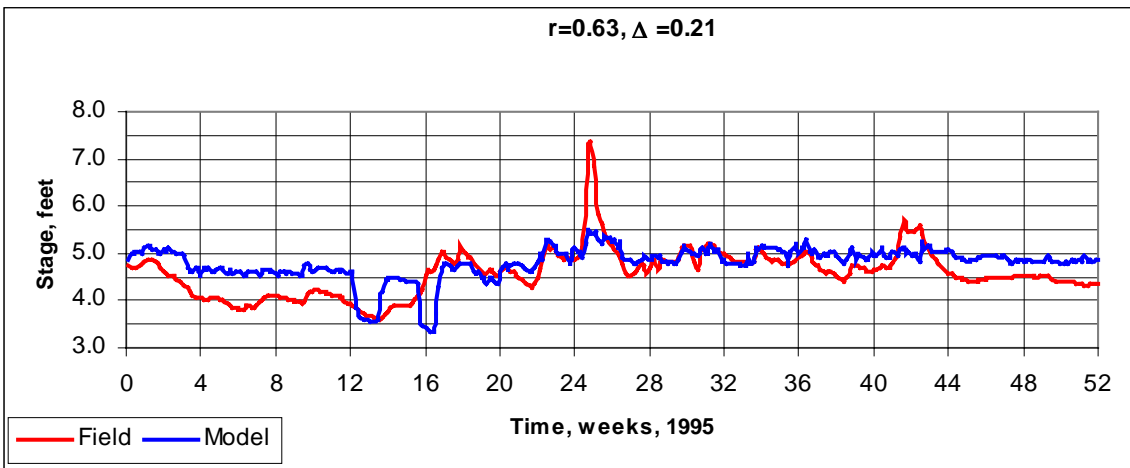
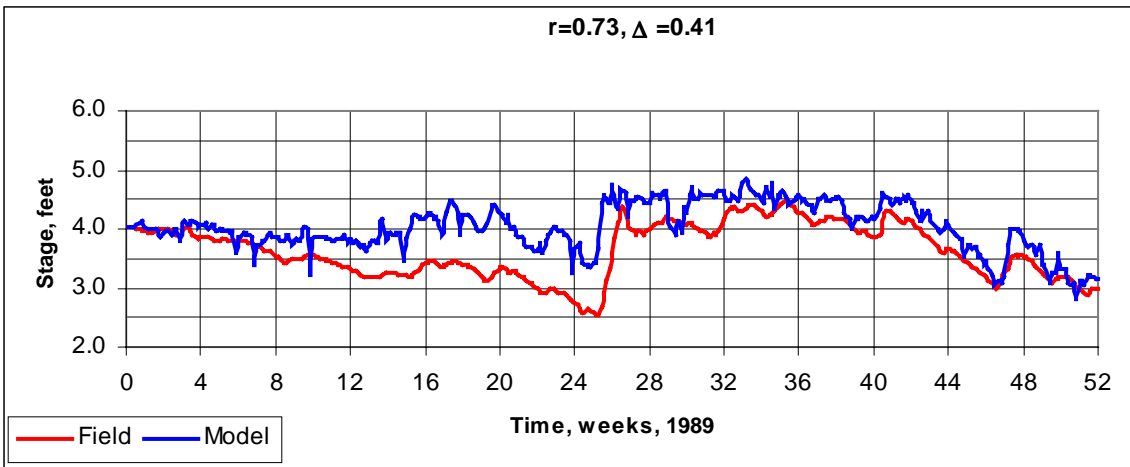
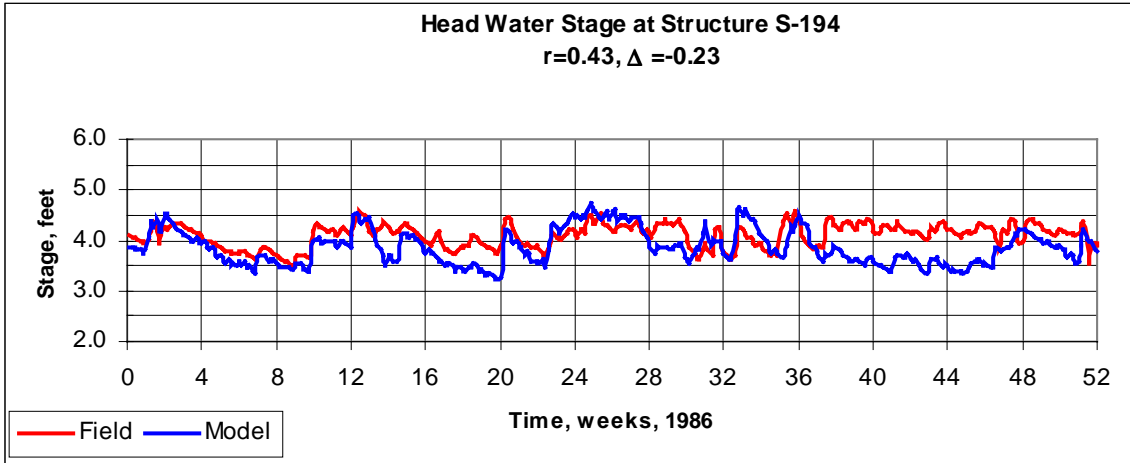


Figure 99: Head Water Stage at S-194

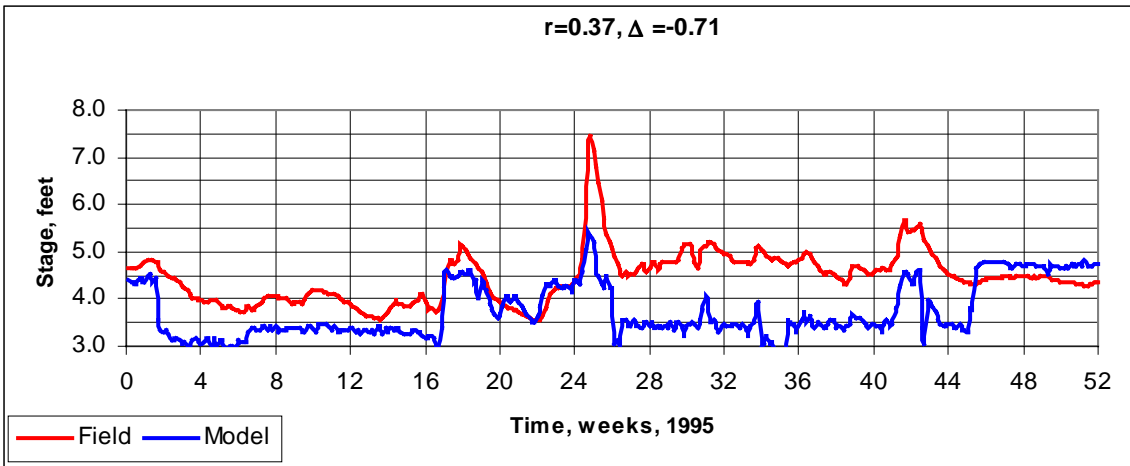
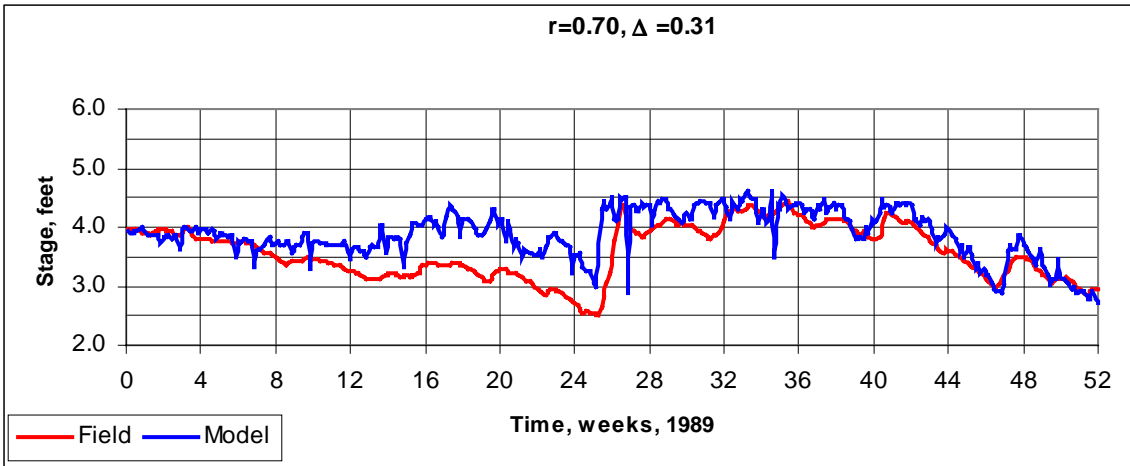
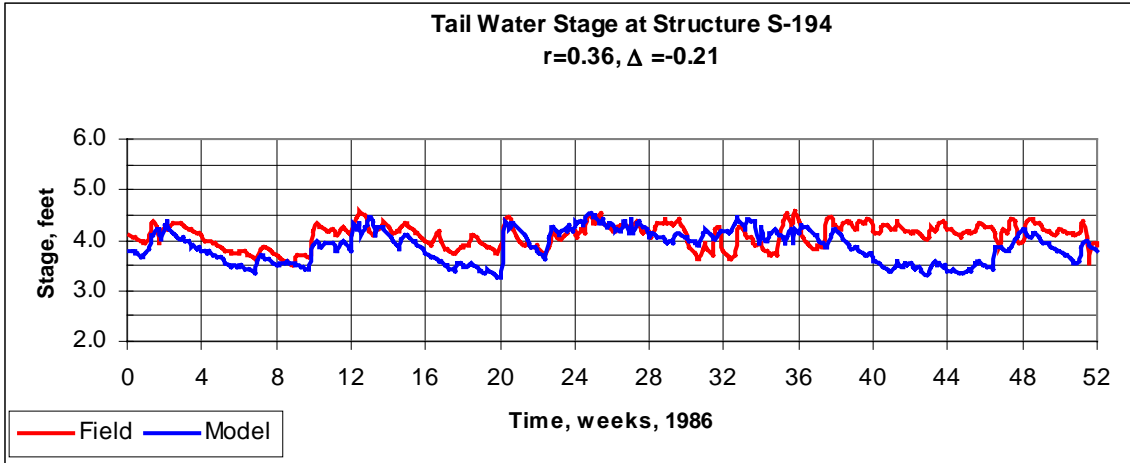


Figure 100: Tail Water Stage at S-194

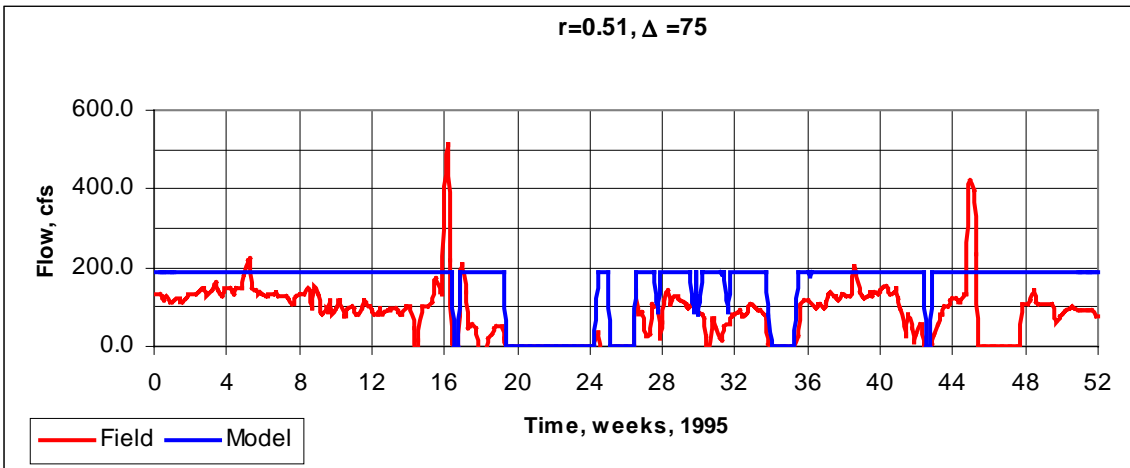
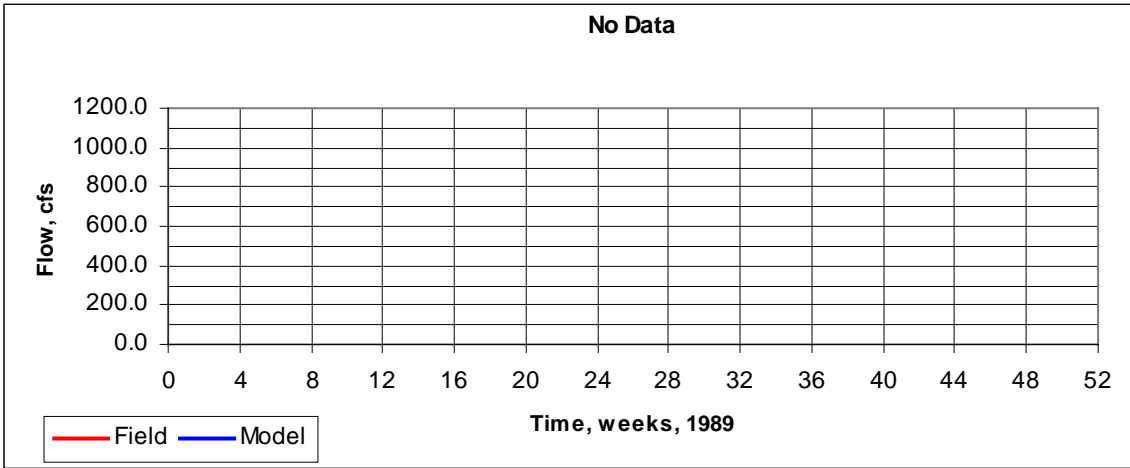
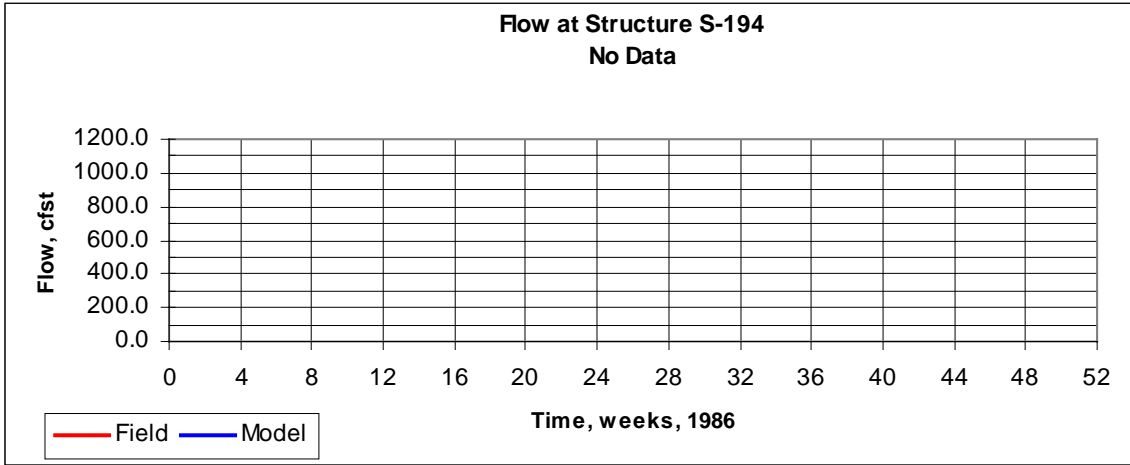


Figure 101: Flow at S-194

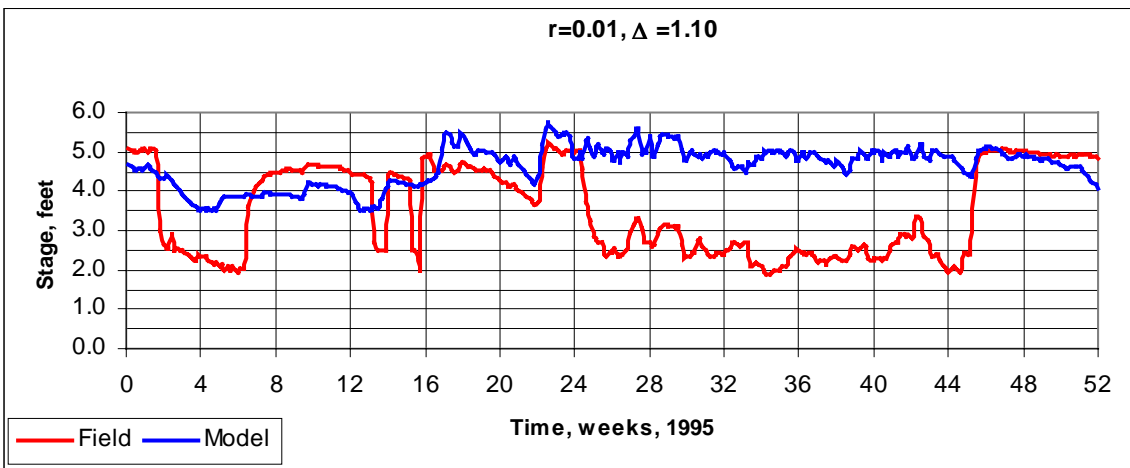
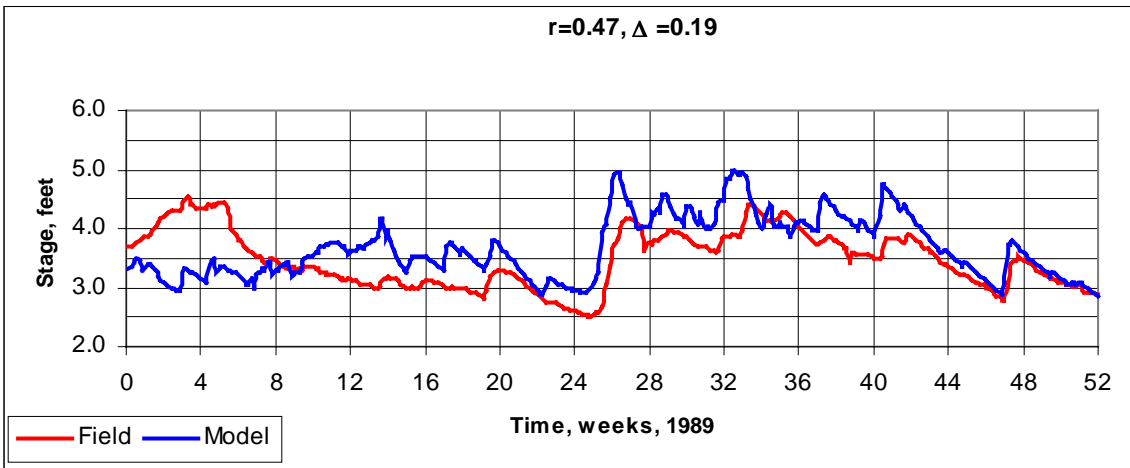
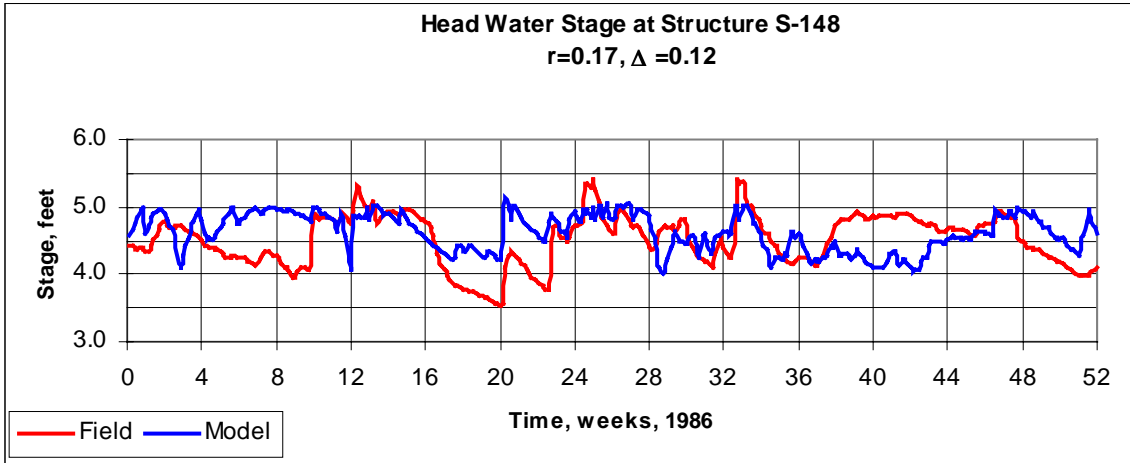


Figure 102: Head Water Stage at S-148

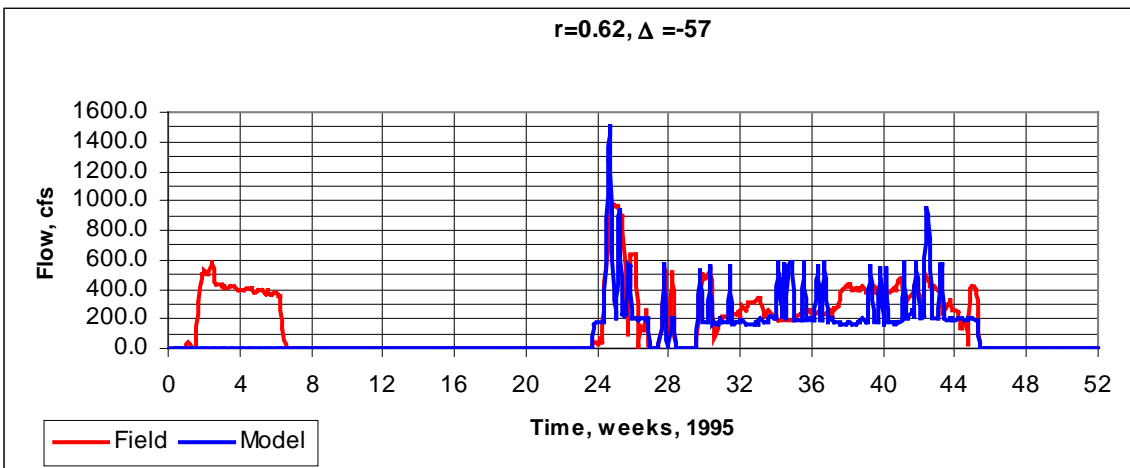
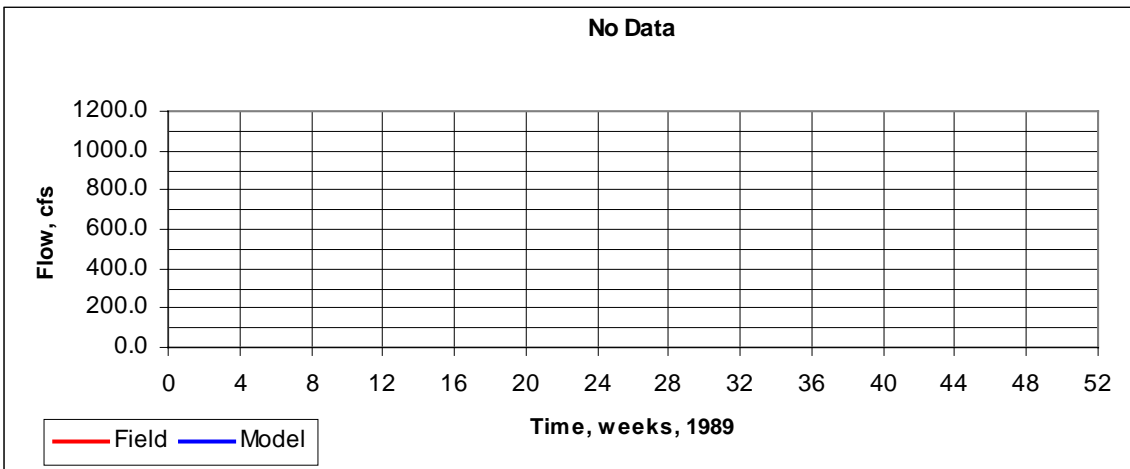
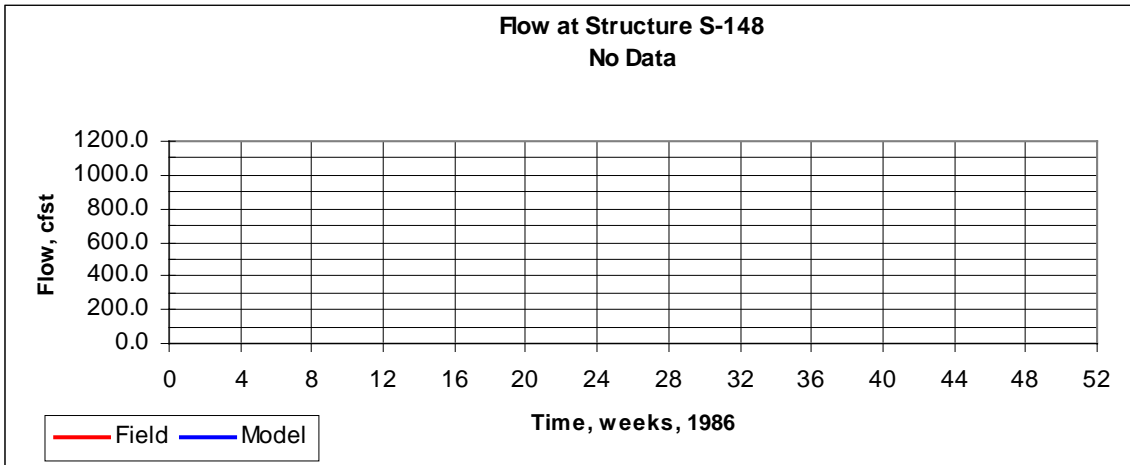


Figure 103: Flow at S-148

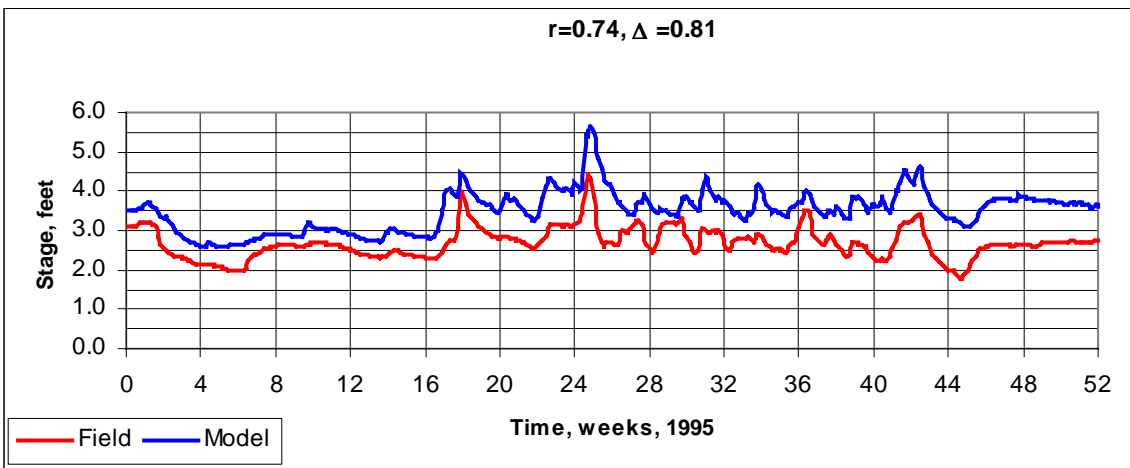
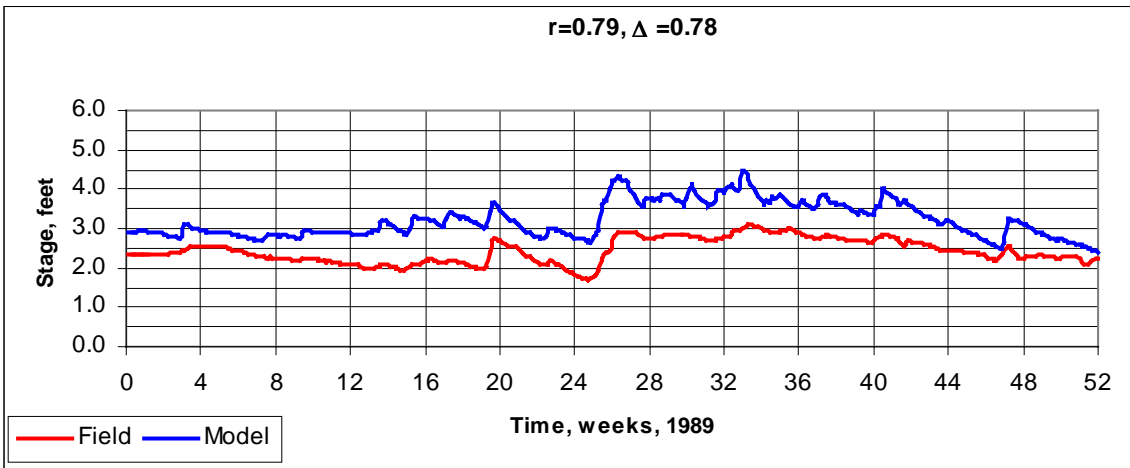
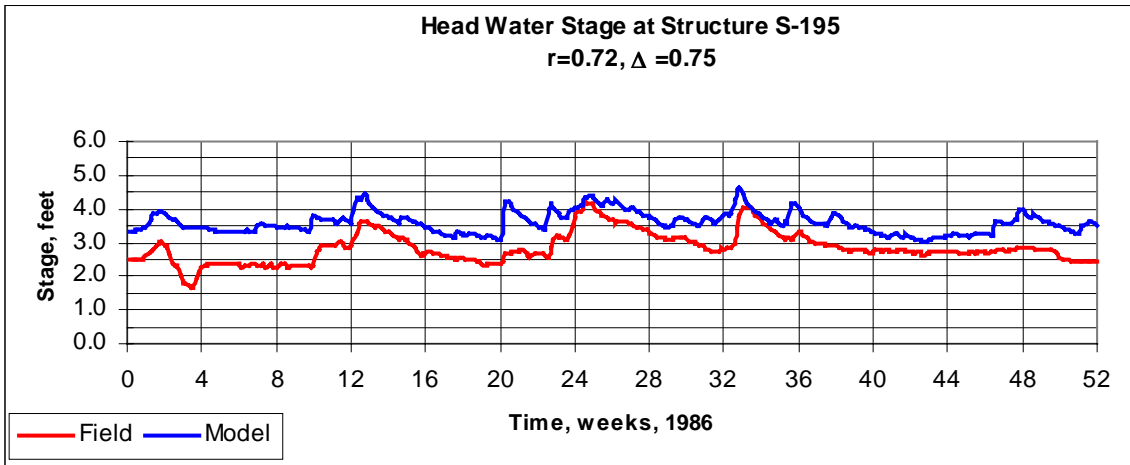


Figure 104: Head Water Stage at S-195

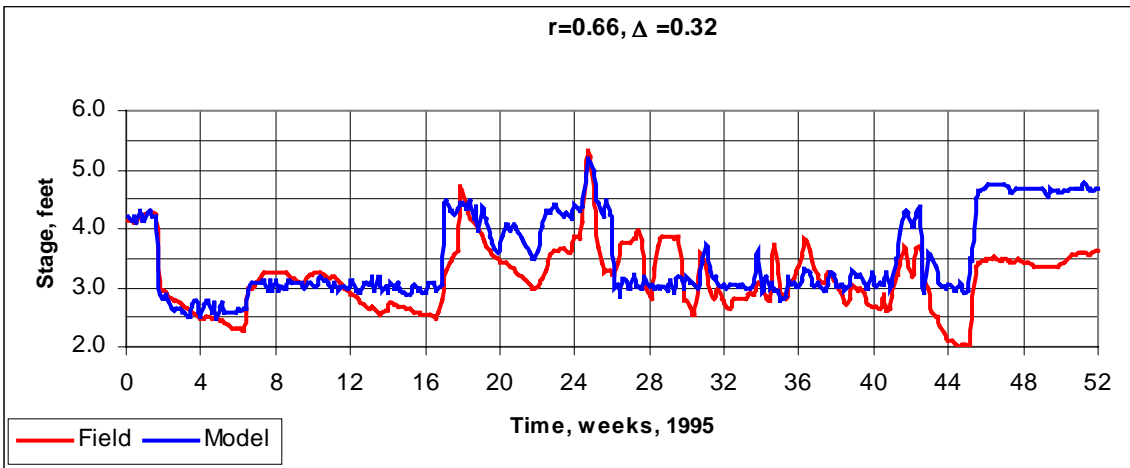
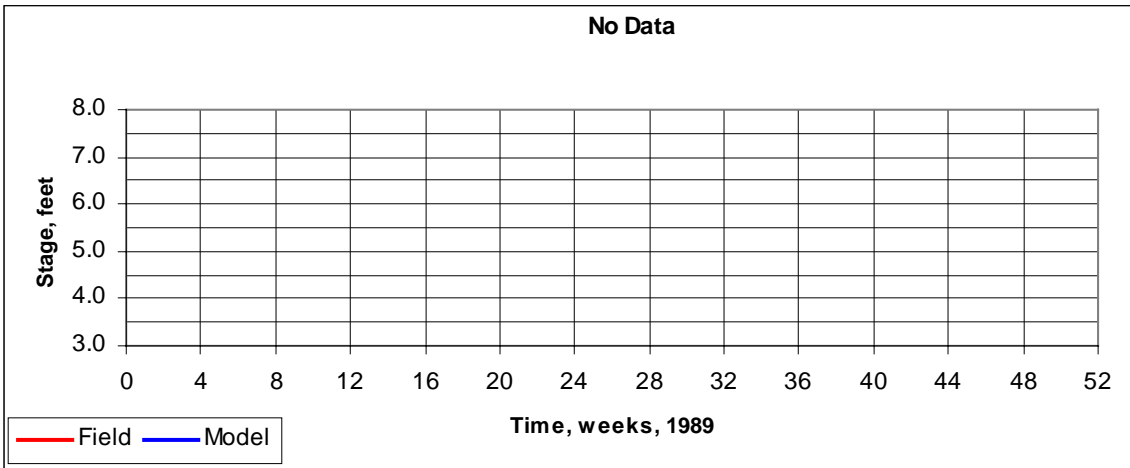
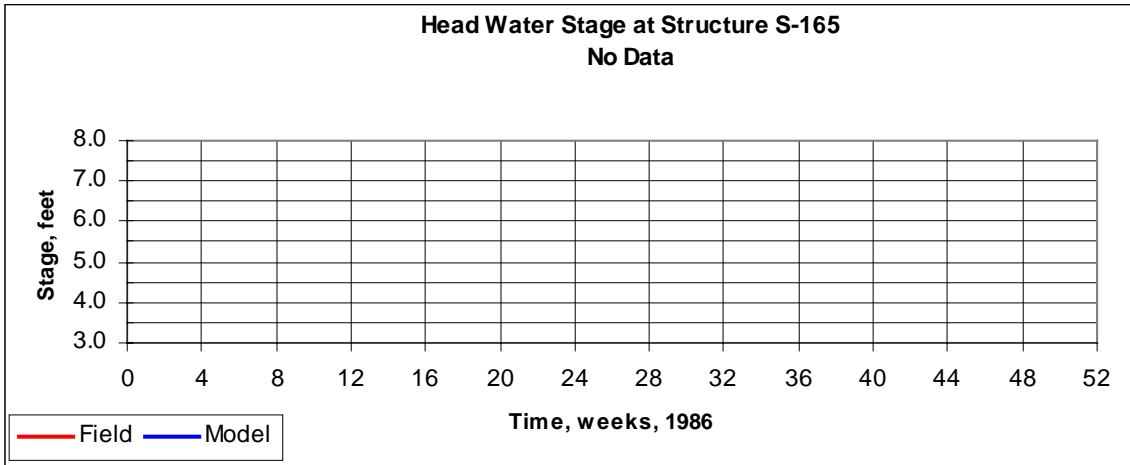


Figure 105: Head Water Stage at S-165

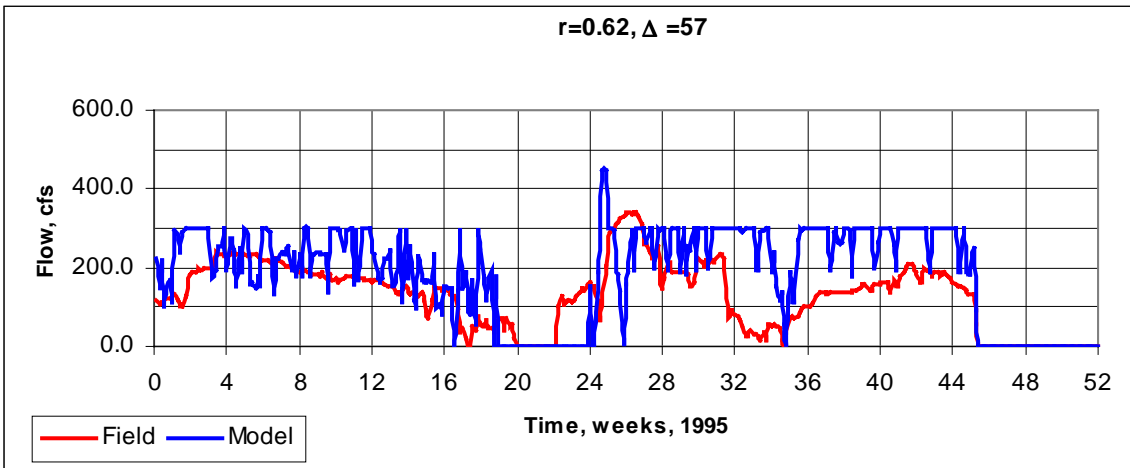
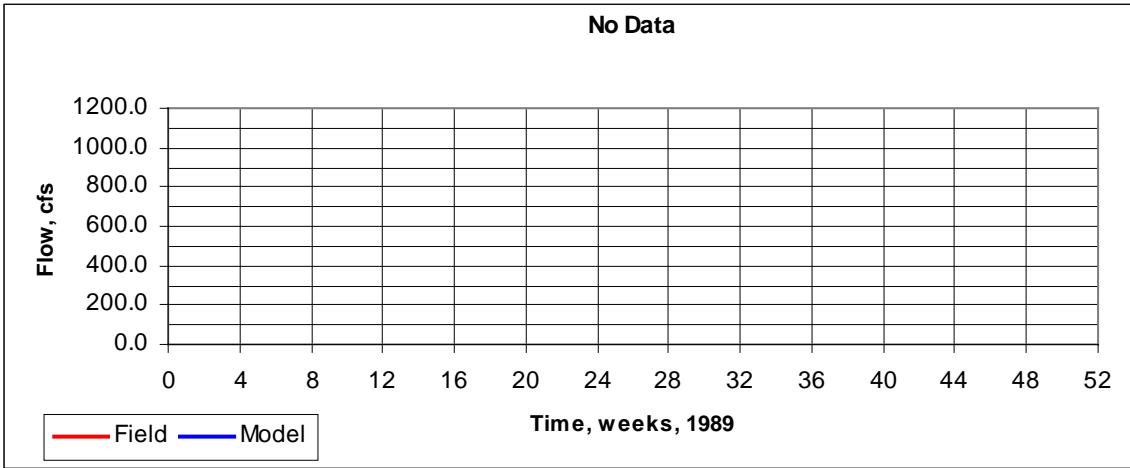
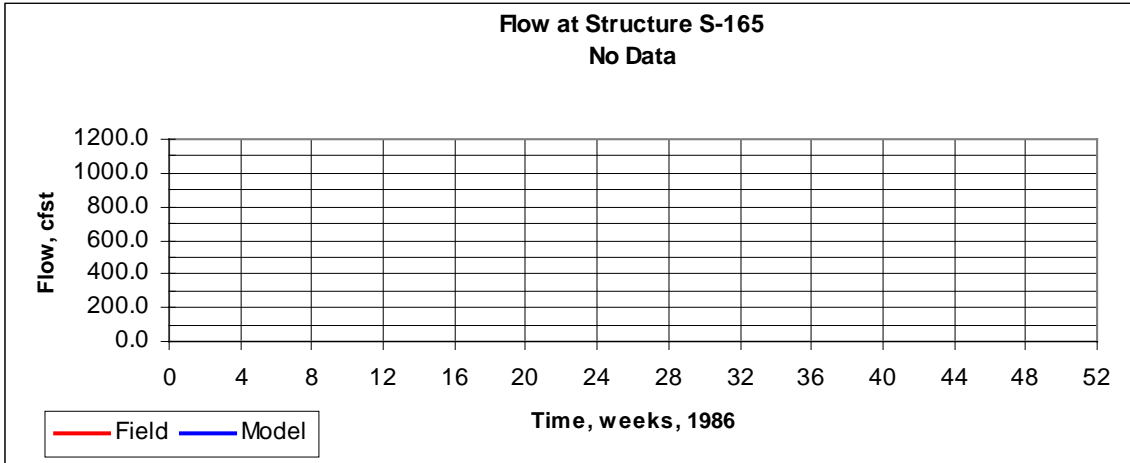


Figure 106: Flow at S-165

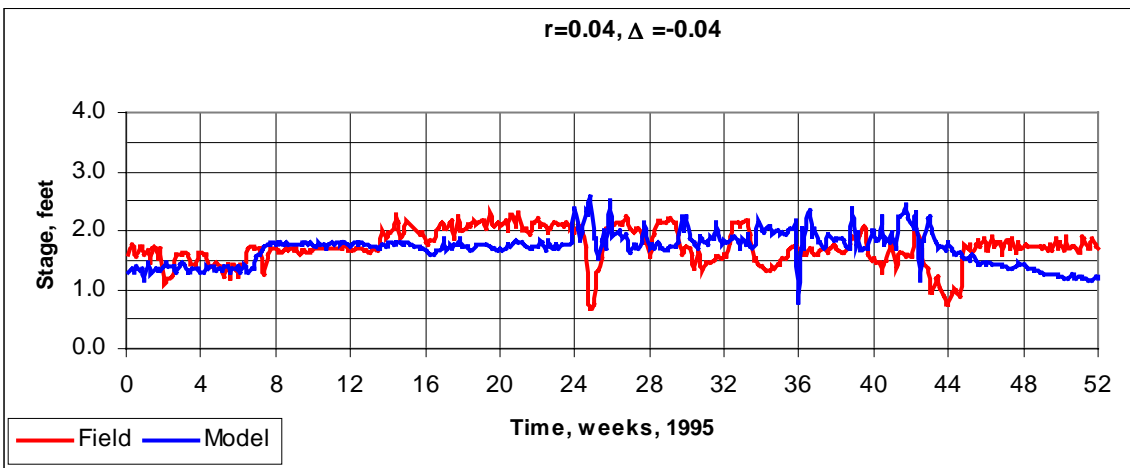
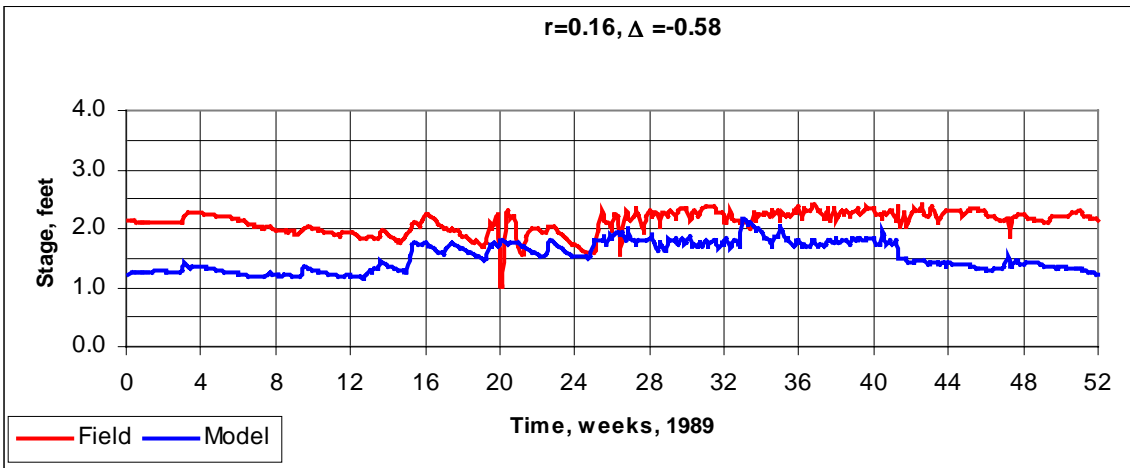
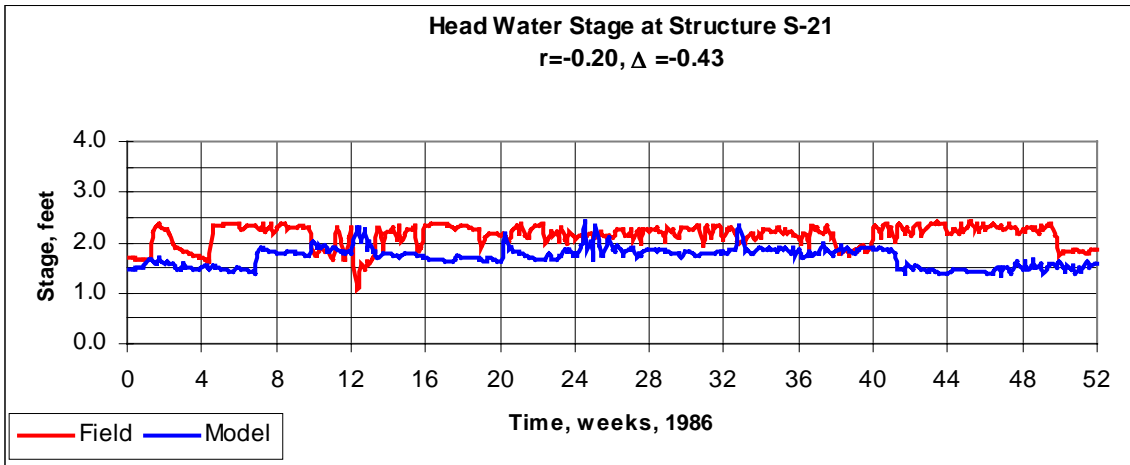


Figure 107: Head Water Stage at S-21

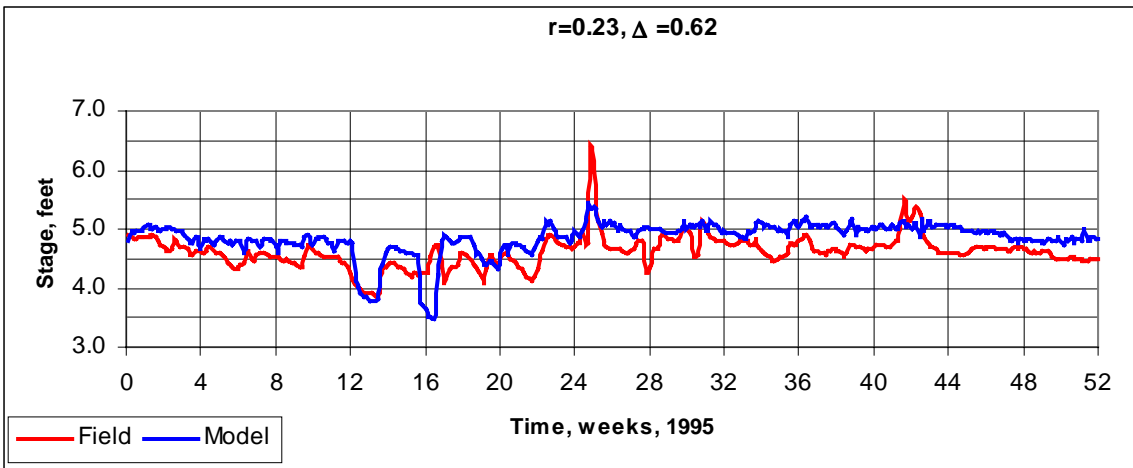
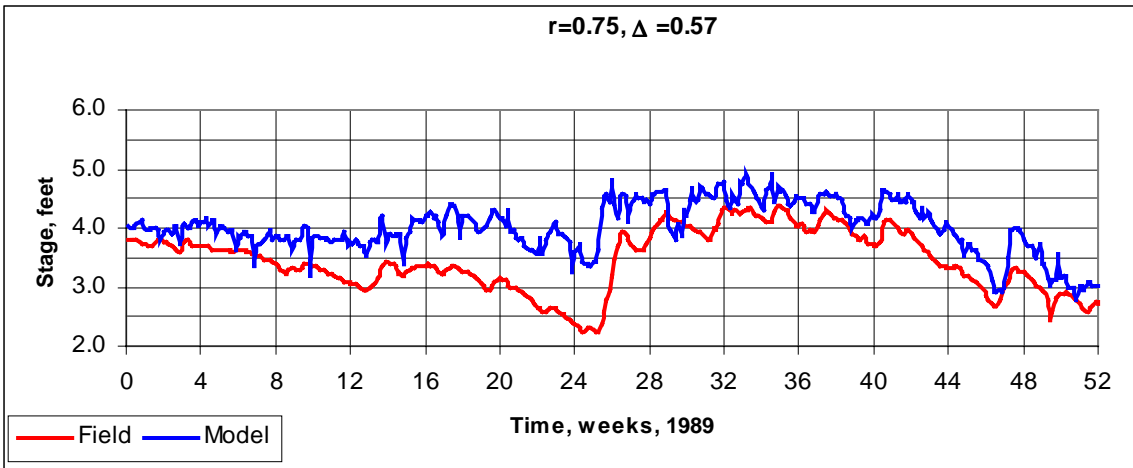
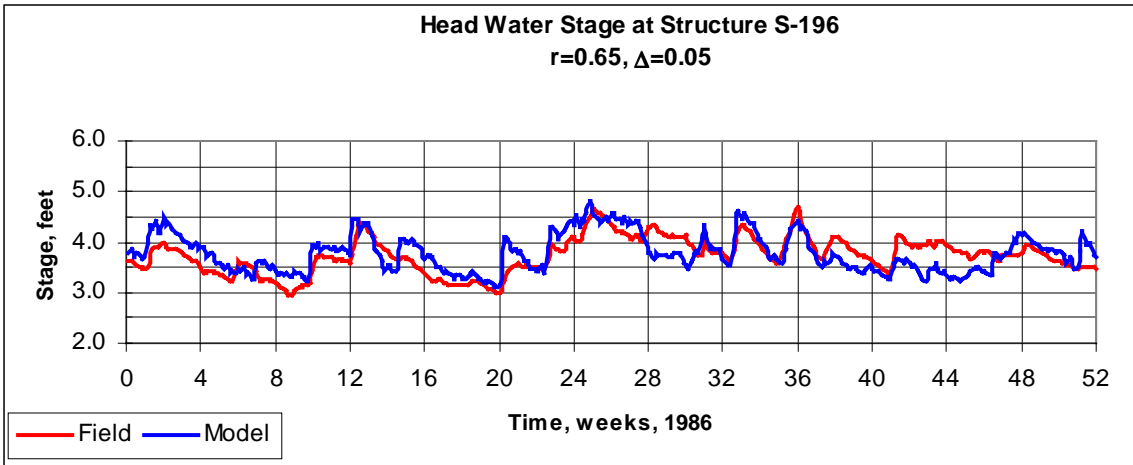


Figure 108: Head Water Stage at S-196

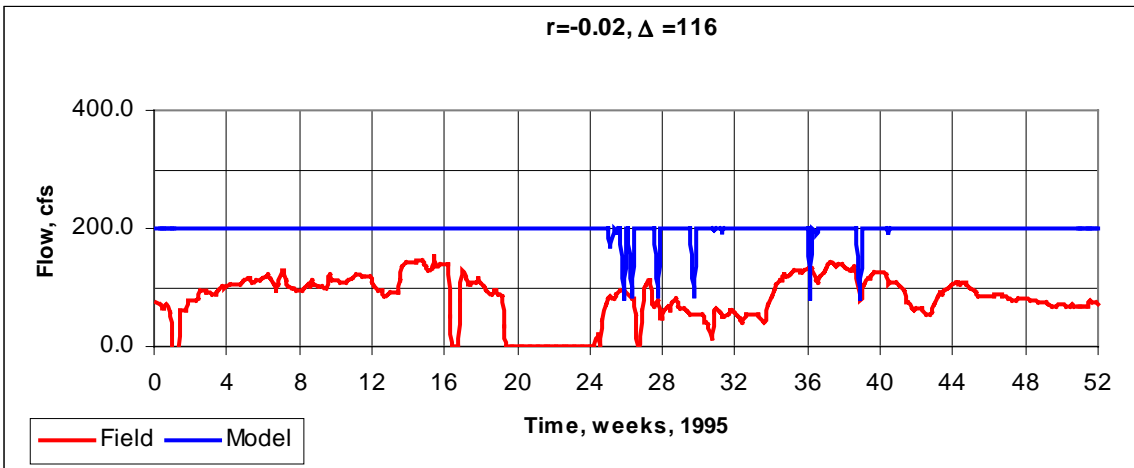
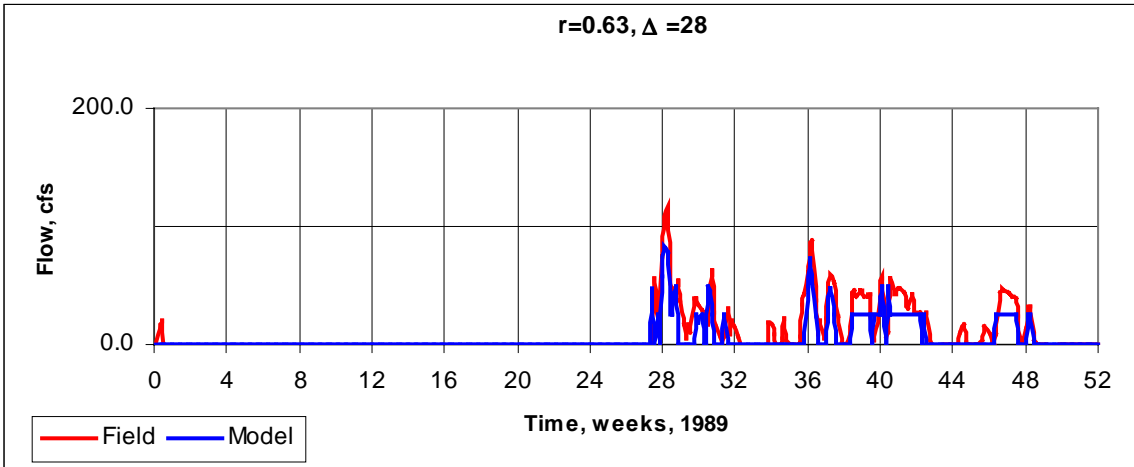
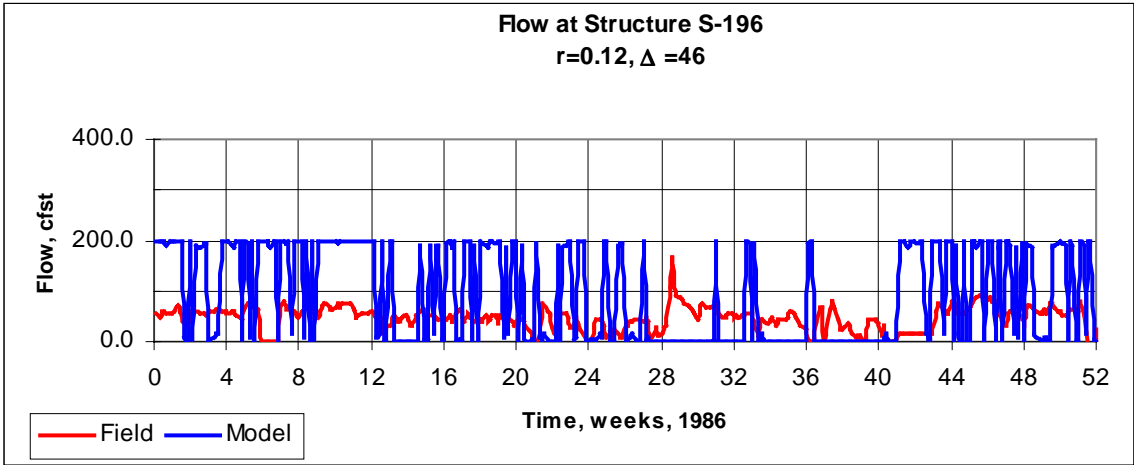


Figure 109: Flow at S-196

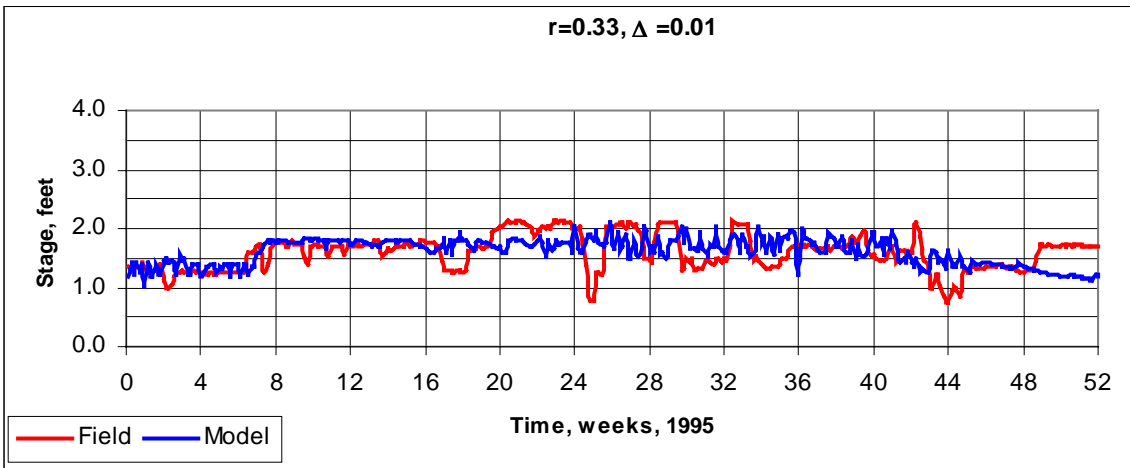
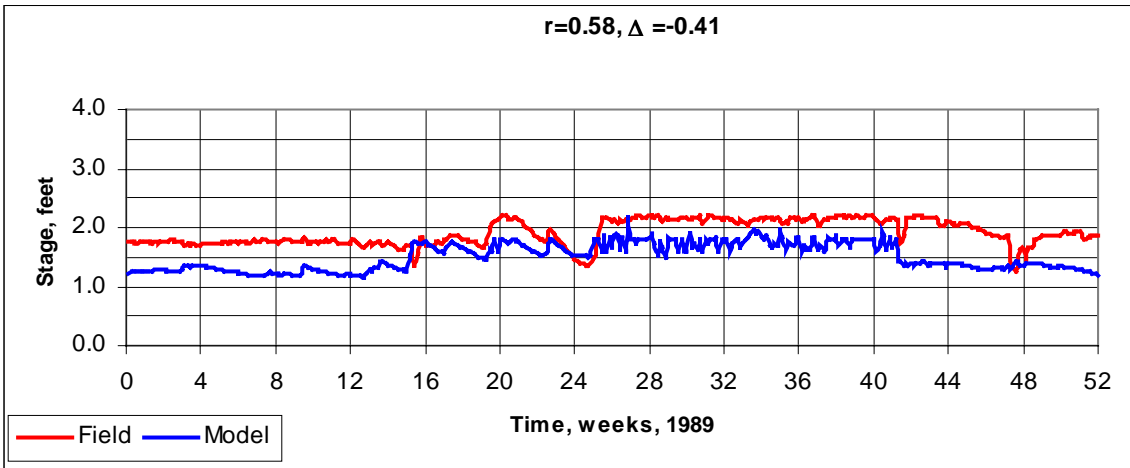
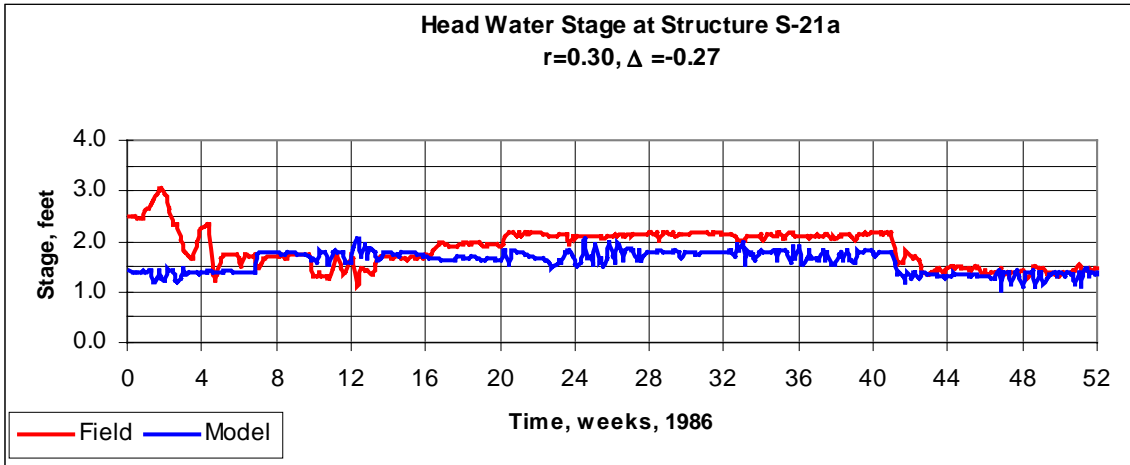


Figure 110: Head Water Stage at S-21a

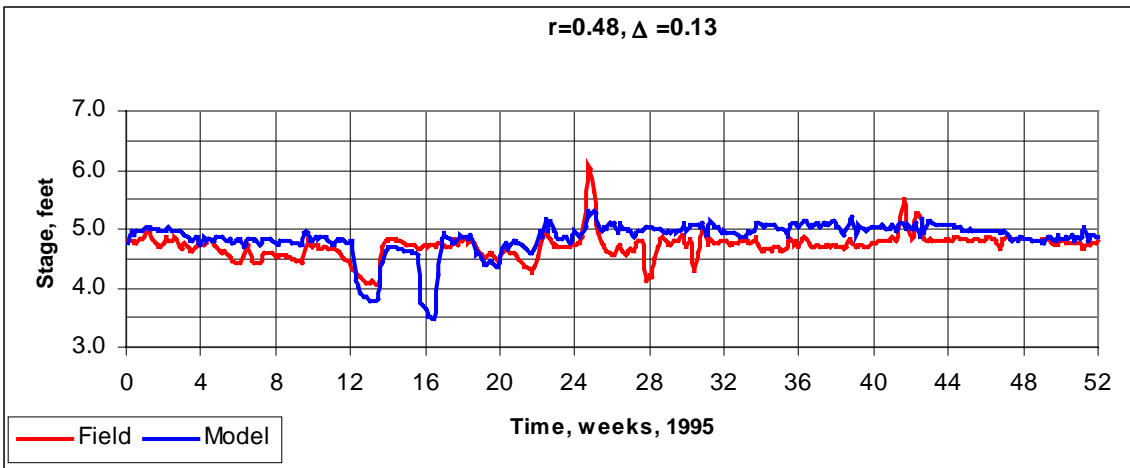
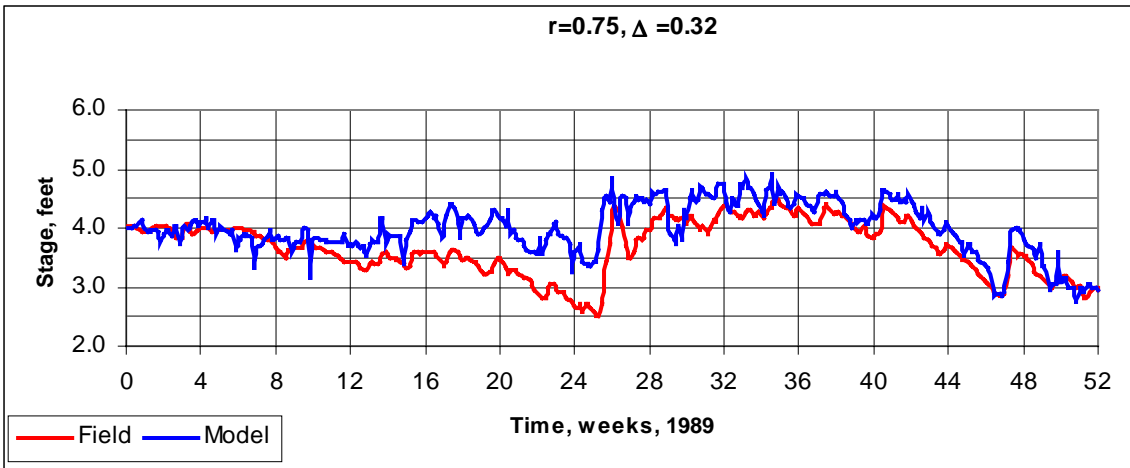
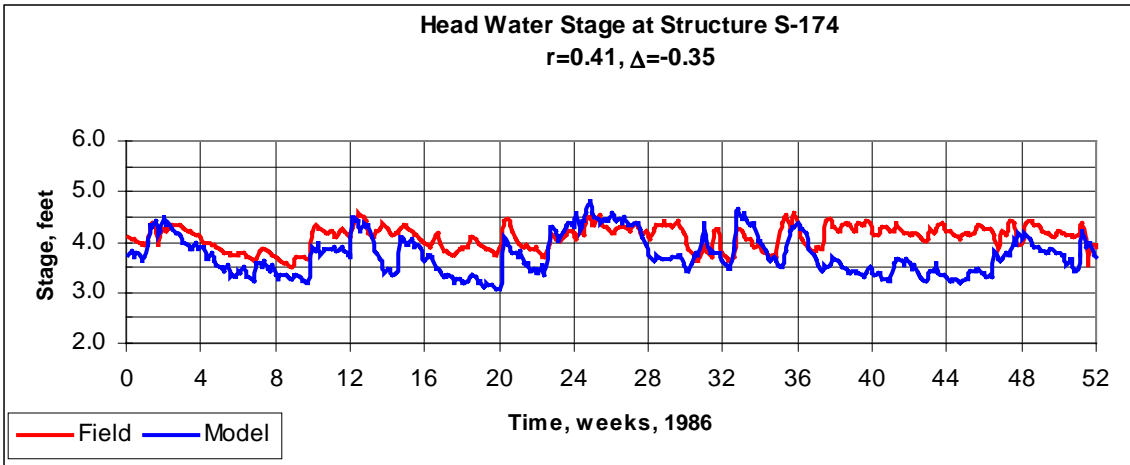


Figure 111: Head Water Stage at S-174

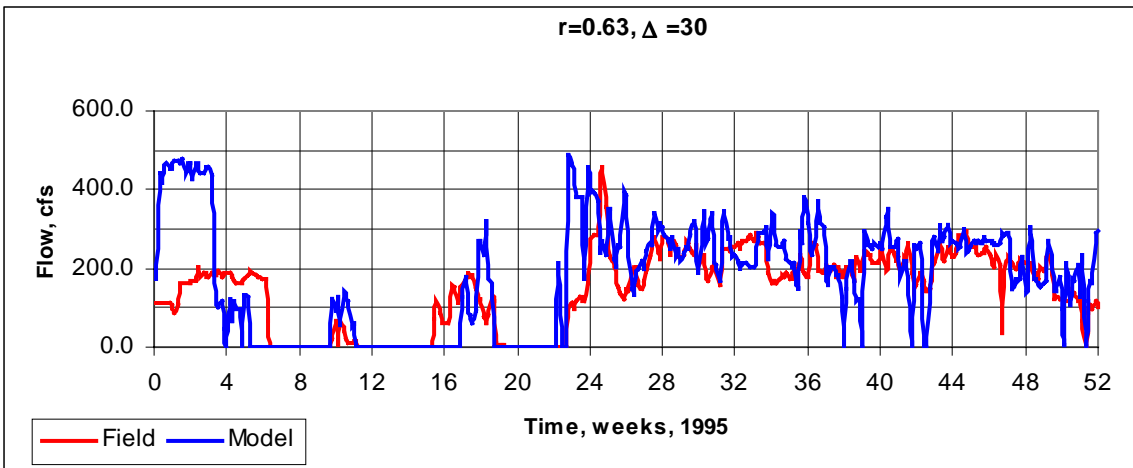
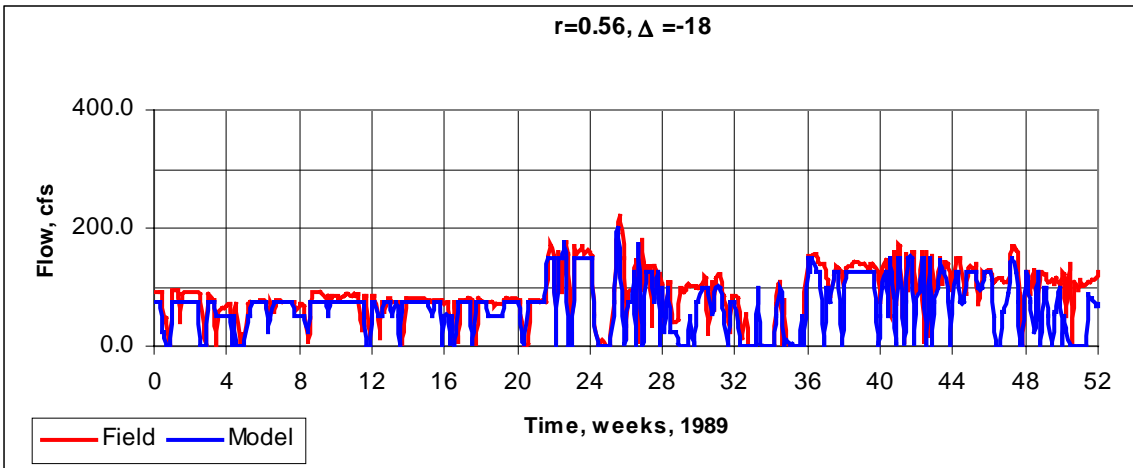
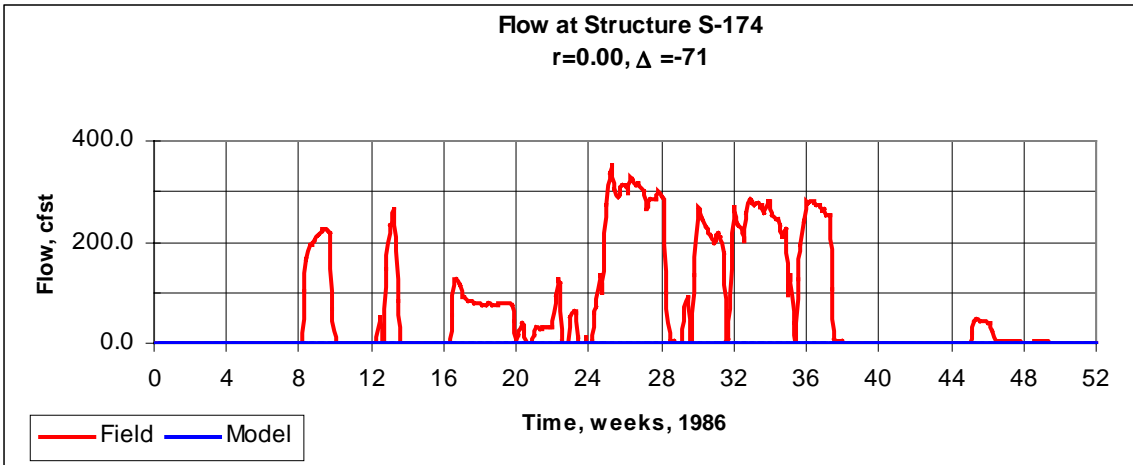


Figure 112: Flow at S-174

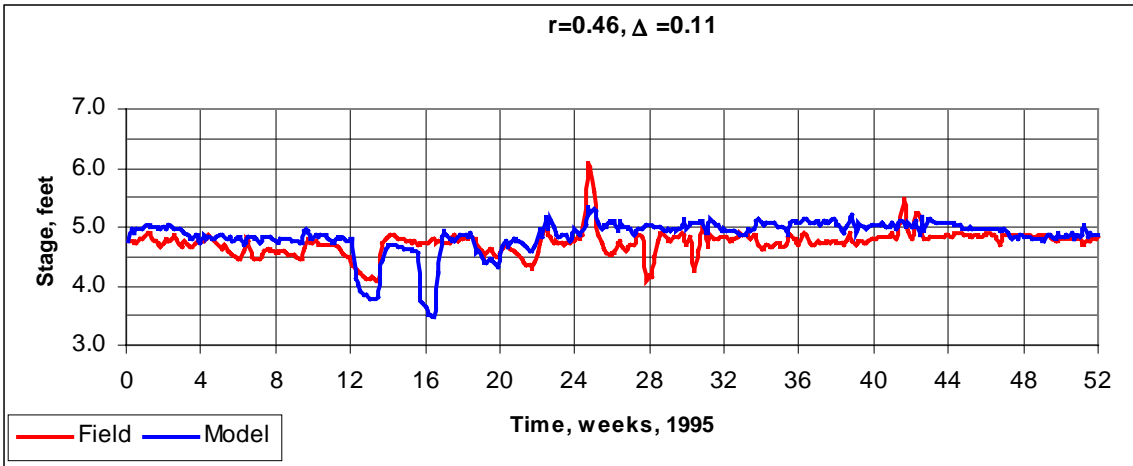
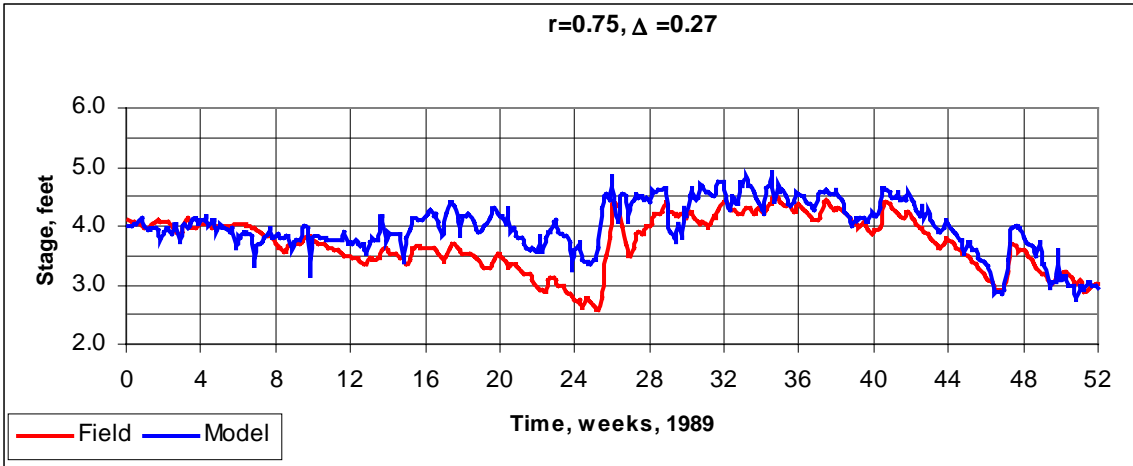
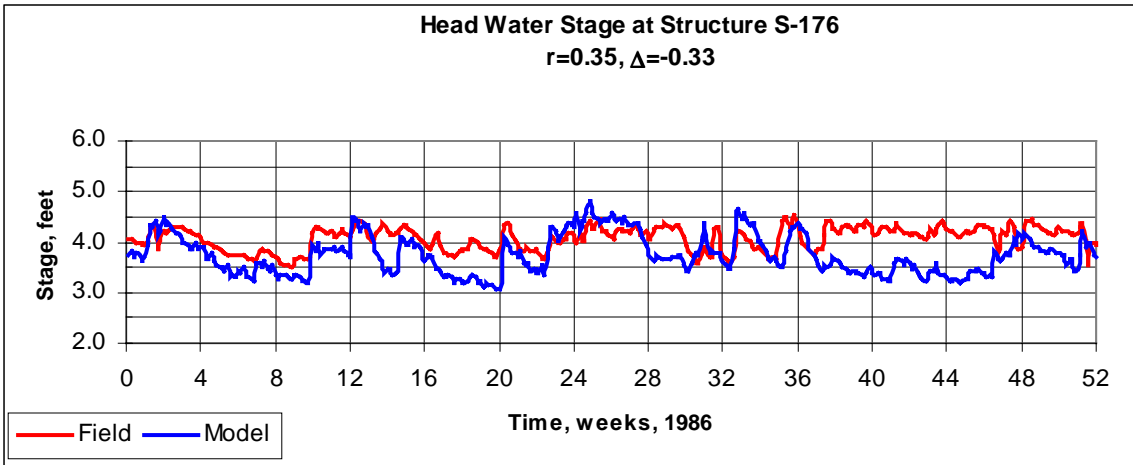


Figure113: Head Water Stage at S-176

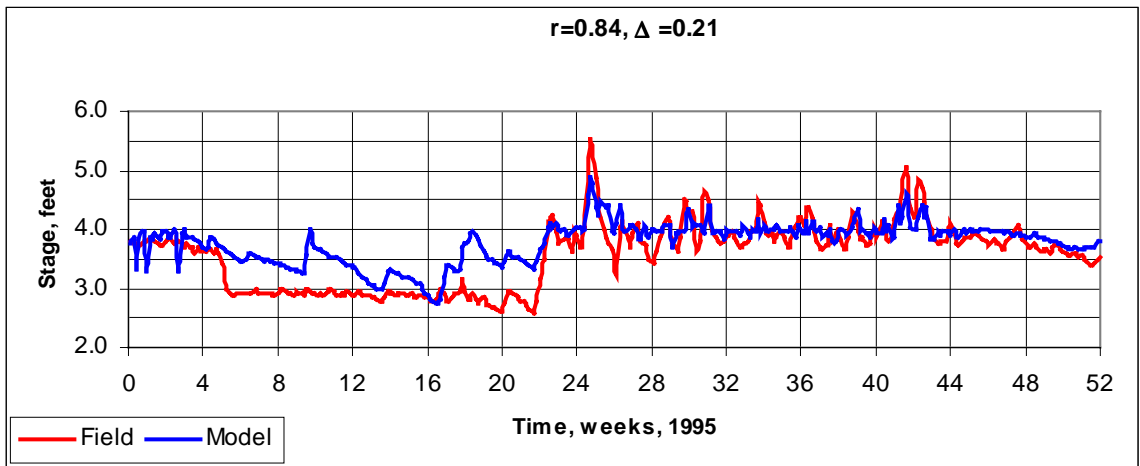
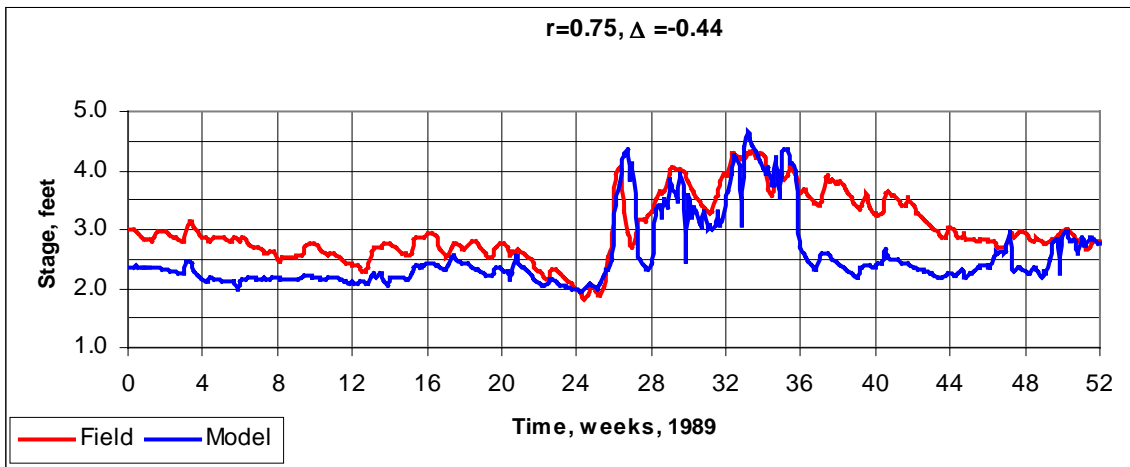
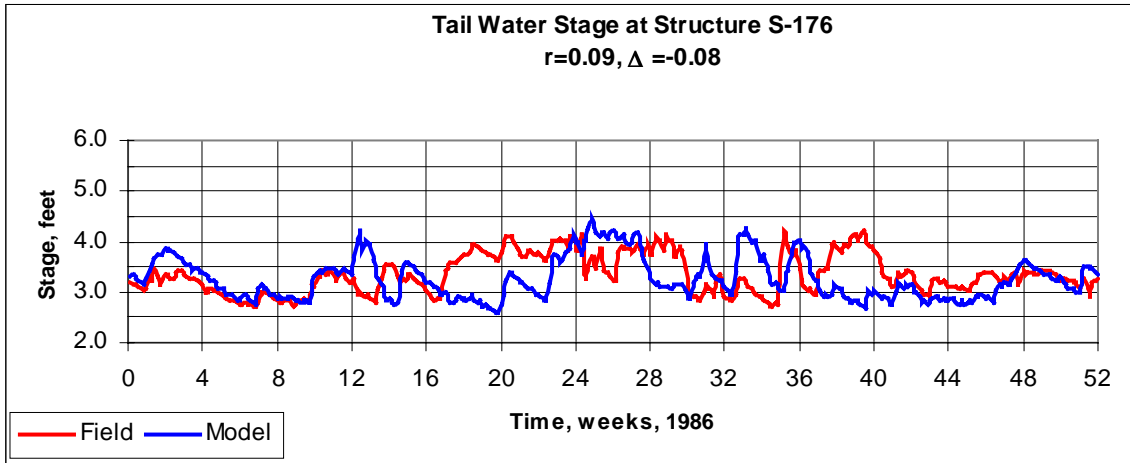


Figure 114: Tail Water Stage at S-176

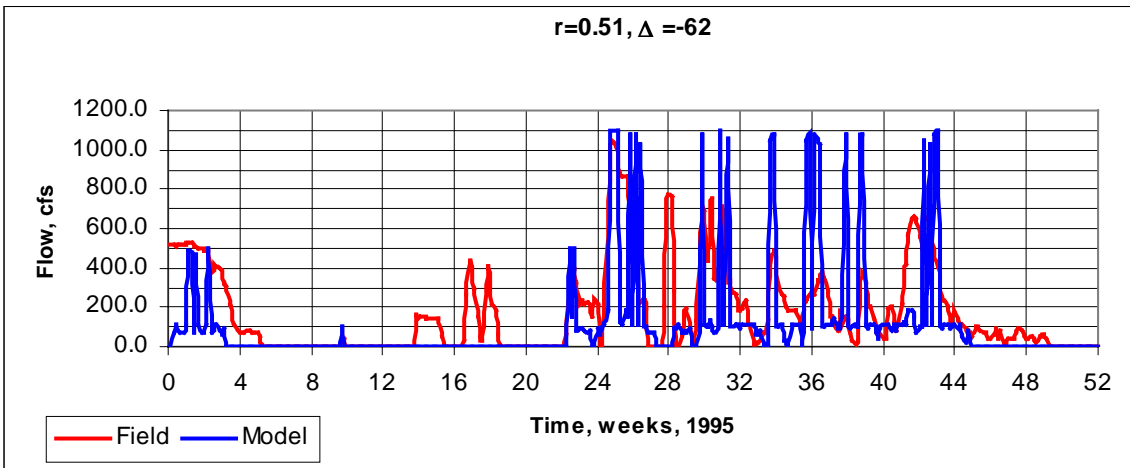
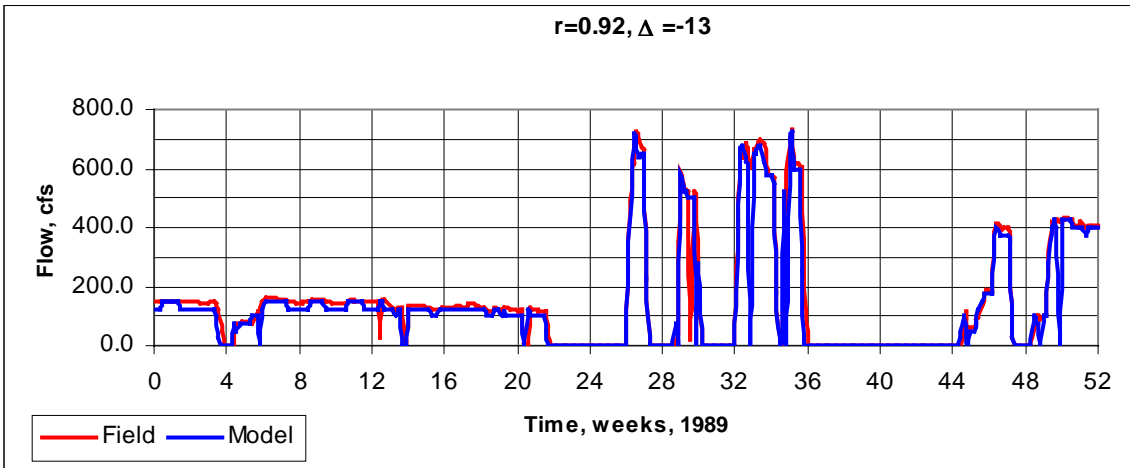
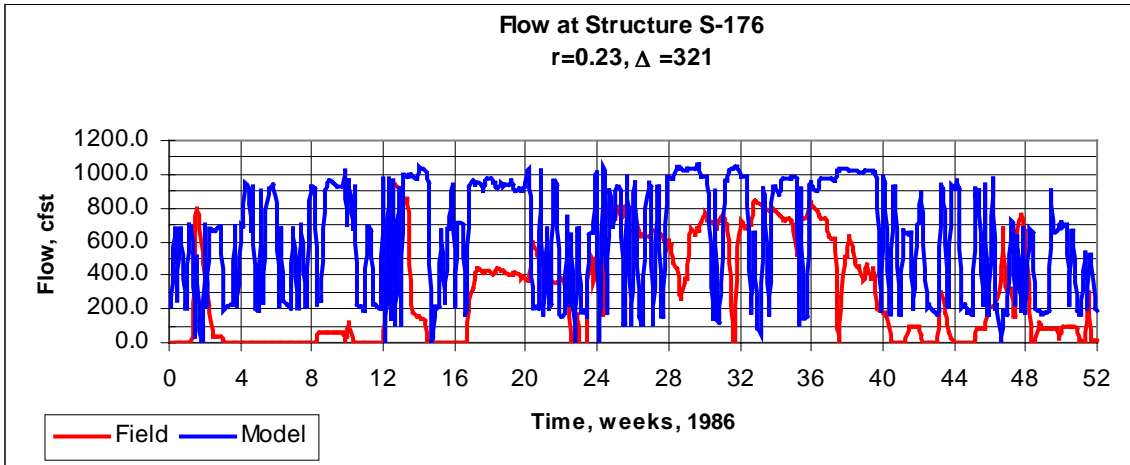


Figure 115: Flow at S-176

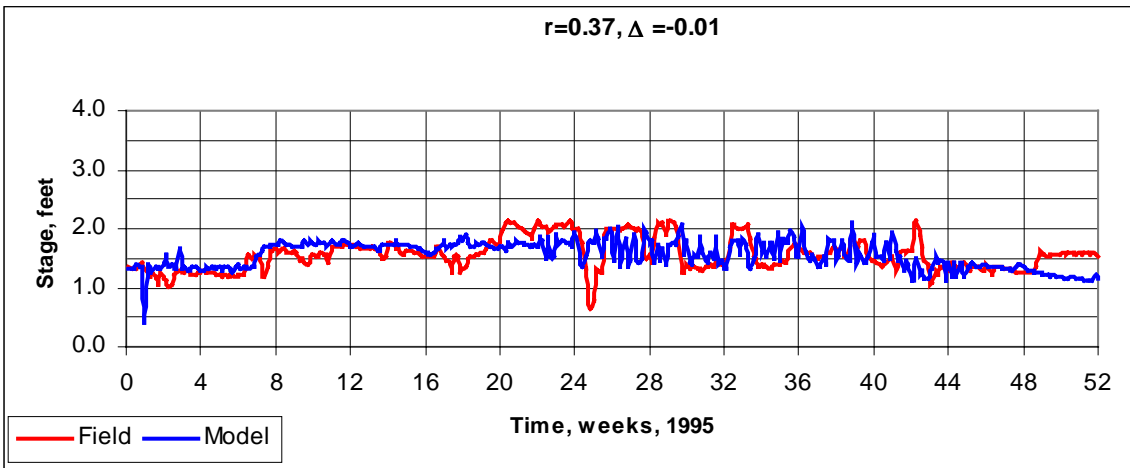
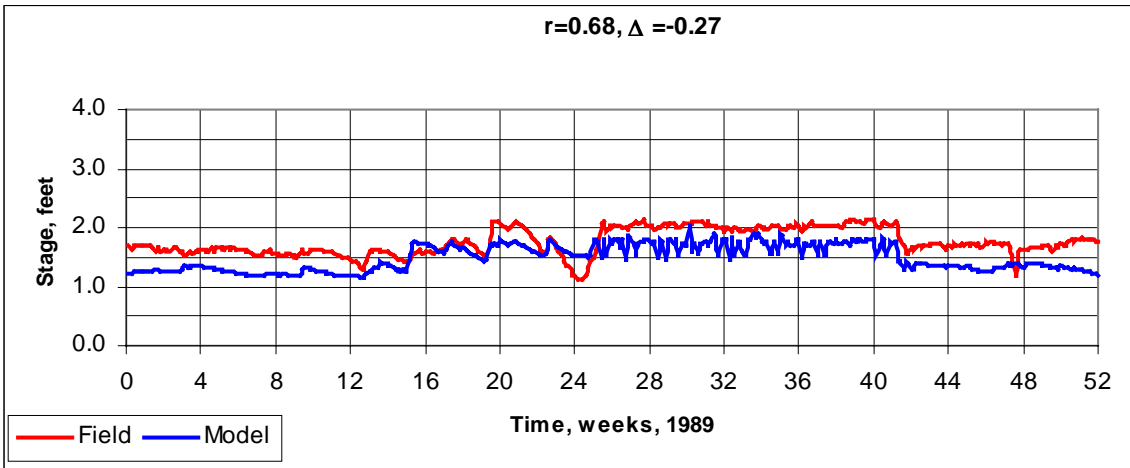
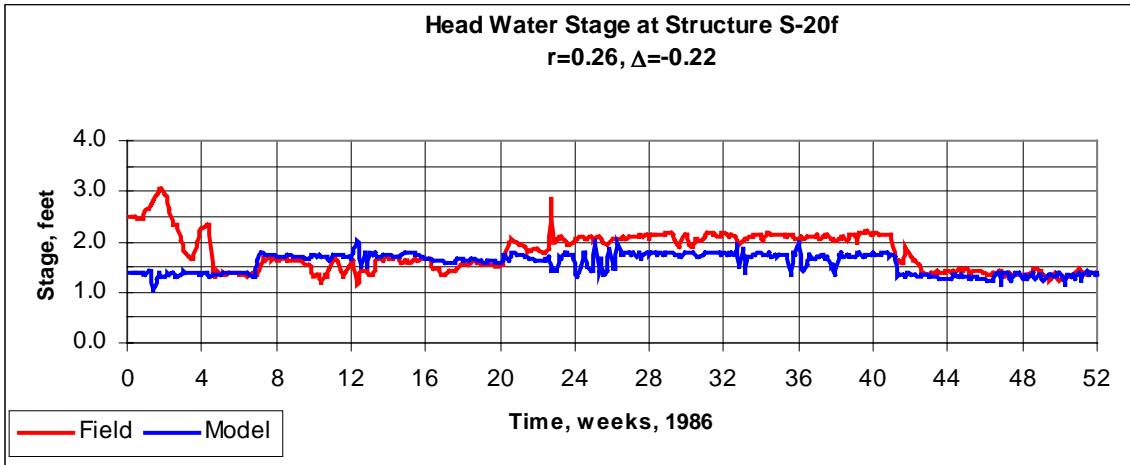


Figure 116: Head Water Stage at S-20f

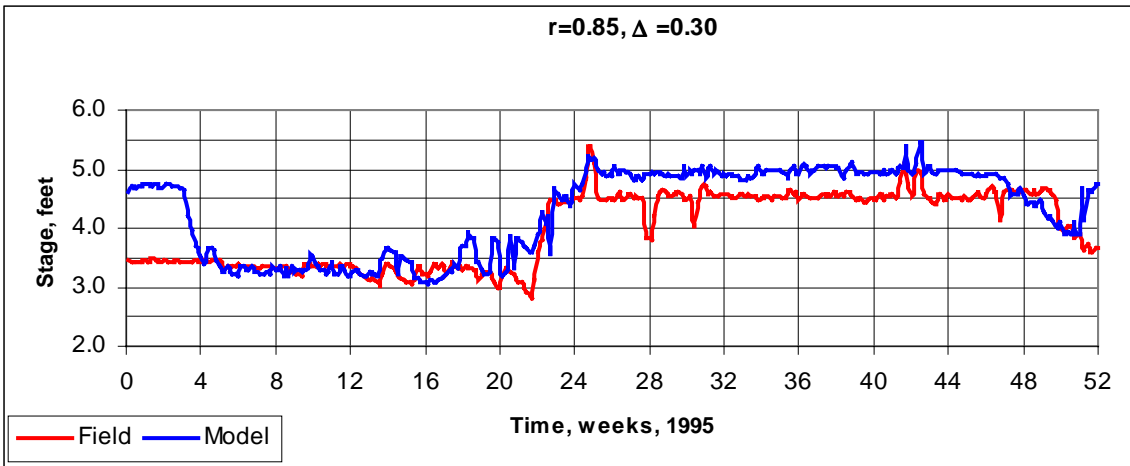
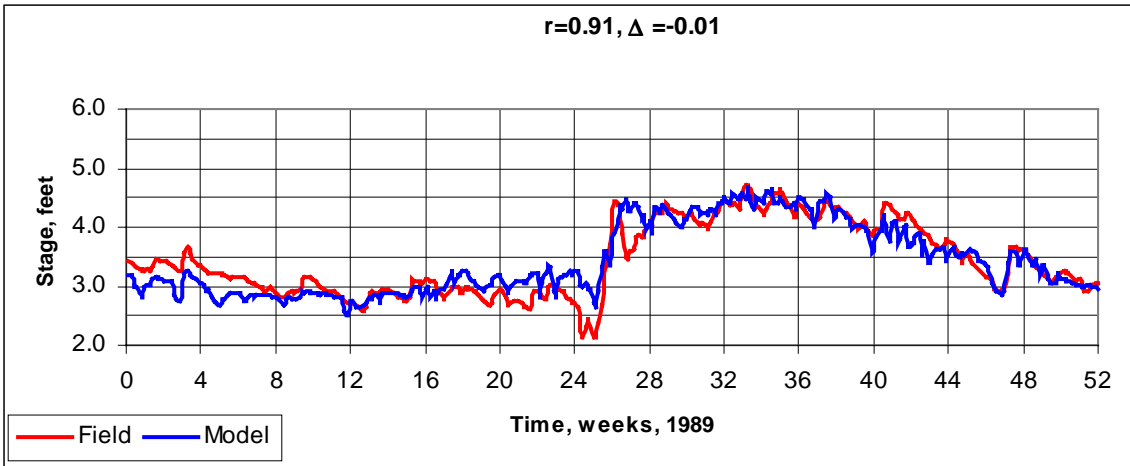
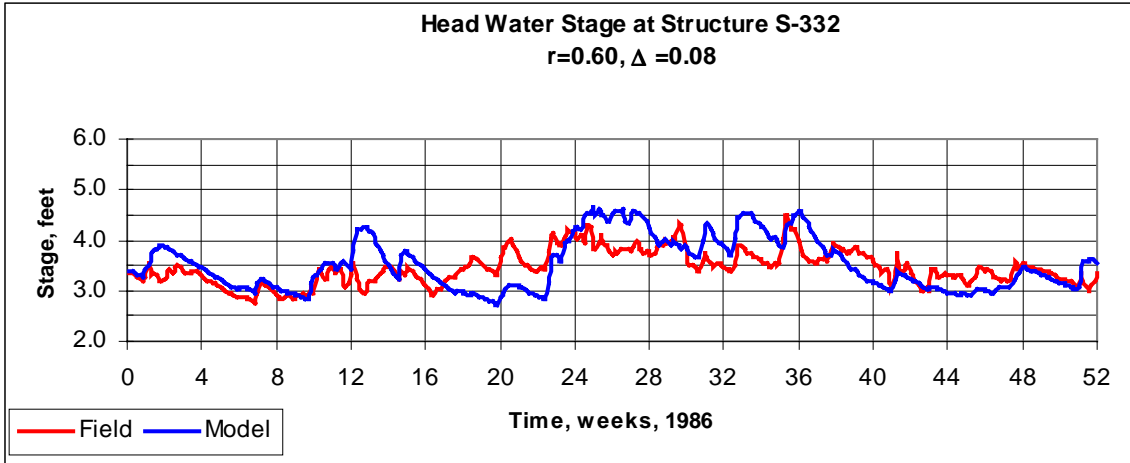


Figure 117: Head Water Stage at S-332

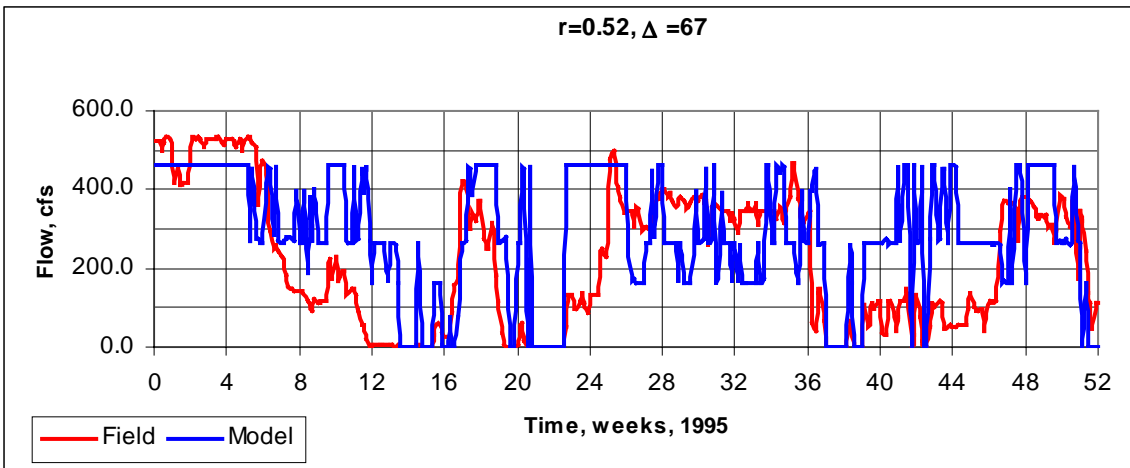
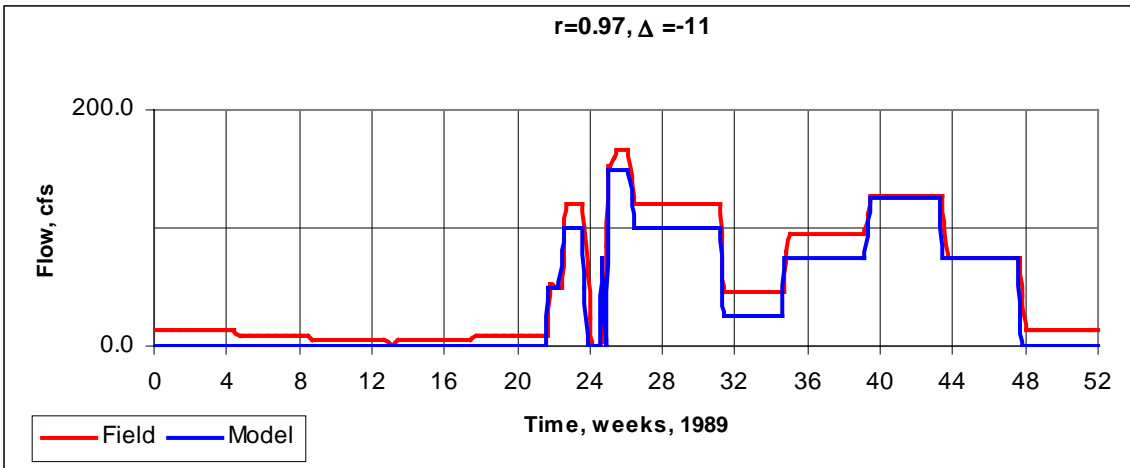
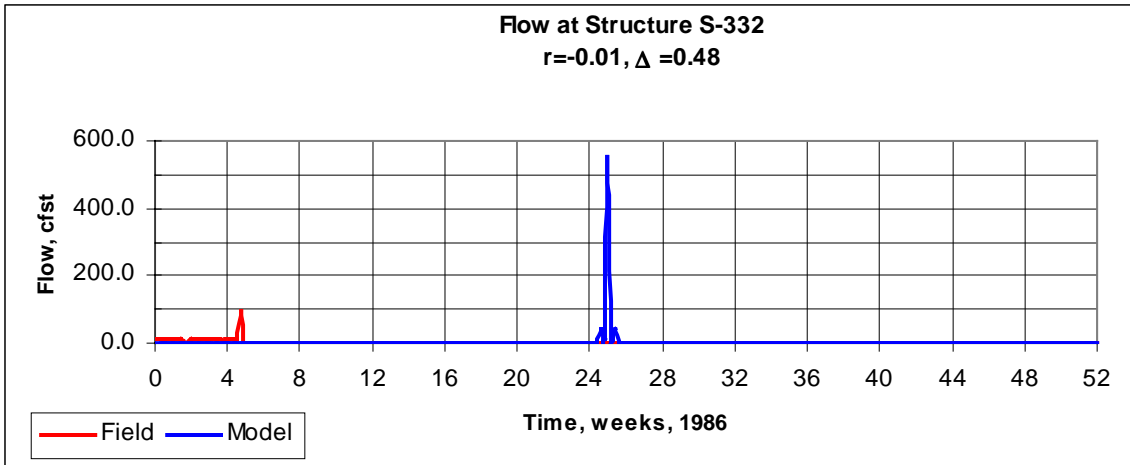


Figure 118: Flow at S-332

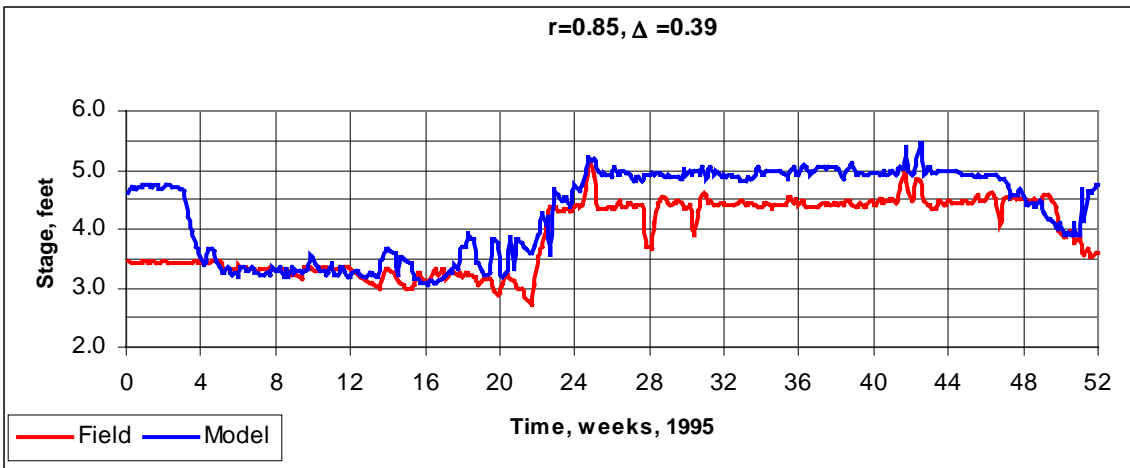
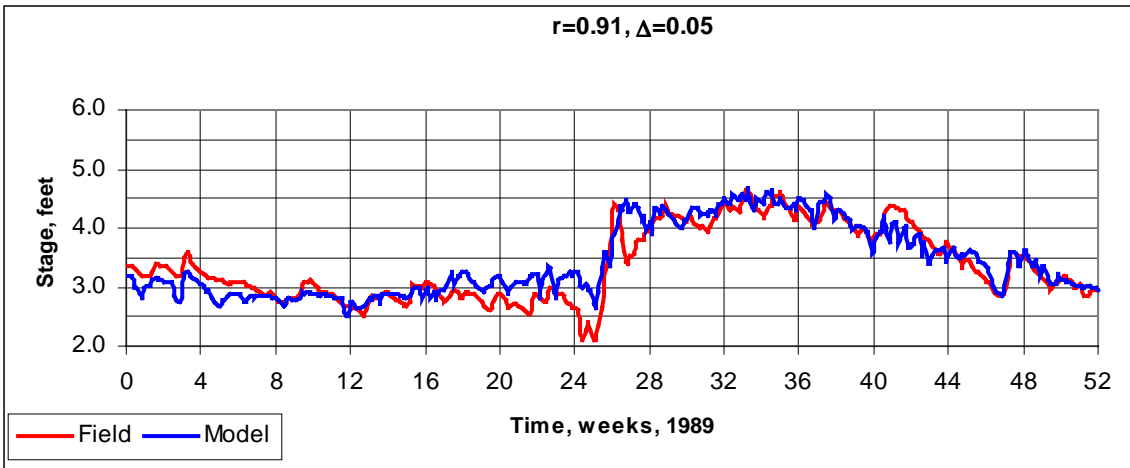
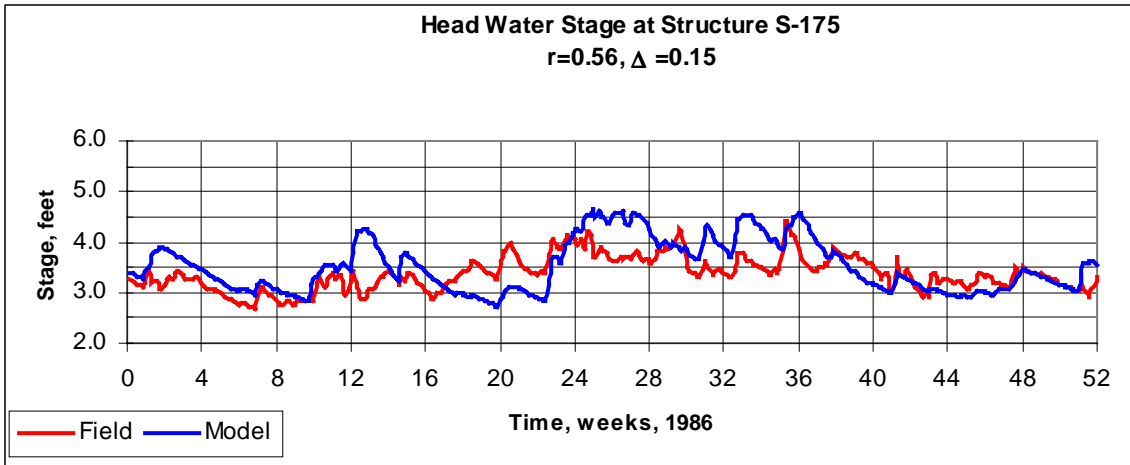


Figure 119: Head Water Stage at S-175

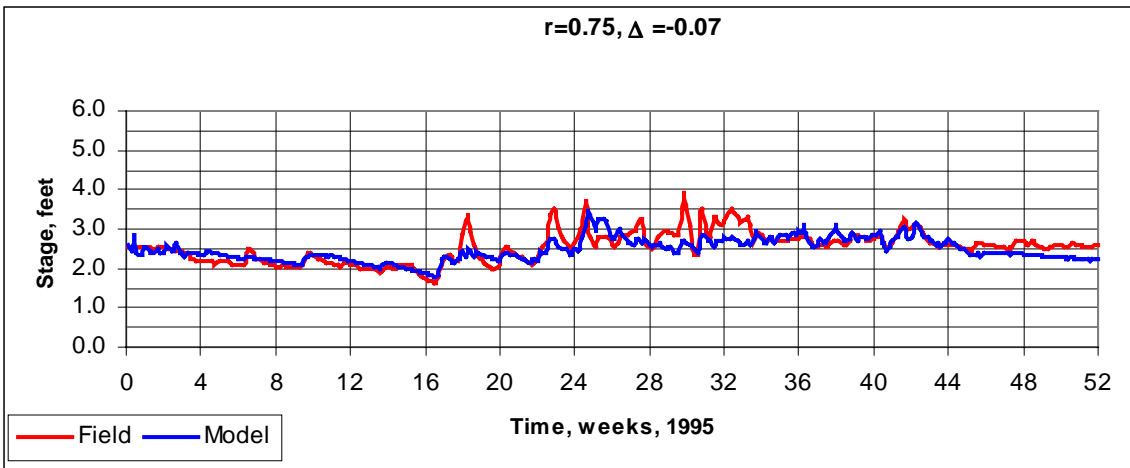
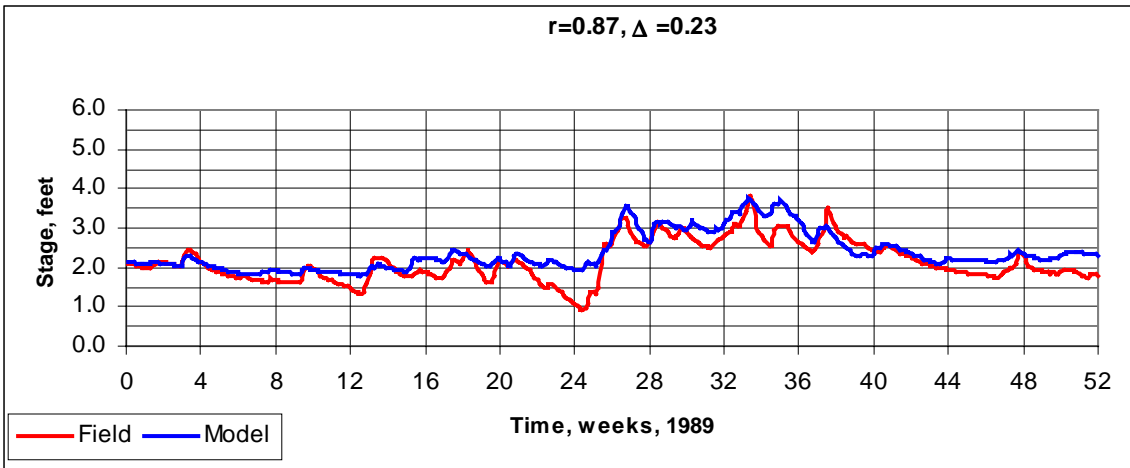
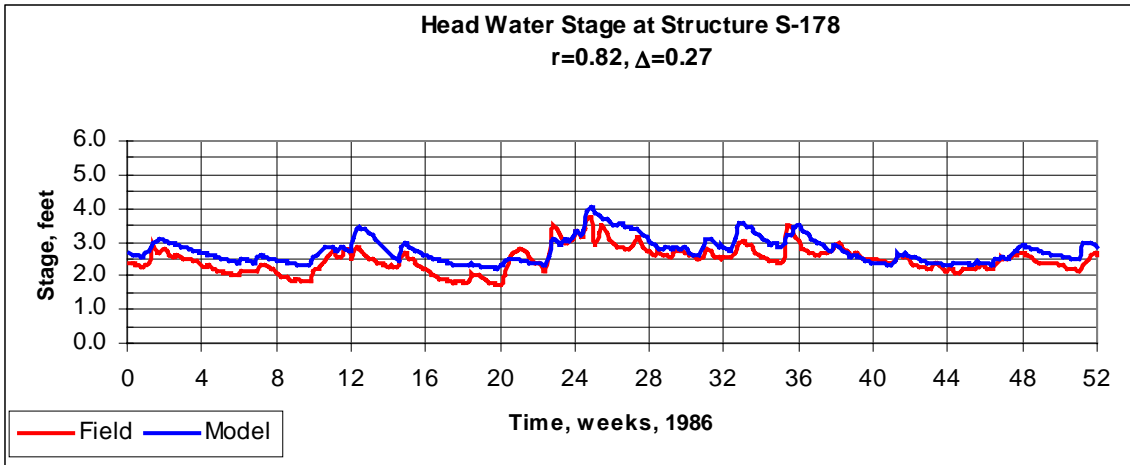


Figure 120: Head Water Stage at S-178

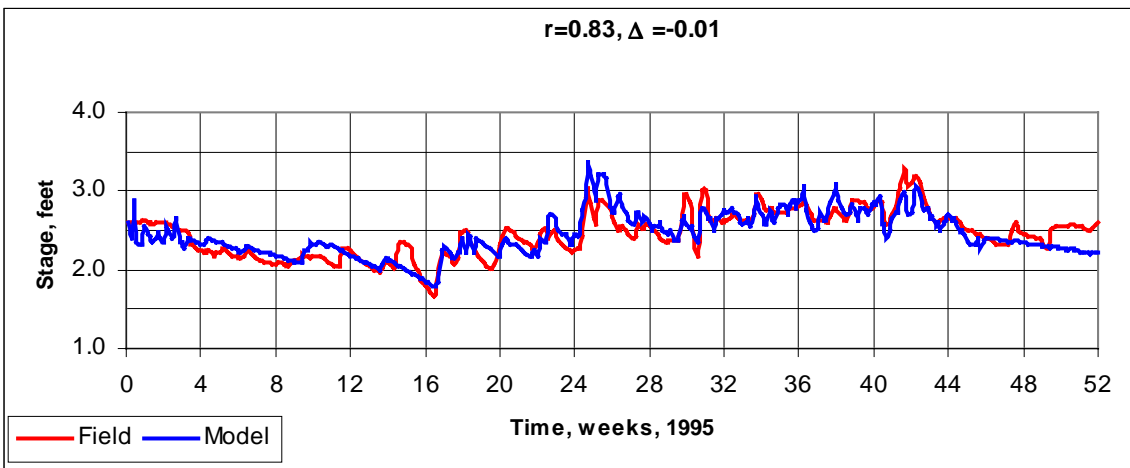
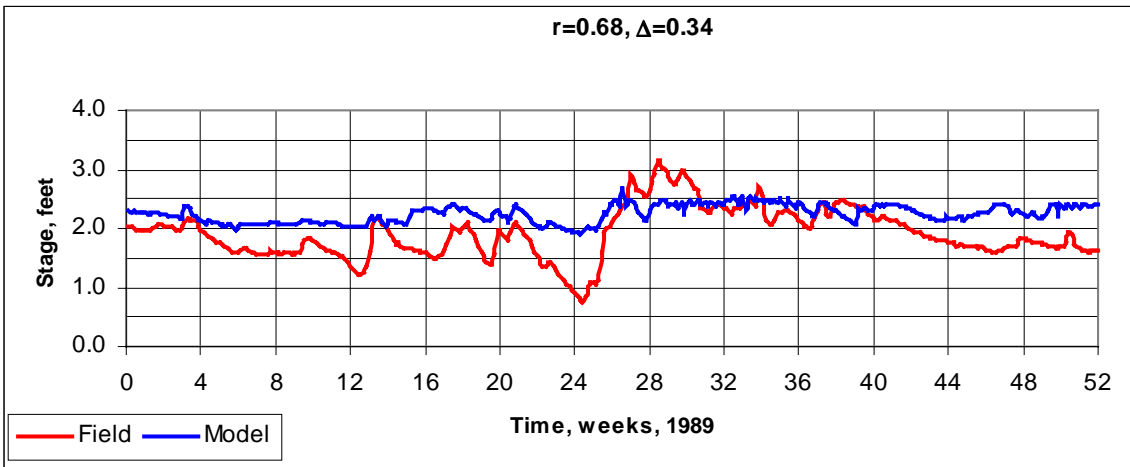
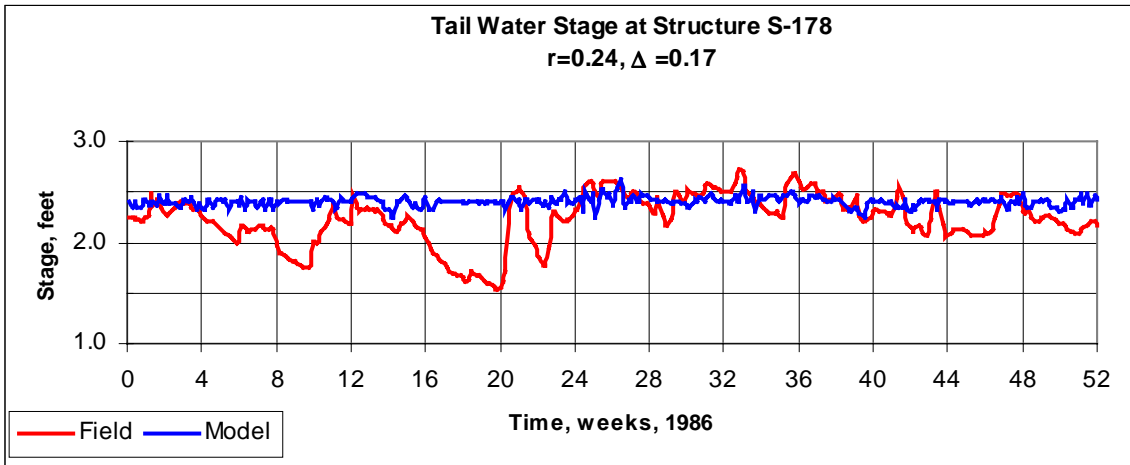


Figure121: Tail Water Stage at S-178

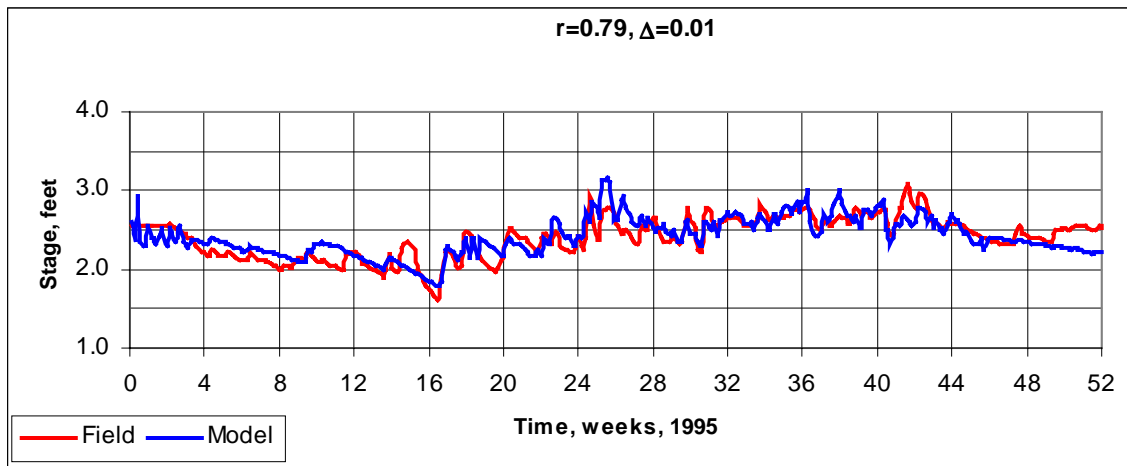
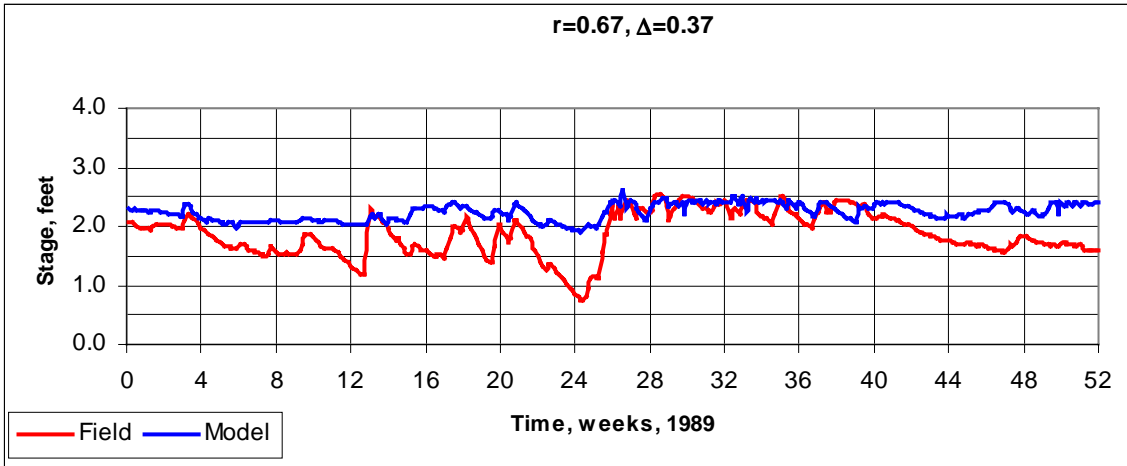
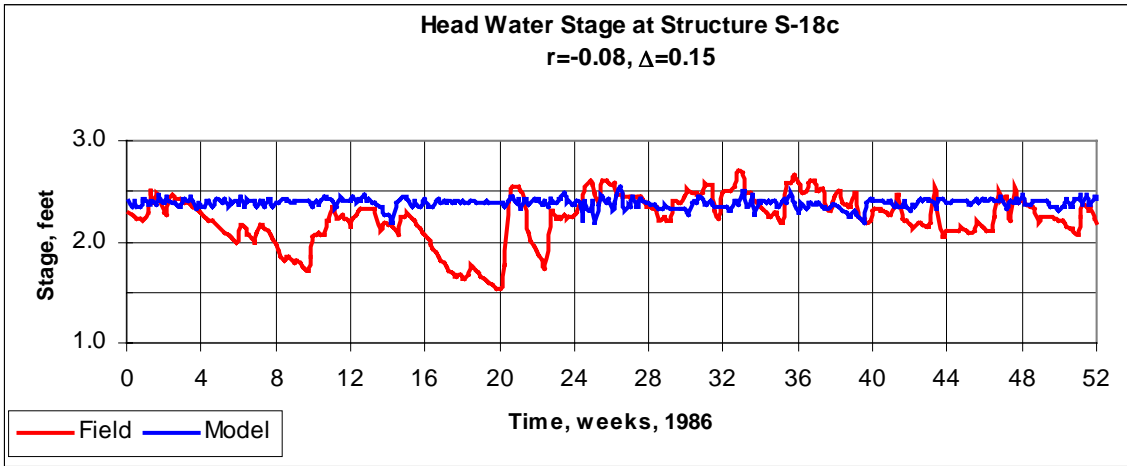


Figure 122: Head Water Stage at S-18c

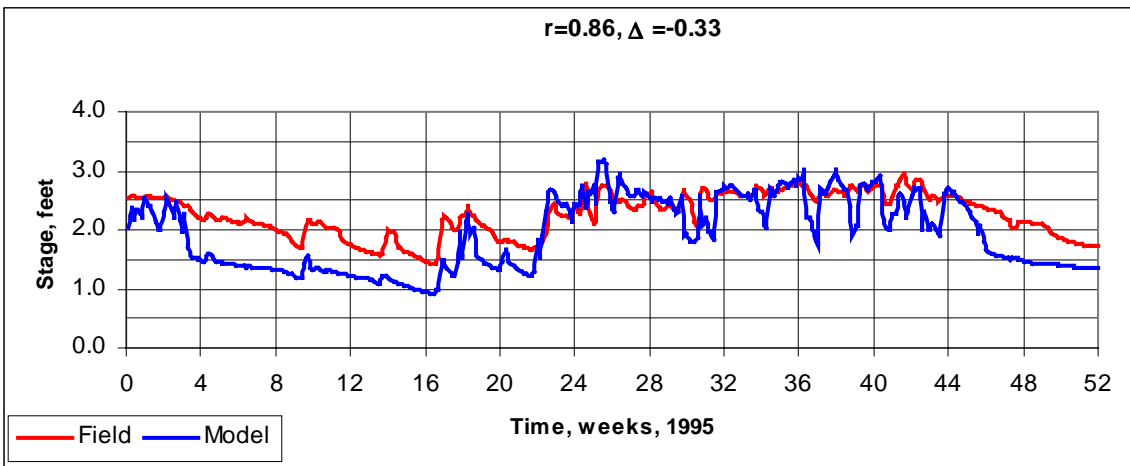
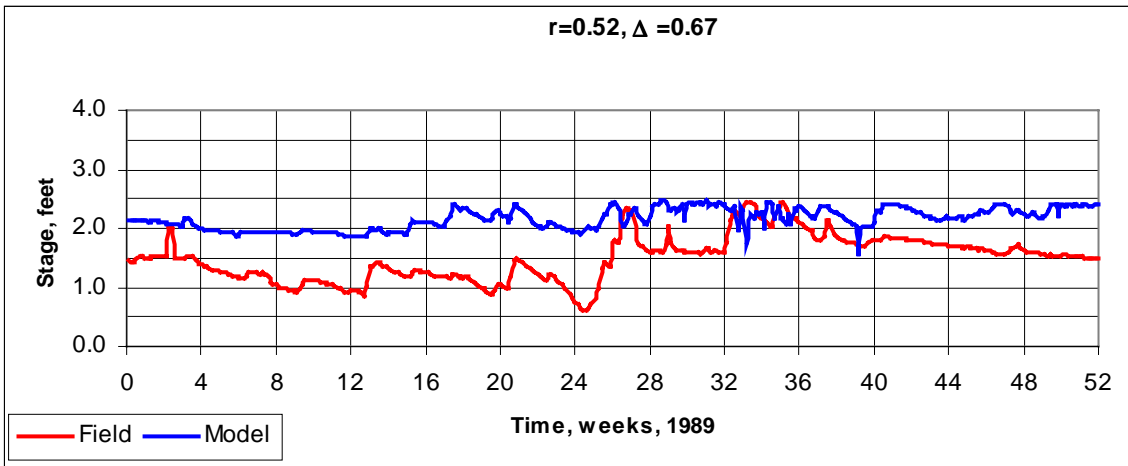
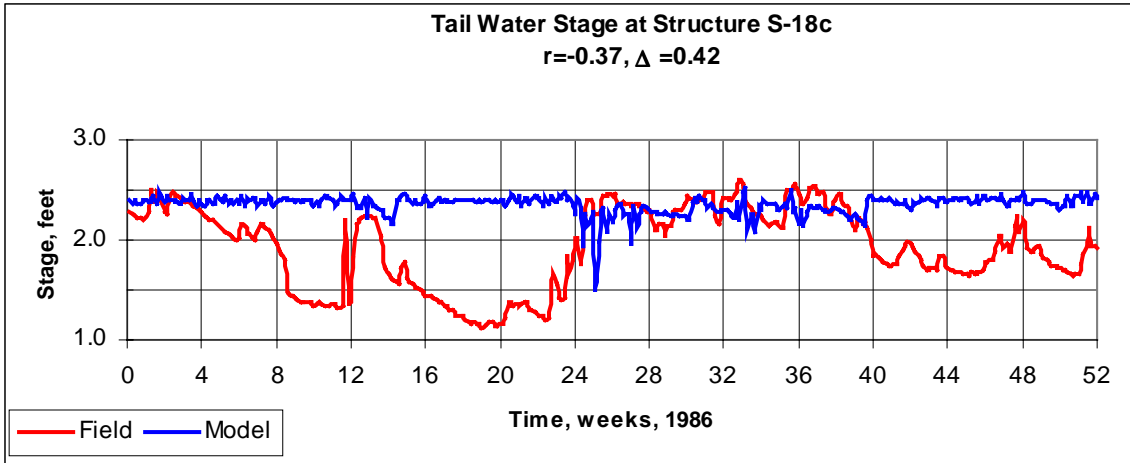


Figure 123: Tail Water Stage at S-18c

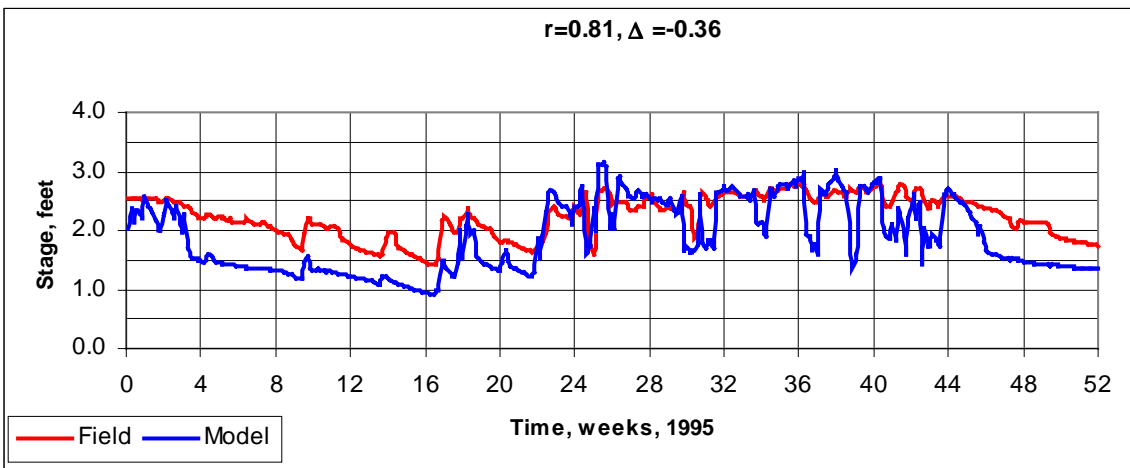
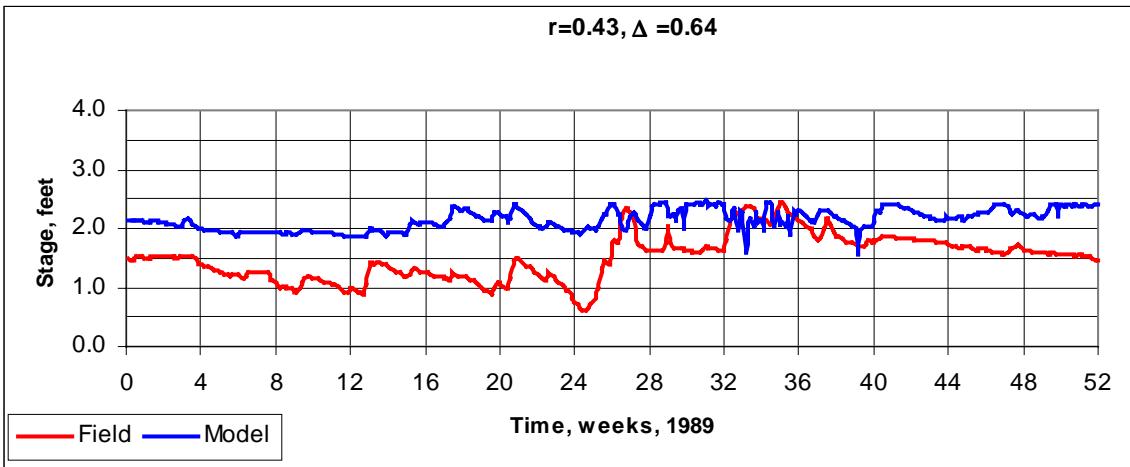
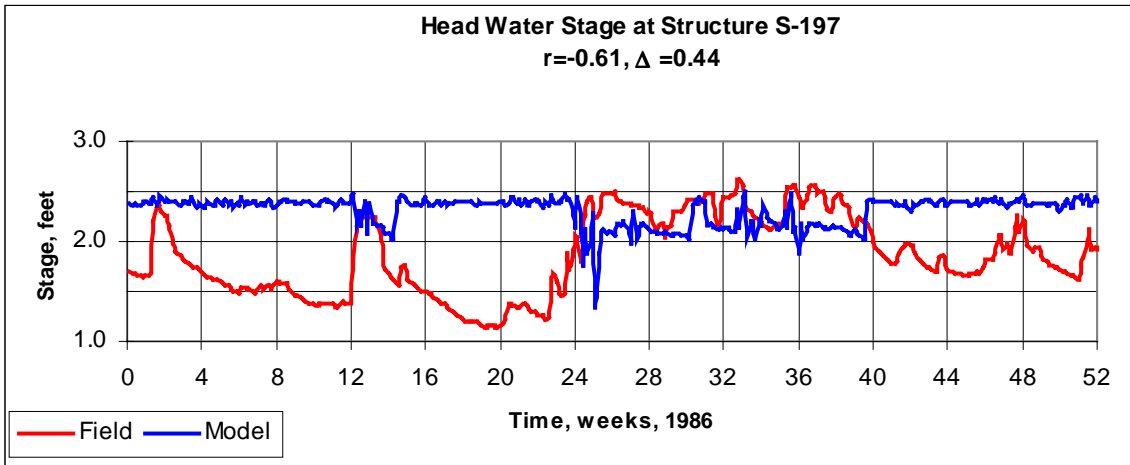


Figure 124: Head Water Stage at S-197

Appendix A

Fresh Water Equivalent Heads of Saline Water General Head Boundaries (GHB) for MODFLOW/MODBRANCH

The General Head Boundary (GHB) package of MODFLOW/MODBRANCH requires that the *Head* at the center of each boundary cell be specified. This head value is usually expressed as a distance above some common reference point. This is straightforward when using fresh water, but is not when the water is saline and the model is not density driven.

Using ρ_s = density of salt water and ρ_f = density of fresh water, an equation expressing the **mass** balance between a column of saline water and an equivalent column of fresh water is derived as follows:

$$\begin{aligned}\text{Mass of saline column} &= \rho_s A (Z_s - Z) \\ \text{Mass of fresh column} &= \rho_f A (Z_f - Z)\end{aligned}$$

where

- Z_s = elevation of the saline water surface (known),
- Z_f = elevation of the fresh water surface (unknown),
- Z = common reference point (known),
- A = area of the base of each column (will cancel).

Since the masses of the column should be equal, we get the following:

$$\begin{aligned}\rho_s A (Z_s - Z) &= \rho_f A (Z_f - Z), \text{ or} \\ \rho_s (Z_s - Z) &= \rho_f (Z_f - Z).\end{aligned}$$

Using a value of fresh water density (ρ) of 1.0 g/cc and for ocean water, a density (ρ_s) of approximately 1.025 g/cc, the equivalent fresh water head Z_f is:

$$Z_f = 1.025 (Z_s - Z) + Z.$$

If we do not take into account salinity, then the head throughout the water column (i.e., for each layer) is constant because the $(\rho_s/\rho_f) = 1$. However, since the density of the ocean water is not equal to the fresh water, the *head* is not constant with depth and must be adjusted.

Example:

Assume we have a 3 layer model. At one specific location (x,y), the elevations of the cell centers are 0., -20., -50 feet. The ocean water elevation is 1.2 feet. If this were fresh water, then the head would be 1.2 (=Z_s) feet at each cell. However, for ocean water (ρ_s = 1.025) there will be a different value of head at each depth.

$$\begin{aligned} \text{Layer 1:} \quad Z_s - Z &= 1.2 - 0.0 = 1.2 \\ T_f &= (1.025)(1.2) + 0.0 = \mathbf{1.23} \text{ feet} \quad (2.5\% \text{ increase}) \end{aligned}$$

$$\begin{aligned} \text{Layer 2:} \quad Z_s - Z &= 1.2 - (-20) = 21.2 \\ T_f &= (1.025)(21.2) + (-20) = \mathbf{1.73} \text{ feet} \quad (44\% \text{ increase}) \end{aligned}$$

$$\begin{aligned} \text{Layer 3:} \quad Z_s - Z &= 1.2 - (-50) = 51.2 \\ T_f &= (1.025)(51.2) + (-50) = \mathbf{2.48} \text{ feet} \quad (107\% \text{ increase}) \end{aligned}$$

For this simple example, the difference in general head boundary specification between the top and bottom layers is over 100%. A problem remains in that, if we specify these general head boundary (ghb) values, the groundwater model will attempt to move water vertically upward instead of horizontally. In order to avoid this, the vertical leakage in the boundary cells is set close to 0.